# EFFECT OF SALT AND POLYELECTROLYTES ON SELF-ASSEMBLED STRUCTURES OF IONIC AMPHIPHILES

by

*Anindya Chowdhury*

A thesis submitted to
the Jawaharlal Nehru University for the degree of
**Doctor of Philosophy**

2022


**Raman Research Institute**
**Banglore 560 080**
**India**

# DECLARATION

I hereby declare that this thesis is composed independently by me at Raman Research Institute, Bangalore under the supervision of Prof. Pramod Pullarkat and Prof. V. A. Raghunathan. The subject matter presented in this thesis has not previously formed the basis of the award of any degree, diploma, associateship, fellowship or any other similar title. I also declare that I have run it through the **Turnitin** plagiarism software.

Anindya Chowdhury

Signature of the Student

(Anindya Chowdhury)

Signature of the Supervisor

(Prof. Pramod Pullarkat)
Raman Research Institute
Bangalore 560080

Signature of the Co-supervisor

(Prof.V.A.Raghunathan)
Raman Research Institute
Bangalore 560080

# CERTIFICATE

This is to certify that the thesis entitled " **EFFECT OF SALT AND POLYELECTROLYTES ON SELF-ASSEMBLED STRUCTURES OF IONIC AMPHIPHILES** " submitted by Anindya Chowdhury for the award of degree DOCTOR OF PHILOSOPHY of Jawaharlal Nehru University is his original work. This has not been published or submitted to any other university for any other degree or diploma.

Signature of the Supervisor

(Prof. Pramod Pullarkat)
Raman Research Institute
Bangalore 560080

Signature of the Co-supervisor

(Prof.V.A.Raghunathan)
Raman Research Institute
Bangalore 560080

Signature of the Director

Director
Raman Research Institute
Bangalore 560080

# Acknowledgements

I am very much thankful to my thesis supervisor Prof. V. A. Raghunathan for providing the support and guidance. I am overwhelmed by his patience and deep understanding of the subject. I will consider myself knowledgeable even if I have a very small fraction of understanding of the subject compared to Raghu. The journey is very long and at end of it I have nothing to say to myself but the famous line by Dylan "..Yet there is no one to beat you/ No one to defeat you/ Except the thoughts of yourself feeling bad".

I am thankful to Prof. Yashodhan Hatwalne and Prof. Pratibha R. for being part of my thesis advisory committee. I would like to thank Prof. Sayantan Majumdar for his suggestions and help. I also would like to thank Prof. Ranjini Bandyopadhyay, Prof. Pramod Pullarkat, Prof. Arun Roy and Prof. Gautam V Soni for all the discussions.

I am thankful to Radhakrishna, Amudha and Chaitanya for their help. I am thankful to Mani, Dhason, Yatheendran, Srinivasa and Serene for all technical support for my experimental work. I am extremely thankful to Vasudha for all her help with my experiments and also for the mental support she always provided. I am thankful to Raja, Venkatesh and Murali for all their help.

I thank all the library staff for their help. I would like to thank everyone at the computer section and in the administrative department. I am very much thankful to everyone in the mechanical workshop, especially Anand and Ibrahim.

I thank all my labmates. I had good time with Madhukar. I thank Meera and Sreeja for teaching me the different experimental techniques and also for keeping the lab atmosphere lively. I thank Surya for all the support. I thank Ayush for all the suggestions.

I thank Madhukar, Mari, Sreyas, Swamy, Athul and Jk for all their help and the care they showed to me. I can't thank you enough. I also thank Jaggu, Gb, Sebanti, Arun, Vardhan, Abhishek, Anjan, Sumanth, Nooman, Subodh, Tiwary, Niranjan, Santanu da for all the good times. I don't know what more to say. I also thank Maheshwar, Avik, Raj da, Dipak, Rajkumar da, Chandan, Sagar, Bapan, Sanjay, Irla, Saumya, Vishnu, Nisanth, Saichand, Subhadip, Arsalan, Rajkumar for support and friendship. I am very very thankful to all the RRI students and the RRI sports community.

I am thankful to my parents for their support and encouragement. I can not forget my younger sister Purba, who always helped me in the tough times. To Ashoya (our pet dog), I just want you live long and healthy. My heartfelt thanks to my wife Sushmita and her family for their unfailing support and encouragement at all times. And finally to ma and Sushmita " I love you".

# Synopsis

Thesis title: "EFFECT OF SALT AND POLYELECTROLYTES ON SELF-ASSEMBLED STRUCTURES OF IONIC AMPHIPHILES"

In this thesis we study the structure, phase behaviour and polymorphism of different self-assembled aggregates of ionic amphiphilic molecules in the presence of polyelectrolytes and salt. In addition, the influence of pH on the phase behaviour of zwitterionic bilayers has also been probed. Various experimental techniques, such as small angle x-ray scattering (SAXS), polarising optical microscopy (POM), cryogenic scanning electron microscopy (cryo-SEM) and differential scanning calorimetry (DSC), are used to probe the structure of different phases and the underlying interactions.

In chapter 1 we give a brief introduction to amphiphilic molecules and principles of their self-assembly[1]. Then we present a short description of the phase behaviour of amphiphile-water systems[2]. We provide an outline of relevant interactions present in systems probed in this study. We also describe the basic principles of experimental techniques, such as x-ray scattering, polarising optical microscopy and cryo-SEM. SAXS data modelling for the determination of various structures observed in our systems is also discussed.

In chapter 2 we describe the structural polymorphism of surfactant-DNA complexes. Double stranded DNA, which has a persistence length of about 50 nm[3], acquires a negative charge in an aqueous solution due to dissociation. Single chain cationic surfactants form complexes with DNA, which have two dimensional crystalline order[4–6]. Structures of complexes of DNA with alkyltrimethylammonium bromide ($C_nTAB$) surfactants, with n varying from 8 to 18 have been studied. Depending on the chain length of the surfactant (n) and the ratio of surfactant to DNA base concentration (R) a variety of columnar structures, such as hexagonal (H), square (S), super hexagonal ($H_s$) are observed. SAXS patterns from different structures have been collected and the data analysed (fig. 1). Electron density maps are constructed from the diffraction data (fig. 2, fig. 3). Composition of some complexes has been determined using elemental analysis.These results indicate the important role played by the surfactant chain length in determining the structure of surfactant-DNA complexes.

In chapter 3 we describe the effect of sodium salt of poly acrylic acid (PAANa) on the phase behaviour of didodecyldimethyl ammonium chloride (DDAC), didodecyldimethyl ammonium bromide (DDAB) and dioctadecyldimethyl ammonium chloride (DOAC) bilayers. SAXS, Cryo-SEM, thermogravimetric analysis (TGA) and POM techniques are used to identify the various phases exhibited by these systems. Concentration and molecular weight of the polyelectrolyte, water content of the solution and salt concentration are varied for studying the phase behaviour. Previous studies have shown a lamellar ($L_\alpha^1$) $\rightarrow$sponge ($L_3$) $\rightarrow$lamellar ($L_\alpha^2$) transition in DDAB-PAANa

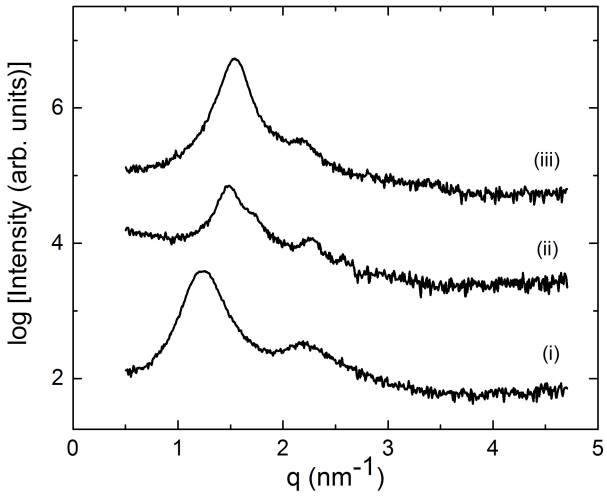


FIGURE 1: SAXS patterns of $C_nTAB - DNA$ complexes in water. (i) H phase in $C_{18}TAB$-DNA complex. (ii) $H_s$ and (iii) S phase in $C_{12}TAB$-DNA complexes.

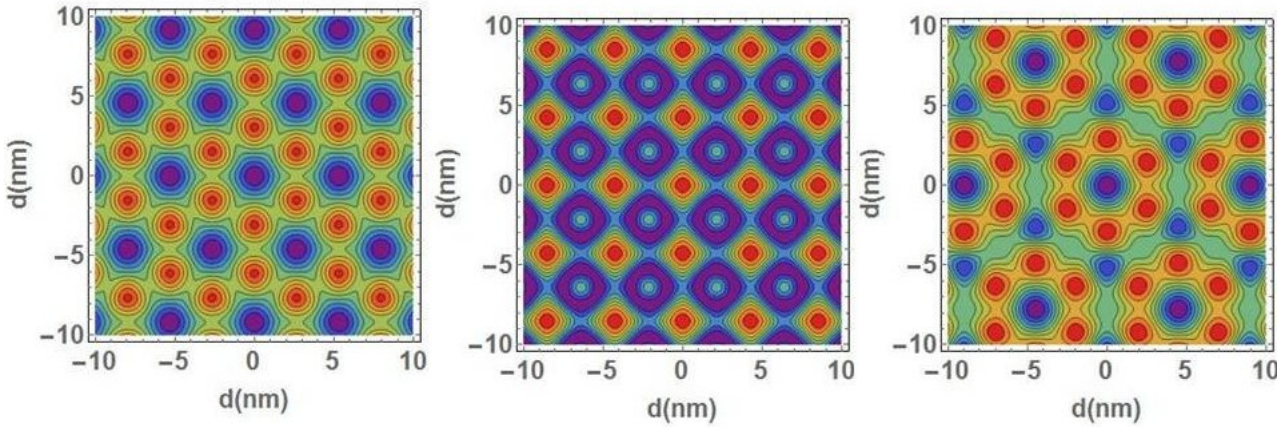


FIGURE 2: Electron density maps of H (left), S (middle) and $H_s$ (right) phases constructed from SAXS data.

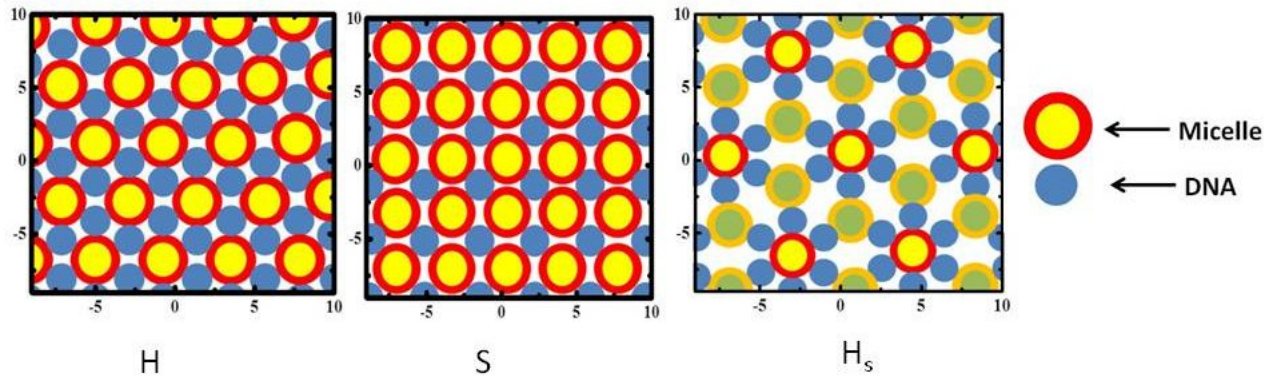


FIGURE 3: Schematics of different structures suggested by the electron density maps.

complexes for PAANa of low molecular weight on decreasing the water content[7]. The sponge phase consists of a disordered network of surfactant bilayers, whereas the lamellar phase is made

up of a periodic stack of bilayers. The $L_\alpha^2$ phase has a slightly lower d-spacing compared to the $L_\alpha^1$ phase. In the case of DDAC, on adsorption of polyelectrolyte of low molecular weight, a collapsed( $L_\alpha^{c1}$ )→swollen($L_\alpha$) →collapsed($L_\alpha^{c2}$) phase sequence is observed on decreasing the water content [8]. We have determined the composition of different phases using thermogravimetric analysis (TGA), which shows the presence of polyelectrolyte in the $L_\alpha^{c1}$ phase but not in the $L_\alpha^{c2}$ phase. A partial phase diagram is also constructed in $\phi$ vs salt concentration plane ($\phi$=$\frac{weight_{DDAC}}{(weight_{DDAC}+weight_{PAANa})}$). The swollen phase ($L_\alpha$) is not found for PAANa of higher molecular weight. The phase behaviour of DOAC-PAANa system is very similar to that of DDAC-PAANa system.

In chapter 4 we discuss the effect of salt on the swelling behaviour of a lamellar phase made of charged membranes at low and intermediate salt concentrations (up to 1M). SAXS, POM and cryo-SEM techniques are used to probe this system. Surfactants such as didodecyldimethylammonium chloride (DDAC), didodecyldimethylammonium bromide (DDAB) and lipids like 1,2-dipalmitoyl-3-trimethylammonium-propane (chloride salt) (DMTAP) are used in the study. Effect of LiCl, NaCl, KCl and CsCl is studied on the swelling behaviour of the lamellar phase of DDAC and DMTAP bilayers while the effect of LiBr, NaBr, KBr and CsBr is studied on the swelling behaviour of the lamellar phase DDAB bilayers. At very low salt concentrations the lamellar phase of charged membranes is stabilized by inter membrane electrostatic repulsion [1]. In the case of highly flexible surfactant membranes, on increasing the salt concentration the system goes from electrostatically stabilized to undulation stabilized lamellar phase [9].Beyond a threshold salt concentrations a collapsed lamellar phase is found whose d-spacing is comparable to the bilayer thickness. In the case of charged lipids, the bending rigidity of the membrane is an order of magnitude higher, and the d-spacing decreases monotonically with increasing salt concentration (fig. 4). We show that these observations can be qualitatively understood in terms of the DLVO (named after Derjaguin, Landau, Verwey and Overbeek) theory of colloidal stability [1].

In chapter 5 we study the effect of salt on the lamellar phase of charged lipids and surfactants in the high salt regime. On increasing the concentration of NaCl and LiCl the d-spacing increases above a threshold concentration for DDAC bilayers but does not change at high concentrations of KCl and CsCl (fig. 5). Similar effect is observed at high concentrations of LiBr, NaBr, KBr and CsBr on DDAB. For LiBr and NaBr the d-spacing increases but it does not change for KBr and CsBr. At the high concentrations of NaBr and LiBr, an optically isotropic phase is observed in the case of DDAB. SAXS data is consistent with the optically isotropic phase being made up of bilayers. The effect of salt on DMTAP is found to be analogous to that on DDAC, with the only difference being that the value of threshold salt concentration, at which the d-spacing starts to increase, is lower than that for DDAC. Earlier studies have shown that the electrostatic screening length increases with increasing salt concentration in concentrated electrolytes [10]. From our study we observe the increase in d-spacing in the high salt regime depends on the nature of the salt. Further work needs to be done in order to understand the origin and ion-specificity of this behaviour.

In chapter 6 we study the effect of pH on the phase behaviour of 1,2-dimyristoyl-sn-glycero-3-phosphocholine (DMPC) and 1,2-dilauroyl-sn-glycero-3-phosphocholine (DLPC) bilayers. SAXS, WAXS, DSC and POM techniques are used to probe their phase behaviour. DMPC bilayers form three lamellar phases in water; the fluid phase above the main-transition temperature ($T_m$), the tilted gel phase below the pre-transition temperature ($T_p$) and the ripple phase in between [11]. $T_m$ and $T_p$ are about 24°C and 14°C, respectively. Phase behaviour of DMPC at pH=4 and pH=3

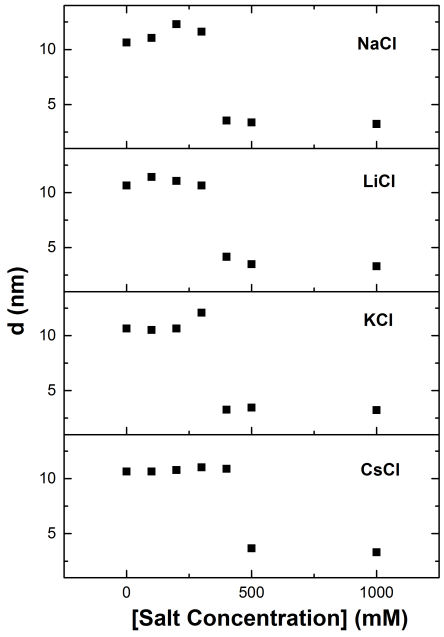


FIGURE 4: Variation of the periodicity (d) of the lamellar phase of DDAC bilayers with salt concentration. The surfactant concentration is 20 wt%. The d-spacing does not change appreciably until a salt concentration of around 300 mM. At a salt concentration of about 400 mM the d-spacing rather abruptly reduces to about 3.2 nm. In the case of CsCl the abrupt decrease in d takes place at a slightly higher concentration.

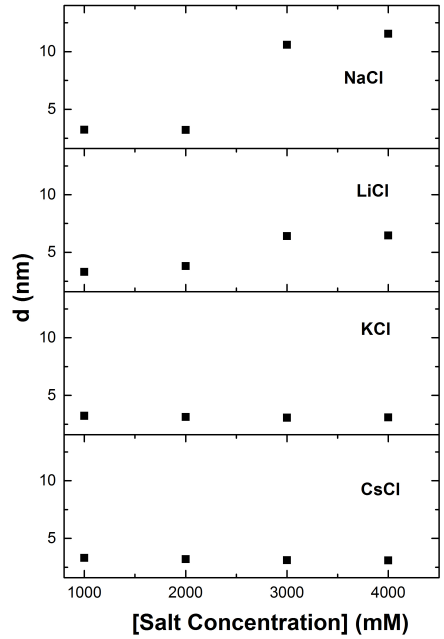


FIGURE 5: Variation of the d-spacing of the lamellar phase of DDAC bilyers with salt concentration in the high-salt regime. Notice that only for NaCl and LiCl the d-spacing increases after a threshold but not for KCl and CsCl.

remains identical to the phase behaviour in water[12]. At lower pH (pH=2 and pH=1) the main-transition temperature increases and the pre transition disappears . The d-spacing in the gel phase is found to be very large, which indicates the charging of bilayers at lower pH (fig. 6). Formation of an untilted gel phase shows the dehydration of the lipid head group at lower pH. After a few days of incubation we notice the formation of DMPC crystallites at low temperatures and the inverted hexagonal phase at high temperatures. Formation of these phases can also be attributed to the de-hydration of the head groups of DMPC molecules. The effect of pH on DLPC bilayers is found to be very similar to that on DMPC bilayers.

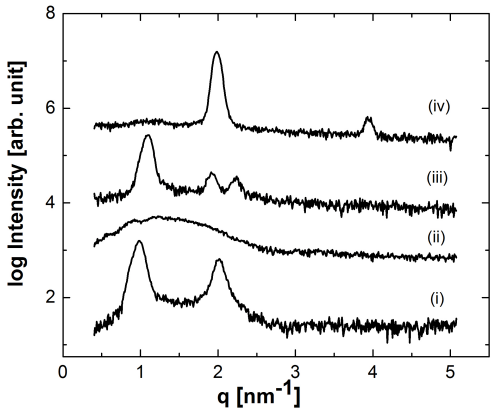


FIGURE 6: SAXS patterns of different phases of DMPC dispersions in HCl solutions of varying pH. (i) A fluid lamellar phase of 6.2 nm periodicity at pH=4, very similar to that seen in the DMPC-water system. (ii) a swollen lamellar gel phase at pH=2, with a periodicity of about 20 nm. (iii) an inverted hexagonal phase at pH=2 with lattice parameter of 6.9 nm. (iv) Crystalline phase observed after a few days of incubation at pH = 1 and 2.

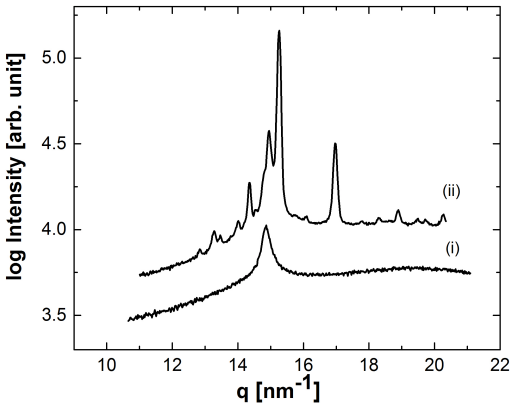


FIGURE 7: WAXS patterns of DMPC dispersions at pH=1. (i) A single sharp peak is observed at room temperature after incubation for 1 day indicating the formation of a non-tilted gel phase. (ii) many peaks are found after incubating the sample for a week. The appearance of multiple peaks in the WAXS pattern can be attributed to the formation of crystallites as a consequence of the de-hydration of the lipid head groups.

In chapter 7 we summarize the main results of the thesis and discuss some directions for future studies.

# Bibliography

[1] Israelachvili JN. Intermolecular and surface forces. Academic press; 2015.

[2] Lombardo D, Kiselev MA, Magazù S, Calandra P. Amphiphiles self-assembly: basic concepts and future perspectives of supramolecular approaches. Adv Condens Matter Phys. 2015;2015:1-22.

[3] Anderson CF, Record Jr MT. Polyelectrolyte theories and their applications to DNA. Ann Rev Phys Chem. 1982;33(1):191-222.

[4] Krishnaswamy R, Pabst G, Rappolt M, Raghunathan V, Sood A. Structure of DNA-CTAB-hexanol complexes. Phys Rev E. 2006;73(3):031904.

[5] Madhukar S. Influence of some sterols and nucleotides on the structure of self-assembled amphiphilic systems. PhD Thesis, Jawaharlal Nehru University, New Delhi. 2017:45-60.

[6] Thomas M. Surfactant-Polyelectrolyte Complexes: Structure and Interactions. PhD Thesis, Jawaharlal Nehru University, New Delhi. 2019:108-16.

[7] Gupta SP, Thomas M, Chowdhury A, Raghunathan V. Effect of adsorbed polyelectrolytes on the interactions and elasticity of charged surfactant bilayers. J Phys: Condens Matter. 2020;32(19):194004.

[8] Thomas M, Swamynathan K, Raghunathan V. Salt-induced swelling transitions of a lamellar amphiphile—Polyelectrolyte complex. J Chem Phys. 2019;150(9):094903.

[9] Roux D, Nallet F, Freyssingeas E, Porte G, Bassereau P, Skouri M, et al. Excess area in fluctuating-membrane systems. Europhys Lett. 1992;17(7):575.

[10] Smith AM, Lee AA, Perkin S. The electrostatic screening length in concentrated electrolytes increases with concentration. J Phys Chem Lett. 2016;7(12):2157-63.

[11] Nagle JF, Cognet P, Dupuy FG, Tristram-Nagle S. Structure of gel phase DPPC determined by X-ray diffraction. Chem Phys Lipids. 2019;218:168-77.

[12] Chowdhury A, Sasidharan S, Xavier P, Viswanath P, Raghunathan V. Effect of pH on the phase behavior of DMPC bilayers. Biochim Biophys Acta. 2021;1863(11):183695.

Signature of the Student

Signature of the Supervisor

Signature of the Co-Supervisor

## List of publications related to studies presented in this thesis

- "Effect of pH on the phase behaviour of DMPC bilayers", **Anindya Chowdhury**, Sreeja Sasidharan, Pinchu Xavier, P. Viswasnath and V A Ragunathan, BBA-Biomembranes (2021), 1863,183695.

- "Columnar liquid crystalline phases of surfactant-DNA complexes", Meera Thomas, **Anindya Chowdhury**, Amit K. Majhi and V. A. Raghunathan, Liquid Crystals (2021), 1-10.

- "Effect of adsorbed polyelectrolyte on the interactions and elasticity of the charged surfactant bilayers", Santosh Kumar Gupta, Meera Thomas, **Anindya Chowdhury**, V A Raghunathan, J.Phys : Condens. Matter (2020) 32,194004.

- "Influence of micellar size on the structure of surfactant-DNA complexes", A. V. Radhakrishnan, S. Madhukar, **A. Chowdhury**, V. A. Raghunathan , Phys. Rev. E (2022), 105, 064504.

# Contents

# List of Figures

# List of Tables

# Chapter 1

# Introduction

In this thesis we study the structure, phase behaviour and polymorphism of different self-assembled aggregates of ionic amphiphilic molecules in the presence of polyelectrolytes and salt. In addition, the influence of pH on the phase behaviour of zwitterionic bilayers has also been probed. Various experimental techniques, such as small angle x-ray scattering (SAXS), polarising optical microscopy (POM), cryogenic scanning electron microscopy (cryo-SEM) and differential scanning calorimetry (DSC), are used to probe the structure of different phases and the underlying interactions. This chapter provides a brief introduction to the different systems studied and experimental techniques employed.

## 1.1 Amphiphiles

An amphiphile is a molecule that consists of two parts, one part is soluble in a particular fluid and the other is not. If the fluid is water then the soluble part is called hydrophilic or the head group and the insoluble part is called hydrophobic or the tail as it ususally is a hydrocarbon chain. Surfactants, lipids, block co-polymers and cholesterol are typical examples of amphiphiles[1–4]. Depending on the nature of their head group amphiphiles can be separated into diffrent groups; ionic, non-ionic and zwitterionic. An ionic ammphiphile is one which acquires a charge in water because of the dissociation of its headgroup (e.g. Sodium dodecyl sulphate (SDS), Cetyltrimythylammonium bromide (CTAB)). A zwitterionc amhiphile will have a dipole moment in the aqueous solution, but no net charge(1,2-dimyristoyl-sn-glycero-3-phosphocholine (DMPC)).

## 1.2 The Hydrophobic effect

Water is a polar molecule. It can create inter molecular hydrogen bonds. Any non-polar molecule such as a hydrocarbon or fluorocarbon cannot create hydrogen bonds in water. When such a non polar molecule is placed in water, water molecules form a cavity to accommodate it. A water molecule in liquid state forms 3 to 3.5 hydrogen bonds on an average with neighbouring molecules, but in the presence of any non polar solute the co-ordination number increases to around 4. Hence the entropy reduces. When many such molecules are present in water, the entropy loss becomes very large and therefore the net change in the free energy becomes positive. For this reason the solubility of non polar molecules in water is very low and this phenomenon is called the hydrophobic effect[1–5], Hydrophobic effect is very important in soft matter systems, especially for the self assembly of amphiphilic molecules.

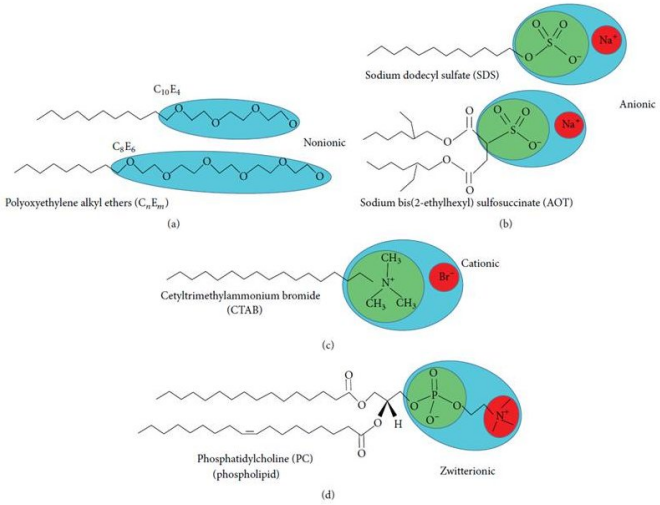


FIGURE 1.1: Examples of (a) nonionic , (b) and (c) ionic, (d) zwitterionic amphiphiles. Figure is taken from [4] .

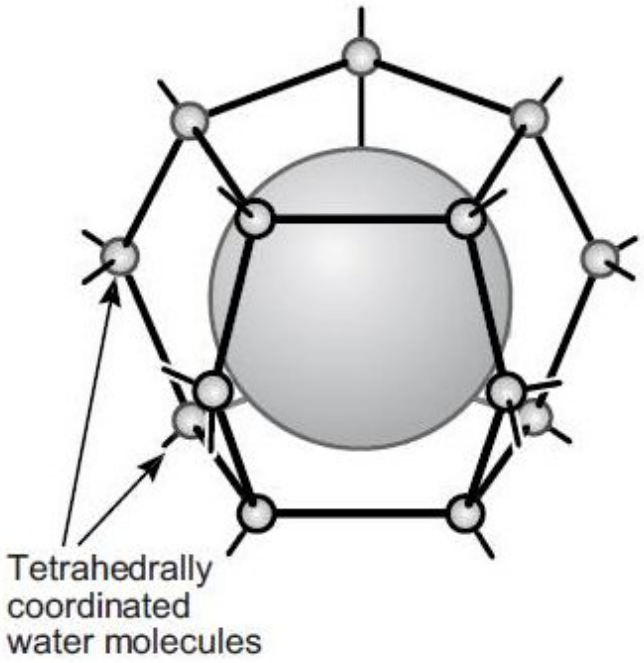


FIGURE 1.2: Cage-like structure formed by water molecules around a non-polar molecule. Schematic is taken from [1]

## 1.3 Self-assembly of amphiphiles

Amphiphiles are dispersed in water at very low concentrations, due to their translational entropy. At comparatively higher concentrations these molecules self assembles into a variety of structures. These structures are called micelles. The concentration above which the process of self assembly occurs is called the critical micellar concetration (CMC). Let us consider an aggregate of size N, where N is the aggregation number, i.e., the number of amphiphiles molecules in the aggregate. The chemical potential of each monomer in such an aggregate can be written as, [1]

$$\mu_N = \mu_N^0 + \frac{k_B T}{N} log \frac{x_N}{N} \tag{1.1}$$

$k_B$ is Boltzmann's constant. $\mu_N^0$ is the reference chemical potential. The second term arises from the entropy of mixing. Now we consider a dilute solution of micelles of varying size. $x_N$ is the concentration of the molecules in aggregates of size N. In equilibrium the chemical potential per monomer will be the same in each aggregate. Thus,

$$\mu_1^0 + \frac{k_B T}{1} log \frac{x_1}{1} = \mu_2^0 + \frac{k_B T}{2} log \frac{x_2}{2} = ..... = \mu_N^0 + \frac{k_B T}{N} log \frac{x_N}{N} \tag{1.2}$$

Solving this equation, we get

$$\frac{x_N}{N} = x_1 exp[\frac{(\mu_1^0 - \mu_N^0)}{k_B T}] \tag{1.3}$$

$$\frac{x_N}{N} = x_1 exp^{\alpha} \tag{1.4}$$

where,

$$\alpha = \frac{(\mu_1^0 - \mu_N^0)}{k_B T} \tag{1.5}$$

$x_1$ is the concentration of the monomers and the total concentration of amphiphiles in solution is give by $x = \sum_N x_N$. The aggregation process depends crucially on the sign of alpha. If it is negative, $x_N$ remains small for all values of x. On the other hand aggregation will occur beyond a threshold values of x, if alpha is positive, as shown below. When $x_1$ is small, $x_N$ also remains small. When $x_1$ reaches a critical value $(x_1)_{critical} \sim exp[-\alpha]$, $x_N$ starts to grow and self-assembly begins. This concentration of monomers $(x_1)_{critical}$ is defined as the CMC. It is also equal to the total concentration of the amphiphile in the solution, since the concentration of aggregates is negligible at this stage. Below CMC the amphiphiles are dispersed as monomers and above CMC there is a co-existence of monomers and micelles. CMC depends on factors, such as the pH, temperature, pressure and the chemical structure of the amphiphiles[6]. The CMC for ionic amphiphilcs is typically of the order of $10^{-3}$-$10^{-2}$ M, for non-ionic amphiphiles it is around $10^{-5}$-$10^{-4}$ M, and for lipids it is around $10^{-9}$M. The reason for such low CMC for lipids is the large hydrophobc effect created by the two hydrocarbon chains. Experimentally CMC can be determined by measuring physical properties of the solution, such as surface tension, equivalent conductivity and osmotic pressure[6,7].

Amphiphilc molecules in water above CMC form micelles. Shape of the micelles can be spherical, cylindrical or bilayer. Shape of the aggregates is governed by the geometry of the molecule. Based on the geometry of the molecule we can define a quantity called the critical packing parameter $C_{pp}$.

$$C_{pp} = \frac{v}{a_0 l_c} \tag{1.6}$$

Where v is the volume of the hydrocarbon chain, $l_c$ is the chain length and $a_0$, the optimal head group area, which is determined by interactions in the system. For spherical micelles $C_{pp} \leq 1/3$, if $1/3 \leq C_{pp} \leq 1/2$, then cylindrical micelles are preferred. If $C_{pp} \sim 1$, bilayers are formed. For amphiphiles having very small head group area usually inverted micelles are formed[1,3,4].

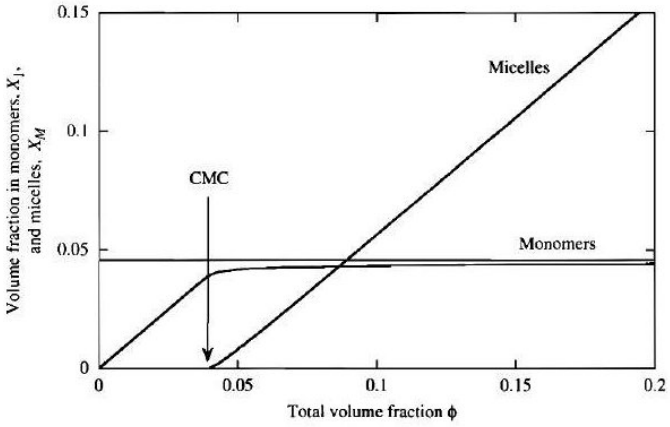


FIGURE 1.3: Monomer and micelle volume fractions vs total volume fraction of the amphiphile in the aqueous solution. After CMC the micelle concentration starts to increase. figure is taken from [3]

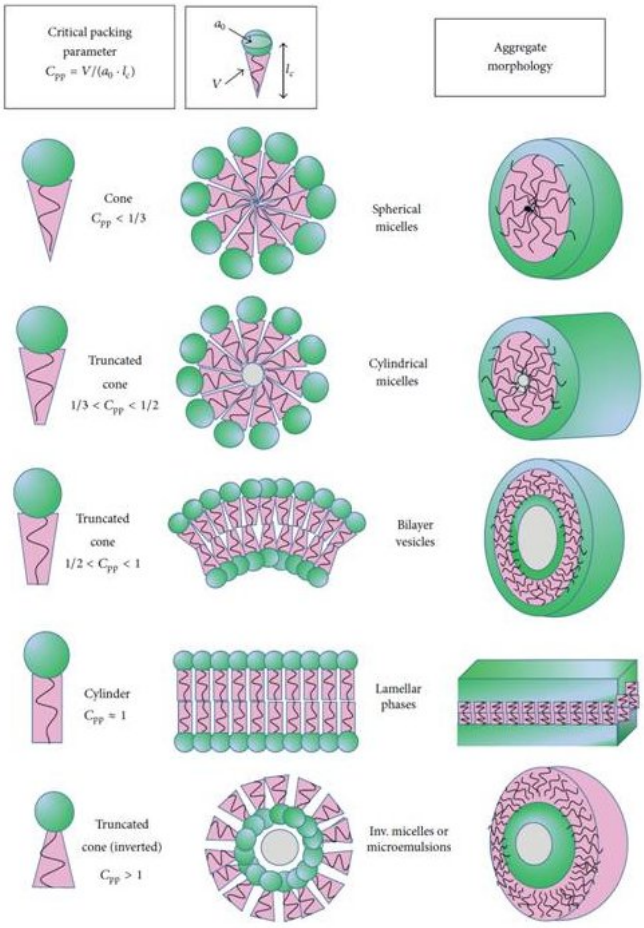


FIGURE 1.4: Different morphologies of amphiphile aggregates based on $C_{pp}$ , taken from [4]

### 1.3.1 Phase behaviour of self-assembled structures of amphiphiles in water

Amphihilic molecules below CMC remain as monomers. Above CMC they start to self-assemble. Just above CMC usually they form spherical micelles, which remain dispersed in water forming an isotropic solution. On increasing the concentration a sphere to rod transformation of the

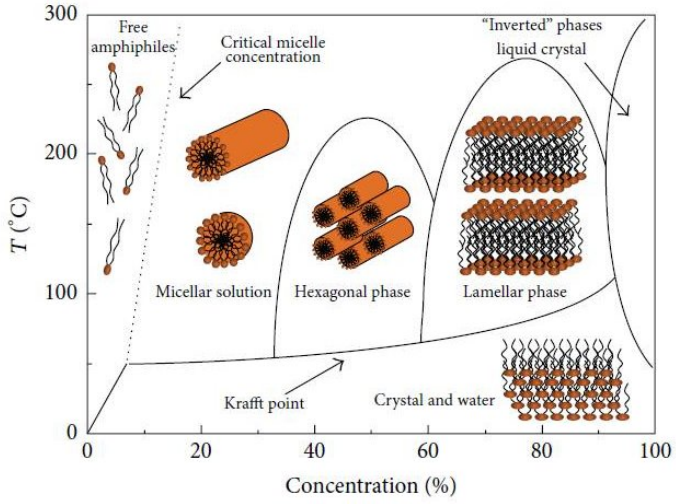


FIGURE 1.5: A typical phase diagram of an amphiphile-water system. Taken from [4]

micellar shape occurs. With increasing concentration a hexagonal phase of cylindrical micelles is observed. As we increase the concentration further the cylindrical micelles transform into bilayers, which form a lamellar phase. At even higher concentration of amphiphiles the inverted phases are formed. The amphiphiles crystallize out of the solution below the Kraft temperature, hence self-assembly can occur only at higher temperatures. [1].

## 1.4 Polyelectrolytes

Polyelectrolytes are polymers in which each or some of the monomers contains an ionizable group, which dissociates in water making the polymer charged. Like acids polymers also can be divided into weak and strong, depending on their ability to ionise in water. Strong polyelectrolytes get completely dissociated in water. A weak polyelectrolyte does not get fully charged in water, it has a dissociation constant associated with it. This dissociation constant can be altered based on the pH of the solution, ionic sterngth etc. Many polyelectrolytes have biological origin such as DNA, RNA etc. If the charge density on the polymer becomes high, then the electrostatic interaction dominates. In that case a fraction of the counter ions stays near the polyelectrolyte. This is called counter-ion condensation [8]. If we consider the polyelectrolyte to be an infinite long, charged straight line, then the electrostatic potential at a distance r varies as a function of ln r. The entropy associated with the counterions also varies proportional to ln r. As both the terms contributing to the free energy vary as ln r, at a given distance r one of these terms dominates. Hence, the phenomenon of counterion condensation can be seen as a competition between entropy and electrostatic energy [9]. Bjerrum length is the characteristic length at which electrostatic interaction between two unit charges is equal to the thermal energy ( $l_b = e^2/\epsilon_0 k_B T$ ). For water at room temperature the value is 0.70 nm [10]. Counterion condensation takes place when the separation between the charged groups along the polymer backbone is less than $l_b$. The persistence length ($l_p$) is a measure of polymer flexibility. It is the distance over which the orientations of two segments along the polymer chain are correlated [11]. If we take two points along the polymer chain separated by a distance l, and if $\theta$ is the angle between the tangents to the polymer backbone at these points, then it can be shown that $< cos\theta >= exp(-l/l_p)$. For double stranded DNA the

value of persistence length is about 50 nm[12]. Salt is a key factor that determines the flexibility of polyelectrolytes. At low salt concentration, the charges on the polymer remains unscreened. The chains remain in an extended configuration. As salt concentration of the solution is increased, the Debye length decreases[1]. As the Debye length becomes smaller, the flexibility increases[13].

## 1.5 Interaction Forces

In this section we briefly discuss some of the inter particle interactions relevant to the soft matter systems studied in this thesis.

### 1.5.1 Van der Waals interaction

Van der Waals interaction is a distance dependent interaction between two atoms or molecules. Van der Waals interaction arises from three sources : dipole-dipole interaction, dipole- induced dipole interaction and dispersion interaction[1]. Among these the third one is purely quantum mechanical in origin. At any given moment if the centers of positive and negative charges in a molecule do not coincide,that will give rise to a instantaneous dipole moment. Even though the time average of this dipole moment may be zero, the instantaneous dipole moment can induce a dipole moment in the neighbouring molecule, resulting in an attracting force between the molecules. Between two molecules it is weak and diminishes as $1/r^6$ with distance. But due to the additive nature of this interaction it is comparatively large between two macroscopic bodies. For two parallel surfaces separated by a distance D, the interaction energy per unit area is

$$W(D) = \frac{-A}{12\pi D^2} \tag{1.7}$$

Where A is the Hamaker constant, which is a function of the dielectric permittivities of the interacting particles and medium in between. It can be either positive or negative. It is always positive for two like surfaces interacting through any other medium[1]. Hence in these cases van der Waals force is always attractive.

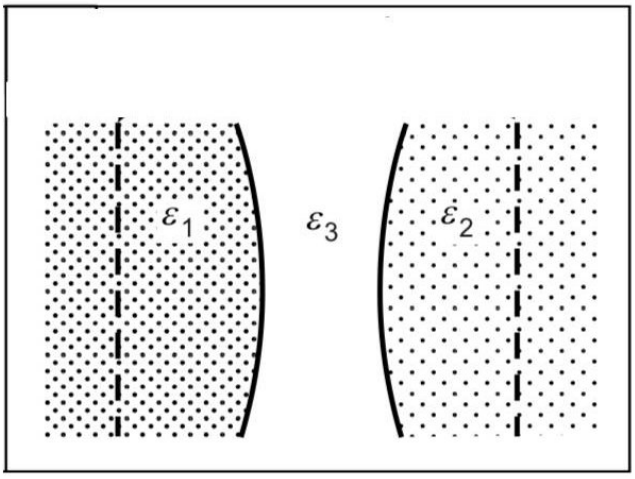


FIGURE 1.6: Schematic for presenting van der Waals interaction between two dissimilar media. Taken from[1]

### 1.5.2 Electrostatic interaction

As mentioned above the van der Waals force between two particles in a medium is always attractive. If van der Waals force was acting alone on the particles dissolved in a solution, then we can expect them to coagulate and precipitate out of the solution. One of the reasons that prevents it is the electrostatic repulsive force. If we imagine a bilayer made up of a cationic surfactant such as didodecyldimethyl ammonium bromide (DDAC), it releases $Cl^{-1}$ ion (counterion) in water and the surface of the bilayer remains positively charged. Some of these counterions bind strongly to the surface forming the Stern layer, while others form an atmosphere of ions near the surface, called the diffuse electric double layer[(1)].

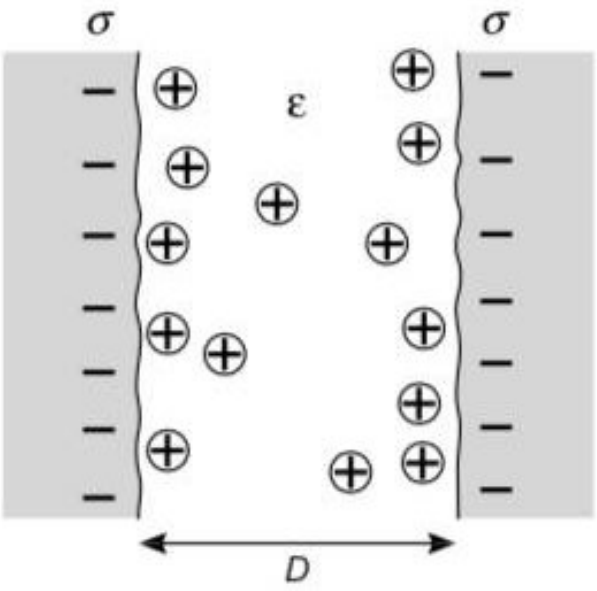


FIGURE 1.7: Schematic of two charged surfaces in water. Taken from[(1)]

The chemical potential of a counterion at any point in the solution is given by,

$$\mu = ze\psi + k_B T log\rho \tag{1.8}$$

Here $\psi$ is the electrostatic potential, $\rho$ is the number density of counterions of valency z at that point x between the surfaces. At equilibrium the chemical potential will be same everywhere in the solution. Using this condition we obtain the counterion density at any point x as,

$$\rho = \rho_0 exp(-ze\psi/k_B T) \tag{1.9}$$

Where $\rho = \rho_0$ is the counterion density at the mid plane between the surfaces (x=0) where $\psi$ is taken to be 0. Hence the Poisson's equation can be written as

$$\frac{d^2\psi}{dx^2} = \frac{-ze\rho_0}{\epsilon\epsilon_0} exp(\frac{-ze\psi}{kT}) \tag{1.10}$$

This is known as the Poisson-Boltzmann eqn. The solution of this equation is given by,

$$\psi(x) = \frac{kT}{ze} ln\ cos^2(Mx) \tag{1.11}$$

Where

$$M^2 = \frac{(ze)^2\rho_0}{2\epsilon\epsilon_0 kT} \tag{1.12}$$

In the presence of salt the PB equation gets modified as,

$$\frac{d^2\psi}{dx^2} = \sum_i \frac{-z_i e\rho_0^i}{\epsilon\epsilon_0} exp(\frac{-z_i e\psi}{kT}) \tag{1.13}$$

For small $\psi$ we can write,

$$\frac{d^2\psi}{dx^2} = \sum_i \frac{-z_i e\rho_0^i}{\epsilon\epsilon_0}(1 - \frac{z_i e\psi}{kT}) \tag{1.14}$$

Under valid boundary condition the solution of this equation is,

$$\psi = \psi_0\, exp(-\kappa x) \tag{1.15}$$

where, $\kappa^{-1}$ is called the Debye screening length and is given by,

$$\kappa = \sqrt{\frac{2e^2\rho_0 z_i^2}{\epsilon\epsilon_0 kT}} \tag{1.16}$$

AS the salt concentration in the solution increases, the Debye length decreases. For monovalent salts it is given by,

$$\kappa = \frac{0.304}{\sqrt{C}} \tag{1.17}$$

Where C is the molar concentration of the salt. The electric double layer interaction free energy per unit area between two planar surfaces held at a constant potential and separated by a distance D is,

$$W(D) = \frac{64kT\rho_0}{\kappa} tanh^2(\frac{e\psi_0}{4kT})\kappa\, exp^{-\kappa D} \tag{1.18}$$

### 1.5.3 Undulation interaction

Flexible membranes whose bending rigidity is of the order of $k_B$T show pronounced thermal fluctuations. A single membrane can fluctuate freely. But when two such membranes are brought closer, they tend to suppress each others out of plane fluctuations. This causes a reduction in the entropy of the membrane system. This leads to a repulsion between the bilayers, which tends to push them away. This long range repulsion is called Helfric interaction, which is a function of membrane bending rigidity[1,14,15] The magnitude of this interaction between two fluctuating membranes, separated by a distance D is given by

$$W(D) = \frac{3\pi^2(kT)^2}{128\kappa D^2} \tag{1.19}$$

Where $\kappa$ is the bending modulus of the membrane, and T is the temperature. Bending rigidity of a membrane depends on its surface charge density, since the repulsion between the charged

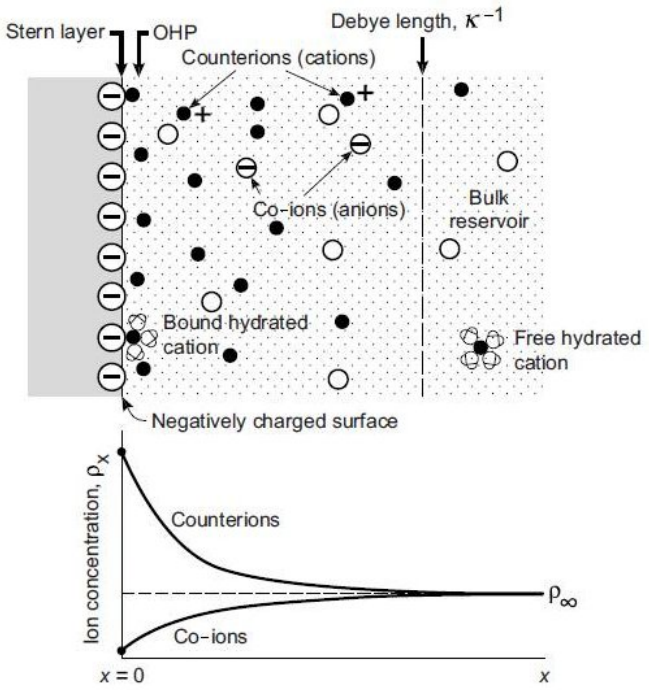


FIGURE 1.8: Schematic of distribution of co-ions and counter ions near a charged surface. The bottom plot gives the charge densities as function of distance from the surface. Taken from [1]

headgroups gives a positive contribution to $\kappa$ [11]. Therefore charged bilayers in water (for example DDAC) remains rigid and flat. But upon addition of salt the charges on the bilayer get screened and the electrostatic contribution of the bending rigidity is reduced [11].

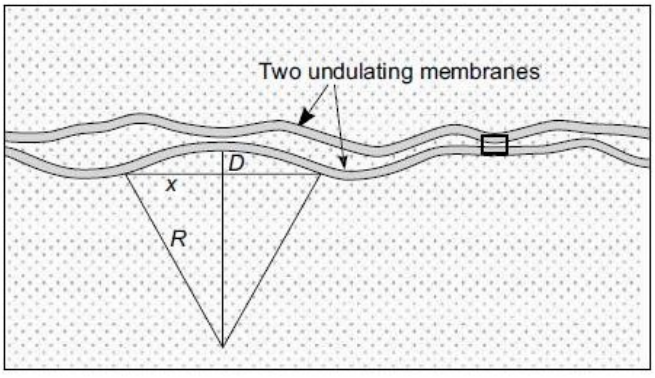


FIGURE 1.9: Schematic of thermally undulating bilayers. [1]

### 1.5.4 Hydration repulsion

Along with Van der Waals attraction and electrostatic repulsion, there is a short range repulsion in the case of lipid bilayers, arising from the ordering of the water molecules around the polar head group. This repulsion is called hydration repulsion [1,16]. This force dominates when separation between the bilayers is less than 2 nm. Physical origin of this force can be viewed as the work

needed to remove water molecules from the polar head groups, as two surfaces come close to each other[17]. Mathematically the potential can be written as[18],

$$V_H(l) = P_H \lambda_H e^{-\frac{l}{\lambda_H}} \tag{1.20}$$

where, $P_H$ is the hydration pressure and $\lambda_H$ is the characteristic decay length, which is around 0.2 nm-0.3 nm. $\lambda_H$ for different lipids are given in[19].

## 1.6 Experimental techniques

In this section we discuss the basic principles of the different experimental techniques employed in this study.

### 1.6.1 Principles of x-ray diffraction

X-rays are electromagnetic waves. The wavelength of x-rays varies from 0.1 nm to 10 nm. X-rays get scattered by the electrons present in the material and hence the scattered intensity depends on the electron density of the material[20,21]. In this section we will discuss the theory of x-ray diffraction briefly.

Let us consider an incident wave

$$\phi_{inc} = \phi_0 e^{(i\vec{K}_0.\vec{r})} \tag{1.21}$$

falling on a scatterer situated at the origin. As scattered wave is spherical then at a sufficiently large distance R the scattered wave can be written as,

$$\phi_{sc} = \frac{\phi_0 a}{R} e^{(i\vec{K}_0.\vec{R})} \tag{1.22}$$

Where a is the scattering length, determining the strength of the scattering. If the scatterer is not at the origin, but at some distance $\vec{r}$,then we have to introduce a phase factor $(\vec{K}_1 - \vec{K}_0).\vec{r}$, in order to take care of the path differences of incident and scattered waves (fig. 1.10). Now we introduce a new a vector $\vec{q} = \vec{K}_1 - \vec{K}_0$. If we assume $R >> r$, then the scattered wave can be written as

$$\phi_{sc} = \frac{\phi_0 a}{R} e^{i(\vec{K}_0.\vec{R} - \vec{q}.\vec{r})} \tag{1.23}$$

For an assembly of N point scatters situated at different positions $r_i$ $(i = 1, 2, 3, ....N)$ the above equation looks like,

$$\phi_{sc} = \frac{\phi_0 a}{R} e^{i(\vec{K}_0.\vec{R})} \sum_{i=1}^{N} e^{-i(\vec{q}.\vec{r}_i)} \tag{1.24}$$

The above equation can be written as Fourier transform of a density function $\rho(\vec{r}) = \delta(\vec{r} - \vec{r}_i)$.Hence,

$$\phi_{sc} = \frac{\phi_0 a}{R} e^{i(\vec{K}_0.\vec{R})} \int \rho(\vec{r}) e^{-i(\vec{q}.\vec{r})} d\vec{r} \tag{1.25}$$

The intensity of the scattered radiation is given by,

$$I(q) = |\phi_{sc}|^2 = |\frac{\phi_0 a}{R} e^{i(\vec{K}_0.\vec{R})} \int \rho(\vec{r}) e^{-i(\vec{q}.\vec{r})} d\vec{r}|^2 \tag{1.26}$$

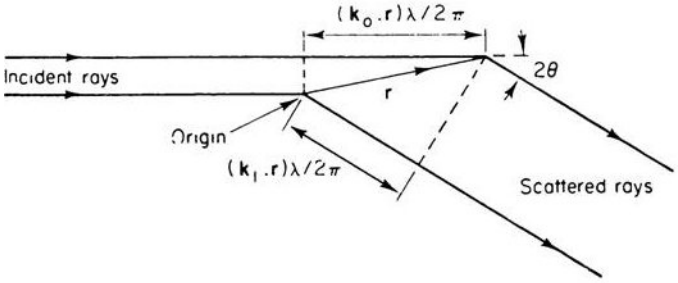


FIGURE 1.10: Schematic of x-ray scattering. The 2 point scatterers are separated by a distance r. Taken from [22]

Electron density of any periodic lattice can be written as the convolution of a lattice function $\rho_l(\vec{r})$ and a basis $\rho_b(\vec{r})$, which describes the electron density of the repeating unit cell.[21,22].

$$\rho(\vec{r}) = \rho_l(\vec{r}) \otimes \rho_b(\vec{r}) \tag{1.27}$$

According to the convolution theorem Fourier transform of the convolution of two functions is the product of their Fourier transform[21,22]. So the Fourier transform of the above equation gives,

$$F(\vec{q}) = f_l(\vec{q}) * f_b(\vec{q}) \tag{1.28}$$

The intensity of the diffraction pattern is given by,

$$I(\vec{q}) = |F(\vec{q})|^2 = S(\vec{q}) * |f_b(\vec{q})|^2 \tag{1.29}$$

$S(\vec{q})$ is called the structure factor and gives information about lattice structure. $f_b(\vec{q})$ is called the form factor and contains information about contents of the unit cell. The observed intensities have to be modified to take into account experimental factors including the detector geometry[23]. The observed intensity should be multiplied by $q^2$ in the case of a 1D detector, for a 2D detector it should be multiplied by q. The polarisation factor, which is given by ,$P \sim \frac{1+Cos^2(2\theta)}{2}$ , will be $\sim 1$, for small angles. Multiple planes can satisfy the Bragg condition simultaneously and hence contribute to the observed intensity. The intensities should be corrected by taking into account this multiplicity factor.

**Construction of electron density maps from SAXS data**

**Electron density of the lamellar phase**

We have used the model described in ref.[24] to find out the electron density profile $\rho(z)$ across the bilayer from the scattering data of the lamellar phase. According to this model $\rho(z)$ can be written in terms of three Gaussians, two for the two head group regions, positioned at $z = \pm z_h$ and one for the bilayer mid-plane. The bilayer centre is taken as z=0 (fig. 1.11). Combining these $\rho(z)$ can be written as,

$$\rho(z) = \rho_{CH_2} + \bar{\rho_h}[exp(-\frac{(z-z_h)^2}{2\sigma_h^2}) + exp(-\frac{(z+z_h)^2}{2\sigma_h^2})] + \bar{\rho_c}[exp(-\frac{z^2}{2{\sigma_c}^2})] \tag{1.30}$$

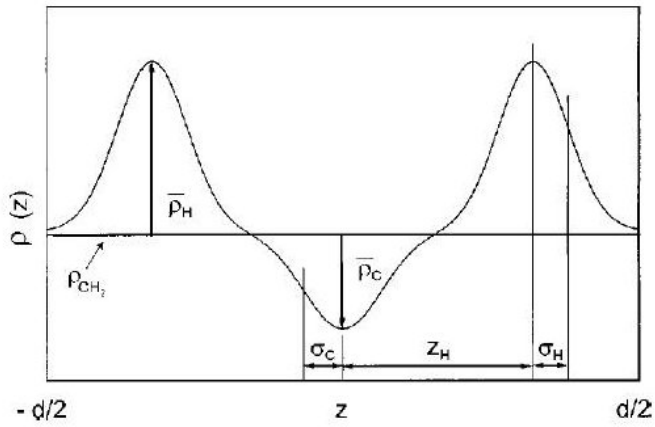


FIGURE 1.11: Electron density profile across the bilayer accoding to the three- Gaussian model. Taken from[24]

where, $\bar{\rho_h}$ and $\bar{\rho_c}$ are the electron densities of head group and hydrocarbon chain regions respectively, with respect to the methylene group ($\rho_{CH_2}$). $\sigma_h$ and $\sigma_c$ are related to the widths of the Gaussians. The form factor (F(q)), which is given by the Fourier transform of the electron density function ($\rho(z)$), can be written as,

$$F(q) = 2\sqrt{2\pi}\sigma_h\bar{\rho_h}exp(-\frac{\sigma_h^2q^2}{2})Cos(qz_h) + \sqrt{2\pi}\sigma_c\bar{\rho_c}exp(-\frac{\sigma_c^2q^2}{2}) \tag{1.31}$$

The structure factor S(q) of the lamellar phase is given by[25],

$$S(q) = N + 2\sum_{k=1}^{N-1}(N-k)Cos(kqd)exp[-(\frac{d}{2\pi})^2q^2\eta\gamma]\pi k^{-(\frac{d}{2\pi})^2q^2\eta} \tag{1.32}$$

Where N is the number of correlated bilayers, $\gamma$ is Euler's constant , d is the lamellar periodicity. $\eta$ depends on the bulk (B) and bending moduli (K) of the lamellar stack, and is given by

$$\eta = \frac{q^2K_BT}{8\pi\sqrt{KB}} \tag{1.33}$$

The magnitude of scattered intensity from a dispersion of bilayers is,

$$I(q) = (S(q)|F(q)|^2 + N_d|F(q)|^2)/q^2 \tag{1.34}$$

$N_d$ is the number of uncorrelated bilayers in the scattering volume. The data was fitted to the above equation by adjusting the fitting parameters ( $\bar{\rho_h}, \bar{\rho_c}, \sigma_h, \sigma_c, N_d, z_h, \eta$).

**Electron density of the hexagonal phase**

In this section we will describe the protocol used to find the electron density map of the two dimensional hexagonal phase. Any point $\vec{r}$ in a lattice can be represented in terms of the primitive lattice vectors $\vec{a_1}$ and $\vec{a_2}$[21],

$$\vec{r} = m\vec{a_1} + n\vec{a_2} \tag{1.35}$$

In the case of 2D hexagonal phase,

$$\vec{a_1} = a\hat{x} \tag{1.36}$$

$$\vec{a_2} = -\frac{a}{2}\hat{x} + \frac{a\sqrt{3}}{2}\hat{y} \tag{1.37}$$

where a is the lattice parameter. Using the orthogonality condition we find,

$$\vec{b_1} = (\frac{4\pi}{a\sqrt{3}})(\frac{\sqrt{3}}{2}\hat{x} + \frac{1}{2}\hat{y}) \tag{1.38}$$

$$\vec{b_2} = \frac{4\pi}{a\sqrt{3}}\hat{y} \tag{1.39}$$

Where $\vec{b_1}$ and $\vec{b_2}$ are the primitive transnational vectors in the reciprocal space. In the case of the 2D hexagonal phase the peak positions are found in the ratio of $1:\sqrt{3}:2:\sqrt{7}:3..$, since we have used a 1D detector for collecting the data, the intensity of each peak, which is obtained from the area under the peak, had to be multiplied by $q^2$ [26–29]. The electron density is obtained by using the equation,

$$\rho_{hk} = \sum_{hk} p_{hk} A(\vec{q}_{hk}) Cos(\vec{q}_{hk}.\vec{r}) \tag{1.40}$$

where, $\vec{q}_{hk}$ is the reciprocal lattice vector, $p_{hk}$ and $A(\vec{q}_{hk})$ are the phase and amplitude of the reflections, respectively. The phases of the reflections can be either +1 or -1, due to the centrosymmetric structure (i.e. $\rho(r) = \rho(-r)$). If n is the number of peaks in the diffraction pattern, a total of $2^{n-1}$ combinations of phases are possible, and electron density maps are obtained corresponding to each of them (fig. 1.12). Based on these maps different models are constructed (fig. 1.13).

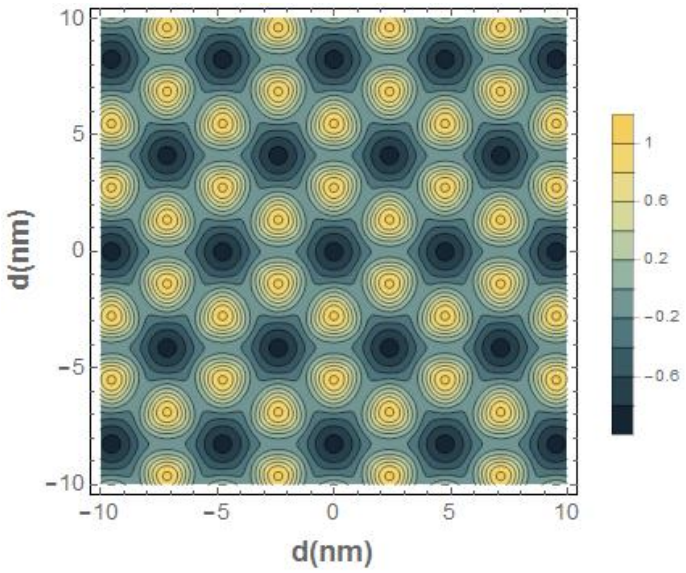


FIGURE 1.12: Electron density map of a hexagonal phase of surfactant-DNA complexes

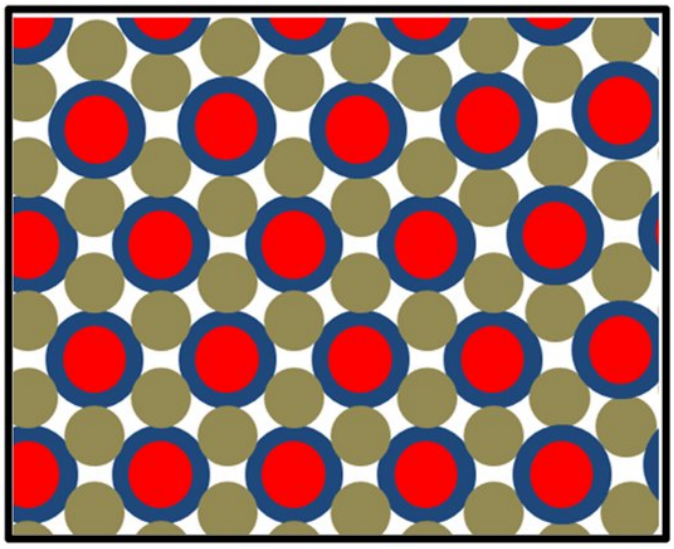

FIGURE 1.13: Schematic based on the map. Red region represents the hydrocarbon part of the micelles, blue part the head group region. The grey circles represent the DNAs.

### 1.6.2 Polarising optical microscopy

Anisotropic liquid crystalline phases show birefringence. Polarising optical microscopy (POM) is a standard technique to identify the different phases shown by liquid crystals[30]. For our study usually the samples were taken in a rectangular capillary and was flame sealed at both the ends to avoid any loss of water. In some cases samples were sandwiched between a coverslip and glass slide. Such samples were studied under crossed polarisers.

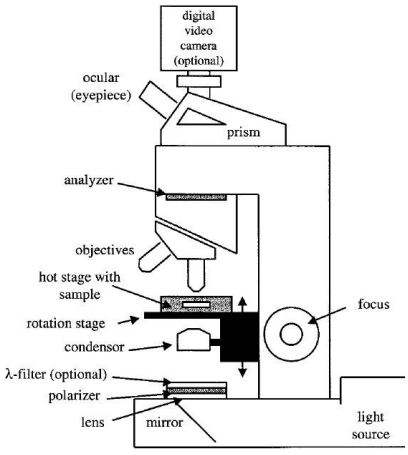


FIGURE 1.14: schematic of a POM set up. Taken from[30]

A schematic of a polarising optical microscope is shown in fig. 5.10. The source, which generally emits white light is placed at the bottom, from which the emitted light passes through a polariser. A condenser, which is kept after the polariser focuses the lineraly polarised light on the sample. The temperature of the sample stage can be varied by an external temperature controller. Linearly polarised light passing through an optically anisisoropic liquid crystalline medium, gets

divided into ordinary and extra-ordinary waves, which pass through the objective and analyzer and eventually get collected by an eye piece.

### 1.6.3 Cryogenic scanning electron microscopy (cryo-SEM)

Cryo-SEM is an effective imaging technique which is used to study many soft matter and biological systems[31,32]. In this technique the samples are quenched using liquid nitrogen. Because of this there is no water loss from the sample and the structure and morphology of the sample remain frozen. 20 - 30 $\mu$l of the sample is taken in a cuvette and quenched in liquid nitrogen. The sample is then transferred to a high vacuum cryo-unit (PP3000T cryo unit), where the temperature is typically maintained around -180°C, After fracturing the sample with a cold knife, they are sublimated and then coated with platinum. Image formation in this technique depends on the interaction between incident electrons and the specimen used for the study. Secondary electrons (SE) are generated due to in-elastic scattering between the incident electron and the atoms of the sample. These electrons are collected by a detector. SEM is used mainly to detect surface structure and roughness of sample. Other detectors are used to detect back scattered electrons (BSEs) and x-rays. In our case imaging was done by using Zeiss Ultra Plus Cryo-SEM.

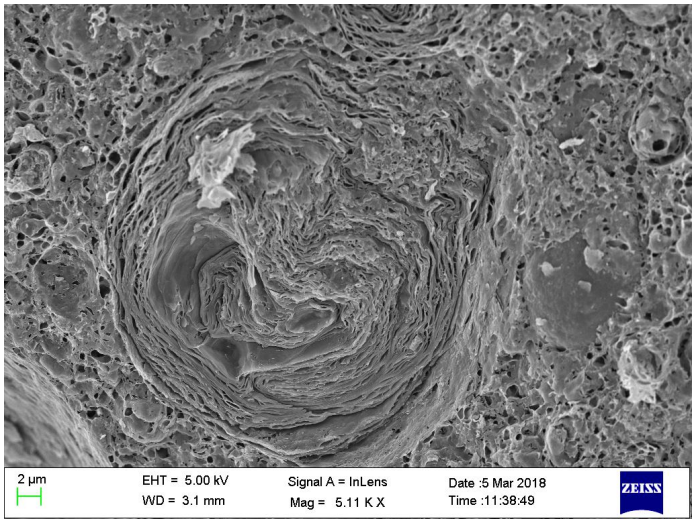


FIGURE 1.15: Typical Cryo-SEM image of multi lamellar vesicles (MLVs)

### 1.6.4 CHNS analysis

The amount of carbon, hydrogen, nitrogen and sulphur present in a compound can be determined using a CHNS analyser[33]. High temperature combustion ($\sim$ 1100 °C ) in an oxygen rich environment is required to carry out the analysis. During this process the compounds get oxidized (e.g. carbon turns to carbon dioxide, sulphur becomes sulphur dioxide etc). The combustion products are then passed through a high temperature copper chamber ($\sim$ 600 °C), where the extra oxygen of the combustion process in removed and nitrogen oxides are converted to nitrogen gas. These products are then passed through subsequent absorbent traps to leave out only the oxides of carbon, hydrogen, nitrogen and sulphur. For detection of the gases GC (gas chromatography) separation technique is used.

### 1.6.5 Differential scanning calorimetry (DSC)

Differential scanning calorimetry is a technique where a reference and a sample are heated simultaneously and difference in the heat flow as a function of temperature is measured[34]. Different transitions such as melting, glass transition, phase changes can be detected by using DSC. From the difference in the heat flow between the sample and the reference during the phase transition transition enthalpies is measured. As discussed later in the thesis using DSC we have found the transition enthalpy corresponding to pre and main transition of lipids and also the Kraft temperature as a function of salt concentration for charged surfactants. The heat capacity ($C_p$) of a material as a function of temperature also can be measured using DSC.

# Bibliography


[1] Israelachvili JN. Intermolecular and surface forces. Academic press; 2011.

[2] Holmberg K, Jönsson B, Kronberg B, Lindman B, et al. Polymers in aqueous solution. Wiley-Blackwell New York; 2002.

[3] Jones RAL, Jones RA, Jones R, et al. Soft condensed matter. vol. 6. Oxford University Press; 2002.

[4] Lombardo D, Kiselev MA, Magazù S, Calandra P. Amphiphiles self-assembly: basic concepts and future perspectives of supramolecular approaches. Adv Condens Matter Phys. 2015;2015:1-22.

[5] Tanford C. The hydrophobic effect: formation of micelles and biological membranes 2d ed. J. Wiley.; 1980.

[6] Hunter RJ. Foundations of colloid science. Oxford university press; 2001.

[7] Menger FM. The structure of micelles. Accounts of Chemical Research. 1979;12(4):111-7.

[8] Manning GS. Limiting laws and counterion condensation in polyelectrolyte solutions. III. An analysis based on the Mayer ionic solution theory. The Journal of Chemical Physics. 1969;51(8):3249-52.

[9] Oosawa F. A simple theory of thermodynamic properties of polyelectrolyte solutions. Journal of Polymer Science. 1957;23(103):421-30.

[10] Oosawa F. Polyelectrolytes. M. Dekker; 1971.

[11] Andelman D. Introduction to electrostatics in soft and biological matter. Soft condensed matter physics in molecular and cell biology. 2006;6.

[12] Anderson CF, Record Jr MT. Polyelectrolyte theories and their applications to DNA. Ann Rev Phys Chem. 1982;33(1):191-222.

[13] Dias R, Lindman B. DNA interactions with polymers and surfactants. John Wiley & Sons; 2008.

[14] Helfrich W. Effect of thermal undulations on the rigidity of fluid membranes and interfaces. Journal de Physique. 1985;46(7):1263-8.

[15] Servuss R, Helfrich W. Mutual adhesion of lecithin membranes at ultralow tensions. Journal de Physique. 1989;50(7):809-27.

[16] Parsegian VA, Fuller N, Rand RP. Measured work of deformation and repulsion of lecithin bilayers. Proceedings of the National Academy of Sciences. 1979;76(6):2750-4.

[17] Rand R. Interacting phospholipid bilayers: measured forces and induced structural changes. Annual review of biophysics and bioengineering. 1981;10(1):277-314.

[18] Lu BS, Gupta SP, Belička M, Podgornik R, Pabst G. Modulation of elasticity and interactions in charged lipid multibilayers: monovalent salt solutions. Langmuir. 2016;32(50):13546-55.

[19] Rand R, Fuller N, Parsegian V, Rau D. Variation in hydration forces between neutral phospholipid bilayers: evidence for hydration attraction. Biochemistry. 1988;27(20):7711-22.

[20] Sherwood D, Cooper J. Crystals, X-rays and proteins: comprehensive protein crystallography. OUP Oxford; 2010.

[21] Chaikin PM, Lubensky TC, Witten TA. Principles of condensed matter physics. vol. 10. Cambridge university press Cambridge; 1995.

[22] Champeney DC, Fuoss RM. Fourier transforms and their physical applications. Physics Today. 1973;26(10):57.

[23] Buerger M. The correction of X-ray diffraction intensities for Lorentz and polarization factors. Proceedings of the National Academy of Sciences of the United States of America. 1940;26(11):637.

[24] Pabst G, Rappolt M, Amenitsch H, Laggner P. Structural information from multilamellar liposomes at full hydration: full q-range fitting with high quality x-ray data. Physical Review E. 2000;62(3):4000.

[25] Zhang R, Suter RM, Nagle JF. Theory of the structure factor of lipid bilayers. Physical Review E. 1994;50(6):5047.

[26] Radhakrishnan A, Ghosh SK, Pabst G, Raghunathan V, Sood A. Tuning DNA-amphiphile condensate architecture with strongly binding counterions. Proceedings of the National Academy of Sciences. 2012;109(17):6394-8.

[27] Thomas M. Surfactant-Polyelectrolyte complexes: Structure and Interactions. Raman Research Institute, Bangalore.; 2019.

[28] Krishnaswamy R, Pabst G, Rappolt M, Raghunathan V, Sood A. Structure of DNA-CTAB-hexanol complexes. Phys Rev E. 2006;73(3):031904.

[29] Madhukar S. Influence of some sterols and nucleotides on the structure of self-assembled amphiphilic systems. Raman Research Institute, Bangalore.; 2019.

[30] Dierking I. Textures of liquid crystals. John Wiley & Sons; 2003.

[31] Strey R, Jahn W, Porte G, Bassereau P. Freeze fracture electron microscopy of dilute lamellar and anomalous isotropic (L3) phases. Langmuir. 1990;6(11):1635-9.

[32] Meyer H, Richter W. Freeze-fracture studies on lipids and membranes. Micron. 2001;32(6):615-44.

[33] Wachberger E, Dirscherl A, Pulver K. Automatic procedure for the CHN-analysis of organic substances in the milligram range. Microchemical Journal. 1971;16(2):318-28.

[34] Gill P, Moghadam TT, Ranjbar B. Differential scanning calorimetry techniques: applications in biology and nanoscience. Journal of biomolecular techniques: JBT. 2010;21(4):167.

# Chapter 2

# Polymorphism in surfactant-DNA complexes

## 2.1 Introduction

DNA is a semirigid polyelectrolyte having a persistence length of about 50 nm [1]. It acquires a negative electric charge in aqueous solutions, due to the release of its counterions into the medium. However, not all the counterions are dispersed and a large fraction of them remain close to the DNA backbone. This phenomenon, called counterion condensation, is known to occur if the charge density of the polyelectrolyte is sufficiently high, and results from the competition between the electrostatic and entropic contributions to the free energy of the solution [2]. Polyelectrolytes, such as DNA, form complexes with oppositely charged macroions added to the solution.These macroions could be polyelectrolytes, colloidal particles or self-assembled structures of amphiphilic molecules [3–6]. The counterions that are initially bound to the two types of macroions are released on complexation, and the gain in the translational entropy of these counterions is the main factor driving the process [7]. Such complexes have been widely studied due to their potential applications in industry and medicine [8,9].

Complexes of DNA with cationic single-chain surfactants have been the subject of many structural investigations [10–15]. Most of these studies have used the cationic surfactant, cetyltrimethylammonium bromide ($C_{16}$ TAB), which self-assembles into rod-like micelles in water at concentrations slightly above its critical micellar concentration (CMC). If the contour length of the DNA is very long, typically of the order of a few $\mu$m, these complexes form two-dimensional crystals, with the long axes of the DNA and the rod-like micelle normal to the plane of the lattice. These structures do not have translational order along the direction normal to the lattice plane, and hence have the same symmetry as columnar liquid crystals [16].

In this chapter, we describe the structural polymorphism observed in complexes of DNA with a homologous series of cationic surfactants, namely, alkyltrimethylammonium bromide ($C_n$ TAB), as n is varied from 18 to 8. For $n \geq 14$ the complexes exhibit a hexagonal columnar (H) phase, irrespective of the relative surfactant to DNA base molar concentration (R) in the solution. Similarly, for $n \leq 10$ a square columnar (S) phase is observed at all values of R. However, in the intermediate case of n = 12, two different structures are found depending on the value of R; the S phase for R = 5, and a super-hexagonal columnar ($H_s$) phase at R = 1. The $H_s$ structure can be distinguished from H by its much larger lattice parameter. The observed structural polymorphism of these complexes can be qualitatively accounted for by considering the different contributions to their free

energy[17].

## 2.2 Materials and methods

All surfactants and sodium salt of calf thymus DNA were obtained from Sigma Aldrich. Complexes were prepared by adding appropriate amounts of DNA to an aqueous solution of the surfactant, to obtain the desired value of the surfactant to DNA base molar ratio, R. CMCs of the surfactants, taken from the literature, with the value of n given in parentheses, are: 0.1 mM (18)[18], 0.9 mM (16), 3.6 mM (14), 15.8 mM (12)[19], 67 mM (10)[20], and 293 mM (8)[21]. Surfactant concentration in the solution was higher than the corresponding CMC. On adding DNA to the surfactant solution, the complexes form a gel-like precipitate suspended in the natant. Samples were equilibrated for about a week at room temperature. For small-angle x-ray scattering (SAXS) studies, the complex along with some of the supernatant was taken in 1 mm glass capillaries, which were flame sealed to avoid any loss of water. Data were collected over a range of the magnitude of the scattering vector (q) from 0.01 to 5.0 nm $^{-1}$, using a Hecus S3-Micro system, fitted with a one- dimensional position-sensitive detector. Typical exposure time was 30 min and error in the measurement of peak positions was $\pm$ 0.02 nm. Data from all samples were collected at 30 °C, except from C18 TAB-DNA complexes, which were maintained at 50 °C, due to the higher Kraft temperature of this surfactant.

Elemental analysis of the complexes was conducted using a CHNS elemental analyser (vario MICRO cube, Elementar), which gives the relative amounts of C, H and N in the material to an accuracy of 0.3 %, Complexes were prepared at the chosen compositions and the entire complex was transferred into tin boats after equilibration. Care was taken to minimise the amount of the surfactnatant taken along with the complex. Samples were dried thoroughly by placing them in an evacuated desiccator for 3 days, and were then removed and crimped immediately to avoid rehydration. The total number of carbon ($C_t$) and nitrogen atoms ($N_t$) in the sample, obtained from the experiment, can be expressed as, $C_t = n_s C_s + n_b C_b$, and $N_t = n_s N_s + n_b N_b$, where $C_s$, $C_b$, $N_s$, $N_b$ are the number of carbon and nitrogen atoms in a surfactant molecule and DNA base, respectively. $n_s$ and $n_b$ are the total number of surfactant molecules and DNA bases in the sample. Recasting the above equations, we get,$C_t/N_t = (C_s R_c + C_b)/(R_c + N_b)$, where $R_c$ is the surfactant to DNA base molar ratio in the complex, which can be different from its bulk value R. Thus the composition of the complex can be determined from the values of $C_t$ and $N_t$ obtained from the experiment.

## 2.3 Results

Polarising microscopy images show that the complexes are highly birefringent. The birefringence persists, but becomes weak at NaCl concentrations of the order of 500mM (fig.2.1 and fig. 2.2). Complexes do not form beyond a salt concentration of 600 mM.

SAXS patterns of $C_{18}$TAB- DNA complexes are shown in fig. 2.3 and fig. 2.4, for two values of R above and below R=1, which is the isoelectric point of the system, where the total number of surfactant ions is equal to the total number of DNA bases. The peaks observed can be indexed to a two-dimensional hexagonal lattice; the lattice parameters are presented in Table 2.1. In the

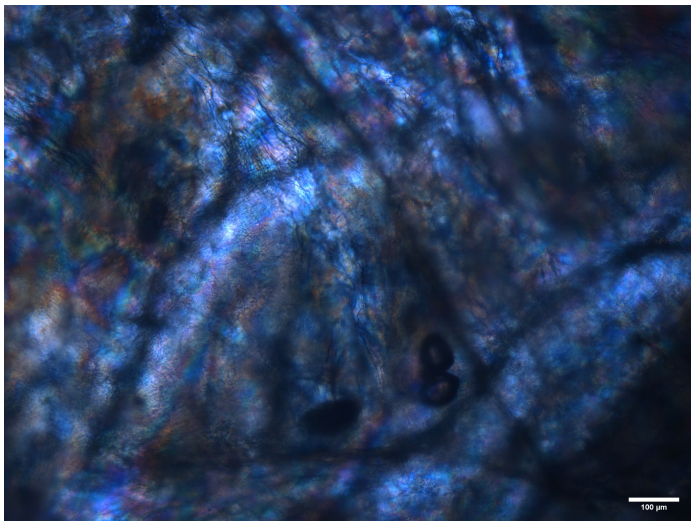

FIGURE 2.1: POM images of DTAB-DNA complexes in Water.

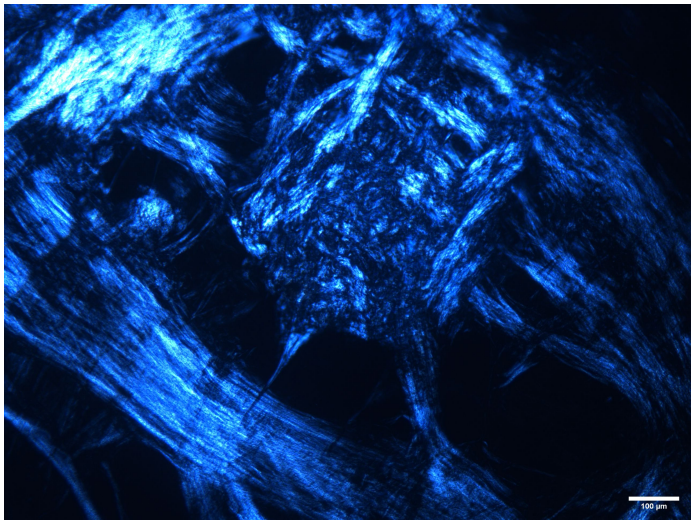

FIGURE 2.2: POM images of DTAB-DNA complexes in 500mM NaCl.

presence of the salt the peaks become sharper and one extra peak is observed. $a$ is found to be slightly higher at the higher value of R and higher salt concentration.

SAXS patterns of $C_{16}$TAB-DNA complexes are very similar (fig. 2.5 and fig. 2.6)and show sharper peaks in the presence of salt. As in the previous case, $a$ is found to be slightly higher at the higher value of R and higher salt concentration (Table 2.1). SAXS profiles of $C_{14}$TAB-DNA complexes are also simililar to those of $C_{18}$TAB-DNA and $C_{16}$TAB-DNA complexes[22].

SAXS pattern of $C_{12}$TAB (DTAB)-DNA complexes are very different. For R=5.0 samples in the absence of NaCl the SAXS pattern shows a abroad peak, indicating the absence of long range transnational order in the system (fig. 2.7). We refer to this as the Nematic Gel I. This structure is observed up to [NaCl] $\approx$ 200 mM. As [NaCl] is increased further sharper and distinct diffraction peaks are observed. These patterns show two peaks with their q' s in the ratio of 1: $\sqrt{2}$, and can be indexed to a two dimensional the square lattice with $a \approx 4.1$ nm. We label this phase as square (S) phase. Peaks in the diffraction pattern become again broad with further increase in [NaCl]. These complexes are birefringent and we label this structure as the Nematic Gel II (fig.5.10).

SAXS patterns obtained at R = 0.5 for different values of [NaCl] are given in fig. 2.8. The

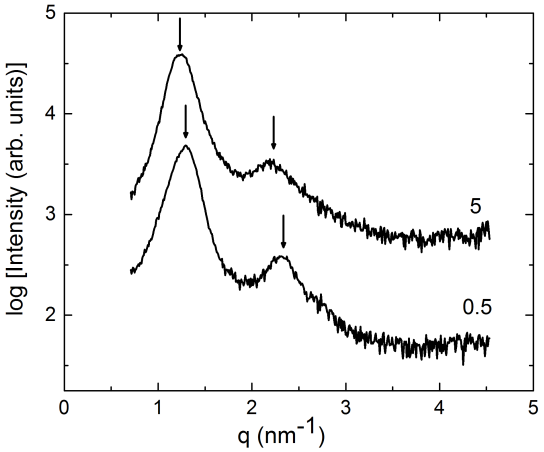


FIGURE 2.3: SAXS patterns of $C_{18}$TAB- DNA complexes in water. Surfactant concentration was fixed at 50mM, the values of R is indicated against each pattern. Expected positions of the diffraction peaks are indicated by arrows in all the patterns presented.

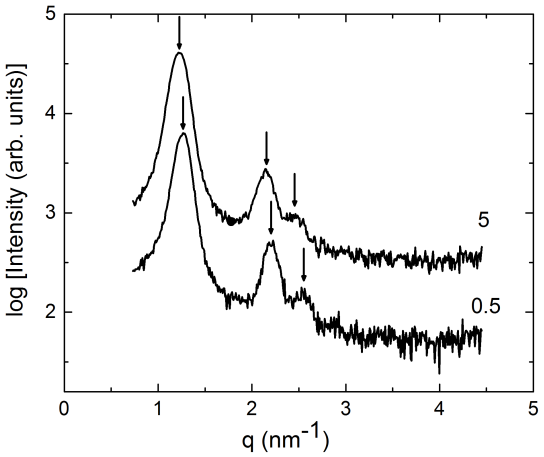


FIGURE 2.4: SAXS patterns of $C_{18}$TAB- DNA complexes in 200mM NaCl. Surfactant concentration was fixed at 50mM, the values of R is indicated against each pattern. Expected positions of the diffraction peaks are indicated by arrows in all the patterns presented.

behavior at R = 0.5 is very similar to that at R = 5.0, with the appearance of SAXS patterns with sharp peaks only over an intermediate range of [NaCl]. Both at higher and lower [NaCl] the birefringent complexes give only a very broad peak in their SAXS patterns. However, the ordered structure found at R = 0.5 corresponds to a two-dimensional hexagonal lattice and not a square lattice. Moreover, in all these patterns the (1 0) peak is always absent and only higher order peaks with their q's in the ratio $\sqrt{3} : 2 : \sqrt{7} : 3$ are observed. The lattice parameter ($a$) of this phase is $\approx$ 9.0 nm and we label this phase as the super hexagonal ($H_s$) phase.

A partial phase diagram of the system, as a function of R and [NaCl], deduced from the SAXS data is presented in fig. 2.9. Nematic phases are found at lower and higher [NaCl] for all values

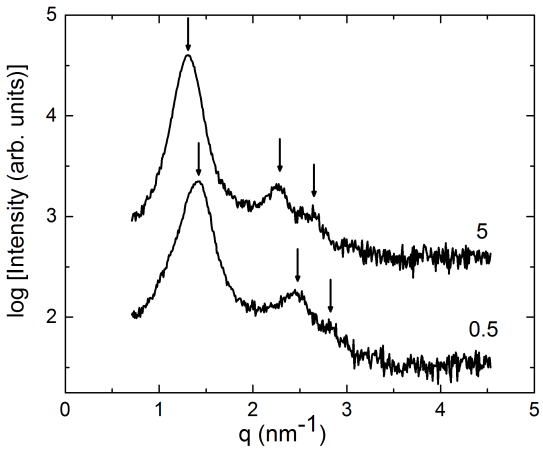


FIGURE 2.5: SAXS patterns of $C_{16}$TAB- DNA complexes in water. Surfactant concentration was fixed at 50mM, the values of R is indicated against each pattern.

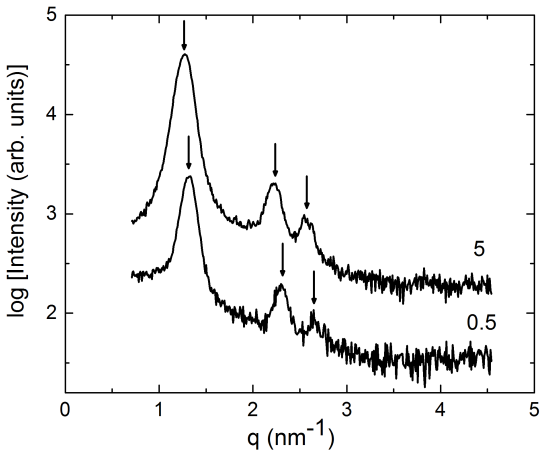


FIGURE 2.6: SAXS patterns of $C_{16}$TAB- DNA complexes in 200mM NaCl. Surfactant concentration was fixed at 50mM, the values of R is indicated against each pattern.

of R. Over intermediate values of [NaCl] the S phase is observed for $R > 3$, whereas the $H_s$ structure is observed at lower R. Fig. 2.10 shows the phase behavior as a function of R and surfactant concentration in the absence of salt. Here the nematic phase is observed at lower DTAB concentrations, irrespective of the value of R. The $H_s$ phase appears on increasing [DTAB] to 150 mM for $R \leq 1$, whereas the S phase occurs for [DTAB] $\geq$ 350 mM for $R \geq 2$.

SAXS patterns of $C_{10}$TAB- DNA complexes are shown in fig. 2.11 and fig. 2.12 for R = 0.5 and 5. Complexes do not form at a surfactant concentration of 50 mM, but appear on increasing it to 100 mM. In this case also the peaks become sharper in the presence of salt. Patterns at both values of R correspond to a two-dimensional square lattice. Values of $a$ in this (S) phase are given in table 2.1.

$C_8$ TAB-DNA complexes are found only over a narrow range of surfactant concentration around 500 mM. Their SAXS patterns are given in fig. 2.13 for two values of R. At R = 0.5, the pattern has a broad peak and the complex has a nematic-like structure. At R = 5 the pattern shows one sharp

| n | R | [NaCl] (mM) | Phase | $a$(nm) |
|---|---|---|---|---|
| 18 | 0.5 | 0 | H | 5.35 |
| | 0.5 | 200 | H | 5.63 |
| 18 | 5 | 0 | H | 5.67 |
| | 5 | 200 | H | 5.80 |
| 16 | 0.5 | 0 | H | 5.09 |
| | 0.5 | 200 | H | 5.44 |
| 16 | 5 | 0 | H | 5.51 |
| | 5 | 200 | H | 5.65 |
| 14 | 0.5 | 0 | H | 5.01 |
| | 0.5 | 200 | H | 5.10 |
| 14 | 5 | 0 | H | 5.30 |
| | 5 | 400 | H | 5.43 |
| 12 | 0.5 | 200 | $H_s$ | 8.41 |
| | 5 | 200 | S | 4.07 |
| 10 | 0.5 | 0 | S | 3.43 |
| | 0.5 | 200 | S | 3.68 |
| 10 | 5 | 0 | S | 3.56 |
| | 5 | 200 | S | 3.75 |

TABLE 2.1: Lattice parameter of $C_n$TAB-DNA complexes. H

peak indicating that the complex has long-range positional order. However, the absence of additional peaks makes it impossible to unambiguously identify its structure. These complexes do not form in a 200 mM NaCl solution.

Composition ($R_c$) of $C_{10}$TAB-DNA complexes was determined using elemental analysis for different values of the bulk composition (R) of the solution. Variation of $R_c$ with R, obtained from these experiments, is shown in fig.2.14. For $R \leq 1.0$, $R_c$ is almost equal to R. At higher values of R, however, $R_c$ increases very slowly with increasing R and saturates at around 1.7.

Cryo-SEM images of DTAB-DNA complexes are presented in fig. 2.15 and fig. 2.16. Two samples were taken from two different parts of the phase diagram.The first sample was taken at lower R which corresponds to the $H_s$ phase in the phase diagram and the second sample was taken at higher R, corresponding to the S phase. Both the images show bundle-like features, whose diameter is around 30 nm - 50 nm. Similar images have been observed for other $C_n$TAB-DNA complexes[16].

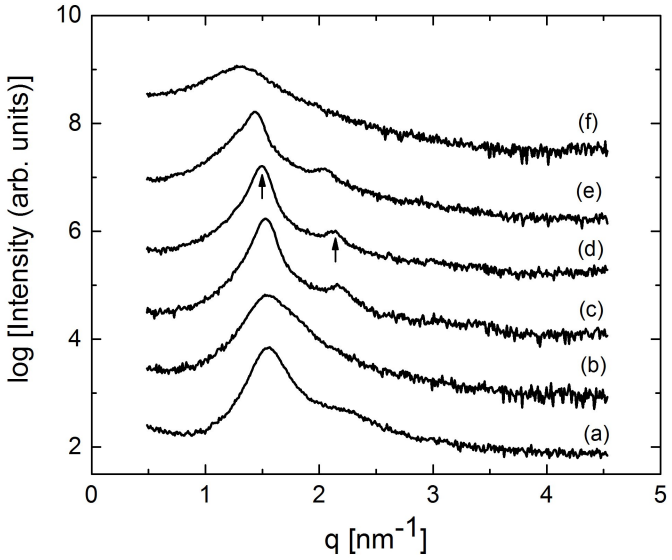


FIGURE 2.7: SAXS patterns of DTAB-DNA complexes at R = 5.0 for [NaCl] = 0 mM (a), 100 mM (b), 200 mM (c), 300 mM (d), 400 mM (e) and 500 mM (f). Arrows indicate positions of the (1 0) and (1 1) peaks from a square lattice.

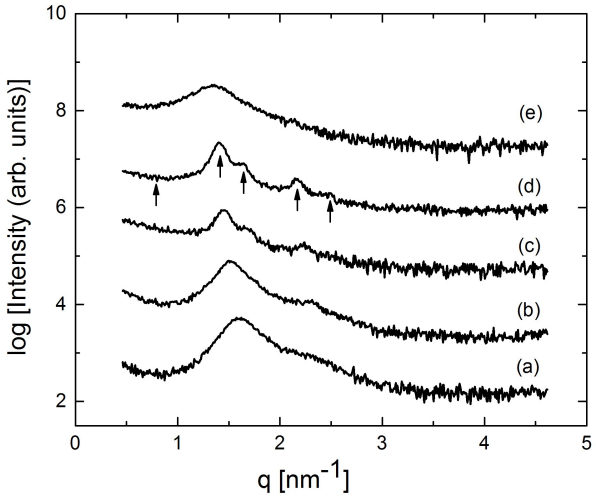


FIGURE 2.8: SAXS patterns of DTAB-DNA complexes at R = 0.5 for [NaCl] = 0 mM (a), 100 mM (b), 200 mM (c), 300 mM (d) and 400 mM (e). Arrows indicate positions of the (1 0), (1 1), (2 0), (2 1) and (3 0) peaks from a hexagonal lattice. Note the absence of the (1 0) peak.

### 2.3.1 Madelung energy

CTAB-DNA complexes exhibit only the hexagonal (H) structure irrespective of the value of R. In contrast, this structure is absent in DTAB-DNA complexes and the S structure is observed for R $>$ 3. In order to gain a qualitative understanding of the relative stability of the S and H structures we have estimated the electrostatic energy of these structures. Assuming the micelles to be infinitely long, the electrostatic energy of these two-dimensional macroion crystals can be estimated using the pair interaction potential per unit length between two dissimilar parallel cylinders, separated by a distance r, given by[24]

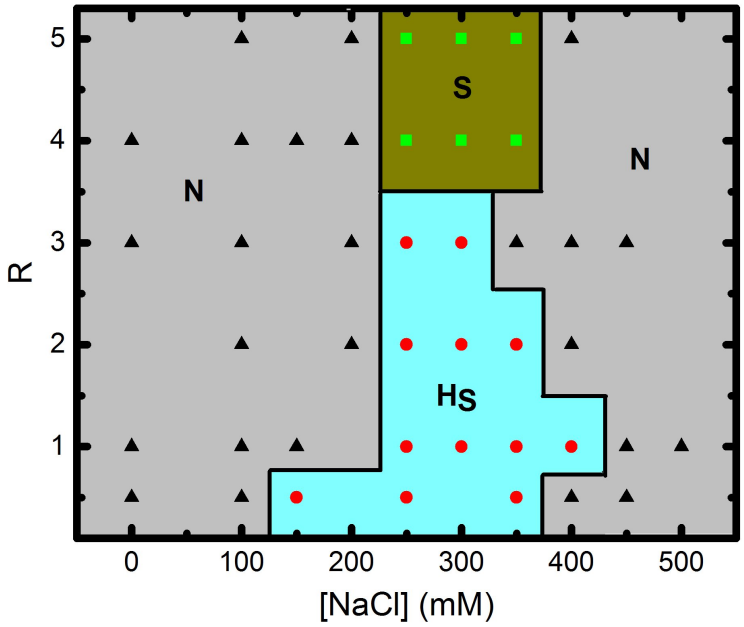


FIGURE 2.9: Partial phase diagrams of DTAB-DNA complexes determined from SAXS and polarizing microscopy data, as a function of R and NaCl concentration. N - nematic, S - square and $H_s$ - superhexagonal. For reconstructing the phase diagram, data were taken from [23].

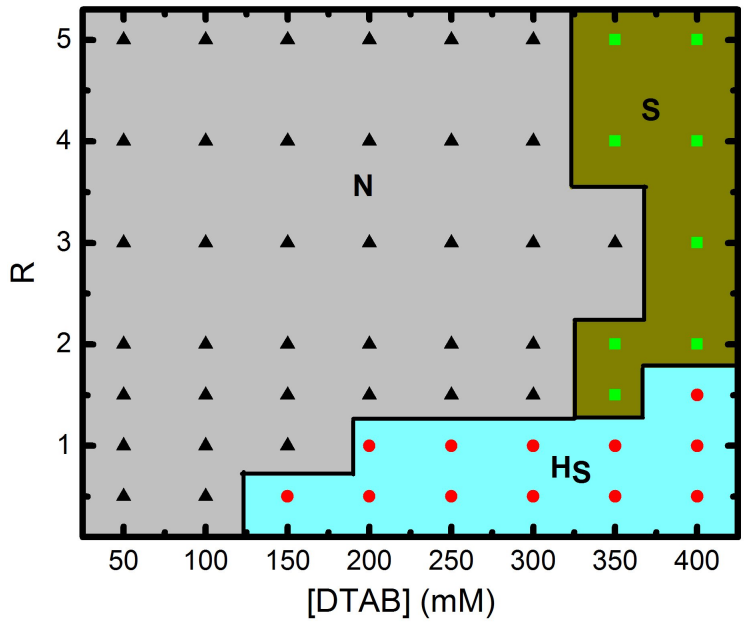


FIGURE 2.10: Partial phase diagrams of DTAB-DNA complexes determined from SAXS and polarizing microscopy data, as a function of R and DTAB concentration [17]

$$V(r) = 2(\nu_1\nu_2/\epsilon)K_0(\kappa r) \tag{2.1}$$

Where, $\nu_i = 2\pi\sigma_i/\kappa K_1(\kappa a_i)$, $\sigma_i$ is the surface charge density of the cylinder of radius $a_i$ (i=1,2) and $\kappa$ the inverse Debye length. $K_0$ and $K_1$ are Bessel functions of the second kind of order 0 and 1, respectively. The energy U of the macroion crystal per unit cell can be obtained by summing the interactions of each particle in the unit cell with all other particles in the system, analogous to the calculation of the Madelung energy of ionic crystals [25–28],

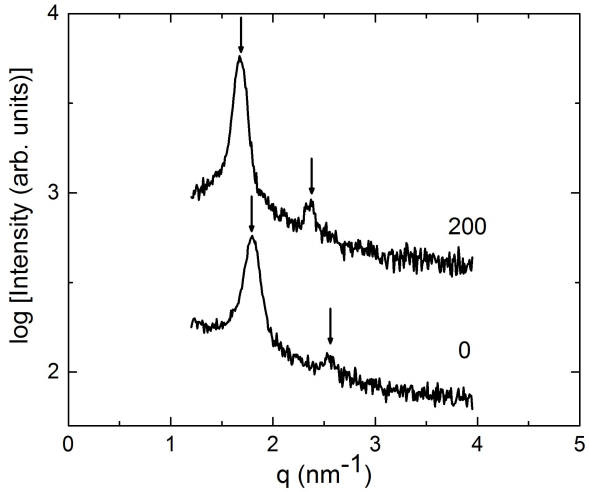


FIGURE 2.11: SAXS patterns of $C_{10}$TAB- DNA complexes at R = 0.5. NaCl concentration (mM) in the solution is indicated against each pattern. Surfactant concentration in the solution is 100 mM.

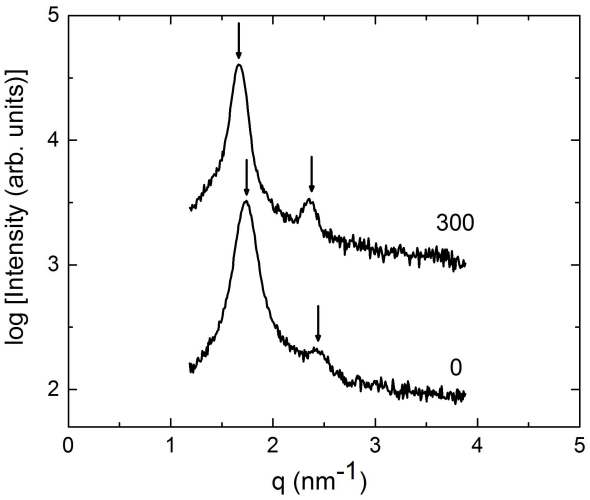


FIGURE 2.12: SAXS patterns of $C_{10}$TAB- DNA complexes at R = 5. NaCl concentration (mM) in the solution is indicated against each pattern. Surfactant concentration in the solution is 100 mM.

$$U = \frac{1}{2}\sum V_{mm}(r) + \sum V_{md}(r) + \frac{1}{2}\sum V_{dd}(r) \tag{2.2}$$

The three terms in the above equation correspond to the micelle-micelle, micelle-DNA, and DNA-DNA interactions, respectively. The surface charge density of the micelle is estimated to be 1.56 e/nm$^2$ taking the area per head group to be 0.64 nm$^2$ [29], whereas that of the DNA is estimated to be -0.75 e/nm$^2$ from its radius of 1.25 nm [30]. The energy of the two structures have been calculated by summing over these interactions using the Sum routine from Mathematica [31]. Since the electrostatic interactions are screened by salt, the summation converges rapidly over a few unit cells.

The energy per particle, u = U/n, n being the number of particles within a unit cell, of the H

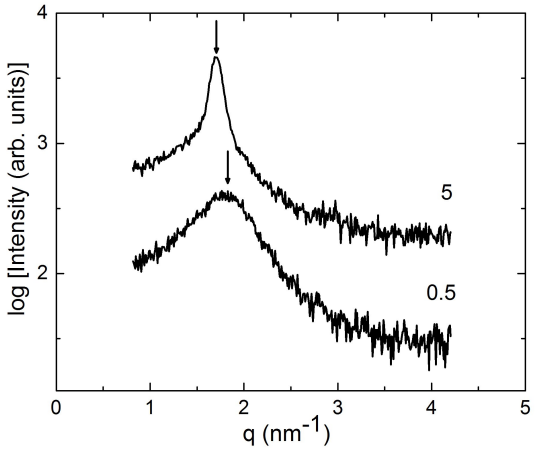


FIGURE 2.13: SAXS patterns of $C_8$TAB- DNA complexes in water at two values of R, indicated against each curve. Surfactant concentration in the solution is 500 mM.

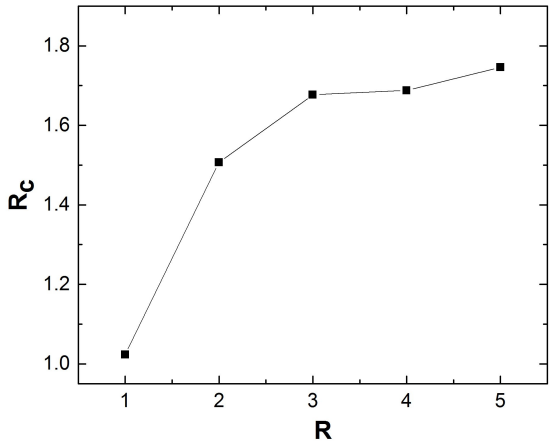


FIGURE 2.14: Variation of the composition of the complex ($R_c$) with the bulk solution composition (R) obtained from elemental analysis of $C_{10}$ TAB-DNA complexes.

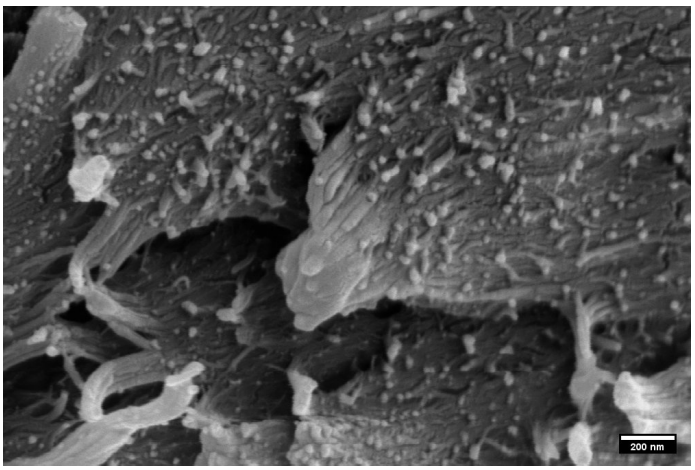


FIGURE 2.15: Cryo-SEM images of DTAB-DNA complexes at R=1.

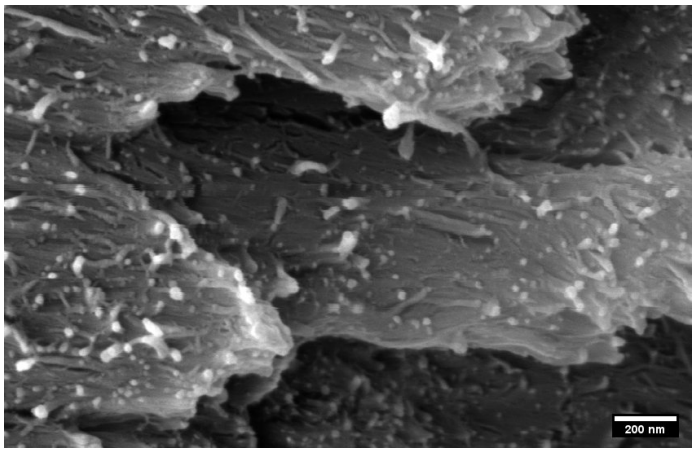


FIGURE 2.16: Cryo-SEM images of DTAB-DNA complexes at R=5.

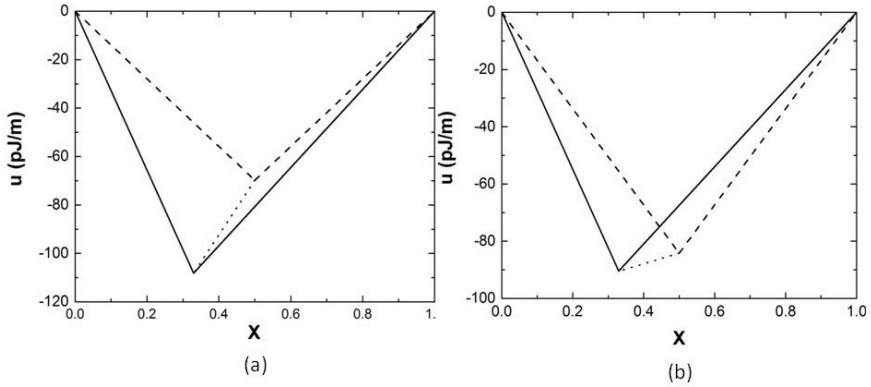


FIGURE 2.17: Electrostatic energy per particle of the S and H structures obtained from the calculations. x is the ratio of number of micelles to the total number of particles (DNA+micelles) in a unit cell. x = 1/3 for H and x = 1/2 for S. x = 0 and x = 1 correspond to dilute solutions of DNA and micelles, respectively. The straight line segments are Maxwell constructions joining any two of the four energy minima corresponding to the four phases in the system. The two phases coexisting at any value of x are indicated by the endpoints of the lowest straight line segment at that composition. [NaCl] = 300 mM. $r_m$ = 2.0 nm (a) and $r_m$ = 1.5 nm (b).

and S structures obtained from the calculations are given in fig.2.17 for $r_m$ = 2.0 nm and 1.5 nm. Here x is the micelle/(DNA+micelle) fraction in the structure, values of x for H and S being 1/3 and 1/2, respectively. The points x = 0 and x = 1 represent dilute solutions of DNA and micelles, respectively, whose electrostatic energy is assumed to vanish. Coexistence of different structures can be inferred from the slopes of the straight lines joining the points representing their energies, a procedure analogous to the well-known Maxwell construction[(28)]. H is found to be the only stable structure for $r_m$ = 2.0 nm. It coexists with a dilute DNA solution between x = 0 and x = 1/3, and with a dilute micellar solution at higher values of x. On decreasing $r_m$ to 1.5 nm S also becomes stable, leading to its coexistence with H between x = 1/3 and x = 1/2, and with a dilute micellar solution between x = 1/2 and x = 1.

The negative contribution to u from micelle-DNA interaction is comparable in the two structures at a given value of $r_m$. The positive contribution from micelle-micelle interaction is higher in S, due to the lower inter-micellar separation in this structure. For similar reasons, the positive contribution from DNA-DNA interaction is higher in H. Since the surface charge density of the

micelle is fixed, its total charge increases with increasing $r_m$. Hence the magnitudes of the micelle-DNA and micelle-micelle interactions are higher at higher $r_m$. On the other hand, the DNA-DNA contributions are lower at higher $r_m$, since the inter-DNA separation increases with increasing $r_m$. At $r_m$ = 1.5 nm, the two structures have comparable values of u and hence they are both stable, albeit at different compositions. On increasing $r_m$ to 2, DNA-DNA repulsion decreases in H, whereas micelle-micelle repulsion increases in S, leading to the disappearance of the latter from the phase diagram.

### 2.3.2 Effect of micellar length

For CTAB-DNA complexes a H phase is observed, while $H_s$ phase is observed in the case of DTAB-DNA complexes at lower values of R. One major difference between these two surfactants is the tendency of CTAB to form cylindrical micelles, compared to small ellipsoidal micelles in the case of DTAB[32]. In order to probe if this difference is responsible for the occurrence of the two different structures, we have studied the influence of hexanol on the phase behaviour of DTAB-DNA complexes, since hexanol is known to induce the formation of cylindrical micelles[33]. SAXS patterns of the complexes at a hexanol to surfactant molar ratio in the solution, $\beta$ = 1, is shown in fig. 2.18. It has three peaks, which can be indexed on a two-dimensional hexagonal lattice with $a$ = 4.8 nm. Thus the elongation of the micelles drives a $H_s \rightarrow$ H transition of the complex.

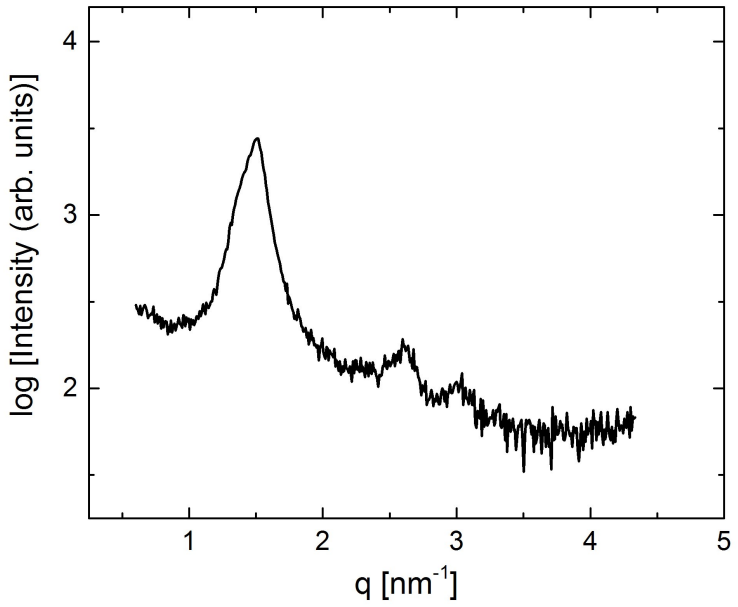


FIGURE 2.18: SAXS pattern showing the formation of the H phase in DTAB-DNA complexes in the presence of hexanol. Hexanol to surfactant molar ratio in the solution is 1.0, R = 0.5, and [DTAB] = 50 mM.

### 2.3.3 Electron density maps

Electron density maps ($\rho(\vec{r})$) of the different structures observed in this study have been determined from the SAXS data, using the relation, $\rho(\vec{r}) = \sum_{hk} |F_{hk}| \phi_{hk} \cos(\vec{q}_{hk}.\vec{r})$ , where $F_{hk}$, $\phi_{hk}$ and $\vec{q}_{hk}$ are the amplitude, phase and scattering vector, respectively, of the (h,k) reflection. Assuming the structure to have a centre of symmetry, $\phi_{hk}$ is taken to be either +1 or -1. $\rho(\vec{r})$ is computed

by trying out all phase combinations and picking out the most suitable map(s) consistent with a close-packed structure of DNA and micelles. Electron density maps, so determined, are shown in fig. 2.19. Schematics of various structures suggested by these maps are given in fig. 2.20.

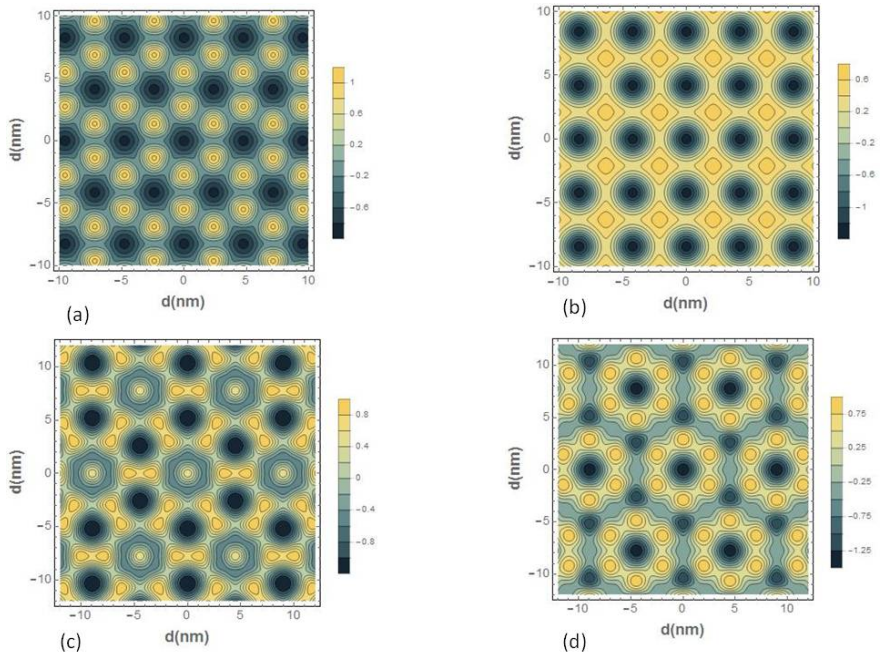


FIGURE 2.19: Electron density maps of the H (a), S (b), and $H_s$ phases (c and d) observed in the present study, determined from the SAXS data. Two possible structure of the $H_s$ phase are shown, which are obtained for different sets of phases of the observed reflections. These maps correspond to the electron density of the complexes projected on the plane of the lattice, which is normal to the DNA axis. The low electron density regions correspond to the hydrocarbon cores of the micelles and the high electron density regions correspond to DNA.

## 2.4 Discussions

Polarising microscopy and SAXS studies clearly show that $C_n$ TAB-DNA complexes have a two-dimensional hexagonal structure for n $\geq$ 14. Electron density map of this (H) phase shows a close-packed intercalated structure, with each cylindrical micelle surrounded by 6 DNA and each DNA surrounded by 3 micelles. Such a packing ensures that the oppositely charged species are in proximity. Since this structure is close-packed, its lattice parameter can be expressed in terms of the micellar radius $r_m$ and the DNA radius $r_d$ as, $a = \sqrt{3}(r_m + r_d)$. Taking $r_d$ to be 1.25 nm[30], $r_m$ is estimated to be 2.0, 1.9 and 1.8 nm for n = 18, 16 and 14, respectively. Value of $r_m$ obtained for $C_{16}$ TAB is in good agreement with that reported in the literature[32]. For n = 10, an intercalated square lattice is observed, where the coordination number of both DNA and micelle is 4. In this (S) phase the lattice parameter, $a = \sqrt{2}(r_m + r_d)$, and the value of $r_m$ estimated for n = 10 is 1.3 nm. Since only one peak is observed in the SAXS pattern for n = 8, its structure cannot be determined.

The n = 12 case is intermediate and shows two different structures depending on the bulk composition R. SAXS data and polarizing optical microscopy observations show the formation of a nematic phase at low DTAB concentrations for all values of R. DATB is known to form small ellipsoidal micelles at lower concentrations[32]. Lack of long-range translational order in these

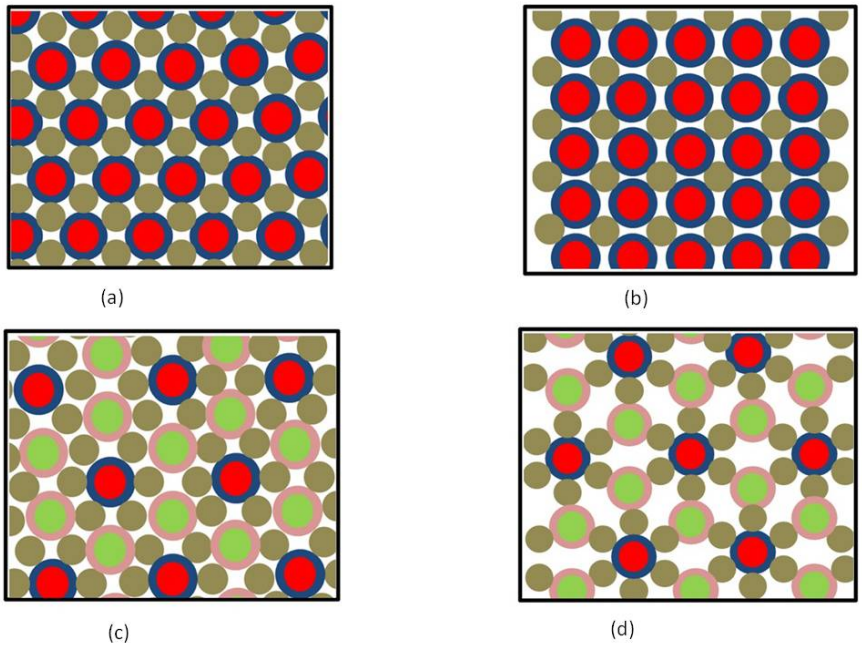


FIGURE 2.20: Schematics of structures of the H (a), S (b) and $H_s$ (c and d) phases observed in the present study, deduced from the electron density maps given in fig. 2.19.

complexes most probably results from these micelles taking different orientations between the DNA strands. Increasing the salt or surfactant concentration results in elongated micelles, which can pack more uniformly between the DNA. As a consequence two-dimensional crystalline structures characterized by long-range translational order are formed under these conditions. A nematic phase is again observed at high NaCl concentrations. This results from the gradual swelling of the complex due to the screening of electrostatic interactions by increasing salt concentration in the solution, which destroys long-range translational order resulting in the orientationally ordered nematic phase. With further increase in the salt concentration, long-rage orientational order is also lost and complexation is completely prevented. As a result a uniform solution is obtained for [NaCl] $>$ 600 mM.

The phase diagrams show the formation of the S and $H_s$ phases in DTAB-DNA complexes, in contrast to CTAB-DNA complexes, where only the H phase is seen. Elemental analysis studies indicate that the composition of the complex, $R_c \sim 1$ in both the phases[23]. Hence concentrations of $Na^+$ and $Br^-$ counterions in the solution can be expected to be comparable to the DTAB concentration. Therefore, it is understandable that the S and $H_s$ phases appear at comparable values of [NaCl] and [DTAB] in the two phase diagrams. However, there are slight differences in the positions of the phase boundaries in figs. 4.1 a and 4.1 b. In the former case concentration of $Br^-$ is around 50 mM and that of $Cl^-$ increases with increasing NaCl in the solution. Whereas in the latter case $Cl^-$ is absent and $Br^-$ concentration increases with DTAB concentration. Therefore, it is possible that the differences in the locations of the phase boundaries is due to the presence of different dominant counterions in the two solutions. The small jump in $R_c$ observed at $R \sim 2.5$ coincides with the $H_s \rightarrow S$ transition observed in SAXS studies, and implies an abrupt increase in the surfactant content of the complex on forming the S phase[23]. Earlier study has shown the formation of S phase at higher R in the CTAT- DNA complexes, which was attributed to the fact

that tosylate counterions binds more strongly to micelle compared to $Br^-$ counterion of DTAB and CTAB[34]. This mechanism cannot explain the formation of the S phase in DTAB-DNA complexes, but not in CTAB-DNA complexes, as this surfactant has the same counterion. The Madelung energy calculations presented above show that the S structure is preferred over the H when the micellar radius is smaller than a threshold value. Hence the stability of the S phase in DTAB-DNA complexes can be attributed to the lower radius of DTAB micelles. The composition variable x, appearing in these calculations, is related to $R_c$. They both describe the composition of the complex; x in terms of number of micelles and DNA, and $R_c$ in terms of the number of surfactant molecules and DNA bases. $R_c$ can be estimated to be 1.4 and 2.8 in the H and S structures of DTAB-DNA complexes, respectively, assuming the micelles to be infinitely long. Hence x = 0, 1/3 , 1/2 and 1 correspond to $R_c$ = 0, 1.4, 2.8 and $\infty$, respectively. Two kinds of electron density maps are obtained for the $H_s$ phase, which can be interpreted in terms of intercalated packings of DNA and micelles. The unit cell in both cases correspond to is a $\sqrt{3} \times \sqrt{3}$ superlattice of the H structure. There are two nonequivalent micellar environments in both maps, creating the superlattice. Both the unit cells contain one micelle of type-1, two micelles of type-2 and six DNA (fig.2.20). They consist of clusters made up of 6 DNA surrounding a central type-1 micelle that are crossed-liked by type-2 micelles. The only difference between these two structures is a relative rotation of the clusters by 30 $^\circ$ with respect to the line joining neighboring type-1 and type-2 micelles. If we ignore the differences between the two types of micelles, these structures have a micelle to DNA stoichiometry of 1:2, similar to that in the H phase (fig.2.20). The observed effect of hexanol on DTAB-DNA complexes suggests that elongation of the micelles leads to the transformation of $H_s$ into H. Structure of the H phase of DTAB- hexanol-DNA complexes, inferred from the scattering data, is identical to that of CTAB- DNA complexes[15]. Hence the occurrence of the $H_s$ structure in this system is somehow related to the propensity of DTAB to self-assemble into small micelles. It is rather surprising that the $H_s$ phase has been observed in complexes of DNA with surfactants that self-assemble into both very long and very short micelles, such as CTAT and DTAB, respectively. Whereas, in complexes of DNA with surfactants that form intermediate rod-like micelles, such as CTAB, this phase is absent. Currently we do not know the precise factors that stabilize this phase; it is conceivable that diferent mechanisms are at play in the two limiting cases of micellar length.

Absence of complexation in the n = 10 and 8 systems at lower surfactant concentrations is due to their higher CMCs. Complex formation increases the entropy of the bound counterions by releasing them in to the solution, whereas the entropy of the surfactant molecules is reduced as they are frozen in the complex. Reduction in the entropy of the surfactant molecules is a relatively minor effect, if they are already in micellar aggregates in the bulk. On the other hand, if the concentration of the surfactant is much below its CMC, the reduction in their entropy on complex formation can be very significant and comparable to the increase in the entropy of the released counterions. Under these conditions complexation can be hindered. Complexes are also not observed for $C_8$TAB concentrations above a narrow range centred around 500 mM. This may be due to the formation of small complex aggregates that do not phase separate from the solution. Similar behaviour has been observed in other systems[35] and has been rationalised in terms of the charging of small aggregates in the presence of excess amount of one of the macroions[36,37].

All the three structures found in this study are characterised by two-dimensional positional ordering, since different DNA strands are not in registry along the direction parallel to their axes.

Hence, they have the same symmetry as columnar liquid crystalline phases. $R_c$ can be calculated using the known values of $r_m$, $r_d$ and surface charge densities of two species. For H phase it is estimated around 1.5 and for S phase it is around 3. Here the micelles are assumed to be infinitely long, just like the DNA. Earlier study on $C_{14}$TAB- DNA complexes have shown that $R_c$ increases with R, attaining a maximum value around 1.6 when R is 5[16]. If we assume the micelles to be very long, the micelle to DNA stoichiometry in the H phase is 1:2 and that in the S phase is 1:1. Hence $R_c$ in the S phase is twice that in the H phase. In the present case the maximum values of $R_c$ can be estimated to be approximately 1.5 and 3 in the H and S phases, respectively. The H phase is, therefore, closer to the isoelectric point and this structure is preferred as more counterions are released on its formation. This is the situation for $n \geq 14$, where only the H phase is observed for all R. On lowering n, $r_m$ decreases and the separation between the DNA surrounding the micelles reduces. This increases the electrostatic repulsion between the DNA and enhances the energy of the system. Below some value of n this contribution to the energy of the H phase offsets the gain due to the release of higher number of counterions. This results in the formation of the S phase, where a lower number of counterions are released, but the DNA–DNA separation is higher than in the H phase at fixed $r_m$ Observation of the S phase for $n \leq 12$ is consistent with the above picture. Fig. 2.14 b shows variation of $R_c$ with R for $C_{10}$ TAB- DNA complexes. This plot shows a lower value of $R_c$ in the S phase. Similar behaviour is observed for DTAB- DNA complexes[23]. This indicates that the micelles in these complexes are not very long and occupy less interstitial volume between the DNA strands.

Cryo-SEM images of the complexes indicate that they are probably made up of fairly monodisperse bundles with a diameter of about 50 nm, which is much higher than the lattice parameter of these structures. It is tempting to attribute the formation of these bundles to the chirality of DNA, since chirality-induced bundle formation is known to occur in actin aggregates[38]. Further studies are required to confirm this possibility.

## 2.5 Conclusions

We have studied the structure of complexes of DNA with cationic alkyltrimethylammonium bromide ($C_n$TAB) surfactants for n varying between 8 and 18. These complexes are found to have a two-dimensional hexagonal structure for $n \geq 14$. On the other hand, a two-dimensional square phase is observed for n = 10. In the intermediate case of n = 12, the square phase is observed at relatively higher surfactant concentrations, but a hexagonal phase, distinct from the one exhibited by complexes of longer chain surfactants, is observed at lower surfactant concentrations. Formation of the square phase at lower surfactant-chain length can be attributed to higher DNA–DNA repulsion in the hexagonal phase. Structural polymorphism of these complexes demonstrate the delicate interplay between entropy and electrostatic energy in these two-dimensional macroion crystals.

# Bibliography

[1] Anderson CF, Record Jr MT. Polyelectrolyte theories and their applications to DNA. Ann Rev Phys Chem. 1982;33(1):191-222.

[2] Manning GS. Limiting laws and counterion condensation in polyelectrolyte solutions. III. An analysis based on the Mayer ionic solution theory. The Journal of Chemical Physics. 1969;51(8):3249-52.

[3] Rumyantsev AM, Jackson NE, De Pablo JJ. Polyelectrolyte complex coacervates: Recent developments and new frontiers. Annual Review of Condensed Matter Physics. 2021;12:155-76.

[4] Van der Gucht J, Spruijt E, Lemmers M, Stuart MAC. Polyelectrolyte complexes: Bulk phases and colloidal systems. Journal of colloid and interface science. 2011;361(2):407-22.

[5] Kizilay E, Kayitmazer AB, Dubin PL. Complexation and coacervation of polyelectrolytes with oppositely charged colloids. Advances in colloid and interface science. 2011;167(1-2):24-37.

[6] Gradzielski M, Hoffmann I. Polyelectrolyte-surfactant complexes (PESCs) composed of oppositely charged components. Current Opinion in Colloid & Interface Science. 2018;35:124-41.

[7] Ou Z, Muthukumar M. Entropy and enthalpy of polyelectrolyte complexation: Langevin dynamics simulations. The Journal of chemical physics. 2006;124(15):154902.

[8] Timilsena YP, Akanbi TO, Khalid N, Adhikari B, Barrow CJ. Complex coacervation: Principles, mechanisms and applications in microencapsulation. International journal of biological macromolecules. 2019;121:1276-86.

[9] Kulkarni AD, Vanjari YH, Sancheti KH, Patel HM, Belgamwar VS, Surana SJ, et al. Polyelectrolyte complexes: mechanisms, critical experimental aspects, and applications. Artificial cells, nanomedicine, and biotechnology. 2016;44(7):1615-25.

[10] Ghirlando R, Wachtel EJ, Arad T, Minsky A. DNA packaging induced by micellar aggregates: a novel in vitro DNA condensation system. Biochemistry. 1992;31(31):7110-9.

[11] Leal C, Wadsö L, Olofsson G, Miguel M, Wennerström H. The Hydration of a DNA- Amphiphile Complex. The Journal of Physical Chemistry B. 2004;108(9):3044-50.

[12] Krishnaswamy R, Raghunathan V, Sood A. Reentrant phase transitions of DNA-surfactant complexes. Physical review E. 2004;69(3):031905.

[13] Krishnaswamy R, Pabst G, Rappolt M, Raghunathan V, Sood A. Structure of DNA-CTAB-hexanol complexes. Phys Rev E. 2006;73(3):031904.

[14] Leal C, Moniri E, Pegado L, Wennerström H. Electrostatic attraction between DNA and a cationic surfactant aggregate. The screening effect of salt. The Journal of Physical Chemistry B. 2007;111(21):5999-6005.

[15] Madhukar S, Radhakrishnan A, Majhi AK, Raghunathan V. Structure and stoichiometry of CTAB–DNA complexes. The Journal of Chemical Physics. 2020;153(22):224901.

[16] Thomas M, Chowdhury A, Majhi AK, Raghunathan V. Columnar liquid crystalline phases of surfactant-DNA complexes. Liquid Crystals. 2021:1-10.

[17] Radhakrishnan A, Madhukar S, Chowdhury A, Raghunathan V. Influence of micellar size on the structure of surfactant-DNA complexes. Physical Review E. 2022;105(6):064504.

[18] Blandamer MJ, Briggs B, Cullis PM, Engberts JB, Kevelam J. Titration microcalorimetry of micelle formation in aqueous solutions containing alkylpolyoxyethylene glycol ethers, C 12 H 25 (OCH 2 CH 2) m OH where m= 3, 4 and 5, and octadecyltrimethylammonium bromide. Physical Chemistry Chemical Physics. 2000;2(19):4369-72.

[19] Garcia-Mateos I, Mercedes Velazquez M, Rodriguez LJ. Critical micelle concentration determination in binary mixtures of ionic surfactants by deconvolution of conductivity/concentration curves. Langmuir. 1990;6(6):1078-83.

[20] Yoshida N, Matsuoka K, Moroi Y. Micelle Formation ofn-Decyltrimethylammonium Perfluorocarboxylates. Journal of colloid and interface science. 1997;187(2):388-95.

[21] Zieliński R. Effect of temperature on micelle formation in aqueous NaBr solutions of octyltrimethylammonium bromide. Journal of colloid and interface science. 2001;235(2):201-9.

[22] Thomas M. Surfactant-Polyelectrolyte Complexes: Structure and Interactions. PhD Thesis, Jawaharlal Nehru University, New Delhi. 2019:108-16.

[23] Madhukar S. Influence of some sterols and nucleotides on the structure of self-assembled amphiphilic systems. PhD Thesis, Jawaharlal Nehru University, New Delhi. 2017:45-60.

[24] Brenner SL, Parsegian VA. A physical method for deriving the electrostatic interaction between rod-like polyions at all mutual angles. Biophysical journal. 1974;14(4):327-34.

[25] Leunissen ME, Christova CG, Hynninen AP, Royall CP, Campbell AI, Imhof A, et al. Ionic colloidal crystals of oppositely charged particles. Nature. 2005;437(7056):235-40.

[26] Maskaly GR, García RE, Carter WC, Chiang YM. Ionic colloidal crystals: Ordered, multicomponent structures via controlled heterocoagulation. Physical Review E. 2006;73(1):011402.

[27] Maskaly GR. Attractive electrostatic self-assembly of ordered and disordered heterogeneous colloids. Massachusetts Institute of Technology; 2005.

[28] van den Berg D, van Roij R. Phase Behavior of Ionic Colloidal Crystals. 2009.

[29] Reiss-Husson F, Luzzati V. The structure of the micellar solutions of some amphiphilic compounds in pure water as determined by absolute small-angle X-ray scattering techniques. The Journal of physical chemistry. 1964;68(12):3504-11.

[30] Rädler JO, Koltover I, Salditt T, Safinya CR. Structure of DNA-cationic liposome complexes: DNA intercalation in multilamellar membranes in distinct interhelical packing regimes. Science. 1997;275(5301):810-4.

[31] Inc WR. Mathematica, Version 11.0.0;. Champaign, IL, 2021. Available from: https://www.wolfram.com/mathematica.

[32] Bergström M, Pedersen JS. Structure of pure SDS and DTAB micelles in brine determined by small-angle neutron scattering (SANS). Physical Chemistry Chemical Physics. 1999;1(18):4437-46.

[33] Schmutzler T, Schindler T, Schmiele M, Appavou MS, Lages S, Kriele A, et al. The influence of n-hexanol on the morphology and composition of CTAB micelles. Colloids and Surfaces A: Physicochemical and Engineering Aspects. 2018;543:56-63.

[34] Radhakrishnan A, Ghosh SK, Pabst G, Raghunathan V, Sood A. Tuning DNA-amphiphile condensate architecture with strongly binding counterions. Proceedings of the National Academy of Sciences. 2012;109(17):6394-8.

[35] Lai E, van Zanten JH. Monitoring DNA/poly-L-lysine polyplex formation with time-resolved multiangle laser light scattering. Biophysical journal. 2001;80(2):864-73.

[36] Oskolkov NN, Potemkin II. Complexation in asymmetric solutions of oppositely charged polyelectrolytes: Phase diagram. Macromolecules. 2007;40(23):8423-9.

[37] Hayashi Y, Ullner M, Linse P. Oppositely charged polyelectrolytes. Complex formation and effects of chain asymmetry. The Journal of Physical Chemistry B. 2004;108(39):15266-77.

[38] Grason GM, Bruinsma RF. Chirality and equilibrium biopolymer bundles. Physical review letters. 2007;99(9):098101.

# Chapter 3

# Effect of adsorbed polyelectrolytes on the interactions and elasticity of charged surfactant bilayers

## 3.1 Introduction

Ionic amphiphiles, that self-assemble into bilayers, form a highly swollen lamellar phase in aqueous solutions, as a result of long-range electrostatic inter-bilayer repulsion[1–3]. Addition of an oppositely charged polyelectrolyte to the solution has a very pronounced effect on the inter-bilayer interactions, which depends sensitively on the salt concentration ($[C_s]$) in the solution ([4,5]. At low $[C_s]$ the polyelectrolyte forms a heterogeneous adsorption layer on the bilayer surface, due to the electrostatic repulsion between the chains, as has been observed in the case of polyelectrolyte adsorption on oppositely charged rigid surfaces[6]. The presence of a patchy adsorption layer leads to the creation of polymer bridges between adjacent bilayer surfaces, resulting in an effective inter-bilayer attraction[4,7]. As a consequence, a compact surfactant-polyelectrolyte complex precipitates out of the solution, in which a thin polyelectrolyte layer is sandwiched between successive bilayers[8]. The lamellar periodicity of this complex is only slightly higher than the bilayer thickness. On increasing $[C_s]$ a homogeneous adsorption layer is formed on the bilayer surface due to the screening of inter-chain repulsion[4,6,9]. Bridging of neighboring bilayers is no longer possible[10] and the polyelectrolyte covered bilayers form a swollen complex, stabilized either by steric repulsion[11] between the adsorbed chains on adjacent bilayers or by undulation repulsion[12], if the bilayer bending rigidity, $\kappa$ is sufficiently low. At high $[C_s]$ the polyelectrolyte desorbs from the bilayer surface. Since the electrostatic inter-bilayer repulsion is highly screened, van der Waals attraction dominates and the bilayers again form a lamellar phase with a very low periodicity, but with no polyelectrolyte in the intervening aqueous layer between the bilayers. In this chapter we report such salt induced swellig and de-swelling transition of complexes of ionic surfactants didodecyldimethylammonium chloride (DDAC) and dioctadecyldimethylammonium chloride (DOAC) with sodium salt of poly-acrylic acid (PAANa). Elasticity of a bilayer is described in terms of two moduli; the bending rigidity modulus $\kappa$ and the Gaussian rigidity modulus $\bar{\kappa}$, which are associated with the mean and Gaussian curvatures of the surface, respectively[13,14]. Stability requires $\kappa$ to be positive, whereas there is no such restriction on the sign of $\bar{\kappa}$. Polymer adsorption on a bilayer has been predicted to alter both $\kappa$ and $\bar{\kappa}$[15,16]. $\kappa$ is expected to decrease, whereas $\bar{\kappa}$ is expected to increase in the presence of an adsorption layer. The DDAC-water

system forms a swollen $L_\alpha$ phase when the electrostatic repulsion between the bilayers is screened by the addition of NaCl. The lamellar periodicity of this phase is determined by undulation repulsion between the bilayers, which depends on $\kappa$[12,17]. If the swollen DDAC-PAANa complex is also stabilized by undulation repulsion between the bilayers, it should in principle be possible to ascertain the effect of polymer adsorption on $\kappa$ by comparing the maximal lamellar periodicities of the swollen complex and the DDACwater- NaCl system. But it was not possible to address this issue unequivocally , since the lamellar periodicity of the swollen complex showed a large spread, presumably as a result of the extremely slow equilibration due to the irreversible nature of the adsorption process[18]. In this chapter we also present studies on complexes of the ionic surfactant didodecyldimethylammonium bromide (DDAB) and PAANa. This system also exhibits the swelling and deswelling transitions observed in DDAC-PAANa complexes. However, instead of forming a lamellar phase, the swollen complexes in the present system exhibits the sponge phase. The lamellar to sponge transition of bilayers is known to occur when $\bar{\kappa}$ increases and becomes weakly negative[19–22]. Therefore, the present results confirm that binding of PAANa to DDAB bilayers leads to an increase in $\bar{\kappa}$, in agreement with theoretical predictions. Formation of the sponge phase in DDAB-PAANa complexes, but not in DDAC-PAANa complexes, can be understood in terms of differences in the phase behaviour of aqueous solutions of these two surfactants, which suggest that DDAB bilayers have a higher $\bar{\kappa}$ compared to DDAC bilayers. Hence it should be easier to drive DDAB bilayers into the sponge phase than DDAC bilayers, in agreement with our observations.

## 3.2 Materials and methods

DDAB, DDAC, PAANa ($M_w$ = 2100, 5100, 8000 and 15 000) and NaBr were purchased from Sigma-Aldrich and were used without further purification. Samples were prepared over a wide range of $\phi$ at a few values of R, $\phi$ being the combined weight percentage of surfactant and PAANa, and R the polyelectrolyte to surfactant weight ratio. Values of R chosen were much above the isoelectric point of the system ($R_{iso}$ = 0.2), so that the coexisting aqueous solution in all cases contained uncomplexed polyelectrolyte. Ranges of $\phi$ and R were chosen in order to obtain all possible structures of the complexes. Samples were prepared in Millipore water and were kept at 40 °C for about a month for equilibration. Complexes were studied using polarizing optical microscopy (POM), small–angle x-ray scattering (SAXS) and cryogenic-scanning electron microscopy (cryo-SEM). In addition, composition of some of the complexes was probed using thermogravimetric analysis (TGA).

## 3.3 Results

### 3.3.1 Effect on polymer adsorption on DDAC bilayers

By keeping R fixed at 14, DDAC-PAANa2100 samples were prepared by varying the $\phi$ from 20 to 60. At $\phi$=20 a white precipitate is found. The solution becomes turbid at $\phi$=30. SAXS patterns of DDAC-PAANa2100 samples at different $\phi$ are shown in fig. 3.1. The variation of d-spacing with *phi* is given in fig.3.2. At $\phi$= 20, the spacing is 3.4 nm, which is about 1 nm higher than the bilayer

thickness. At $\phi$= 30, the spacing increases to $\sim$ 18 nm. On increasing the $\phi$ to 60, the spacing reduces to $\sim$ 7 nm.

Effect of salt is also studied on the phase behaviour of DDAC-PAANa2100 samples. $\phi$ is fixed at 20 and R=14. The [NaCl] concentration is varied from 0 to 1 M. The SAXS patterns are shown in fig. 3.3. variation of d-spacing with [NaCl] concentration is shown in fig. 3.4. In the absence of externaly added NaCl the spacing is $\sim$ 3.4 nm. At [NaCl]= 300mM, the spacing increases to $\sim$ 18 nm. At higher [NaCl] ([$C_s$ $\sim$ 400 mM]) concentration the spacing reduces to $\sim$ 3.2 nm.

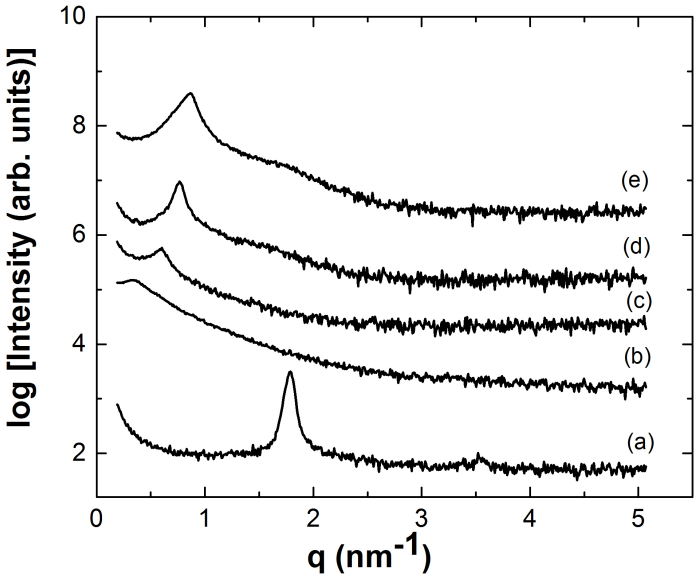


FIGURE 3.1: SAXS patterns of DDAC-PAANa2100 samples at R=14, for $\phi$ ranging from 20 to 60. (a) 20, (b) 30, (c) 40, (d) 50, (e) 60.

From fig. 3.2 and fig. 3.4 it is clear that there is a transition from a collapsed lamellar phase ($L_\alpha^c$) $\rightarrow$ swollen lamellar phase ($L_\alpha$) on decreasing the water content, i.e. on increasing $\phi$, or on increasing the salt concentration at fixed $\phi$. To understand the phase behaviour of DDAC-PAANa2100 samples in greater detail we have studied the phase diagram in the R-[NaCl] plane by keeping the concentration of DDAC fixed at 5wt%. Typical SAXS patterns of samples for varying NaCl concentration are shown in fig.3.5, fig. 3.6 and fig. 3.7. Corresponding variation of d-spacing with salt concentration is shown in fig. 3.8, fig. 3.9 and fig. 3.10. The phase diagram is shown in fig. 3.11. At low values of R, irrespective of the salt concentration only the $L_\alpha^c$ phase is observed. At intermediate values of R (R $>$ 4), a coexistence of swollen lamellar ($L_\alpha$) and a collapsed lamellar phase ( $L_\alpha^c$) is observed up to [NaCl] $\sim$ 300mM. At high values of R (R $>$ 12) and high [NaCl] ($>$ 300 mM) only a swollen lamellar phase ($L_\alpha$) is observed. Cryo-SEM images show a layered morphology, which is typical of a lamellar phase (fig. 3.12).

Effect of polymer chain length is studied by using PAANa of molecular weight 8000. SAXS pattern of DDAC-PAANa8000 samples at R=14 and $\phi$= 20 for varying NaCl concentration is shown in fig. 3.13. Variation of d-spacing with [NaCl] is shown in fig. 3.14. In this case the swollen $L_\alpha$ phase is not found. In water the spacing is $\sim$ 3.3 nm. On increasing the NaCl concentration to 300 mM, the spacing increases to $\sim$ 3.53 nm. At [NaCl]= 1M, the spacing is $\sim$ 3.2 nm.

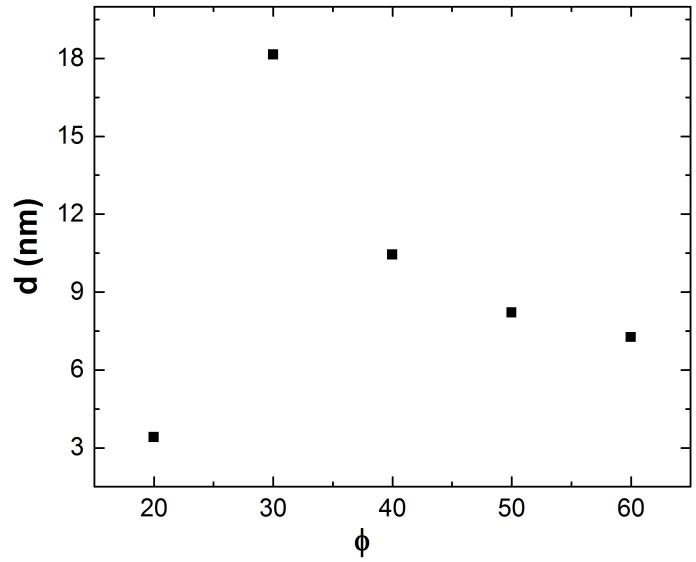


FIGURE 3.2: Variation of d-spacing for DDAC-PAANa2100 samples at R=14; $\phi$ ranging from 20 to 60.

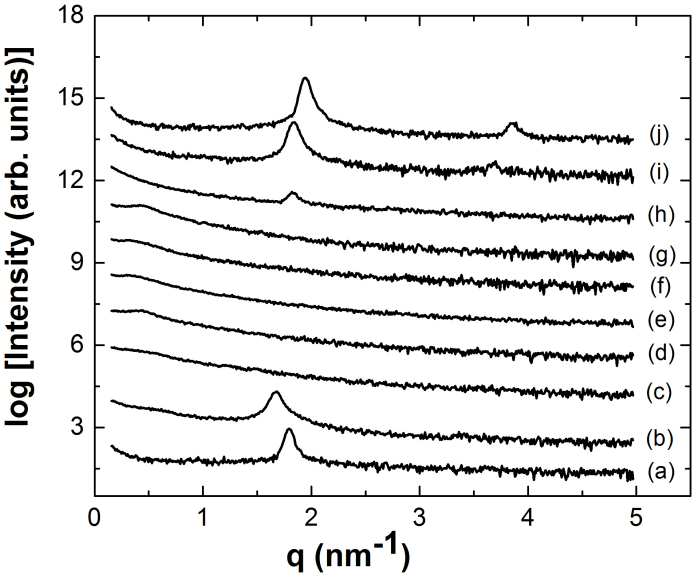


FIGURE 3.3: SAXS patterns of DDAC-PAANa2100 samples at R=14 and $\phi$= 20 in (a) water and in NaCl concentrations of (b) 100 mM, (c) 150 mM, (d) 200 mM, (e) 250 mM, (f) 300 mM, (g) 350 mM, (h) 400 mM, (i) 500 mM and (i) 1 M.

TGA of the two lamellar complexes formed at low and high- [$C_s$] were carried out to determine their composition (fig. 3.15 ). TGA curves of the surfactant and polymer solutions were also collected for reference. Both of them show a step at around 100 °C corresponding to the loss of water. Loss of the surfactant occurs at around 200 °C, whereas that of the polymer occurs at around 400 °C. The large difference in the degradation temperatures of these two species makes it easier to determine their relative abundance in the complex. Three steps can be seen in the TGA curve

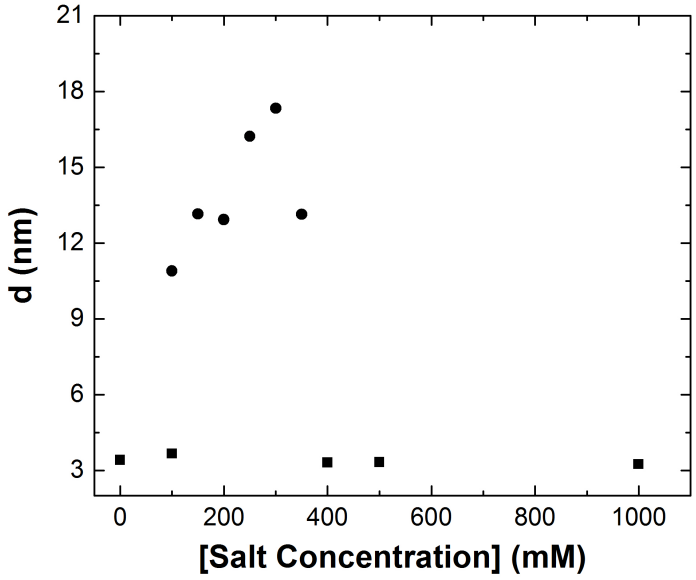


FIGURE 3.4: Variation of d-spacing with NaCl concentration for DDAC-PAANa2100 samples at R=14 and $\phi$= 20.

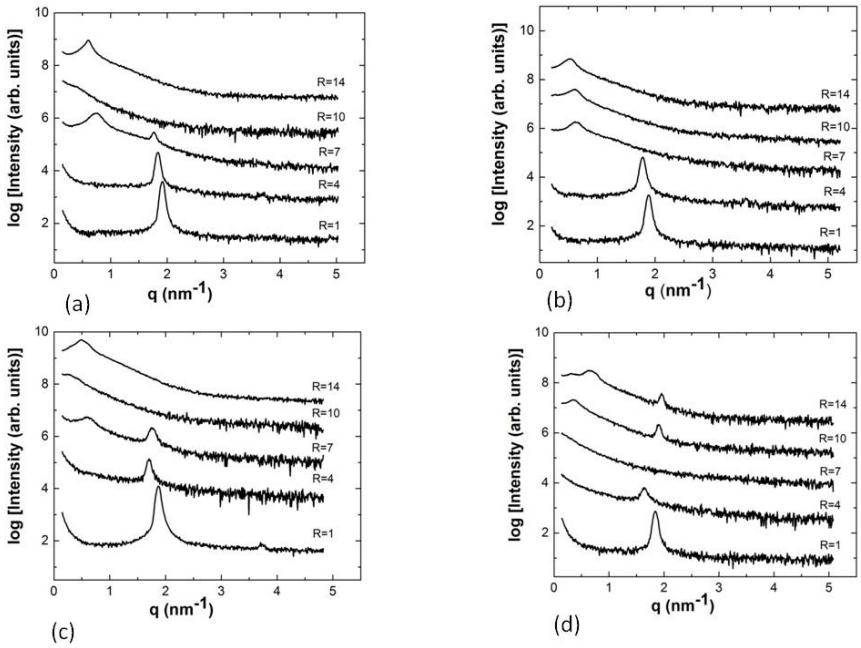


FIGURE 3.5: Typical SAXS patterns of 5 wt% DDAC samples at $\phi$=20 (a) in water, and at NaCl concentration of (b) 100 mM, (c) 150 mM, and (d) 200 mM, for varying R.

of the low-[$C_s$] complex at around 100 °C, 200 °C and 400 °C. The step at 400 °C, corresponding to the polyelectrolyte, is absent in the TGA trace of the high-[$C_s$] complex.

### 3.3.2 Effect on polymer adsorption on DOAC bilayers

By keeping R fixed at 7 and 14, DOAC-PAANa2100 samples were prepared by varying $\phi$ from 20 to 70. SAXS profiles of R=7 samples are shown in fig. 3.16. The observed variation of d-spacing is

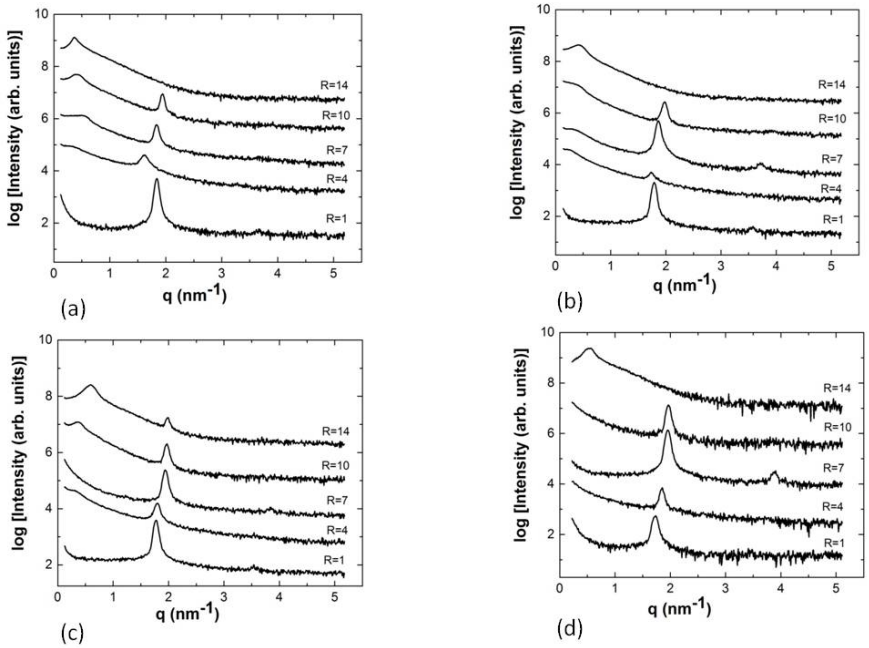


FIGURE 3.6: Typical SAXS patterns of 5 wt% DDAC samples at $\phi$=20 at NaCl concentrations of (a) 250 mM, (b) 300 mM,(c) 350 and (d) 400 mM, for varying R.

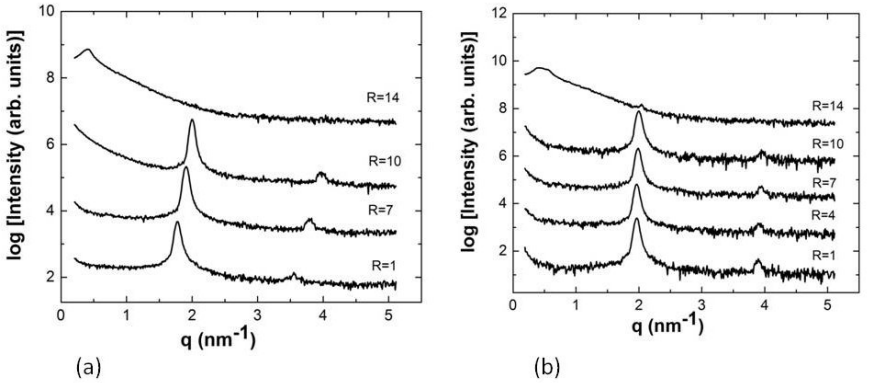


FIGURE 3.7: Typical SAXS patterns of 5 wt% DDAC samples at $\phi$=20 at NaCl concentrations of (a) 500 mM and (b) 1 M, for varying R.

shown in fig. 3.17. At $\phi$= 20, only a collapsed lamellar phase ($L_\alpha^c$) with d $\sim$ 4.4 nm is found. At $\phi$= 30, a coexistence of two lamellar phases with different periodicities are observed ( d $\sim$ 4.2 nm and $\sim$ 14 nm). At $\phi$= 70, the observed spacings are d= 3.79 nm and d= 7.4 nm. SAXS profiles of R=14 samples are shown in fig. 3.18. The observed variation of d-spacing is shown in fig. 3.19. At $\phi$= 20, the observed lamellar periodicity is $\sim$ 4.4 nm. The spacing increases to $\sim$ 11 nm, at $\phi$= 40. At $\phi$= 70, the spacing reduces to $\sim$ 7.5 nm.

Effect of salt is also studied on the phase behaviour of DOAC-PAANa2100 samples. $\phi$ is fixed at 20 and R=14. [NaCl] concentration is varied from 0 to 500 mM. The SAXS patterns are shown in fig. 3.20. Variation of d-spacing with [NaCl] concentration is shown in fig. 3.21. In the absence of externaly added NaCl the spacing is $\sim$ 3.4 nm. At [NaCl]= 300mM, the spacing increases to $\sim$ 18 nm. At higher [NaCl] ([$C_s$] $\sim$ 400 mM) concentration the spacing reduces to $\sim$ 3.2 nm. For other set of experiments, DOAC concentration was fixed at 5wt%, and NaCl concentration is varied from 0 to 500 mM. Typical SAXS patterns of 5wt% DOAC samples for varying R and NaCl

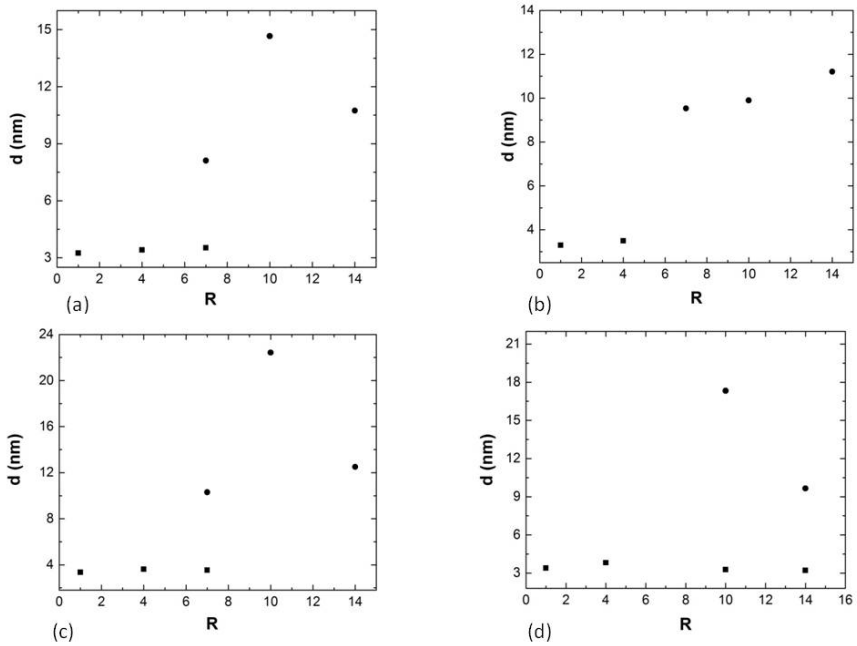


FIGURE 3.8: Typical variation of d-spacing of 5 wt% DDAC samples at $\phi$=20 in (a) water, and at NaCl concentrations of (b) 100 mM, (c) 150 mM, and (d) 200 mM, for varying R.

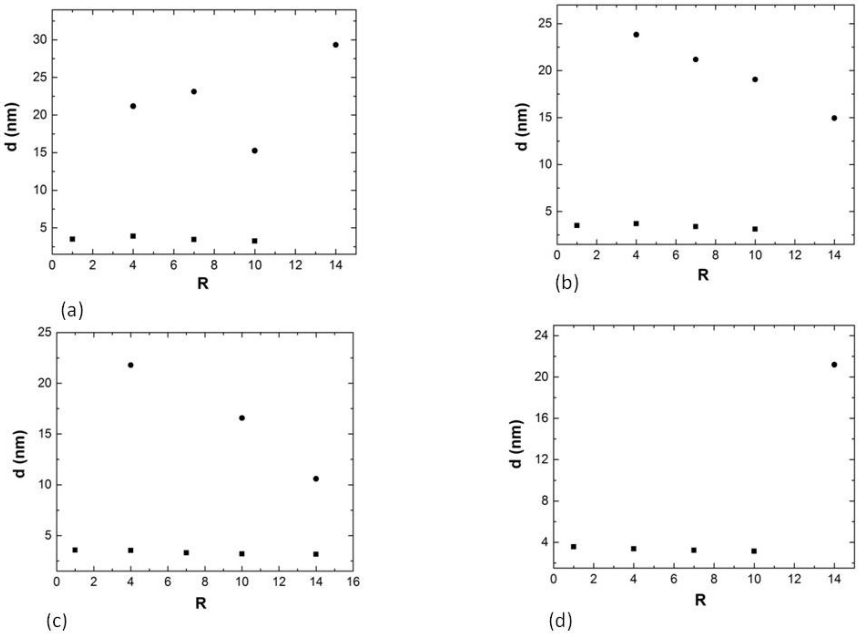


FIGURE 3.9: Typical variation of d-spacing of 5 wt% DDAC samples at $\phi$=20 at NaCl concentrations of (a) 250 mM, (b) 300 mM,(c) 350 and (d) 400 mM, for varying R.

concentration is shown in fig. 3.22 and fig. 3.23. Variation of d-spacing is shown in fig. 3.24 and fig. 3.25. Cryo-SEM images show layered morphology, which is typical of the lamellar phase (fig. 3.26).

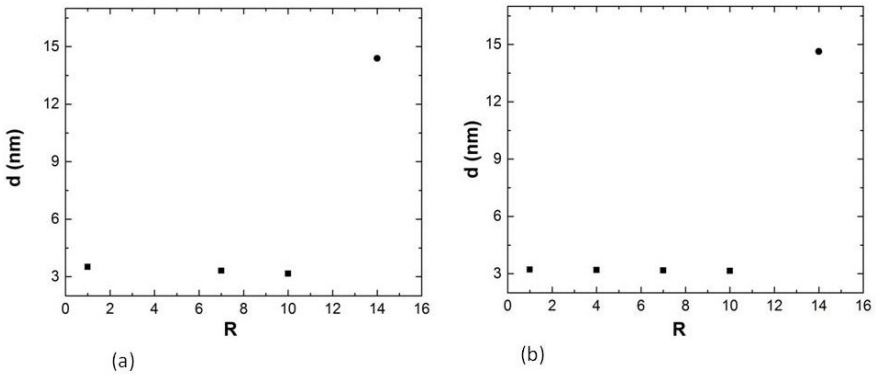


FIGURE 3.10: Typical variation of d-spacing of 5 wt% DDAC samples at $\phi$=20 at NaCl concentrations of (a) 500 mM, and (b) 1 M, for varying R.

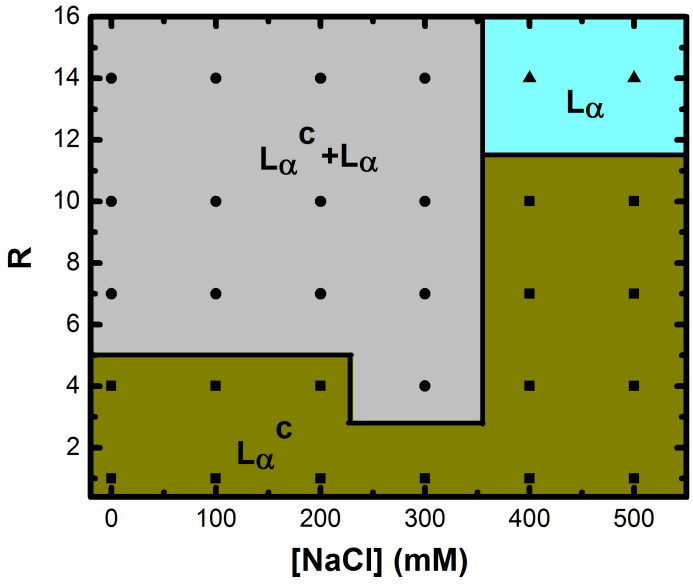


FIGURE 3.11: Phase diagram of DDAC-PAANa2100 samples in the R- [NaCl] plane.

### 3.3.3 Effect of polymer absorption on DDAB bilayers

Keeping R fixed at 14, $\phi$ is varied for DDAB-PAANa5100 samples from $\phi$= 20 to 70. SAXS pattern of DDAB-PAANa5100 samples are shown in fig. 3.27. Variation of d-spacing with $\phi$ is shown in fig. 3.28. At $\phi$= 20, the spacing is $\sim$ 3.5 nm. At $\phi$=40, two distinct peaks are observed correspond to spacings of 3.1 nm and $\sim$ 24 nm. At $\phi$=70, a single sharp peak is observed correspond to a spacing of $\sim$ 2.8 nm. POM images of the precipitate formed at $\phi$ = 70 show a Maltese cross texture typical of a dispersion of multilamellar vesicles (fig. 5.27).

Effect of chain length is also studied. Fig. 3.30 shows the SAXS patterns of DDAB- PAANa8000 samples, for varying $\phi$. R is kept fixed at 14. Variation of d-spacing with $\phi$ is shown in fig. 3.31. At $\phi$= 20, the spacing is 3.35 nm. At $\phi$=30, the spacing increases to 3.52 nm. At $\phi$=70, the observed spacing is 2.84 nm. Effect of salt is also studied by varying the NaBr concentration , at $\phi$= 20 and R= 14. Fig. 3.32 shows SAXS patterns of DDAB-PAANa8000 samples for varying NaBr concentration. Variation of d-spacing is shown in fig. 3.33. Effect of salt is also studied for DDAB-PAANa15000

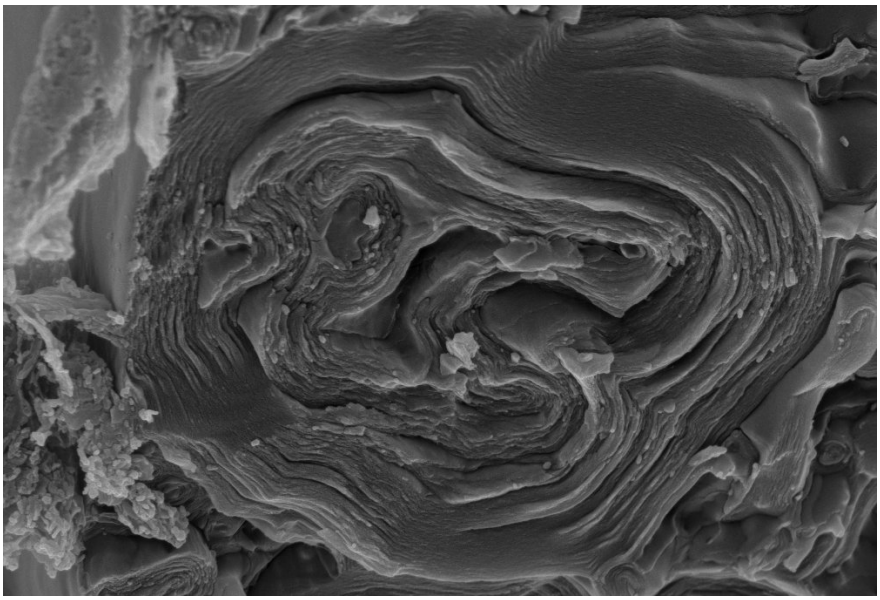

FIGURE 3.12: Cryo-SEM image of a DDAC-PAANa2100 sample at 5wt% DDAC, R=10.

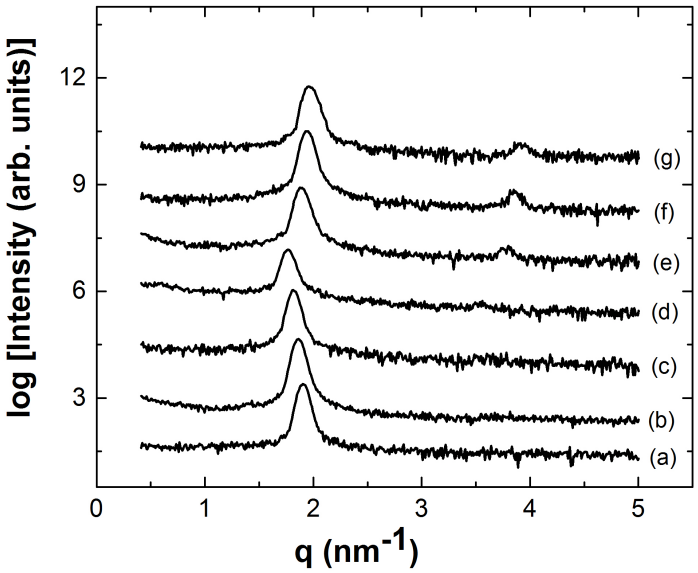


FIGURE 3.13: SAXS patterns of DDAC-PAANa2100 samples at R=14 and $\phi$= 20 in (a) water and at NaCl concentrations of (b) 100 mM, (c) 200 mM, (d) 300 mM, (e) 450 mM, (f) 500 mM, and (g) 1 M.

samples. The effect is found to be very similar to that observed in PAANa8000 samples. SAXS patterns are shown in fig. 3.34. Variation of d-spacing is shown in fig. 3.35.

TGA of the two lamellar complexes formed at low and high-[$C_s$] were carried out to determine their composition (fig. 3.36 ). TGA curves of DDAB and polymer solutions were also collected for reference. Both of them show a step at around 100 °C corresponding to the loss of water. Loss of the surfactant occurs at around 200 °C, whereas that of the polymer occurs at around 400 °C. The large difference in the degradation temperatures

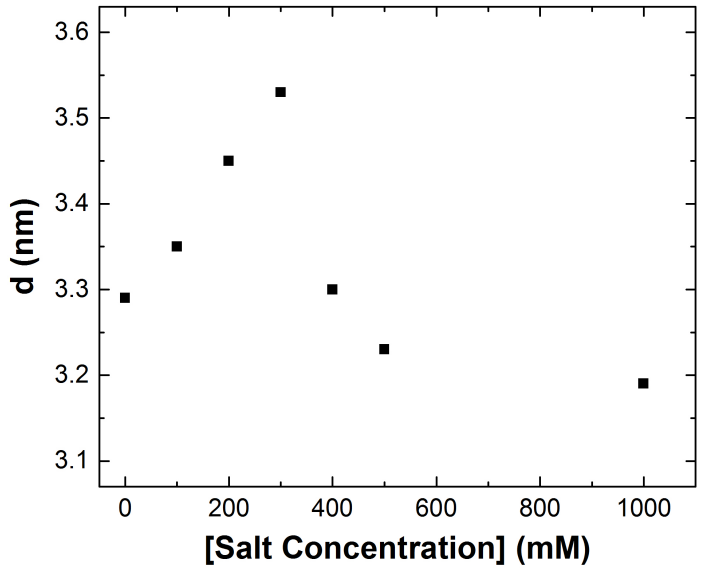


FIGURE 3.14: Variation of d-spacing with NaCl concentration for DDAC-PAANa8000 samples at R=14 and $\phi$= 20.

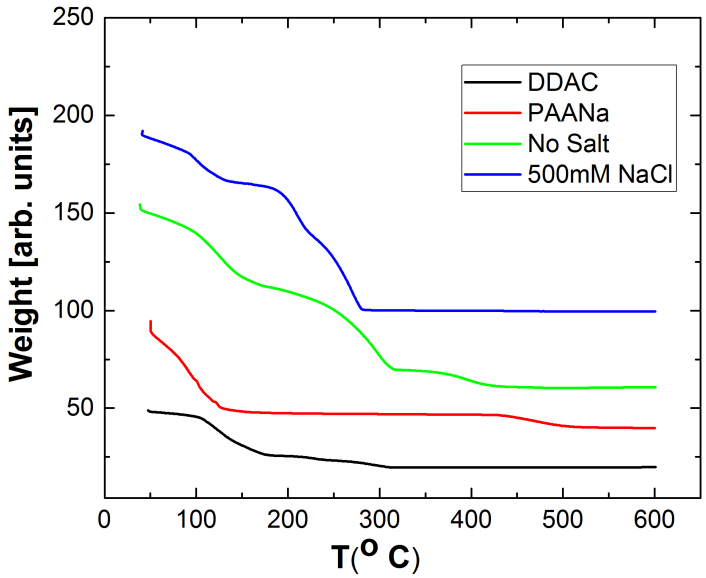


FIGURE 3.15: TGA traces of DDAC, PAANa, and DDAC-PAANa complexes at [NaCl] = 0 and 500 mM.

## 3.4 Discussions

DDAC in water forms a lamellar phase over a wide range of concentrations[23]. A detailed discussion of the formation of oppositely charged surfactant- polymer complex is presented in the introduction and in chapter 2 of the thesis. In this chapter we have studied the phase behaviour of DDAC-PAANa complexes by varying the polymer to surfactant weight ratio (R) and also the chain length of the polymer. R is varied from 1 to 14, which is much above the isoelectric point of

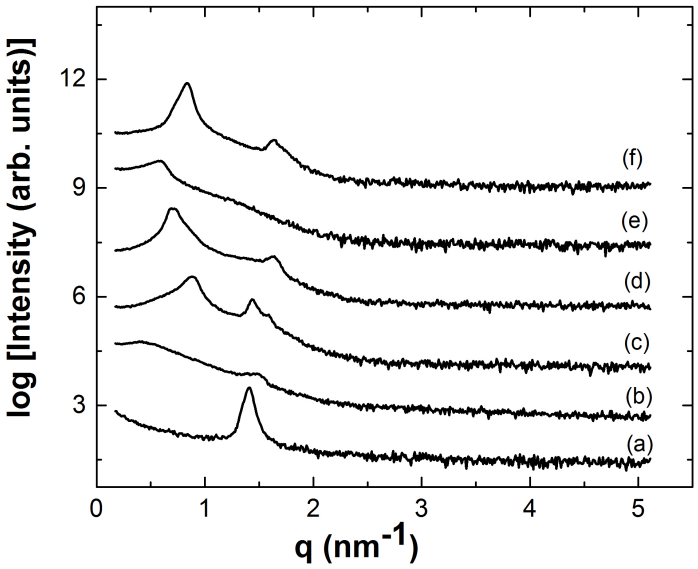


FIGURE 3.16: SAXS patterns of DOAC-PAANa2100 samples at R=7; $\phi$ ranging from 20 to 70. (a) 20, (b) 30, (c) 40, (d) 50, (e) 60, (f) 70.

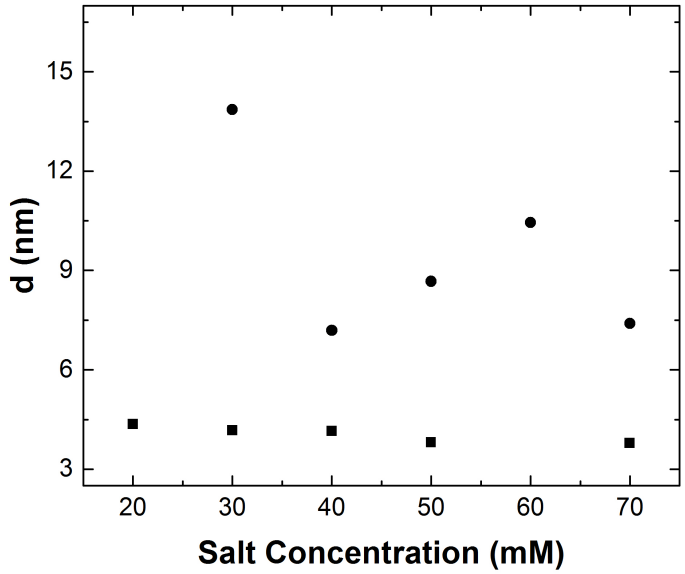


FIGURE 3.17: Variation of d-spacing for DOAC-PAANa2100 samples at R=7; $\phi$ ranging from 20 to 70.

the system ( $R_{iso}$= 0.2). At low $\phi$ only a collapsed lamellar phase in found ($L_{\alpha}^{c}$), irrespective of the length of the polymer. The charge density of PAANa (1/0.25 nm) is higher than the charge density of DDAC (1/0.68 $nm^2$)[24,25]. The polyelectrolyte adsorption layer formed at low salt concentration is heterogeneous as a result of inter-chain electrostatic repulsion[6]. Hence it is reasonable to assume that the collapsed lamellar complex occurring at low salt concentration is stabilized by bridging of adjacent bilayers by the polyelectrolyte chains or by the patch charge interactions between the bilayers[7,26,27]. Absence of the swelling transition for higher molecular weights of

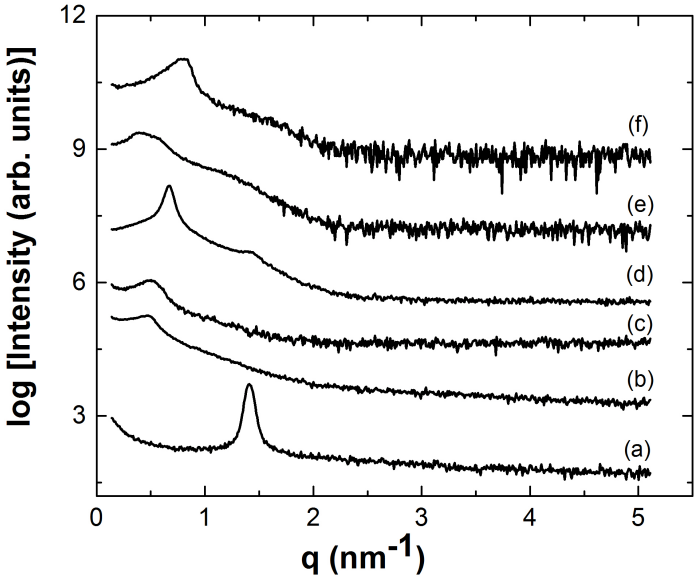


FIGURE 3.18: SAXS patterns of DOAC-PAANa2100 samples at R=14; $\phi$ ranging from 20 to 70. (a) 20, (b) 30, (c) 40, (d) 50, (e) 60, (f) 70.

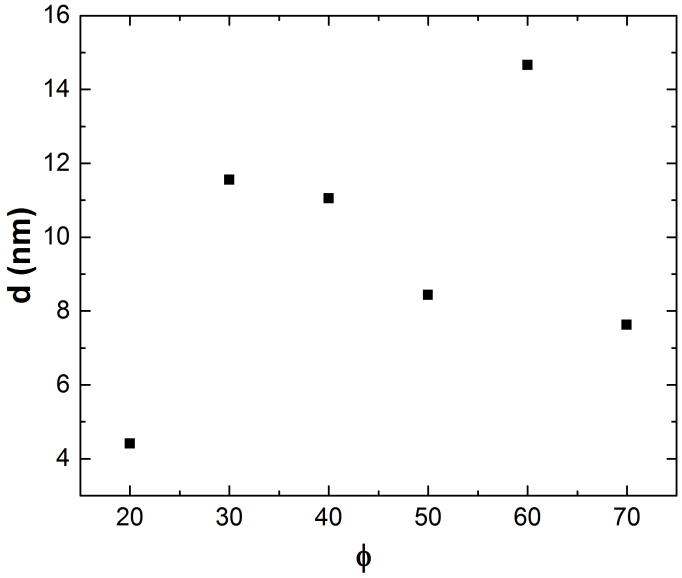


FIGURE 3.19: Variation of d-spacing for DOAC-PAANa2100 samples at R=14; $\phi$ ranging from 20 to 70.

the polyelectrolyte, as seen in DDAC-PAANa complexes can be attributed to the enhancement of the bridging attraction with increasing contour length of the polymer[7]. With increase in $\phi$, a swollen lamellar phase ($L_\alpha$) phase is found in the case of DDAC-PAANa2100 complexes. An increase is $\phi$ results an increase in salt concentration. This will reduce the repulsive interaction between the polymer chains. Hence there maybe an enhancement of the polymer adsorption on the bilayer surface. An abrupt increase of polyelectrolyte adsorption on incrasing the salt concentration is reported in[6,28]. The $L_\alpha^c \rightarrow L_\alpha$ transition observed in the present case can be attributed

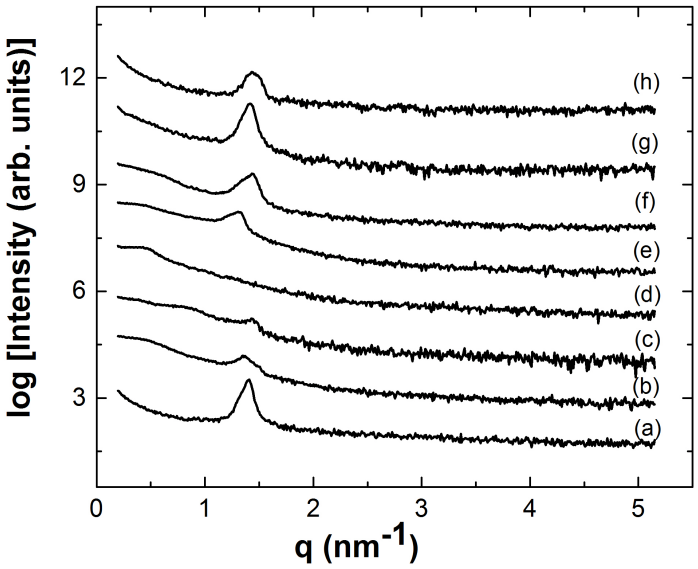


FIGURE 3.20: SAXS patterns of DOAC-PAANa2100 samples at R=14 and $\phi$= 20 in (a) water and at NaCl concentrations of (b) 100 mM, (c) 200 mM, (d) 250 mM, (e) 300 mM, (f) 350 mM, (g) 400mM, and (h) 500 mM.

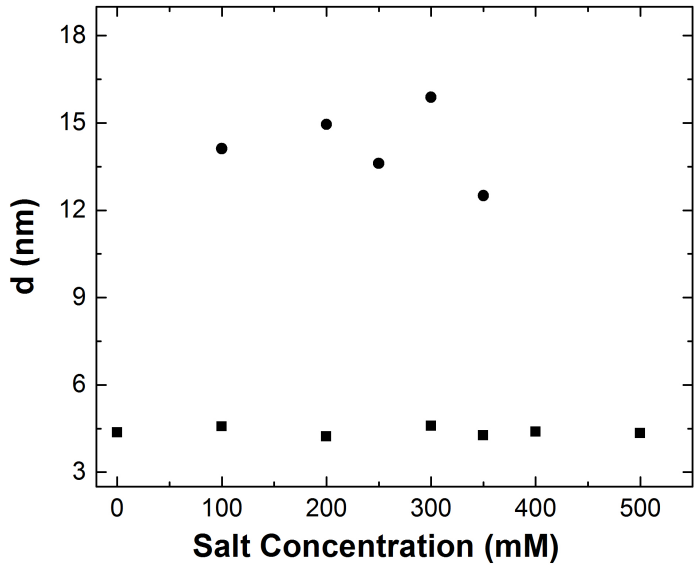


FIGURE 3.21: Variation of d-spacing with NaCl concentration for DOAC-PAANa2100 samples at R=14 and $\phi$= 20.

to the increase of polymer adsorption on the bilayer surface[5]. From fig. 3.2 and fig. 3.4 it is clear that increase of $\phi$ and increase in salt concentration at fixed $\phi$ have similar effects on the phase behaviour of DDAC-PAANa complexes. This is because at fixed R, an increase in $\phi$ increases NaCl concentration in the solution, which is similar to increasing the NaCl concentration at fixed $\phi$. At high salt concentration ([NaCl]$\sim$ 0.4 M) another collapsed lamellar phase ($L_\alpha^{c2}$) is observed. Even for DDAC-PAANa8000 samples, where no swelling is observed at intermediate

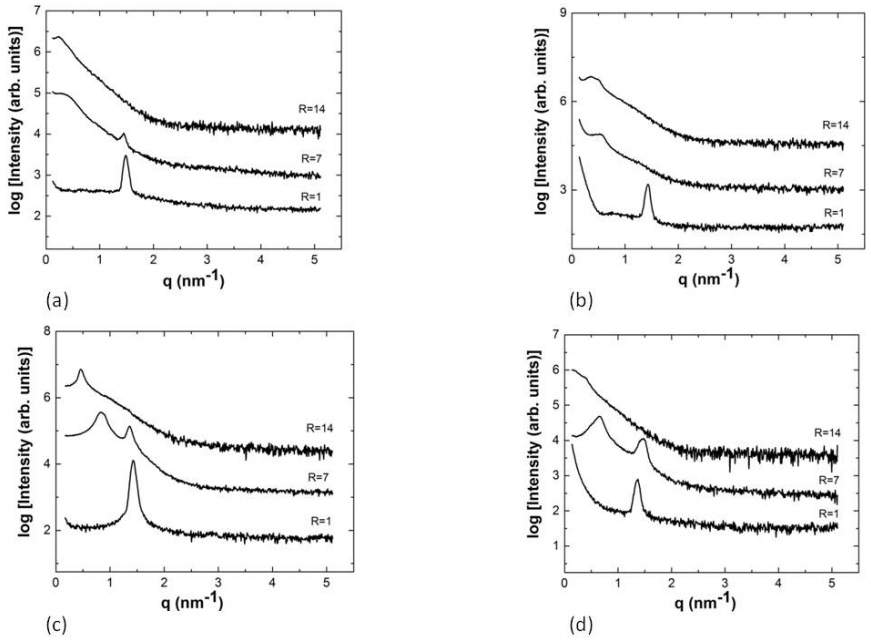


FIGURE 3.22: Typical SAXS patterns of 5 wt% DOAC samples at $\phi$=20 (a) in water, and at NaCl concentrations of (b) 100 mM, (c) 200 mM, and (d) 300 mM, for varying R.

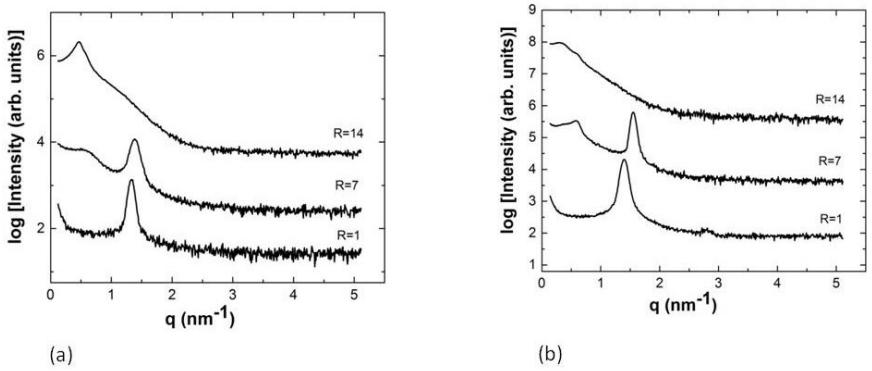


FIGURE 3.23: Typical SAXS patterns of 5 wt% DOAC samples at $\phi$=20 at NaCl concentrations of (a) 400 mM and (b) 500 mM,for varying R.

salt concentration, the lamellar periodicity decreases at high salt concentration. Xie et al. report that [$C_s$] $\sim$ 1 M, polyelectrolytes desorb from the surface[9]. TGA thermograms of the complexes clearly show that the low salt concentration lamellar phase contains both the surfactant and the polyelectrolyte, whereas the high salt concentration lamellar phase is composed of only the surfactant. This is in conformity with the reported inability of the polyelectrolyte chains to adsorb on the bilayer at high salt concentration, when the electrostatic attraction between the chains and the bilayer is fully screened. This observation supports the hypothesis that the collapsed lamellar phase at high salt concentration is stabilized by inter-bilayer van der Waals attraction. Phase diagram of DDAC-PAANa2100 complexes in the R-NaCl plane is shown in fig. 3.11. It is clear that at low R only a collpased lamellar phase is observed irrespective of the salt concentration. After a threshold value of R a coexistence between a collapsed lamellar phase and swollen lamellar phase is observed. So it is clear that the presence of excess polymer in the solution is needed to

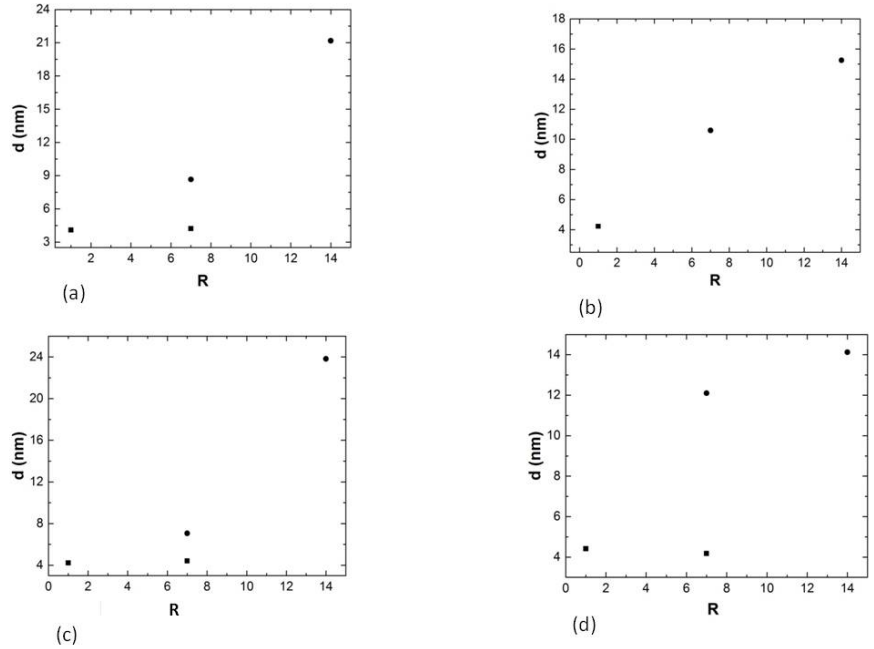


FIGURE 3.24: Typical variation of d-spacing of 5 wt% DOAC samples at $\phi$=20 in (a) water, and in NaCl concentrations of (b) 100 mM, (c) 200 mM, and (d) 300 mM, for varying R.

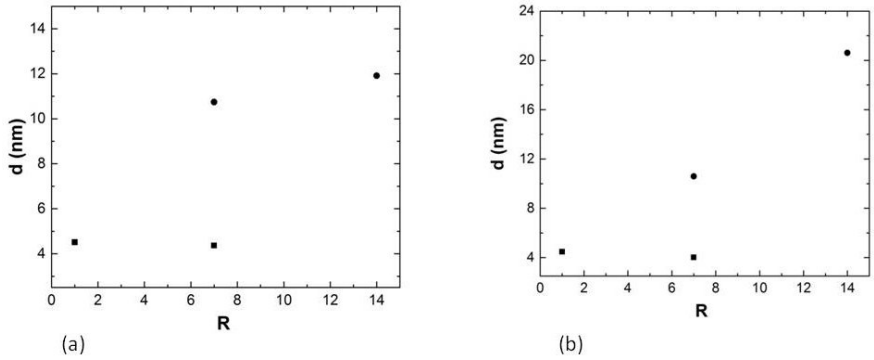


FIGURE 3.25: Typical variation of d-spacing of 5 wt% DOAC samples at $\phi$=20 in NaCl concentrations of (a) 400 mM, and (d) 500 mM, for varying R.

observe the swelling. In the coexistence range a large spread of d-spacing is observed (10-25 nm). At present we do not know what precisely determines the spacing of the swollen phase. Further work needs to be done to understand this behaviour. At high value of R and high salt concentration only a swollen lamellar phase is observed. This phase maybe similar to the swollen lamellar phase of pure DDAC bilayers, since at that high salt concentration we expect polymers to desorb from the bilayer surface.

The phase behaviour DOAC-PAANa samples are found to be similar to that of DDAC-PAANa samples. The d-spacing in the collapsed phase is found to be slightly higher than in the DDAC-PAANa complexes. This is due to the higher chain length of DOAC compared to DDAC, resulting in a thicker bilayer. In the case of DOAC also a spread in the d-spacing (10-25 nm) is observed in the $L_\alpha$ phase. This shows that changing the surfactant chain length fron 16 ( DDAC) to 18 ( DOAC), does not have any significant impact on the phase behaviour of their complexes with PAANa.

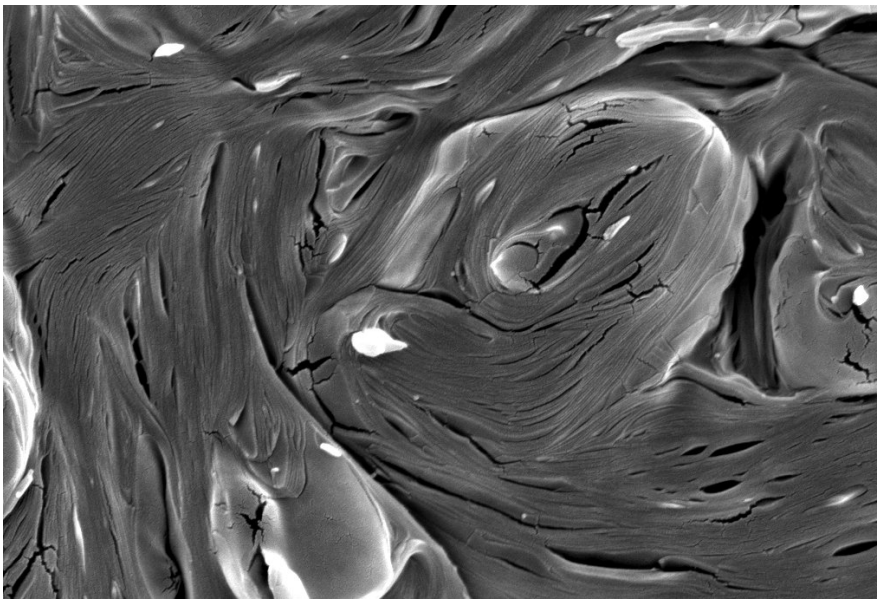

FIGURE 3.26: Cryo-SEM image of DOAC-PAANa2100 sample at 5wt% DOAC, R=14.

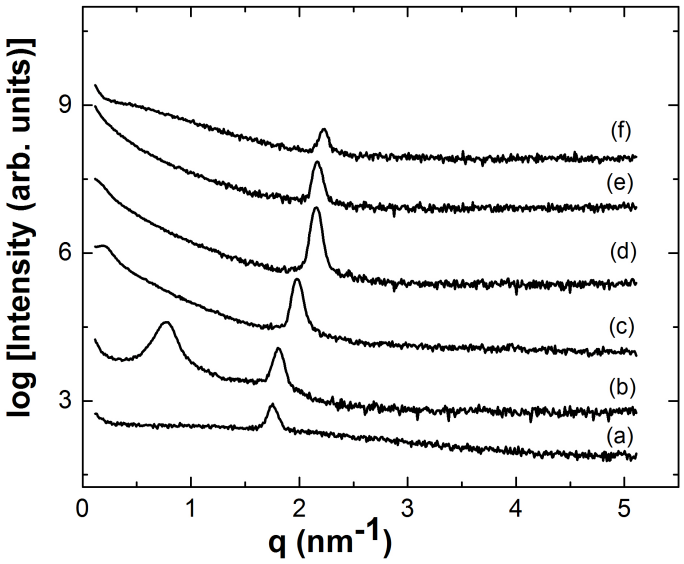


FIGURE 3.27: SAXS patterns of DDAB-PAANa5100 samples at R=14; $\phi$ ranging from 20 to 70. (a) 20, (b) 30, (c) 40, (d) 50, (e) 60, (f) 70.

The phase behaviour of DDAB-PAAna complexes are found to be different from that of DDAC-PAANa (or DOAC- PAANa) complexes. At $\phi$=20, a lamellar phase is found with d $\sim$ 3.5 nm. On increasing $\phi$ for DDAB-PAANa5100 complexes a swollen phase is observed fig. 3.28.At $\phi$= 70 again a lamellar phase is found with d $\sim$ 2.8 nm. But unlike in the previous cases where the swollen phase also was a lamellar phase, here the swollen phase is a sponge phase ($L_3$). A detailed analysis of the phase behaviour of DDAB-PAANa complexes is given in ref.[29,30]. The swollen phase was found to be optically isotropic. SAXS data of the isotropic complexes were fitted to a model of the sponge ($L_3$) phase described in the literature[31]. DDAB-PAANa8000 and DDAB-PAANa15000 do not exhibit the swelling behavior and they form a lamellar phase of very

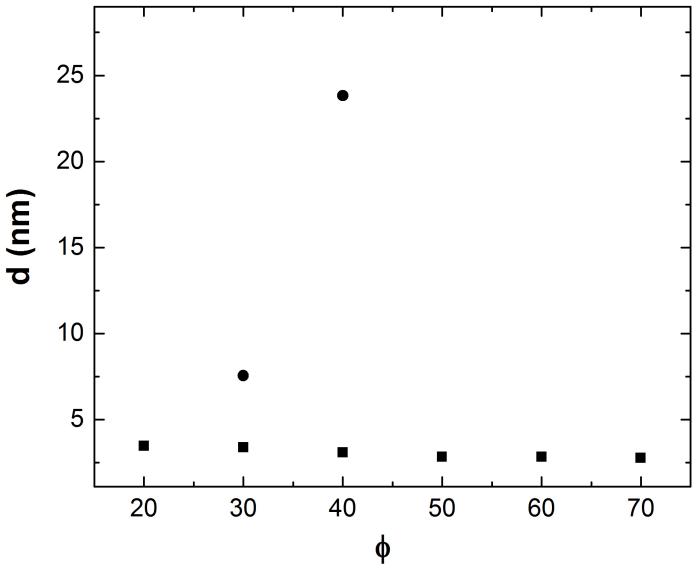


FIGURE 3.28: Variation of d-spacing for DDAB-PAANa5100 samples at R=14; $\phi$ ranging from 20 to 70.

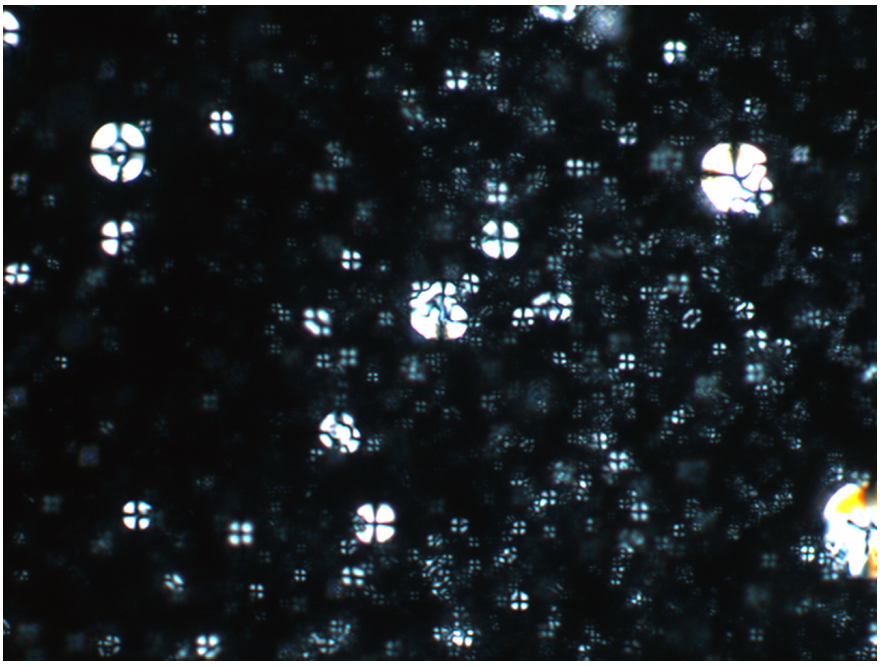

FIGURE 3.29: POM image of the second collapsed phase at R = 14 and $\phi$ = 70, showing a dispersion of multilamellar vesicles.

low periodicity for all values of $\phi$. However, the lamellar periodicity shows a non-monotonic dependence on $\phi$, with a maximum at $\phi \sim 30$. TGA analyses of the complexes clearly show that the low salt concentration lamellar phase contains both the surfactant and the polyelectrolyte, whereas the high salt concentration lamellar phase is composed of only the surfactant, similar to the behaviour of DDAC-PAANa complex.

As mentioned in the introduction, this swollen phase can in principle be stabilized by two types of repulsive interactions; steric repulsion between the adsorption layers and undulation

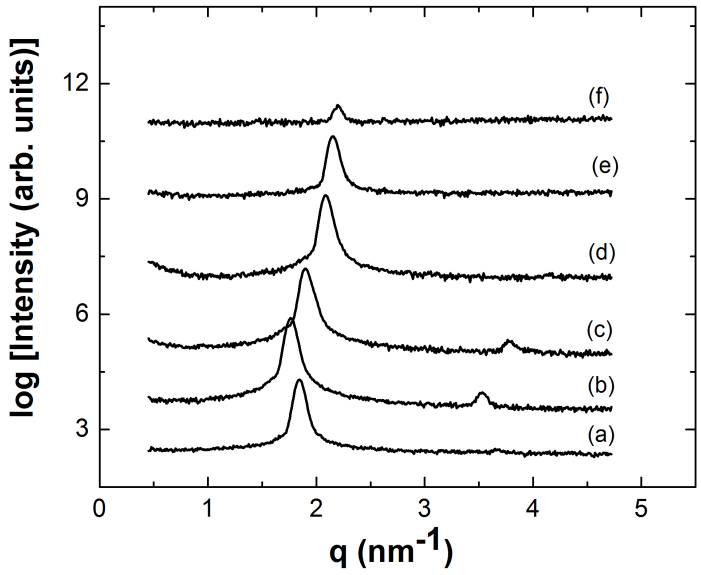


FIGURE 3.30: SAXS patterns of DDAB-PAANa8000 samples at R=14; $\phi$ ranging from 20 to 70. (a) 20, (b) 30, (c) 40, (d) 50, (e) 60, (f) 70.

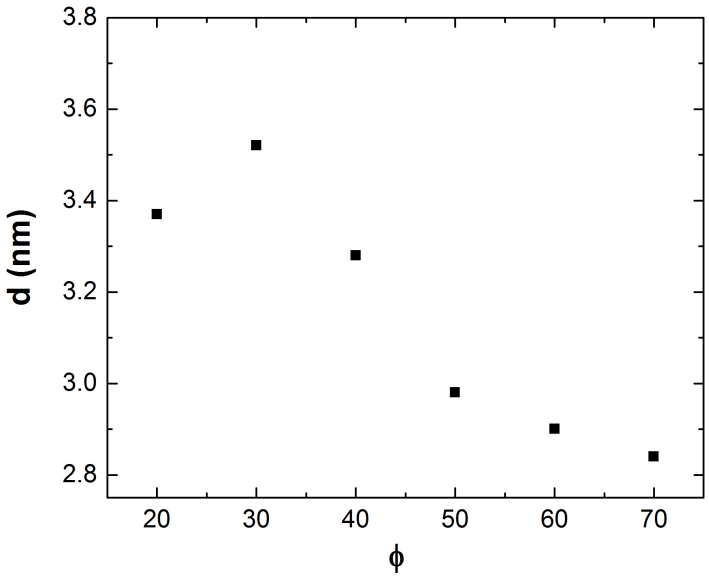


FIGURE 3.31: Variation of d-spacing for DDAB-PAANa8000 samples at R=14; $\phi$ ranging from 20 to 70.

repulsion between the polymer-adsorbed bilayers. In the case of steric repulsion, the maximum swelling will be decided by the thickness of the polymer layer, whereas it will depend on the value of $\kappa$ in the case of undulation repulsion. In swollen complexes of DDAB-PAANa2100 as well as of DDAC-PAANa2100, the separation between the bilayers in the swollen phase is much longer than the contour length of the polymer[5]. Hence steric repulsion between the bilayers can be ruled out and one can attribute the large swelling of these complexes to undulation repulsion. In support of this proposal DDAC bilayers are found to exhibit an undulation stabilized lamellar phase, when

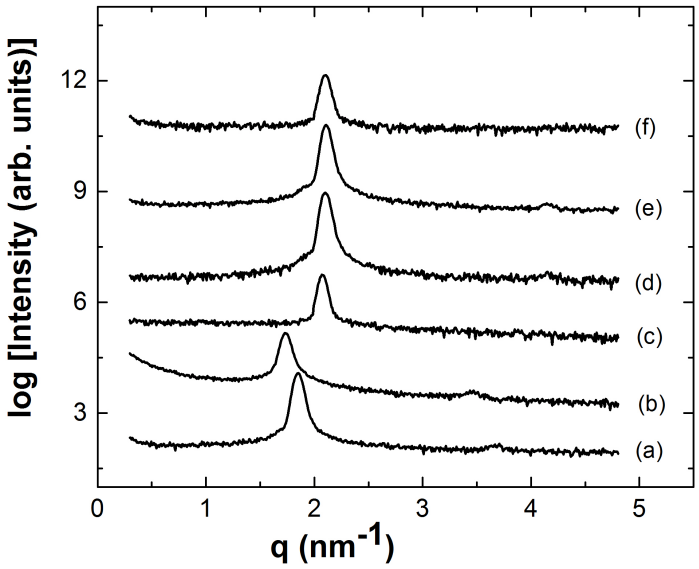


FIGURE 3.32: SAXS patterns of DDAB-PAANa8000 samples at R=14 and $\phi$= 20 in (a) water and at NaBr concentrations of (b) 100 mM, (c) 200 mM, (d) 400 mM, (e) 500 mM, and (f) 1 M.

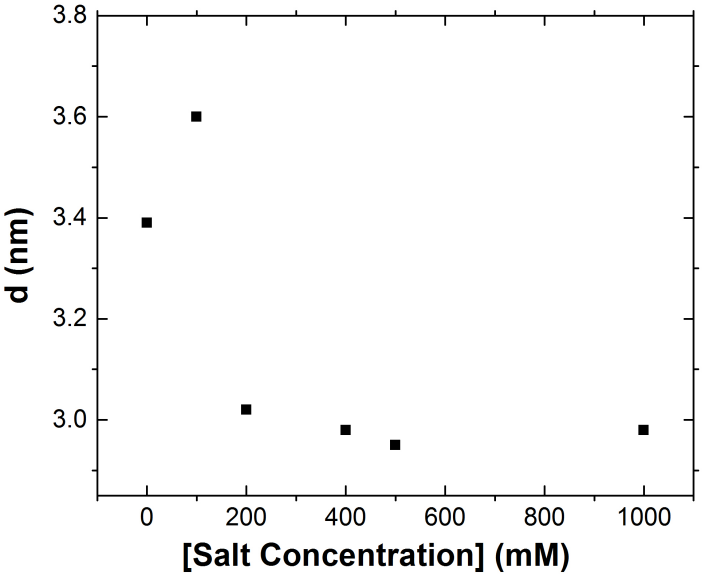


FIGURE 3.33: Variation of d-spacing with NaBr concentration for DDAB-PAANa8000 samples at R=14 and $\phi$= 20

the electrostatic inter-bilayer repulsion is screened out by salt, indicating a low value of $\kappa$. From the structural similarity of DDAB and DDAC, DDAB bilayers can also be expected to have a low value of $\kappa$, which will allow them to swell in the presence of salt. As mentioned earlier, theoretical studies have shown that the $L_\alpha$ phase is stable over a narrow range of values of $\bar{\kappa}/\kappa$ centered around -1. For higher values of this ratio the $L_3$ phase is stable, whereas lower values favor vesicles[21,22]. Polymer adsorption on a bilayer is expected to modify both $\kappa$ and $\bar{\kappa}$[15,16]. $\kappa$ is expected

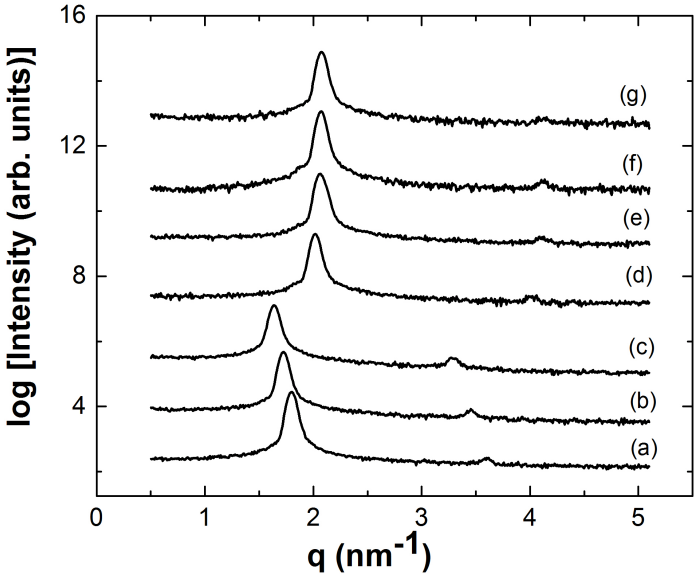


FIGURE 3.34: SAXS patterns of DDAB-PAANa15000 samples at R=14 and $\phi$= 20 in (a) water and at NaBr concentrations of (b) 50 mM, (c) 100 mM, (d) 200 mM, (e) 300 mM, (f) 400 mM and (g) 500 mM.

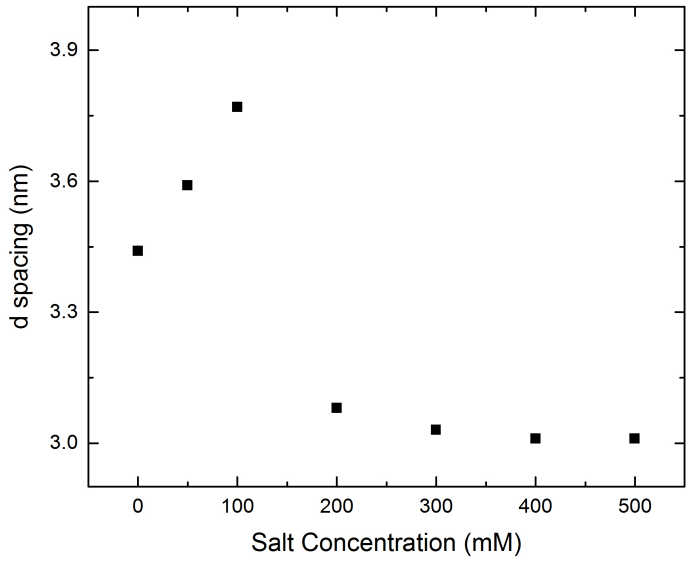


FIGURE 3.35: Variation of d-spacing with NaBr concentration for DDAB-PAANa15000 samples at R=14 and $\phi$= 20.

to decrease, whereas $\bar{\kappa}$ is expected to increase in the presence of an adsorption layer. Hence the ratio $\bar{\kappa}/\kappa$ will increase in the presence of the adsorption layer, driving the $L_\alpha$-$L_3$ transition. Experimental observations have been reported that are consistent with these predictions[32]. Formation of the sponge phase in the present system clearly shows that the presence of the adsorption layer increases the value of $\bar{\kappa}$. The DDAB-water system also forms the $L_\alpha$ phase over a broad concentration range, but there are some striking differences in their phase behaviour. The DDAB-water

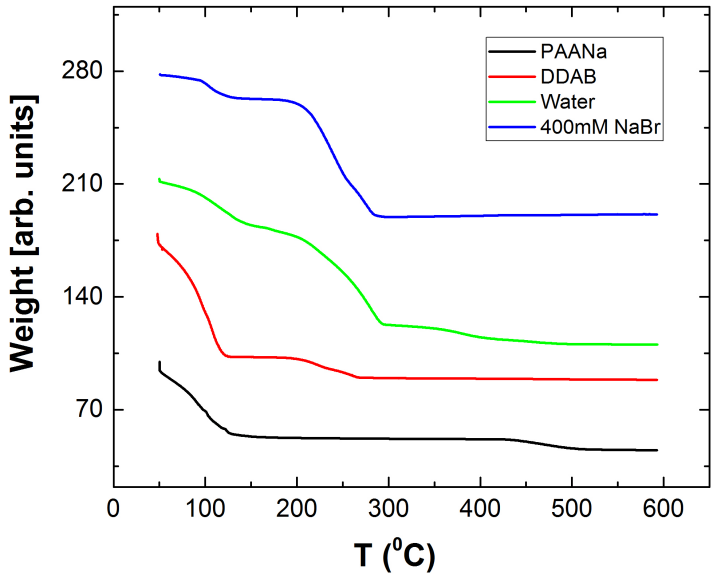


FIGURE 3.36: TGA traces of DDAB, PAANa, and DDAB-PAANa complexes at [NaBr] = 0 and 400 mM.

system is known to exhibit a metastable $L_3$ phase, which is absent in the DDAC-water system[1]. This suggests that DDAB bilayers have a higher value of $\bar{\kappa}$, close to the threshold value required to exhibit the $L_3$ phase. Another major difference between the two surfactant-water systems is the occurrence of a $L_\alpha$–$L_\alpha$ transition in DDAB that is absent in DDAC. This behaviour is attributed to the presence of a strong short-range inter-bilayer attraction, arising from the tendency of $Br^-$ counterions to adsorb back on to the charged bilayers[2]. The coexistence region decreases with increasing temperature and disappears above a critical temperature. At higher temperatures an isotropic phase is found near this composition range, which is absent in the DDAC-water system. The structure of this phase has not been probed in any detail, but it is known that the SAXS pattern of this phase shows a broad correlation peak as in the case of the $L_3$ phase. If this is indeed the $L_3$ phase, then it would be another indication that DDAB bilayers have a higher value of $\bar{\kappa}$, so that a smaller increase in $\bar{\kappa}$ is sufficient to push them into the $L_3$ phase compared to DDAC bilayers.

## 3.5 Conclusions

We have studied the effect of an oppositely charged polyelectrolyte on the interaction between ionic surfactant bilayers, as a function of salt concentration in the solution. At low salt concentrations, polymer bridging between adjacent bilayers creates an effective inter-bilayer attraction, that results in a condensed lamellar complex. At high salt concentration the polyelectrolyte does not bind to the bilayers and the van der Waals inter-bilayer attraction leads to the formation of a collapsed lamellar phase. A swollen complex occurs over intermediate salt concentrations, which forms a bicontinuous sponge phase in the case of DDAB and a swollen lamellar phase for DDAC and DOAC. Formation of the sponge phase can be attributed to an increase in the Gaussian rigidity of the bilayers due to polymer adsorption, as has been theoretically predicted.

# Bibliography


[1] Dubois M, Zemb T. Phase behavior and scattering of double-chain surfactants in diluted aqueous solutions. Langmuir. 1991;7(7):1352-60.

[2] Dubois M, Zemb T, Fuller N, Rand R, Parsegian V. Equation of state of a charged bilayer system: measure of the entropy of the lamellar–lamellar transition in DDABr. The Journal of chemical physics. 1998;108(18):7855-69.

[3] Israelachvili JN. Intermolecular and surface forces. Academic press; 2011.

[4] Dahlgren MA, Waltermo A, Blomberg E, Claesson PM, Sjoestroem L, Aakesson T, et al. Salt effects on the interaction between adsorbed cationic polyelectrolyte layers: theory and experiment. The Journal of Physical Chemistry. 1993;97(45):11769-75.

[5] Thomas M, Swamynathan K, Raghunathan V. Salt-induced swelling transitions of a lamellar amphiphile—Polyelectrolyte complex. J Chem Phys. 2019;150(9):094903.

[6] Szilagyi I, Trefalt G, Tiraferri A, Maroni P, Borkovec M. Polyelectrolyte adsorption, interparticle forces, and colloidal aggregation. Soft Matter. 2014;10(15):2479-502.

[7] Podgornik R. Self-consistent-field theory for confined polyelectrolyte chains. The Journal of Physical Chemistry. 1992;96(2):884-96.

[8] Gradzielski M, Hoffmann I. Polyelectrolyte-surfactant complexes (PESCs) composed of oppositely charged components. Current Opinion in Colloid & Interface Science. 2018;35:124-41.

[9] Xie F, Nylander T, Piculell L, Utsel S, Wagberg L, Åkesson T, et al. Polyelectrolyte adsorption on solid surfaces: theoretical predictions and experimental measurements. Langmuir. 2013;29(40):12421-31.

[10] Biggs S. Steric and bridging forces between surfaces bearing adsorbed polymer: an atomic force microscopy study. Langmuir. 1995;11(1):156-62.

[11] De Gennes PG. Polymers at an interface. 2. Interaction between two plates carrying adsorbed polymer layers. Macromolecules. 1982;15(2):492-500.

[12] Helfrich W. Steric interaction of fluid membranes in multilayer systems. Zeitschrift für Naturforschung A. 1978;33(3):305-15.

[13] Helfrich W. Elastic properties of lipid bilayers: theory and possible experiments. Zeitschrift für Naturforschung c. 1973;28(11-12):693-703.

[14] Chaikin PM, Lubensky TC, Witten TA. Principles of condensed matter physics. vol. 10. Cambridge university press Cambridge; 1995.

[15] Brooks J, Marques C, Cates M. The effect of adsorbed polymer on the elastic moduli of surfactant bilayers. Journal de Physique II. 1991;1(6):673-90.

[16] Clement F, Joanny JF. Curvature elasticity of an adsorbed polymer layer. Journal de Physique II. 1997;7(7):973-80.

[17] Roux D, Safinya C. A synchrotron X-ray study of competing undulation and electrostatic interlayer interactions in fluid multimembrane lyotropic phases. Journal de Physique. 1988;49(2):307-18.

[18] Dahlgren MA. Effect of counterion valency and ionic strength on polyelectrolyte adsorption. Langmuir. 1994;10(5):1580-3.

[19] Porte G, Appell J, Bassereau P, Marignan J. L$\alpha$ to L3: a topology driven transition in phases of infinite fluid membranes. Journal de Physique. 1989;50(11):1335-47.

[20] Roux D, Coulon C, Cates M. Sponge phases in surfactant solutions. The Journal of Physical Chemistry. 1992;96(11):4174-87.

[21] Morse DC. Topological instabilities and phase behavior of fluid membranes. Physical Review E. 1994;50(4):R2423.

[22] Golubović L. Passages and droplets in lamellar fluid membrane phases. Physical Review E. 1994;50(4):R2419.

[23] Robb ID. Specialist surfactants. Springer Science & Business Media; 1996.

[24] Kogej K, Skerjanc J. BINDING OF CETYLPYRIDINIUM CATION BY POLY (ACRYLIC ACID). EFFECT OF POLYMERCHARGE DENSITY. Acta chimica slovenica. 1999;46(2):269-79.

[25] Brotons G, Dubois M, Belloni L, Grillo I, Narayanan T, Zemb T. The role of counterions on the elasticity of highly charged lamellar phases: A small-angle x-ray and neutron-scattering determination. The Journal of chemical physics. 2005;123(2):024704.

[26] Perkin S, Kampf N, Klein J. Long-range attraction between charge-mosaic surfaces across water. Physical review letters. 2006;96(3):038301.

[27] Podgornik R. Polyelectrolyte-mediated bridging interactions. Journal of Polymer Science Part B: Polymer Physics. 2004;42(19):3539-56.

[28] Popa I, Cahill BP, Maroni P, Papastavrou G, Borkovec M. Thin adsorbed films of a strong cationic polyelectrolyte on silica substrates. Journal of colloid and interface science. 2007;309(1):28-35.

[29] Gupta SP, Thomas M, Chowdhury A, Raghunathan V. Effect of adsorbed polyelectrolytes on the interactions and elasticity of charged surfactant bilayers. J Phys: Condens Matter. 2020;32(19):194004.

[30] Gupta SP. Studies on novel phase behavior of ionic amphiphile-water systems. Raman Research Institute, Bangalore.; 2014.

[31] Porcar L, Hamilton WA, Butler PD, Warr G. Scaling of structural and rheological response of L3 sponge phases in the "sweetened" cetylpyridinium/hexanol/dextrose/brine system. Langmuir. 2003;19(26):10779-94.

[32] Maugey M, Bellocq A. Effect of adsorbed and anchored polymers on membrane flexibility: a light scattering study of sponge phases. Langmuir. 2001;17(21):6740-2.

# Chapter 4

# Effect of salt on inter-bilayer interactions in the lamellar phase of some ionic amphiphiles: low salt regime

## 4.1 Introduction

In this chapter we describe the influence of salt on the lamellar phase formed by cationic surfactants and lipids at low salt concentrations ( up to 1M ). Bilayers formed by ionic amphiphiles in water remain flat and rigid in the absence of salt and the lamellar periodicity is determined by inter bilayer electrostatic repulsion[1]. As the salt concentration ($C_s$) is increased, the charge on the bilayers gets screened. Hence the electrostatic repulsion between the charged surfaces is decreased[1,2]. Salt also affects the bending rigidity of a bilayer. In the presence of salt the electrostatic contribution to the bending rigidity of the bilayer is reduced[3]. Hence undulation repulsion between the bilayers becomes dominant, i.e.,the system goes from a electrostatically stabilized phase to an undulation stabilized phase[4]. Previous studies on charged lipid bilayers have also shown the reduction of bending rigidity as the salt concentration is increased[5,6]. Studies on single chain anionic surfactants have shown an increase in the undulation repulsion in the fluid lamellar phase ($L_\alpha$) on suppressing the electrostatic repulsion between the bilayers by the addition of salt[7,8].

We have studied the effect of alkali metal chlorides (LiCl, NaCl, KCl and CsCl) on the lamellar phase formed by didodecyldimethylammonium chloride (DDAC) and DMTAP (1,2-dimyristoyl-3-trimethylammonium-propane (chloride salt)) bilayers and that of alkali metal bromides (LiBr, NaBr, KBr and CsBr) on the lamellar phase of didodecyldimethyl-ammonium bromide (DDAB) bilayers using SAXS, POM and cryo-SEM techniques. DDAC, DDAB and DMTAP form lamellar phase in water over a wide range of concentration[9,10] . The phase diagrams of DDAC and DDAB are shown in fig. 4.1. In water the fluid lamellar phase ($L_\alpha$) is stabilizied by electrostatic repulsion. In that case the bilayers remain rigid and flat and multiple sharp peaks are obtained in the SAXS pattern. In the presence of salt the bilayer bending rigidity reduces. So the system gets stabilized by inter bialyer undulation repulsion. In that case usually only one broad peak is observed in the SAXS pattern in the case of lamellar phase made of DDAC and DDAB. For 20 wt% samples, the d-spacing does not vary significantly up to a salt concentration of $\sim$ 300 mM. In the case of DMTAP, the d-spacing reduces monotonically with salt concentration. This is due to the higher intrinsic bending rigidity of lipid bilayers[11], so the magnitude of the undulation repulsion is lower. At moderate salt concentration another lamellar phase ($L_\alpha^c$) is found at room temteperature

whose d-spacing is comparable to the bilayer thickness[12,13]. The critical salt concentration at which the $L_\alpha \hookrightarrow L_\alpha^c$ transition occurs depends on the salt. The stability of the lamellar phase formed by charged bilayers can be understood in terms of the DLVO theory. The $L_\alpha^c$ phase can be viewed as corresponding to the primary minimum of the DLVO potential, with a difference that in this case there is a thin layer of water that separates adjacent bilayers, which is caused by the hydration repulsion[14]. In the case of DDAC, the d-spacing is found to increase gradually with increasing temperature at higher salt concentrations, where the $L_\alpha^c$ phase is found at 30°C.The extent of swelling over a fixed temperature range decreases with increasing salt concentration. The effects of different alkali metal chlorides on the $L_\alpha$ phase of DDAC and DMTAP and different bromide salts on the $L_\alpha$ phase of DDAB are found to be similar.

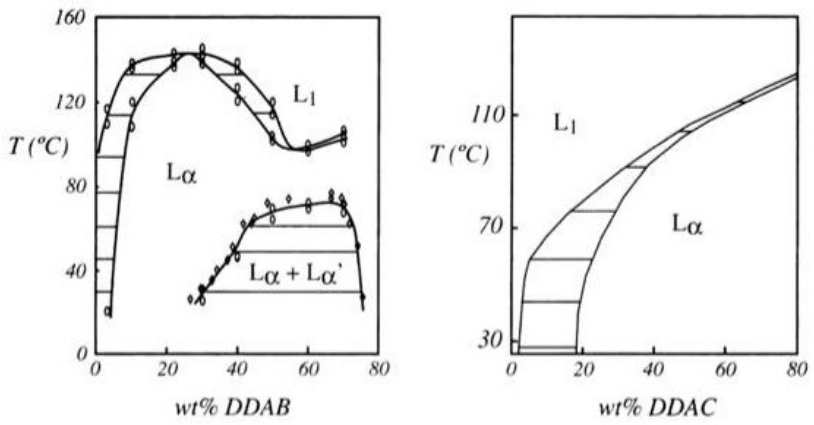


FIGURE 4.1: Phase diagrams of DDAB and DDAC dispersions in water.[9]

## 4.2 Materials and methods

Surfactants (DDAC and DDAB) and salts (NaCl, KCl, CsCl, LiCl, NaBr, KBr, LiBr and CsBr) were purchased from Sigma-Aldrich. DMTAP was purchased from Avanti polar lipids. All the chemicals were used without further purification. The data presented in this chapter is for samples having $\phi$ =20 and $\phi$ =30. $\phi$ is the wt% of the samples, defined as $\phi = \frac{W_s}{W_s+W_w} \times 100$ , $W_s$ is the weight of the surfactant (or lipid) and $W_w$ is the weight of water (or salt solution). Samples are prepared in the desired salt solution, and then left for equilibration for a few days. Samples were mixed thoroughly to ensure homogeneity. Some DDAC samples were left for equllibriation without mixing. Milli-Q water was used for the preparation of the salt solutions. SAXS and POM data for DDAC samples were collected at 30°C and those for DMTAP were collected at 50°C, to ensure that the data were collected in the fluid lamellar ($L_\alpha$) phase.

## 4.3 Results

### 4.3.1 Effect of salt on DDAC bilayers

#### DSC studies

DSC thermograms of DDAC samples in water and at different salt concentrations ($C_s$) of different alkali metal salts are presented in fig. 5.6. In the absence of any salt the transition temperature is observed to be around 10°C. The transition temperature is found to increase slightly with increasing salt concentration. At [$C_s$]= 1M, the transition temperature observed is $\sim$ 15°C. The typical transition enthalpy is found to be close to 6 kJ/mol. The peak position corresponds to the Krafft temperature, above which the bilayers are formed.

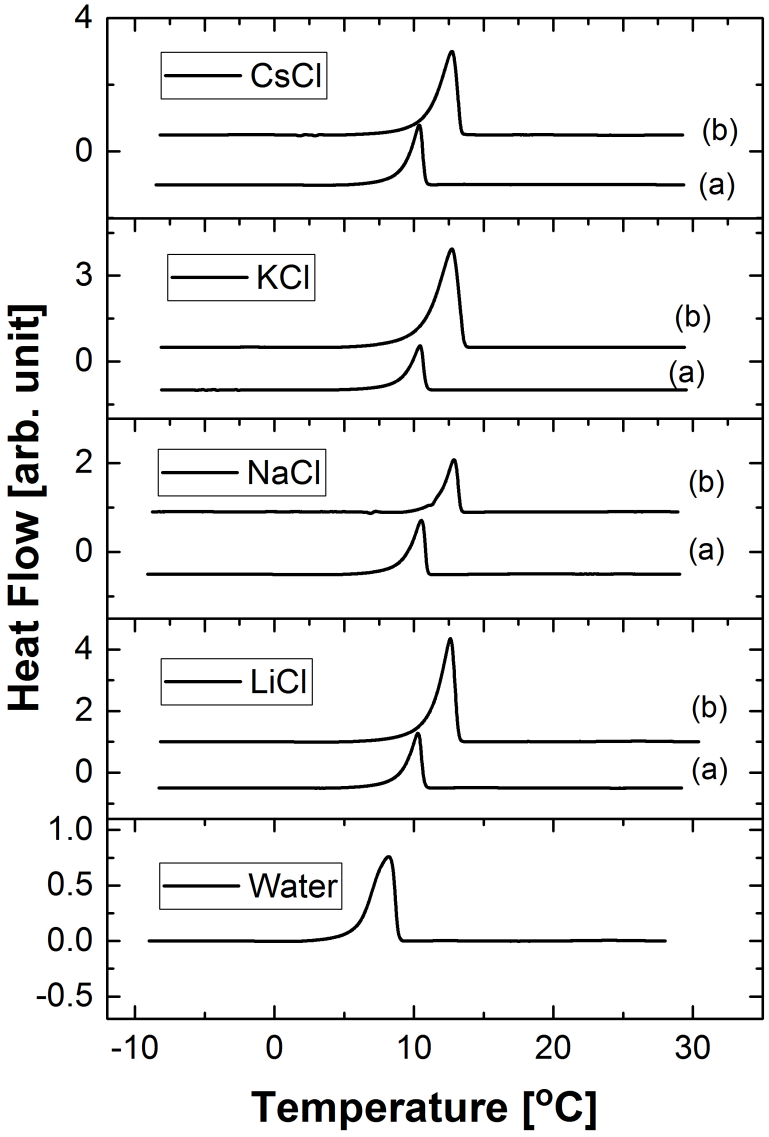


FIGURE 4.2: DSC thermograms of DDAC dispersions in water and in solutions of different alkali metal chlorides at $\phi$ = 20. (a) and (b) represents [$C_s$] = 200mM and 1M, respectively. The transition was not observed in the cooling cycle due to the super-cooling of the fluid phase.

**SAXS studies**

In the absence of any salt 20wt% DDAC samples form a lamellar phase ($L_\alpha$) of periodicity (d) $\sim$ 11 nm. SAXS patterns shows 4 peaks, which can be indexed as the 1st, 2nd, 3rd and 4th order peaks of a lamellar structure. SAXS profiles of DDAC-LiCl samples are shown in fig.4.3. At [LiCl]=100mM, only one broad peak is observed. The pattern remains the same up to [LiCl]= 425 mM. At [LiCl]=450 mM, the d-spacing reduces to 4.1nm . The spacing reduces further to 3.6nm at [LiCl]= 500mM. At [LiCl]= 1M the spacing is 3.2 nm. The SAXS profiles of DDAC- NaCl (fig.4.4), DDAC-KCl (fig.4.5) and DDAC-CsCl (fig.4.6) systems are very similar to those of the DDAC-LiCl system. The peaks become broad as [$C_s$] is increased to 100mM. The diffraction pattern remains unaltered till a threshold value of salt concentration, after which the d-spacing reduces abruptly, indicating the formation of the $L_\alpha^c$ phase. The peaks become sharper in the $L_\alpha^c$ phase. The change of d-spacing with salt concentration for different salts is presented in fig.4.7. The typical error in each measurement is around $\pm$ 0.5 nm,which is indicated for the DDAC-Water system. The threshold value of salt concentration at which the spacing reduces abruptly, depends on the salt. For NaCl and KCl it is $\sim$ 375 mM , where as for LiCl and CsCl it is $\sim$ 450mM. The d-spacing depends on the temperature above the threshold salt concentration. At 30°C the peak remains sharp. As the temperature is increased the d-spacing increases , the peaks also become broad. In a few cases no peaks are observed. At high temperatures a fully swollen phase is found, where d is maximum. SAXS profiles of DDAC-NaCl and DDAC-KCl samples with varying temperature are shown in fig.5.16 and fig.5.17. The temperature at which the swelling transition take place increases with salt concentration. At [$C_s$]= 1M, only the $L_\alpha^c$ phase is found over the whole temperature range (30°C - 70°C) (Tables 4.1,4.2,4.3,4.4).

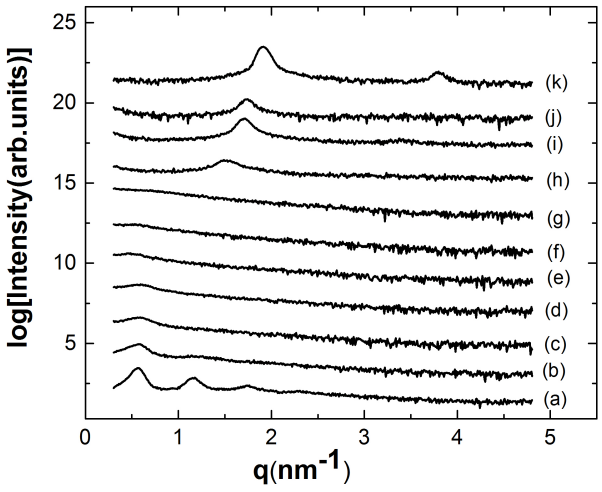


FIGURE 4.3: SAXS profiles of DDAC dispersions in (a) water, and in LiCl solutions of (b) 100mM, (c) 200mM, (d) 300mM, (e) 350mM, (f) 400mM, (g) 425mM, (h) 450mM, (i) 475mM, (j) 500mM, and (k) 1M concentration at $\phi$= 20.

From table 4.1 and fig. 5.16 it is clear that the peaks become broad over an intermediate temperature range and in a few cases no peak is observed in the SAXS profiles for DDAC-NaCl samples. On increasing the temperature when the peak reappears, the position of the peak corresponds to maximum swelling. To verify whether this behaviour is independent of the wt% of the sample or

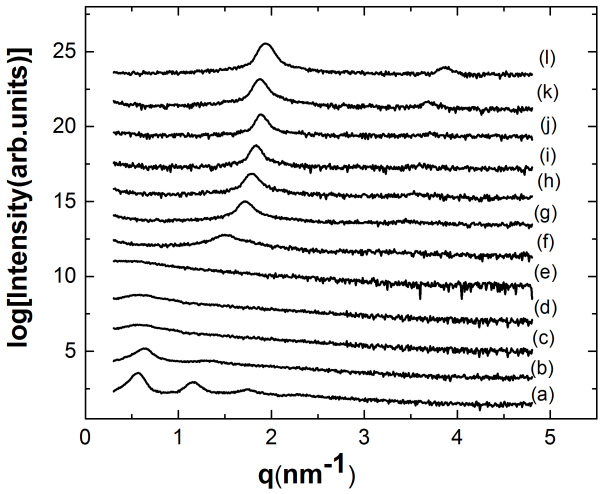


FIGURE 4.4: SAXS profile of DDAC dispersions in (a) water, and in NaCl solutions of (b) 100mM, (c) 200mM, (d) 300mM, (e) 350mM, (f) 375mM, (g) 400mM, (h) 425mM, (i) 450mM, (j) 475mM, (k) 500mM and (l) 1M concentration at $\phi$= 20.

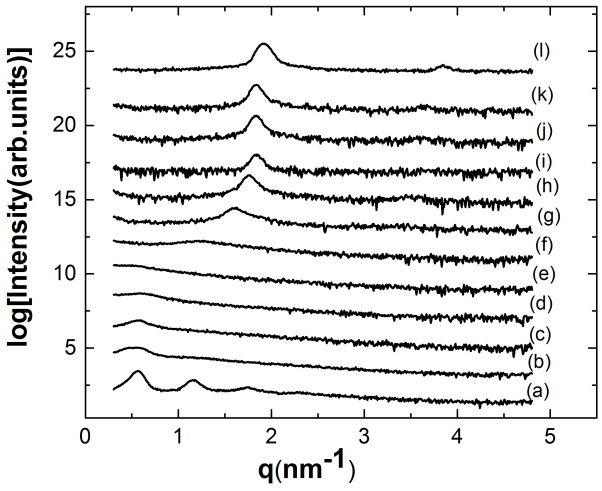


FIGURE 4.5: SAXS profiles of DDAC dispersions in (a) water, and in KCl solution of (b) 100mM, (c) 200mM, (d) 300mM, (e) 350mM, (f) 375mM, (g) 400mM, (h) 425mM, (i) 450mM, (j) 475mM, (k) 500mM and (l) 1M concentration at $\phi$= 20.

not, we have carried out a similar study with 30 wt% samples. The SAXS profiles of the 30 wt% DDAC-NaCl samples are given in fig. 4.10. The peak becomes broad on increasing the temperature, but it does not disappear. No difference in the SAXS profiles is observed between the heating and cooling cycles (fig. (b) and (c) of fig.4.10). Variation of d-spacing with temperature is shown in table 4.5.

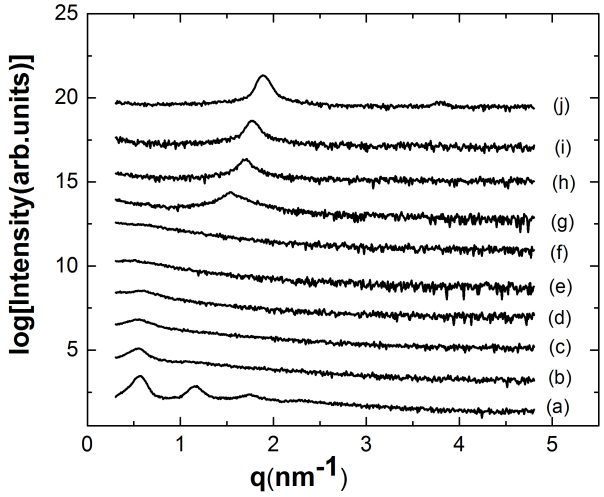


FIGURE 4.6: SAXS profiles of DDAC dispersions in (a) water, and in CsCl solution of (b) 100mM, (c) 200mM, (d) 300mM, (e) 400mM, (f) 425mM, (g) 450mM, (h) 475mM, (i) 500mM and (j) 1M concentration at $\phi$= 20 .

| T (°C) | d (nm) | | | | | | |
|---|---|---|---|---|---|---|---|
| | 375 mM | 400 mM | 425 mM | 450 mM | 475 mM | 500 mM | 1M |
| 30 | 4.1 | 3.6 | 3.5 | 3.4 | 3.3 | 3.3 | 3.1 |
| 35 | 7.6 | 3.9 | 3.6 | - | - | - | - |
| 40 | 11.2 | 5.0 | 4.1 | 3.6 | 3.4 | 3.4 | - |
| 45 | - | 7.5 | 5.5 | - | - | - | - |
| 50 | 12.1 | 11.1 | 7.1 | 4.1 | 3.7 | 3.6 | - |
| 55 | - | - | * | - | - | - | - |
| 60 | 12.3 | 12.3 | * | 5.6 | 4.8 | 3.9 | - |
| 65 | - | - | * | - | - | - | - |
| 70 | 12.71 | 12.3 | 12.5 | * | * | 4.6 | 3.2 |

TABLE 4.1: Temperature dependence of d-spacing for 20 wt% DDAC dispersions at different NaCl concentrations. '-' denotes that data was not taken at that temperature and '*' denotes no peak in the SAXS was observed at that temperature.

### 4.3.2 Effect of salt on DMTAP bilayers

#### DSC studies

DSC thermograms of DMTAP samples are shown in fig. 4.11. A large hytersis is found in heating and cooling cycles ($\sim$ 10°C). A slight increase in the transition temperature is observed in the presence of salt. Two distinct peaks are found in the cooling cycle in some cases. The SAXS data are taken at 50°C, to make sure that the system is in the fluid phase. The typical transition enthapy found is 12 kJ/mol, corresponds to chain melting transition.

#### SAXS studies

The SAXS profiles of DMTAP-LiCl samples are shown in fig. 4.12. 20wt% DMTAP samples form a lamellar phase of d=15.64 nm. Multiple peaks which are found in SAXS pattern can be indexed

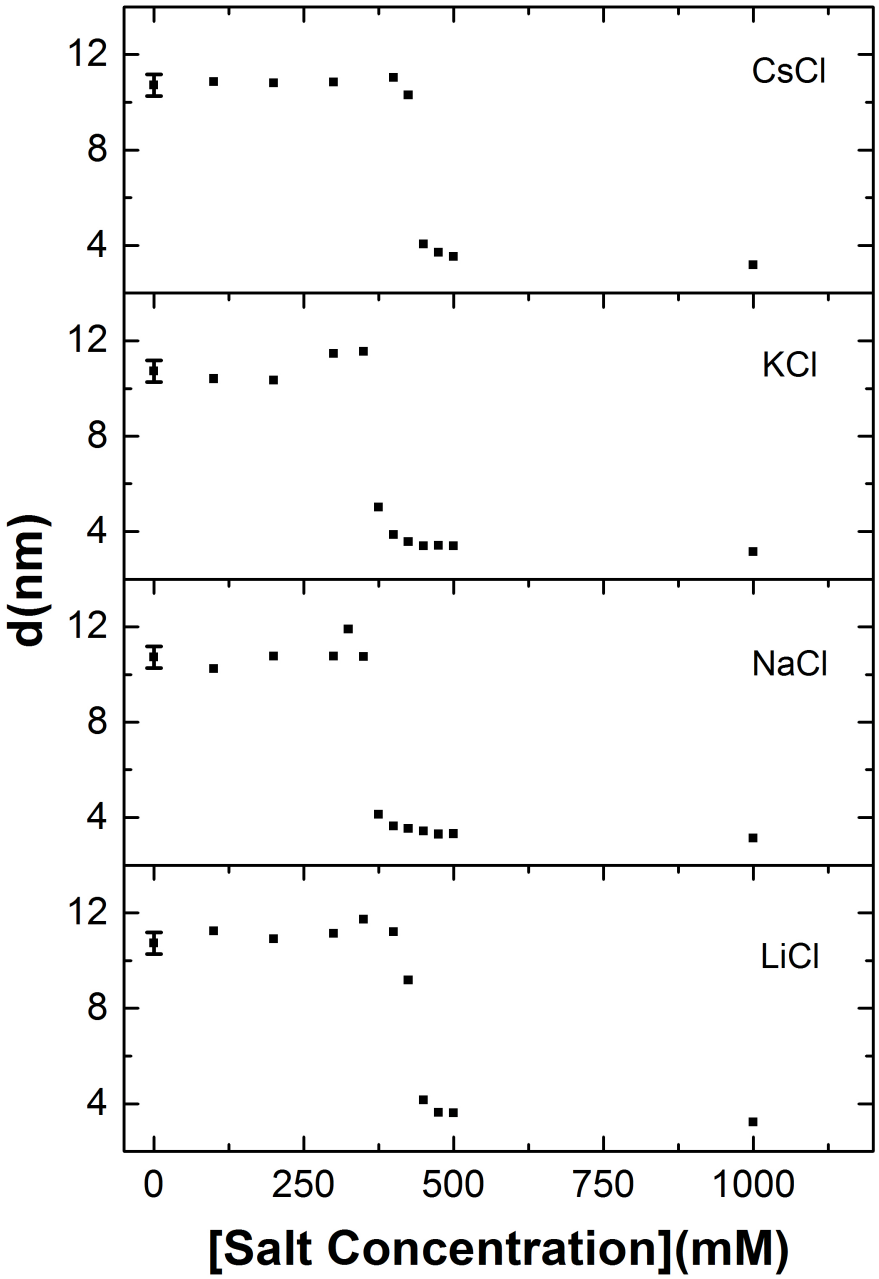


FIGURE 4.7: Variation of d of the $L_\alpha$ phase of 20 wt% DDAC dispersions with salt concentration for different salts. Typical error bar in the swollen phase is indicated. In the collapsed phase the error is smaller than the size of the symbol.

as h=1,2,3 and 4 of a lamellar phase($L_\alpha$). As the salt concentration is increased the d-spacing is reduced till it reaches the minimum at [$C_s$]= 700mM. The SAXS profiles of DMTAP- NaCl (fig. 4.13), DMPAP-KCl (fig. 4.14), DMTAP- CsCl (fig. 4.15) are qualitatively similar to that of DMTAP-LiCl system. The variation of d-spacing with salt concentration is presented in fig. 4.16. and table 4.6.

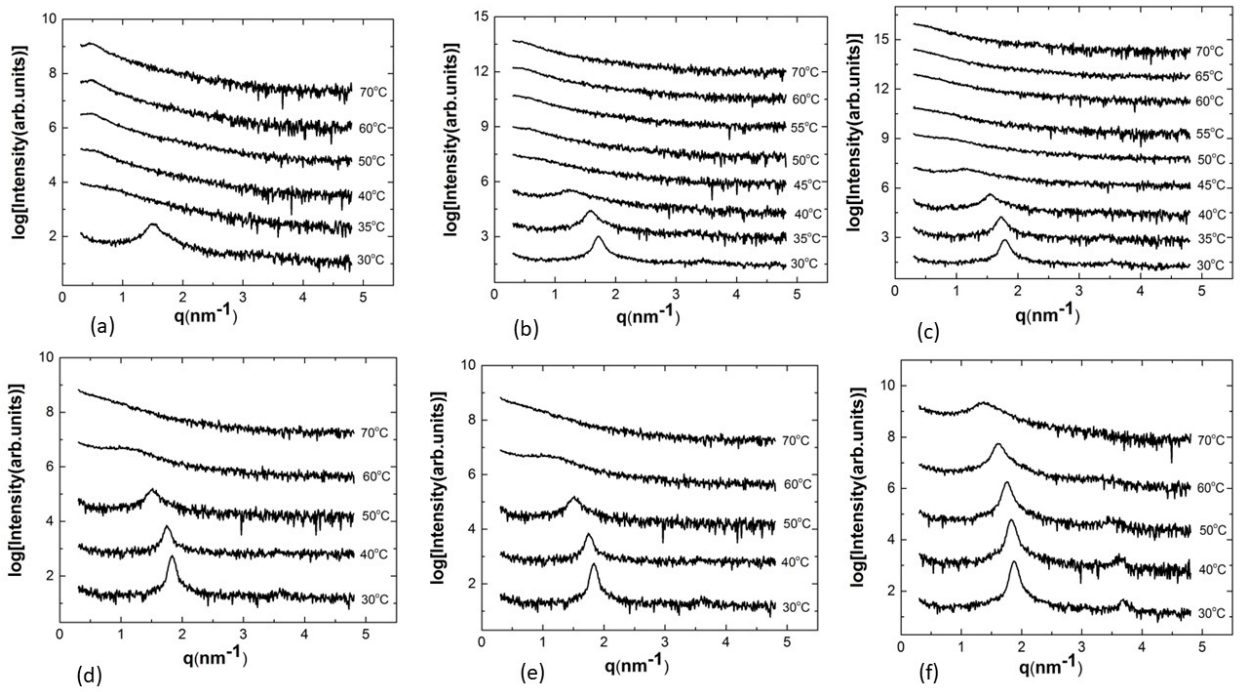


FIGURE 4.8: SAXS profiles of DDAC dispersions in NaCl solutions of (a) 375mM, (b) 400mM, (c) 425 mM, (d) 450mM, (e) 475mM and (f) 500mM concentration at different temperatures at $\phi$ =20.

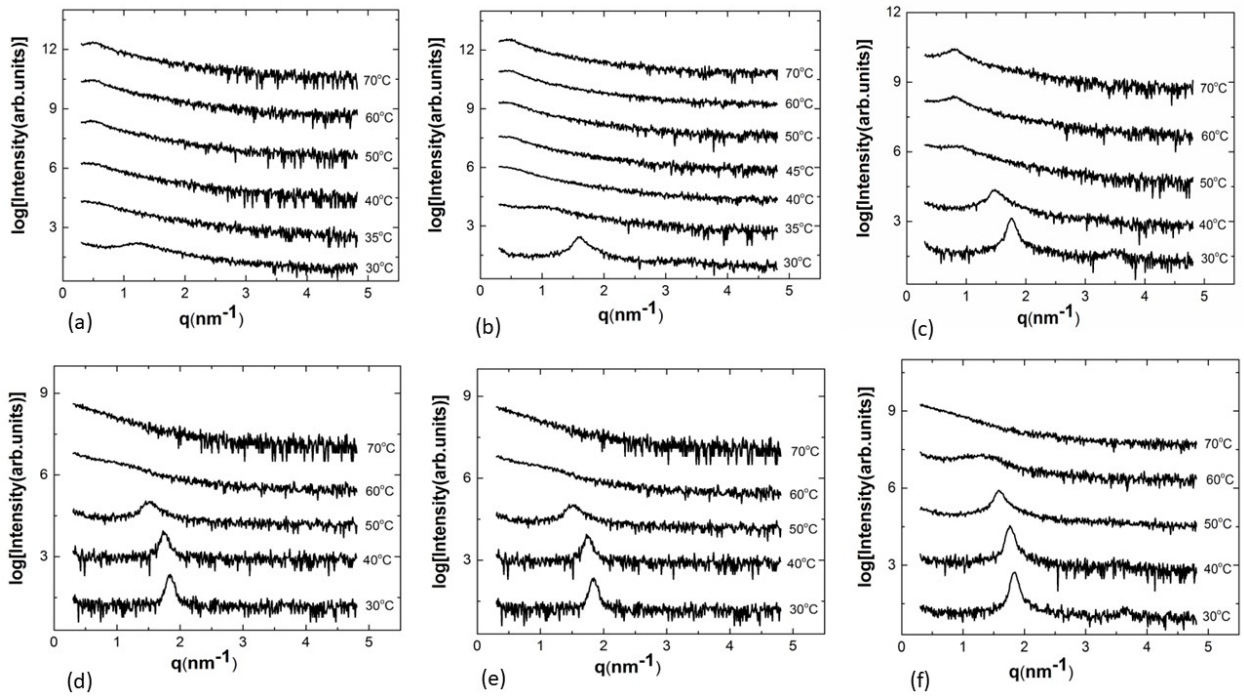


FIGURE 4.9: SAXS profiles of DDAC dispersions at KCl solutions of (a) 375mM, (b) 400mM, (c) 425 mM, (d) 450mM, (e) 475mM and (f) 500mM concentration at different temperatures at $\phi$ =20.

### 4.3.3 Effect of salt on DDAB bilayers

20 wt% DDAB dispersion in water forms a lamellar phase ($L_\alpha$), with a periodicity of 11.9 nm. All the alkali metal bromides are found to have similar effects on DDAB bilayers. SAXS profiles of

| T (°C) | d (nm) | | | | | | |
|---|---|---|---|---|---|---|---|
| | 375 mM | 400 mM | 425 mM | 450 mM | 475 mM | 500 mM | 1 M |
| 30 | 5.0 | 3.9 | 3.6 | 3.4 | 3.4 | 3.4 | 3.1 |
| 35 | 11.6 | 6.0 | - | - | - | - | - |
| 40 | 12.7 | 11.1 | 4.3 | 3.6 | 3.6 | 3.6 | - |
| 45 | - | 12.3 | 5.5 | - | - | - | - |
| 50 | 12.7 | 12.9 | 7.1 | 4.2 | 3.2 | 4.0 | - |
| 55 | - | - | * | - | - | - | - |
| 60 | 12.5 | 12.3 | 7.6 | * | 5.2 | 4.7 | - |
| 65 | - | - | * | - | - | - | - |
| 70 | 11.9 | 12.5 | 7.8 | * | * | * | 3.2 |

TABLE 4.2: Temperature dependence of d-spacing for 20 wt% DDAC dispersions at different KCl concentrations. '-' denotes that data was not taken at that temperature and '*' denotes no peak in the SAXS was observed at that temperature.

| T (°C) | d (nm) | | | |
|---|---|---|---|---|
| | 450 mM | 475 mM | 500 mM | 1 M |
| 30 | 4.1 | 3.7 | 3.6 | 3.2 |
| 70 | * | 8.2 | * | 3.4 |

TABLE 4.3: Temperature dependence of d-spacing for 20 wt% DDAC dispersions at different LiCl concentrations. '*' denotes no peak is observed in the SAXS profile was observed at that temperature.

DDAB-LiBr, DDAB-NaBr, DDAB-KBr and DDAB-CsBr are shown in fig.4.17 , fig.4.18, fig.4.19 and fig. 4.20 respectively. In the absence of salt three peaks are seen in the SAXS pattern. At [$C_s$]= 50mM, two peaks are found, the second order peak being very broad (fig. 4.18, 4.19) , but the d-spacing is comparable to that in water. At [$C_s$]= 100mM, d reduces to $\sim$ 3.1 nm. The value of d does not change further upto [$C_s$]= 1M. Variation of d-spacing with salt concentrations for different salts is shown in fig. 4.21 and table 4.7.

### 4.3.4 Effect of salt on unmixed samples

DDAC - XCl (X= Na, Li, K, Cs) samples which were mixed during preparation, show d-spacing almost similar to that of DDAC-water system at low salt concentrations (up to $\sim$ 300 mM) . Samples which were not mixed during preparation show a monotonic decrease of d with salt concentration before it goes to the $L_\alpha^c$ phase. The d-spacing vs salt concentration data for the unmixed samples is presented in table 4.8 and fig.4.26. Figs. 4.22 ,4.23,4.24 and 4.25 give the SAXS patterns of unmixed DDAC samples in different salt solutions. The peaks become broad on increasing the salt concentration and at [$C_s$] $\sim$ 300mM, only one peak is observed. At [$C_s$] $\sim$ 500mM, two distinct peaks are observed ($L_\alpha^c$ phase), with d $\sim$ 3.5 nm.

## 4.4 Discussions

The periodicity of a lamellar phase is determined by the various inter-bilayer interactions described in chapter 1. In the case of ionic amphiphiles electrostatic repulsion dominates, resulting

| T (°C) | d (nm) | | | |
|---|---|---|---|---|
| | 450 mM | 475 mM | 500 mM | 1 M |
| 30 | 4.1 | 3.7 | 3.5 | 3.2 |
| 70 | 7.1 | 8.2 | 6.3 | 3.3 |

TABLE 4.4: Temperature dependence of d-spacing for 20 wt% DDAC dispersions at different CsCl concentrations.

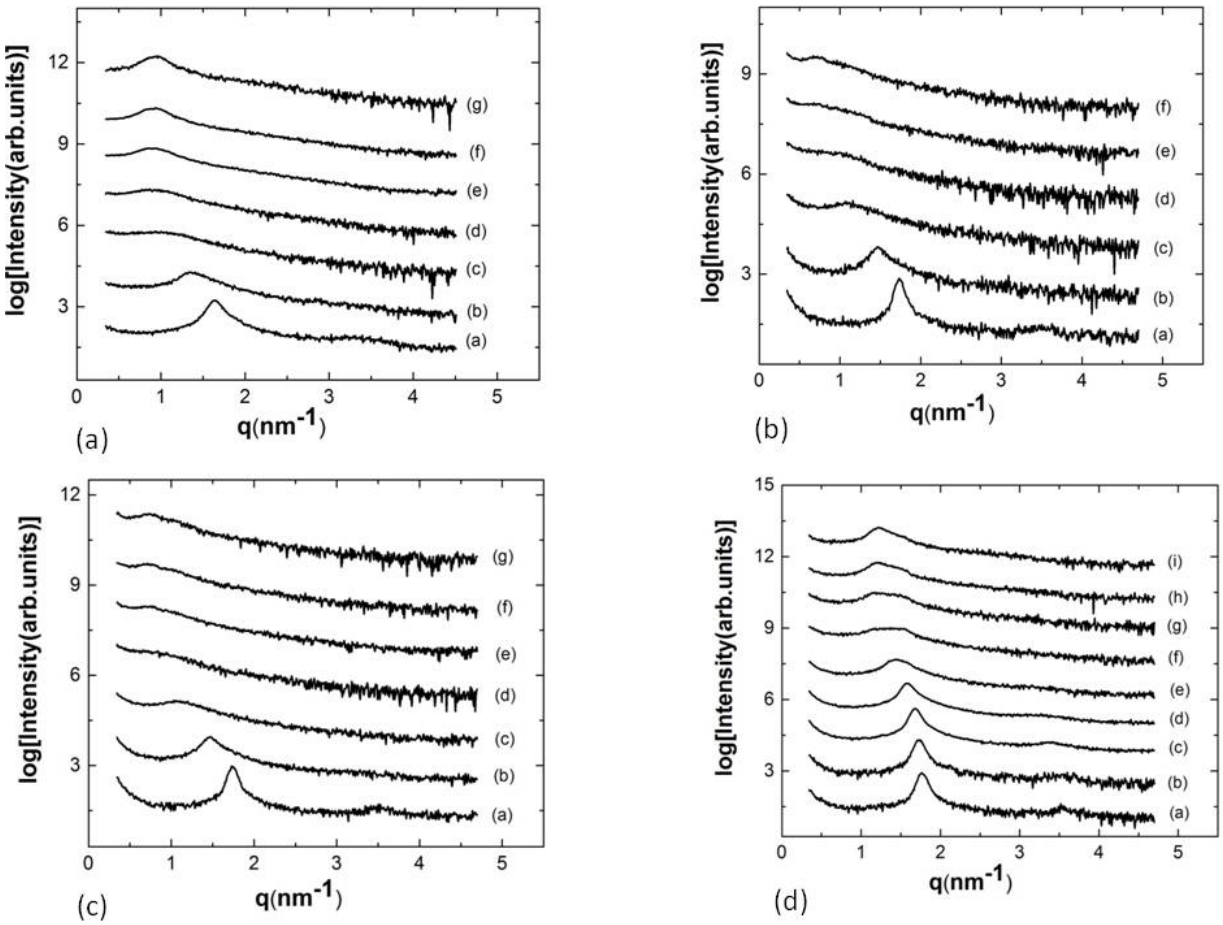


FIGURE 4.10: SAXS profile of DDAC dispersions at NaCl concentration of (a) 350mM, (b) 375mM, (c) 375mM - on cooling and (d) 400 mM at different temperatures at $\phi$ = 30.

in high values of the d-spacing in dilute samples in water. Long-range undulation repulsion is usually negligible in these systems due to the electrostatic contribution to the bilayer bending rigidity, which makes them very rigid. These systems are said to be electrostatically stabilized [1].

The electrostatic contribution to $\kappa$ is reduced in the presence of salt [3]. In the case of a lipid such as DMTAP the bare value of $\kappa$ is of the order of 10 $k_BT$ [15]. Since undulation repulsion, which is inversely proportional to $\kappa$ [4], is relatively small in DMTAP, its d-spacing is primarily determined by electrostatic repulsion. This system is well described by the DLVO theory, which takes into account the electrostatic repulsion and van der Waals attraction. As the salt concentration is increased, the electrostatic repulsion is screened out more and more and the d-spacing gradually decreases due to van der Waals attraction. The d-spacing reaches a minimum value of about 4.7 nm at a salt concentration of 700 mM, corresponding to a Debye length of 0.35 nm. This value

| T (°C) | d (nm) | | | |
|---|---|---|---|---|
| | 350mM | 375mM | 375mM (cooling) | 400mM |
| 30 | 3.8 | 3.6 | 3.6 | 3.5 |
| 35 | 4.6 | - | 3.6 | 3.6 |
| 40 | 6.2 | 4.3 | 4.3 | 3.7 |
| 45 | 6.8 | 5.7 | 5.8 | 4.0 |
| 50 | 6.9 | 6.2 | 7.1 | 4.3 |
| 55 | - | - | 8.1 | - |
| 60 | 6.8 | 8.3 | 8.4 | 4.8 |
| 65 | - | - | - | 5.1 |
| 70 | 6.8 | 8.5 | 8.5 | 5.1 |

TABLE 4.5: Temperature dependence of d-spacing at different NaCl concentrations for 30wt% DDAC samples. '-' denotes that data was not taken at that point.

| [Salt Concentration] (mM) | $d_{CsCl}$ (nm) | $d_{KCl}$ (nm) | $d_{NaCl}$ (nm) | $d_{LiCl}$ (nm) |
|---|---|---|---|---|
| 0 | 15.64 | 15.64 | 15.64 | 15.64 |
| 100 | 14.12 | 13.86 | 14.23 | 13.03 |
| 300 | 12,23 | 11.05 | 9.76 | 10.89 |
| 500 | 8.21 | 6.01 | 5.04 | 5.43 |
| 700 | 4.89 | 4.74 | 4.73 | 4.75 |
| 1000 | 4.67 | 4.59 | 4.62 | 4.79 |

TABLE 4.6: Salt concentration vs d for different salts for DMTAP system at $\phi$= 20.

| [Salt Concentration] (mM) | $d_{CsBr}$ (nm) | $d_{KBr}$ (nm) | $d_{NaBr}$ (nm) | $d_{LiBr}$ (nm) |
|---|---|---|---|---|
| 0 | 11.9 | 11.9 | 11.9 | 11.9 |
| 50 | - | 11.73 | 12.1 | - |
| 100 | 3.07 | 3.14 | 3.07 | 3.14 |
| 200 | 3.1 | 3.07 | 3.10 | 3.13 |
| 300 | 3.1 | 3.1 | - | - |
| 400 | - | 3.08 | - | |
| 500 | 3.06 | * | 3.10 | 3.07 |
| 1000 | 3.05 | 3.0 | 3.01 | 3.07 |

TABLE 4.7: Salt concentration vs d for different salts for DDAB system at $\phi$= 20.

of d-spacing is typically about 1 nm higher than the bilayer thickness[16] due to the presence of short-range hydration repulsion.

The bare value of $\kappa$ for a surfactant such as DDAC, is of the order of $k_BT$[7,12], which is an order

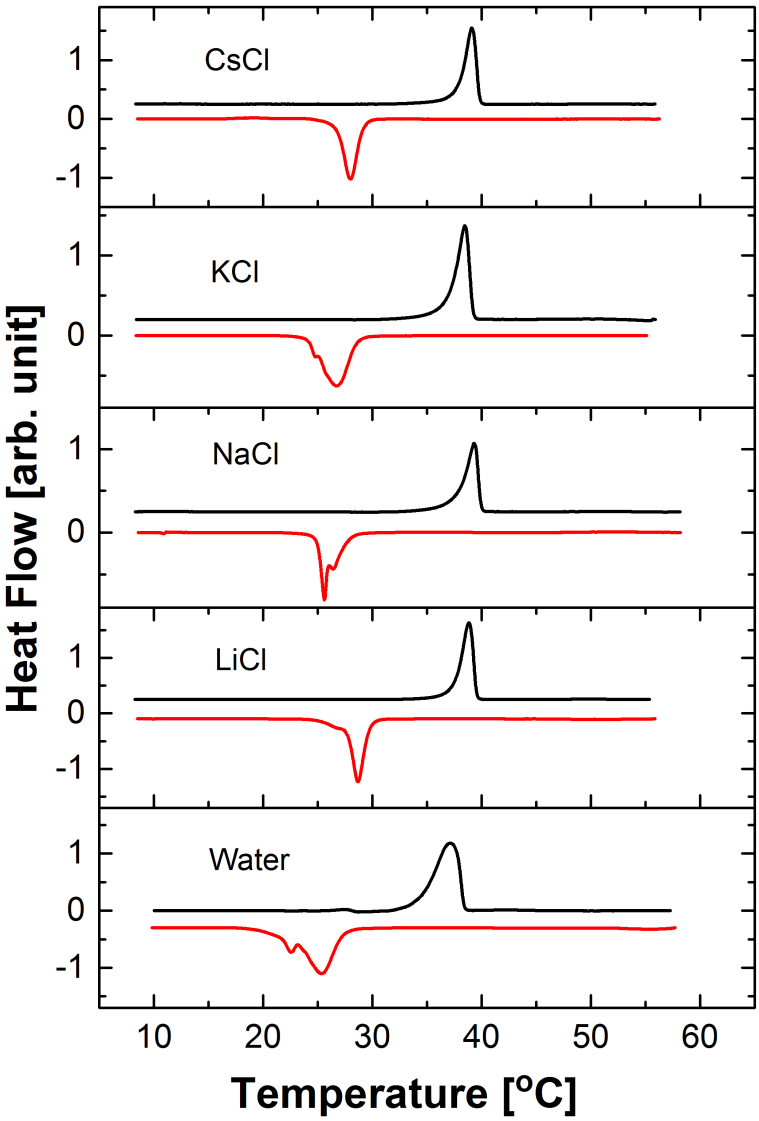


FIGURE 4.11: DSC thermograms of 20 wt% DMTAP dispersions in water and at $[C_s]$= 300mM of different alkali metal chlorides. The black and red traces correspond to the heating and cooling cycles, respectively.

of magnitude lower than the value for DMTAP. This difference in $\kappa$ leads to the striking difference in the variation of d with salt concentration in these two systems. Due to its much lower value of $\kappa$, the amplitude of thermal fluctuations of the DDAC bilayer is much larger, resulting in stronger undulation repulsion between the bilayers. Consequently, the lamellar phase of DDAC is able to swell considerably in the presence of salt, and the system is said to be undulation stabilized. We have observed a maximum swelling of about 18 nm in this system, corresponding to $\phi \sim 10$ (fig.4.27). Since the maximum swelling of both the electrostatically-stabilized salt-free lamellar phase and the undulation-stabilized phase in the presence of salt correspond to values of $\phi$ less than 20, the d-spacings of these phases are comparable at $\phi = 20$. However, there are important differences in their SAXS profiles which are discussed later.

DMTAP is a charged lipid ($Cl^-$ counter-ion), which forms a lamellar phase in water. SAXS

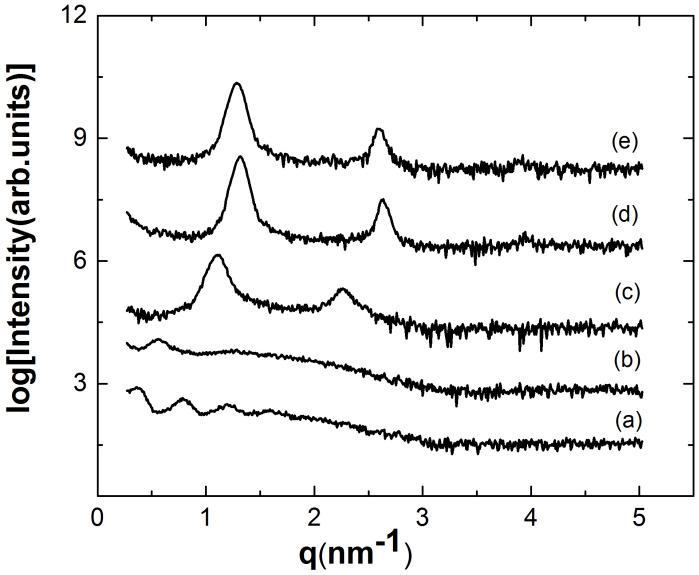


FIGURE 4.12: SAXS profiles of DMTAP dispersions in (a) water, and in LiCl solutions of (b) 300 mM, (c) 500 mM, (d) 700 mM, (e) 1 M concentration at $\phi$ = 20.

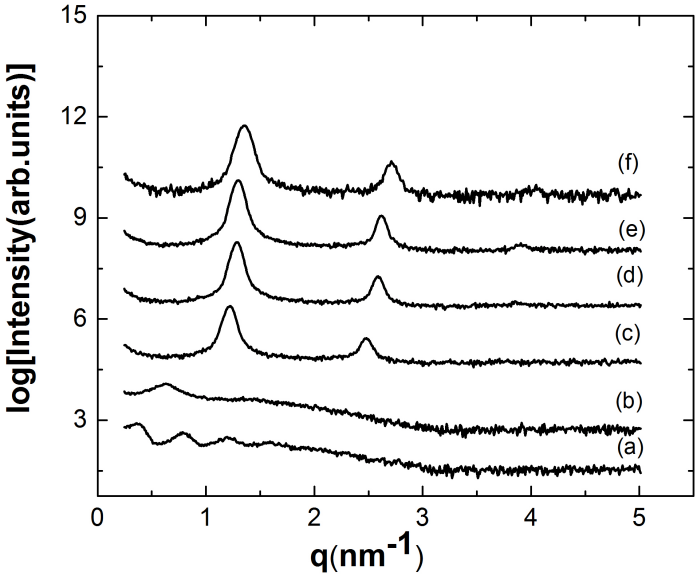


FIGURE 4.13: SAXS profile of DMTAP dispersions in (a) water, and in NaCl solutions of (b) 300 mM, (c) 500 mM, (d) 700 mM, (e) 1 M concentration at $\phi$ = 20.

profile of DMTAP-salt system is shown in fig. 4.12, fg. 4.13, fig. 4.14 and fig. 4.15. 20wt% DMTAP samples form a lamellar phase in water with d= 15.64 nm. Bilayers formed by the charged lipids have a higher bending rigidity ($\sim$ 100 $k_BT$)[6] compared to those formed by neutral lipids ($\sim$ 30 $k_BT$)[15]. Effect of monovalent salts on the reduction of bending rigidity is reported earlier[5,6]. Effect of NaCl on the lamellar periodicity of DOTAP-water system has been studied earlier[17]. In our case a gradual decrease in d-spacing is observed with increasing salt concentration (table 4.6) till it reaches the minimum ($L_\alpha^c$ phase), where two bilayers are separated by a thin water layer.

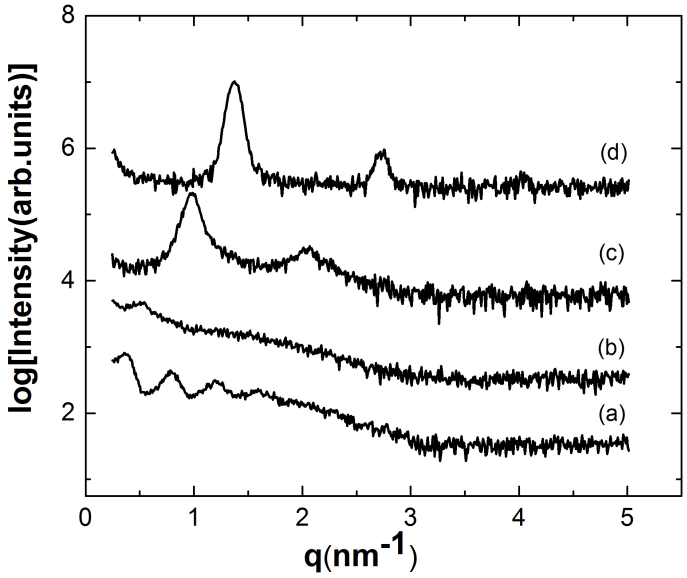


FIGURE 4.14: SAXS profile of DMTAP dispersions in (a) water, and in KCl solutions of (b) 300 mM, (c) 500 mM, (d) 1 M concentration $\phi$ = 20.

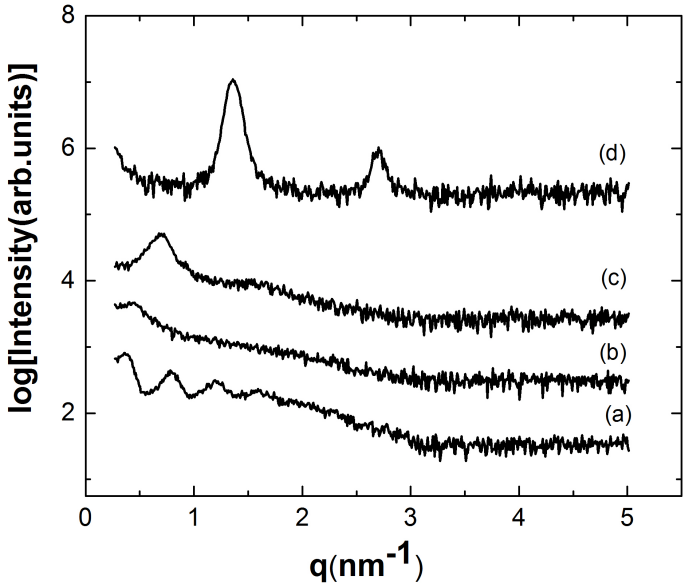


FIGURE 4.15: SAXS profile of DMTAP dispersions in (a) water, and in CsCl solutions of (b) 300 mM, (c) 500 mM, (d) 1 M $\phi$ = 20.

This indicates that the Debye length is gradually decreasing with increasing salt concentration. The amplitude of the undulation repulsion is much lower in the case of lipids, due to the high bare rigidity of the system[11]. The value of observed d-spacing is higher in the case of CsCl, compared to the other salts, when [$C_s$] = 300mM or 500mM. The reason for such behaviour we were unable to figure out at present.

A 20 wt% DDAC dispersion in water forms a lamellar phase of d $\sim$ 11 nm. Several distinct sharp peaks are observed in the SAXS pattern, which as discussed below,reveals that DDAC forms

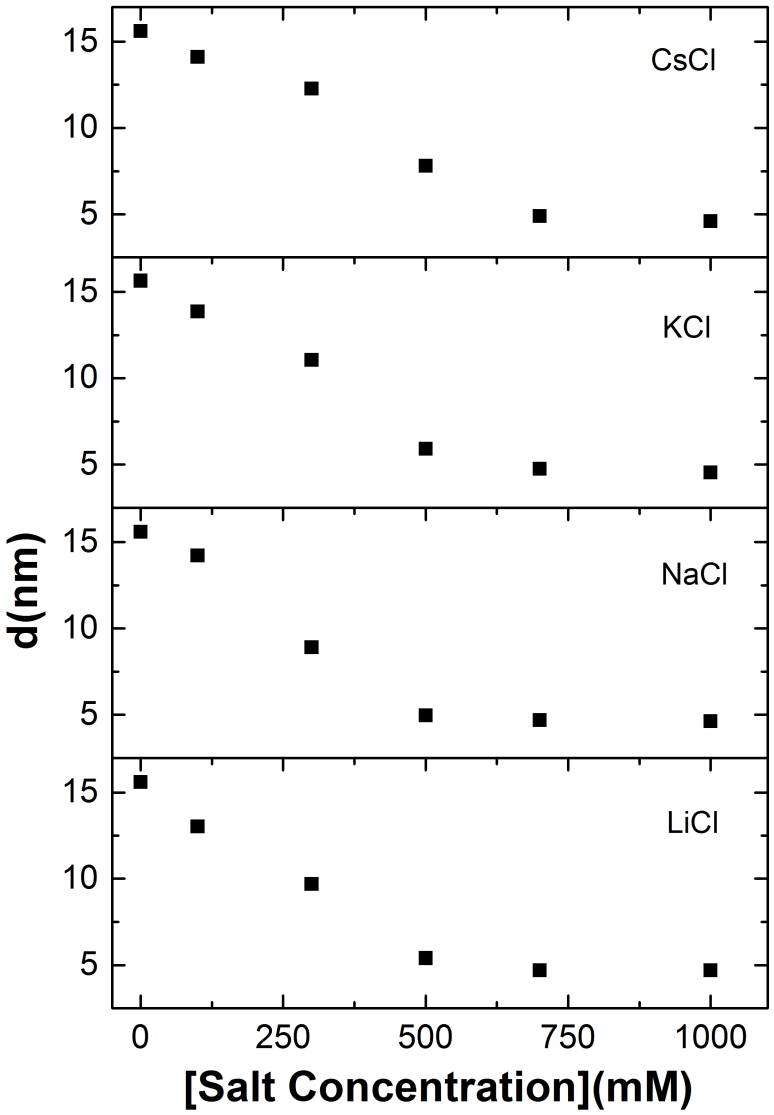


FIGURE 4.16: Variation of d-spacing with salt concentration for different salts for DMTAP samples at $\phi$ = 20. Typical error bar for the fully swollen $L_\alpha$ phase is $\pm$ 0.3nm, where as for the $L_\alpha^c$ phase it is $\pm$ 0.02nm.

rigid, flat bilayers in water and that the lamellar phase is stabilized by inter bilayer electrostatic repulsion. As the salt concentration is increased only one or two broad peaks are observed. This indicates that the lamellar phase is no longer stabilized by electrostatic repulsion, but by steric repulsion between the thermally undulating bilayers[4,7,8], since the bending rigidity of charged bilayers is reduced in the presence of salt[5,6]. In order to confirm this hypothesis, SAXS data for 20wt% DDAC samples in water and in 200 mM NaCl are fitted to a model by following the protocol described in[18].As discuused in the earlier chapter, the scattered intensity, I(q), from a lamellar phase can be expressed as the product of a structure factor, S(q), and a bilayer form factor, F(q), given by,

$$S(q) = N + 2\sum_{k=1}^{N-1}(N-k)cos(kqd) \times exp[-(\frac{d}{2\pi})^2 q^2 \eta^2 \gamma](\pi k)^{-(\frac{d}{2\pi})^2 q^2 \eta} \tag{4.1}$$

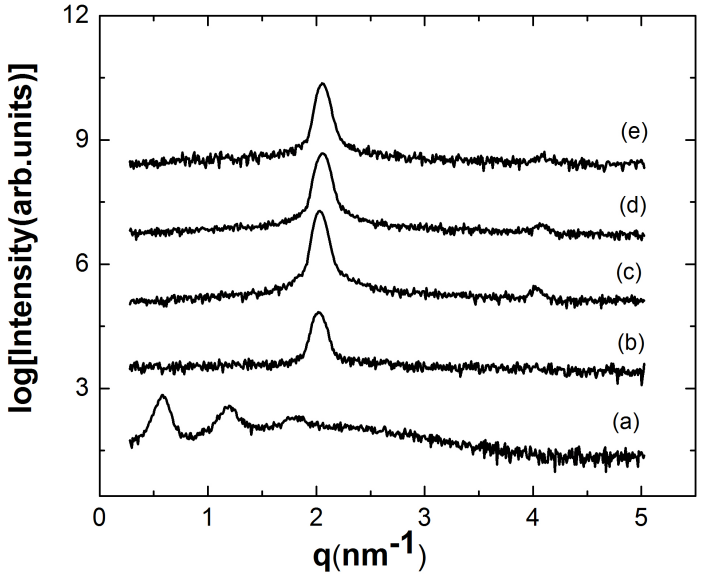


FIGURE 4.17: SAXS profiles of 20 wt% DDAB dispersions in (a) water, and in LiBr solutions of (b) 100 mM, (c) 200 mM, (d) 500 mM and (e) 1 M concentration.

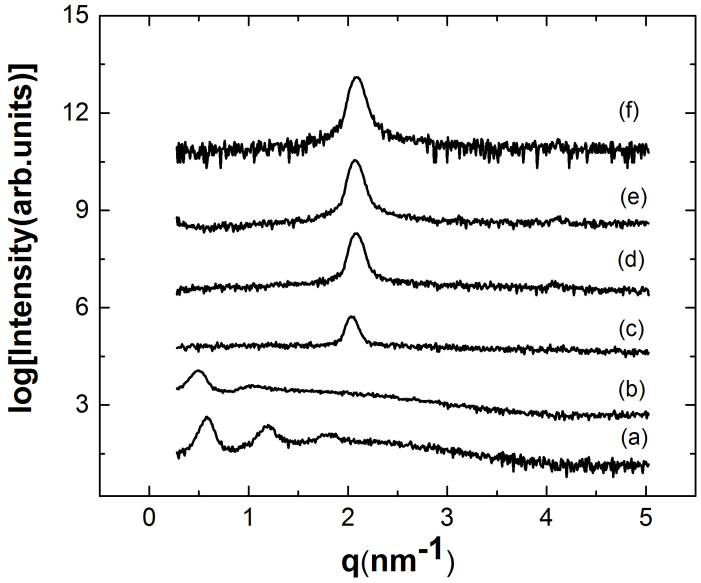


FIGURE 4.18: SAXS profiles of 20 wt% DDAB dispersions in (a) water, and in NaBr solutions of (a) 0 mM. (b) 50 mM, (c) 100 mM, (d) 200 mM, (e) 500 mM and (f) 1 M concentration.

and

$$F(q) = 2\sqrt{2\pi}\sigma_H\bar{\rho_H}exp(-\frac{\sigma_H^2q^2}{2})cos(qz_H) + \sqrt{2\pi}\sigma_c\bar{\rho_c}exp(-\frac{\sigma_c^2q^2}{2}) \quad (4.2)$$

Where N is the number of correlated bilayers in the lamellar stack, $z_h$ is half the bilayer thickness, $\sigma_H$ and $\sigma_C$ are the widths of the Gaussians for the head group and the hydrocarbon tail regions of the bilayers. $\bar{\rho_H}$ and $\bar{\rho_C}$ are the electron density of the head group and tail regions

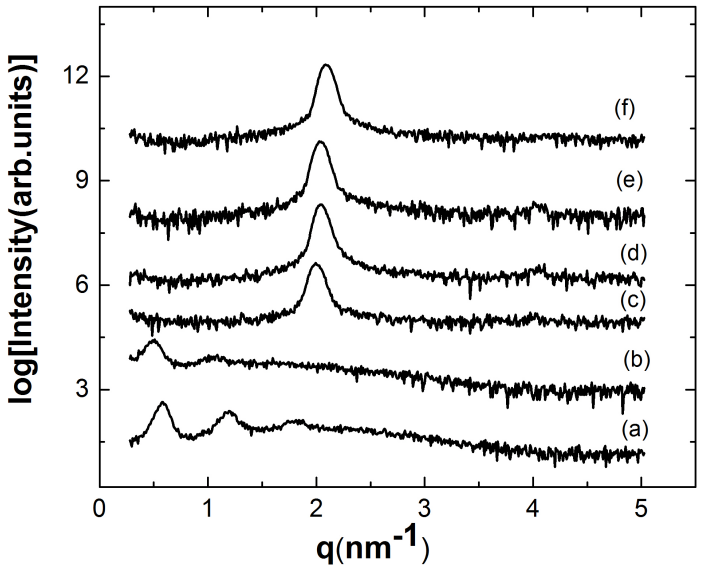


FIGURE 4.19: SAXS profile of 20 wt% DDAB dispersions in (a) water, and in KBr solutions of (b) 50 mM, (c) 100 mM, (d) 200 mM, (e) 300 mM and (f) 1 M concentration.

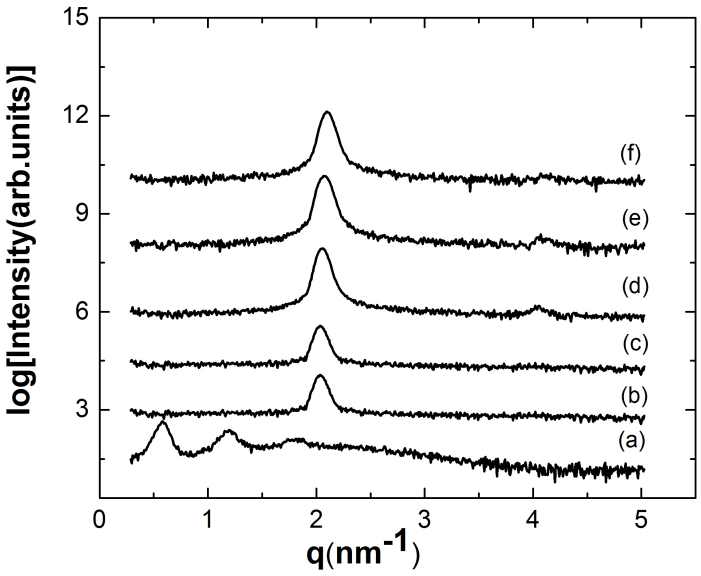


FIGURE 4.20: SAXS profile of 20 wt% DDAB dispersions in (a) water, and in CsBr concentrations of (b) 100 mM, (c) 200 mM, (d) 300 mM, (e) 500 mM and (f) 1 M concentration.

with respect to that of the metylene group. $\eta$ is the Callié parameter, which is a function of both bending rigidity modulus ($\kappa$) and bulk compression modulus ($B$), ($\eta \propto 1\sqrt{kB}$). Fig. 4.28 shows the experimental data and the fit to the model for 20wt% DDAC samples in water and in 200mM NaCl solution. The fitting parameters are given in table. 5.6. The value of $\eta$ increases from 0.08 in water to 0.74 in the presence of 200mM NaCl. This increase in the value of $\eta$ in the presence of salt is in agreement with the previous study[19] and confirms the significant softening of the bilayer in

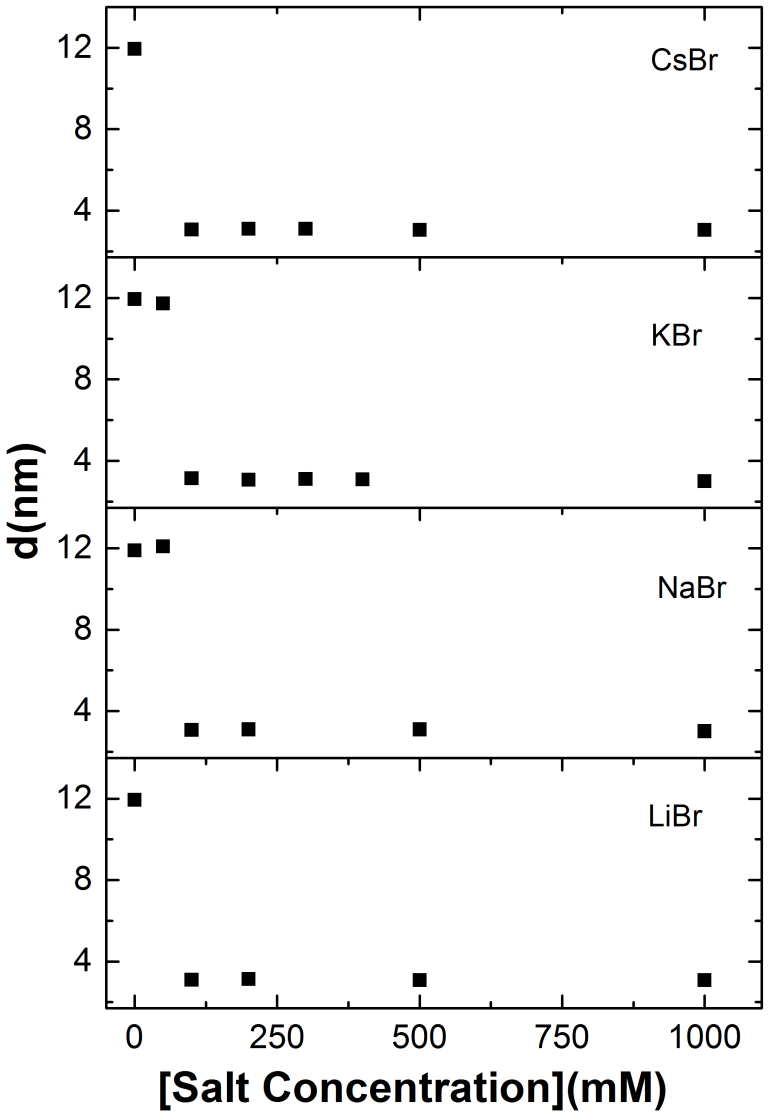


FIGURE 4.21: Variation of d-spacing with salt concentration for different salts for DDAB samples at $\phi = 20$. Typical error bar for the fully swollen $L_\alpha$ phase is $\pm$ 0.3nm, where as for the $L_\alpha^c$ phase it is $\pm$ 0.01nm

the presence of salt.

Fig. 4.7 shows a spread in the d-spacing in the low salt regime. The typical error bar of the measurements is shown for the DDAC- Water system. The spread in the d-spacing can be attributed to the formation of uni lamellar vesicles (ULVs) or small multi lamellar vesicles (MLVs) during sample preparation, which can exert some vestigial osmotic pressure on the system[6]. The value of such osmotic pressure may vary from sample to sample, hence a spread in d is observed. At moderate salt concentration at room temperature (30°C), a lamellar phase with much lower periodicity is observed ($L_\alpha^c$ phase). The threshold value of salt concentration at which the lamellar periodicity abruptly decreases is found to be dependent on the salt. For NaCl and KCl it is $\sim$ 375mM, for LiCl and CsCl it is $\sim$ 450mM. At these salt concentrations the Debye length is about 0.5 nm[1]. So the electrostatic repulsion becomes negligible. The attractive van der Waals force dominates.

| [Salt Concentration] (mM) | $d_{NaCl}$ (nm) | $d_{KCl}$ (nm) | $d_{LiCl}$ (nm) | $d_{CsCl}$ (nm) |
|---|---|---|---|---|
| 0 | 10.06 | 10.06 | 10.06 | 10.06 |
| 100 | 7.02 | 6.96 | 7.26 | 8.24 |
| 200 | 6.8 | 6.49 | 6.12 | 7.51 |
| 300 | 5.29 | 5.21 | 6.02 | 6.46 |
| 400 | 3.82 | 4.1 | 4.34 | 5.52 |
| 500 | 3.48 | 3.56 | 3.55 | 5.32 |
| 1000 | 3.25 | 3.24 | 3.31 | 3.32 |

TABLE 4.8: Variation of d with salt concentration for different salts in the DDAC system at $\phi$= 20. These samples were not mixed during their preparation.

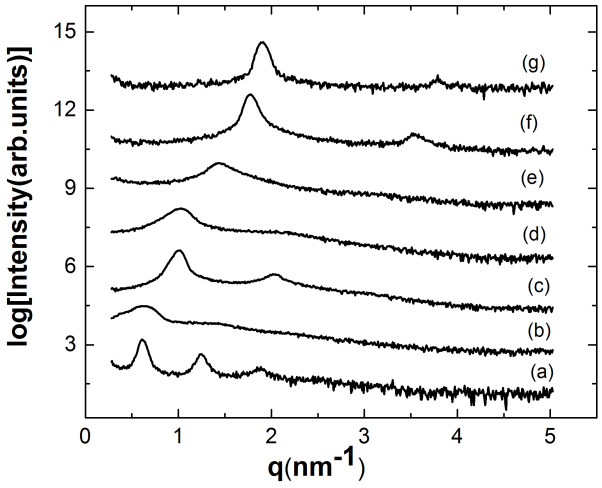


FIGURE 4.22: SAXS profiles of DDAC dispersions in (a) water and in LiCl solution of (b) 100 mM, (c) 200 mM, (d) 300 mM, (e)400 mM, and (f) 500 mM and (g) 1M concentration at $\phi$= 20. These samples were not mixed during preparation.

| [$C_s$] (mM) | $z_h$ (nm) | $\sigma_H$ (nm) | $\sigma_C$ (nm) | $\bar{\rho_H}$ / $\bar{\rho_C}$ | $\eta$ |
|---|---|---|---|---|---|
| 0 | 1.01 | 0.17 | 0.24 | -0.140 | 0.08 |
| 200 | 1.01 | 0.19 | 0.13 | -0.06 | 0.74 |

TABLE 4.9: Values of the model parameters obtained from the best fit.

At $\sim$ 500mM of salt concentration the d-spacing becomes very close to the bilayer thickness[12], so this phase can be viewed as corresponding to the primary minimum of the DLVO potential, where the particles can touch each other, but with a difference. In the case of surfactant or lipid molecules there is a short range hydration repulsion, attributed to the hydration of hydrophilic

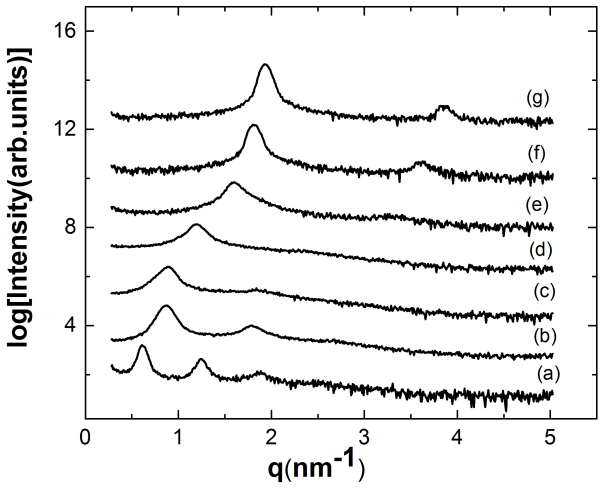


FIGURE 4.23: SAXS profiles of DDAC dispersions in (a) water and in NaCl solutions of (b) 100 mM, (c) 200 mM, (d) 300 mM, (e)400 mM, and (f) 500 mM and (g) 1M concentration at $\phi$= 20. These samples were not mixed during preparation.

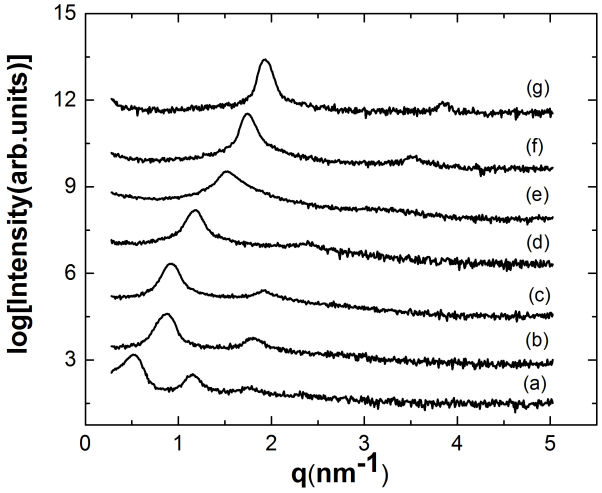


FIGURE 4.24: SAXS profiles of DDAC dispersions in (a) water and in KCl solutions of (b) 100 mM, (c) 200 mM, (d) 300 mM, (e)400 mM, and (f) 500 mM and (g) 1M concentration at $\phi$= 20. These samples were not mixed during preparation.

head groups of the ampphiphilic molecules[14,20]. Therefore, there is a thin layer of water separating the bilayers in the $L_c$ phase. So the primary minimum of DLVO potential is shifted. The details of this hydration repulsion is discussed in chapter 1 of this thesis. In our experiment, the $L_\alpha^c$ phase appears at different concentrations for different salts, we are unable to explain the reason behind such a specific ion-effect. Further work needs to be done for a detailed understanding of this observation.

We have studied the effect of temperature on the collapsed lamellar phase ( $L_\alpha^c$) formed by DDAC bilayers. Fig. 5.16 and fig. 5.17 show the SAXS patterns as function of temperature for 20wt% DDAC- NaCl and DDAC-KCl samples, respectively. The value of d for DDAC-NaCl and DDAC-KCl systems are given in table 4.1 and table 4.2. The d-spacing increases with increasing

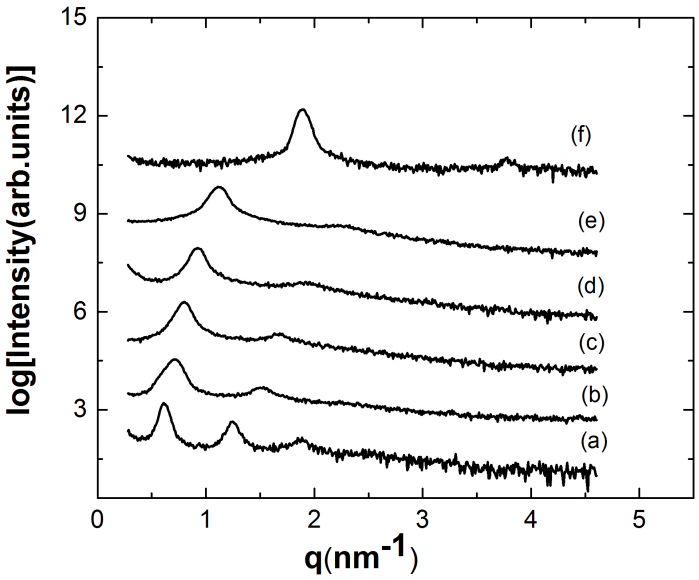


FIGURE 4.25: SAXS profile of DDAC dispersions in (a) water and in CsCl solutions of (b) 100 mM, (c) 200 mM, (d) 300 mM, (e)400 mM, and (f) 500 mM and (g) 1M concentration at $\phi$= 20. These samples were not mixed during preparation.

temperature. The temperature at which the spacing starts to increase, increases with salt concentration. At 1M of salt concentration the spacing does not change even at the highest temperature (70°C). From table 4.1 it is clear that at 70°C a fully swollen phase is found up to [$C_s$] = 425 mM. Over an intermediate temperature range no peak is observed in the SAXS pattern, suggesting the formation of uncorrelated bilayers. To verify whether the formation of uncorrelated bilayers is a general phenomenon or not, 30wt% DDAC samples were prepared over this NaCl concentration range. SAXS profiles of 30wt% DDAC- NaCl samples are shown in fig. 4.10. From fig. 4.10b it is clear that the peak becomes broad on increasing the temperature before it reaches a fully swollen phase, where the peak appears to be sharper. These samples were equilibrated for 30 min before data collection at each temperature in order to avoid artifacts due to slow kinetics. Before going to a fully swollen phase, a lamellar phase with a lower d-spacing is observed. In order to observe a $L_\alpha^c \hookrightarrow L_\alpha$ phase transition on increasing the temperature, there should be enhancement of inter-bilayer repulsion on increasing the temperature or decrease in the attractive interaction. It is very unlikely to have an increase the electrostatic repulsion or a decrease in van der Waals attraction on increasing the temperature over this temperature range. The other possibility is an increase of undulation repulsion with temperature , which has been shown to lead to a gradual swelling of the lamellar phase with increasing temperature[21]. At sufficiently high temperature, the repulsion can be strong enough to lead to the formation of uncorrelated bilayers. Similar binding- unbinding transition has been observed in a mixture of charged and uncharged lipids[22]. On increasing the temperature more, the magnitude of the repulsion increases further. But since the samples only have a limited water content, the increased repulsion can give rise to the ordering of bilayer stacks. Hence the peaks appear in the SAXS pattern for 20 wt% samples at high temperatures. Since in the 30 wt% samples the water content is even less, there is no formation of uncorrelated bilayers over intermediate temperatures. Only a broadening of the peaks is observed. From fig.4.10(b) and

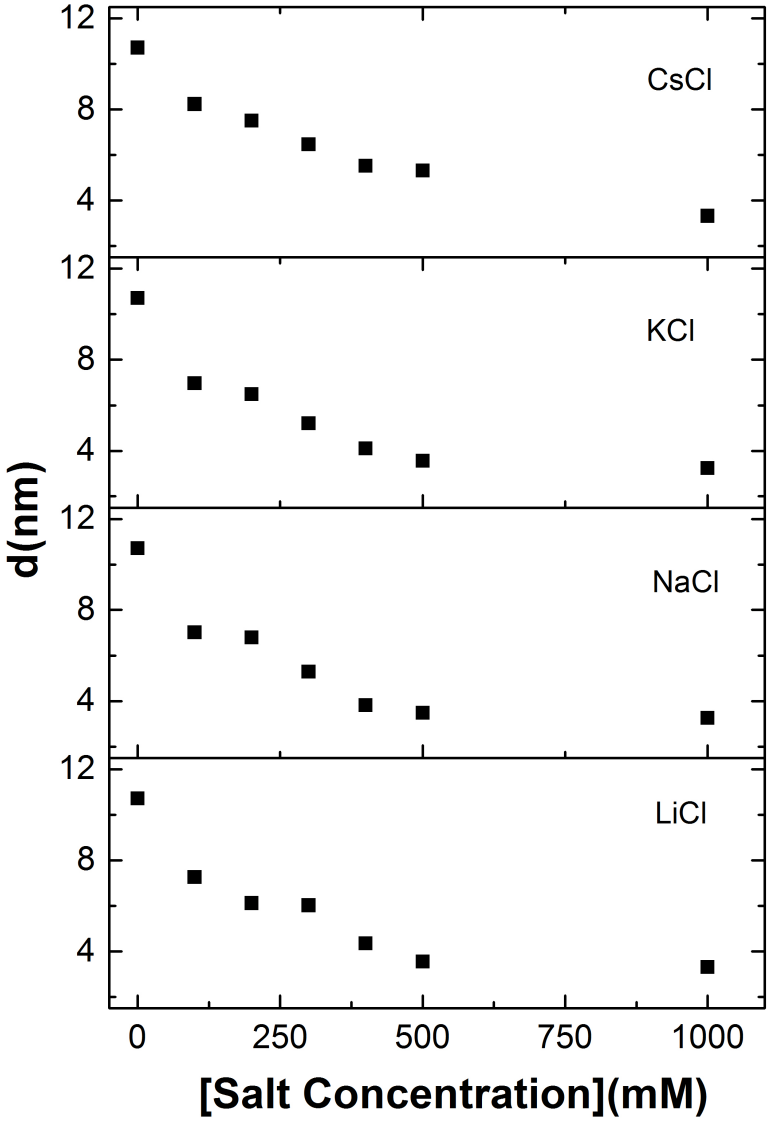


FIGURE 4.26: variation of d-spacing with salt concentration for different salts for DDAC samples at $\phi$ = 20. These samples were not mixed during preparation.

fig.4.10(c), it is clear that the behaviour aphenomen is completely reversible on heating and cooling. There is an increase in the transition temperature with salt concentration. At present we are unable to figure out the precise mechanism for this. Further work needs to be done for a detailed understanding.

Effect of alkali metal bromides (LiBr, NaBr, KBr and CsBr) on the lamellar phase of DDAB, is found to be qualitatively similar to the effect of chloride salts on the lamellar phase of DDAC. The only difference is that the collapsed lamellar phase ($L_\alpha^c$) in the case of DDAB occurs at a much lower salt concentration ($C_s \sim$ 100mM). 20 wt% DDAB in water forms a lamellar phase with d=11.9 nm. Multiple sharp peaks are shown in the SAXS pattern, indicating that the system is stabilized by inter bilayer electrostatic repulsion. At [NaBr]= 50 mM, the periodicity remains almost the same, but the scattering profile shows two broad peaks. Debye length at this salt

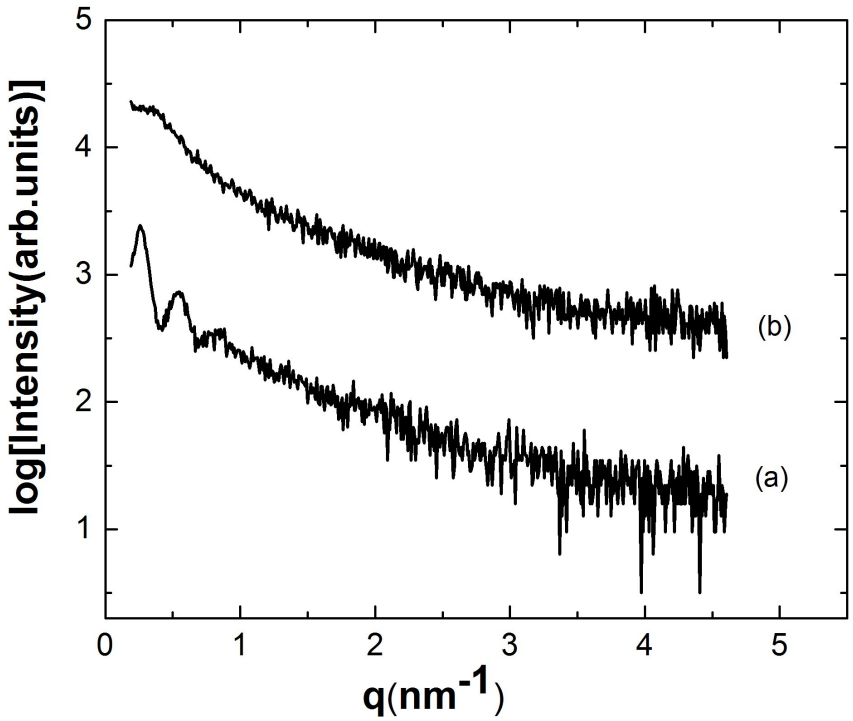


FIGURE 4.27: SAXS profile of DDAC dispersions in (a) water and in NaCl solution of (b) 200mM concentration at $\phi$ = 10.

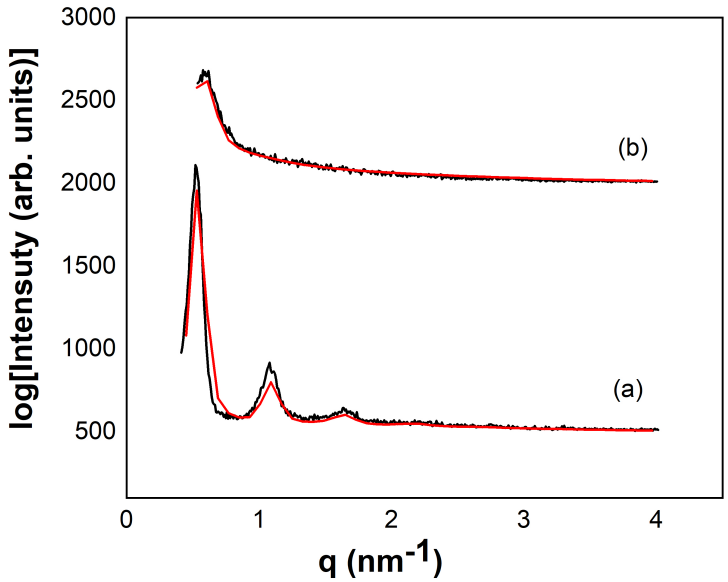


FIGURE 4.28: Fitted data for 20wt% DDAC samples in water (a) and in 200mM NaCl Solution (b). The black line represents the experimental result and the red line represents the best fit profile obtained from the model.

concentration is $\sim$ 1 nm. The much larger periodicity compared to the Debye length and the presence of broad peaks in the scattering profile suggest that this phase is stabilized by undulation repulsion. (fig. 4.18). At [$C_s$]= 100mM, the spacing reduces to 3.1 nm. The appearance of $L_\alpha^c$ phase at lower salt concentration in the case of DDAB compared to the case of DDAC, can be

attributed to the different counter-ions of the two surfactants. Fig.4.1 shows the phase diagram of these two surfactants in water. A two-lamellar phase co-existence region is observed for DDAB, whereas for DDAC only a single lamellar phase is seen. A previous study has shown that the stronger affinity of the $Br^-$ counterion to get absorbed on the bilayer compared to $Cl^-$ can lead to enhanced attraction between the DDAB bilayers[23]. The presence of such an additional attractive interaction between DDAB bilayers can explain the formation of the $L_\alpha^c$ phase at much lower salt concentrations. The effect of different bromide salts on the phase behaviour of DDAB is found to be similar.

The DDAC samples which were not mixed during time of the preparation show a monotonic decrease of d-spacing with increasing salt concentration till it reaches the minimum ($L_\alpha^c$ phase) (table4.8). There is a clear phase separation observed in the non-mixed samples. The top layer of the samples show a lamellar phase ($L_\alpha$). From the bottom part of the sample no significant scattering intensity is observed. Earlier study on DDAB bilayers has shown the formation of a very dilute meta stable sponge phase ($L_3$), which disappears after long incubation time ($\sim$ 90 days)[12]. The presence of such a dilute phase in the present samples can apply an osmotic pressure on the lamellar phase, leading to the observed behaviour.

The effect of salt on the lamellar phase formed by charged surfactant and lipids can be qualitatively explained by using the DLVO theory. The van der Waals interaction energy per unit area of a bilayer can be written as[24],

$$V_a = -\frac{A}{12\pi}\left[\frac{1}{d_W^2} - \frac{2}{((d_W + d_B)^2} + \frac{1}{(d_W + 2d_B)^2}\right] \tag{4.3}$$

Where A is the Hamaker Constant, $d_B$ is the bilayer thickness, $d_W$ is the water layer thickness. The electrostatic interaction per unit area can be express as[25–27],

$$V_r = P_{ES}\lambda_D(coth(\frac{d_W}{2\lambda_D}) - 1) \tag{4.4}$$

Where, $P_{ES} = \sigma_s^2/\epsilon\epsilon_0$, $\sigma_s$ is the surface charge density, $\epsilon$ is the permittivity of salt solution and $\epsilon_0$ is the permittivity of free space, $\lambda_D$ is the Debye length.

Total interaction energy per unit area can be written as,

$$U = V_a + V_r \tag{4.5}$$

Fig. 4.29 shows the DLVO potential for two different values of the Hamaker constant (A). The values of the A were taken from[6,28]. The area per charge is taken as 2.94 $nm^2$ [28]. It is seen from the figures that the height of the barrier reduces as more and more salt is added, before it finally disappears. This is because the electrostatic repulsion between the the surfaces gets screened with increasing salt concentration. The Hamaker constant, which represents the strength of the attractive van der Waals attraction, is more in the second case. Hence the barrier disappears at much lower salt concentration in that case. There is also a secondary minimum in the potential, which is shown in the inset. It is clear from fig.4.29a, that the position of the secondary minimum shifts of lower values of inter bilayer separation ($d_W$ ) as the salt concentration is increased.

Fig. 4.30 represents the effect of surface charge density on the DLVO potential. As the charge density increases the electrostatic repulsion between the charged surfaces increases. Hence, more salt is required to screen the interaction. So, the electrostatic repulsion dominates up to higher

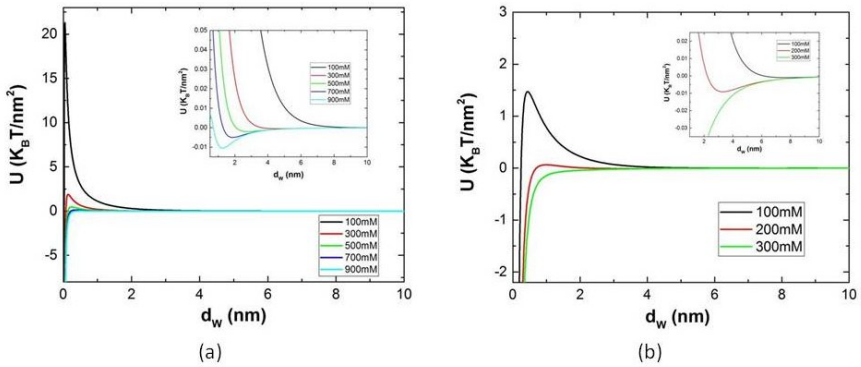


FIGURE 4.29: Total interaction energy per unit area of a bilayer vs water layer thickness for two different values of the Hamaker constant (a) A= 1.8 $k_BT$ (b) A= 16.9 $k_BT$. The position of the secondary minimum is shown in the inset.

salt concentrations. From fig.4.30 b, (where the assumed surface charge density is maximum) it is seen that the barrier does not disappear at even 1M salt concentration. Whereas in the other case ( fig.4.30a ) the barrier disappears at 400 mM. Position of the secondary minimum, for different salt concentrations, is shown in the insets. The value A is taken as 16.9 $k_BT$. The area per charge in fig.4.30b, is 0.65 $nm^2$, which is close to charge density of DDAB and DDAC bilayers at complete dissociation[12]. It is clear from the above discussion that the potential barrier disappears above a critical salt concentration, which increases with the surface charge density of the bilayer. The bilayers become "sticky" above this salt concentration and the undulation-stabilized swollen lamellar phase is no longer stable. This provides a qualitative explanation of the observed abrupt $L_\alpha \hookrightarrow L_\alpha^c$ transformation. The much lower critical salt concentration found in the case of DDAB is consistent with the higher propensity of the $Br^-$ counterions to adsorb back on the bilayer, thus reducing the surface charge density. The absence of such a transition in the case of DMTAP might be a consequence of the much stronger hydration repulsion in this case, due to its much bigger head group, which can prevent the system from accessing the primary minimum.

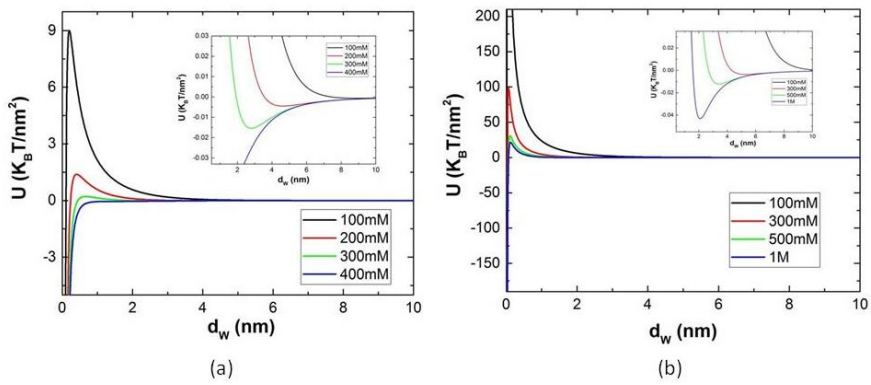


FIGURE 4.30: Total interaction energy of a bilayer per unit area vs water layer thickness for two different values of $\sigma_s$ (a) $e^-/2\ nm^2$ (b) $e^-/\ 0.65\ nm^2$. The position of the secondary minimum is showed in the inset.

## 4.5 Conclusions

In this chapter we have studied the effect of salt on the phase behaviour of fluid lamellar phase formed by ionic surfactants and lipids at low salt regime. In the case of surfactant bilayers (DDAC an DDAB) the sysytem goes from an electrosatically stabilized phase to a undulation stabilized phase on increasing the salt concentration in the solution, before it goes into a collapse lamellar ($L_\alpha^c$) phase. The value of salt concentration at which the collapsed phase appears is different for DDAC and DDAB. This can be attributed to the difference in the counter-ions in the two systems. A specific-ion effect is also observed as the value of $C_s$ at which the $L_\alpha^c$ phase appears in the case of DDAC, is slightly higher for LiCl and CsCl compared to NaCl or KCl. A temperature driven $L_\alpha^c \hookrightarrow L_\alpha$ transition is observed in the case of lamellar phase formed by DDAC. The transition temperature depends on the salt concentration. In the case of charged lipid bilayers (DMTAP), whose bare bending rigidity is a order of magnitude higher compared to the surfactant bilayers, a gradual reduction of d-spacing is observed with increasing $C_s$.

# Bibliography


[1] Israelachvili JN. Intermolecular and surface forces. Academic press; 2011.

[2] Jones RAL, Jones RA, Jones R, et al. Soft condensed matter. vol. 6. Oxford University Press; 2002.

[3] Andelman D. Introduction to electrostatics in soft and biological matter. Soft condensed matter physics in molecular and cell biology. 2006;6.

[4] Helfrich W. Steric interaction of fluid membranes in multilayer systems. Zeitschrift für Naturforschung A. 1978;33(3):305-15.

[5] Faizi HA, Frey SL, Steinkühler J, Dimova R, Vlahovska PM. Bending rigidity of charged lipid bilayer membranes. Soft Matter. 2019;15(29):6006-13.

[6] Lu BS, Gupta SP, Belička M, Podgornik R, Pabst G. Modulation of elasticity and interactions in charged lipid multibilayers: monovalent salt solutions. Langmuir. 2016;32(50):13546-55.

[7] Roux D, Nallet F, Freyssingeas E, Porte G, Bassereau P, Skouri M, et al. Excess area in fluctuating-membrane systems. Europhys Lett. 1992;17(7):575.

[8] Roux D, Safinya C. A synchrotron X-ray study of competing undulation and electrostatic interlayer interactions in fluid multimembrane lyotropic phases. Journal de Physique. 1988;49(2):307-18.

[9] Robb ID. Specialist surfactants. Springer Science & Business Media; 1996.

[10] Kang C, Khan A. Self-assembly in systems of didodecyldimethylammonium surfactants: Binary and ternary phase equilibria and phase structures with sulphate, hydroxide, acetate, and chloride counterions. Journal of colloid and interface science. 1993;156(1):218-28.

[11] Purushothaman S, Cicuta P, Ces O, Brooks NJ. Influence of high pressure on the bending rigidity of model membranes. The Journal of Physical Chemistry B. 2015;119(30):9805-10.

[12] Dubois M, Zemb T. Phase behavior and scattering of double-chain surfactants in diluted aqueous solutions. Langmuir. 1991;7(7):1352-60.

[13] Lewis RN, Tristram-Nagle S, Nagle JF, McElhaney RN. The thermotropic phase behavior of cationic lipids: calorimetric, infrared spectroscopic and X-ray diffraction studies of lipid bilayer membranes composed of 1, 2-di-O-myristoyl-3-N, N, N-trimethylaminopropane (DMTAP). Biochimica et Biophysica Acta (BBA)-Biomembranes. 2001;1510(1-2):70-82.

[14] Parsegian VA, Fuller N, Rand RP. Measured work of deformation and repulsion of lecithin bilayers. Proceedings of the National Academy of Sciences. 1979;76(6):2750-4.

[15] Dimova R. Recent developments in the field of bending rigidity measurements on membranes. Advances in colloid and interface science. 2014;208:225-34.

[16] Nagle JF, Tristram-Nagle S. Structure of lipid bilayers. Biochimica et Biophysica Acta (BBA)-Reviews on Biomembranes. 2000;1469(3):159-95.

[17] Thomas M. Surfactant-Polyelectrolyte complexes: Structure and Interactions. Raman Research Institute, Bangalore.; 2019.

[18] Pabst G, Rappolt M, Amenitsch H, Laggner P. Structural information from multilamellar liposomes at full hydration: full q-range fitting with high quality x-ray data. Physical Review E. 2000;62(3):4000.

[19] Thomas M, Swamynathan K, Raghunathan V. Salt-induced swelling transitions of a lamellar amphiphile—Polyelectrolyte complex. J Chem Phys. 2019;150(9):094903.

[20] Rand R. Interacting phospholipid bilayers: measured forces and induced structural changes. Annual review of biophysics and bioengineering. 1981;10(1):277-314.

[21] Lipowsky R, Leibler S. Unbinding transitions of interacting membranes. Physical Review Letters. 1986;56(23):2541.

[22] Pozo-Navas B, Raghunathan V, Katsaras J, Rappolt M, Lohner K, Pabst G. Discontinuous unbinding of lipid multibilayers. Physical review letters. 2003;91(2):028101.

[23] Tatulian SA. Effect of lipid phase transition on the binding of anions to dimyristoylphosphatidylcholine liposomes. Biochimica et Biophysica Acta (BBA)-Biomembranes. 1983;736(2):189-95.

[24] Safran SA. Statistical thermodynamics of surfaces, interfaces, and membranes. CRC Press; 2018.

[25] Markovich T, Andelman D, Podgornik R. Handbook of Lipid Membranes. Taylor & Francis New York; 2016.

[26] Parsegian VA, Gingell D. On the electrostatic interaction across a salt solution between two bodies bearing unequal charges. Biophysical journal. 1972;12(9):1192-204.

[27] Ben-Yaakov D, Andelman D. Revisiting the Poisson–Boltzmann theory: Charge surfaces, multivalent ions and inter-plate forces. Physica A: Statistical Mechanics and its Applications. 2010;389(15):2956-61.

[28] Zemb T, Belloni L, Dubois M, Marcelja S. Osmotic pressure of highly charged swollen bilayers. Trends in Colloid and Interface Science VI. 1992:33-8.

# Chapter 5

# Effect of salt on inter-bilayer interactions in the lamellar phase of some ionic amphiphiles: high salt regime

## 5.1 Introduction

In this chapter we describe the influence of salt on the lamellar phase formed by cationic surfactants and lipids at high salt concentrations ( up to 4 M ). Earlier study done by Smith et al. showed that there is a long range repulsion between two smooth mica surfaces across a electrolytes at high electrolyte concentration[1]. The experimental decay length ($\lambda_{exp}$) is found to be much greater that the theoritical decay length ($\lambda_D$), which is given by,

$$\lambda_D = \sqrt{\frac{\epsilon_r \epsilon_0 k_B T}{\sum_i \rho_{\infty i} e_i^2 z_i^2}} \tag{5.1}$$

Where T is the temperature, $k_B$ is the Boltzmann's constant, $\epsilon_0$ is the permittivity of free space, $\epsilon_r$ is the relative permittivity, $\rho_{\infty i}$ is the number density of ion type i and $z_i$ is the valency of ion type i. The interaction forces between two mica surfaces were measured using surface force balance apparatus. The electrolytes used were (a) NaCl solution and (b) ionic liquid 1-butyl-1-methylpyrrolidinium bis[(trifluoromethane)sulfonyl]imide. The eperimental findings of Smith et al. in presented are fig. 5.1 and fig. 5.2.

The electrolyte of interest was inserted between two mica sheets and the force between them is measured as a function of their separation. Beyond the oscillatory region a log range repulsion was found between the surfaces which was fitted to a exponentially decaying function ($F_N/R \approx \exp(-D/\lambda_{exp})$), Where $\lambda_{exp}$ is the experimental decay length, which was found to be $\sim$ 8.4 nm for the ionic liquid and $\sim$ 1.1 nm for 2 M NaCl. Fig. 2 shows the comparison between $\lambda_{exp}$ and $\lambda_D$ as a function of concentration. At low concentration $\lambda_{exp} \approx \lambda_D$. After a threshold, $\lambda_{exp}$ starts to increase, showing a significant deviation from $\lambda_D$ ($\lambda_{exp} \gg \lambda_D$). Surface force measurements from Israelachvili's group using ionic liquids shown a decay length of 10-13 nm, much larger than the theoretical Debye length given by eq 1[2]. Such large Debye length would correspond to a concentration of $10^{-4}$ M for a 1 : 1 electrolyte. The explanation was given assuming fractional dissociation of the liquid. The observation of long decay length was explained by Kjellander by taking into account ion-ion correlations[3,4]. A much longer decay length compared to $\lambda_D$ is

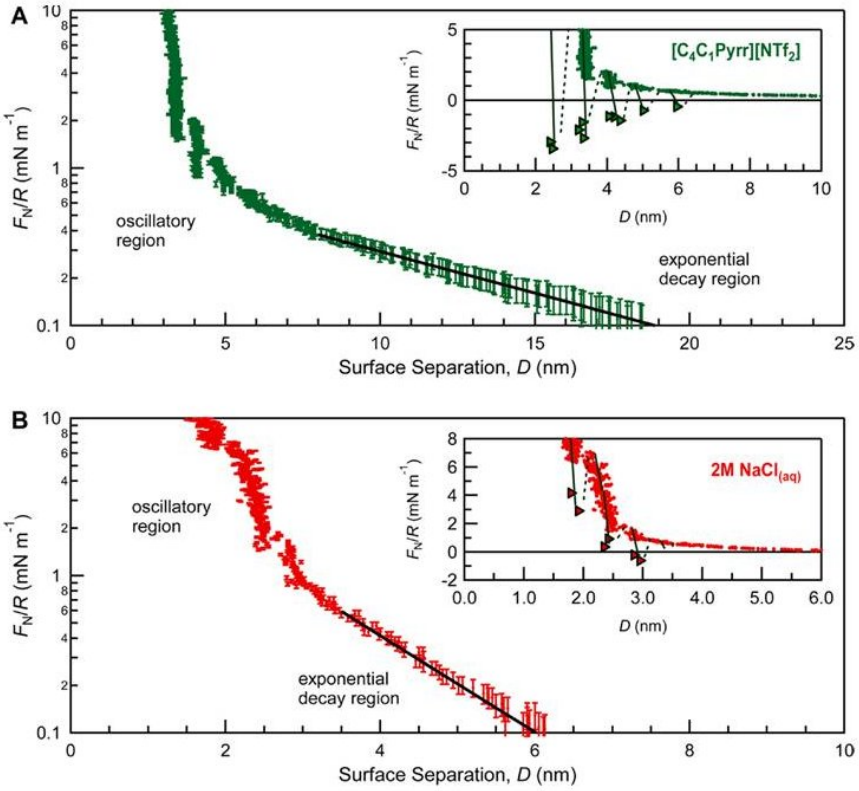


FIGURE 5.1: Normalised force ($F_N/R$) between two mica surfaces placed in a crossed-cylinder configuration across (a) ionic liquid and (b) aqueous solution of 2 M NaCl[1].

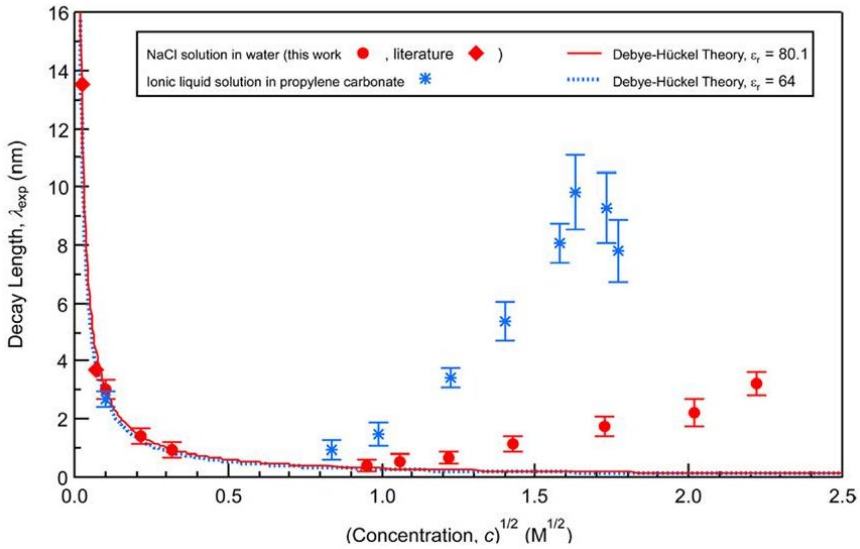


FIGURE 5.2: Decay length vs concentration (c $^{1/2}$) for two different electrolytes[1]

observed in the concentrated solution of LiCl and CsCl is reported in ref.[5]. The general finding of the change in decay length with concentration is expressed in fig. 5.3.

Another study has also reported an increase in the Debye length at salt concentration[6]. Unlike the previous case where measurements were based on surface force apparatus, in this case a new technique was used. In these experiments a small concentration of an ionic fluorescent dye (fluorescein, a dianion) ($10^{-5}$ times of the salt concentration) was added to the solution, whose

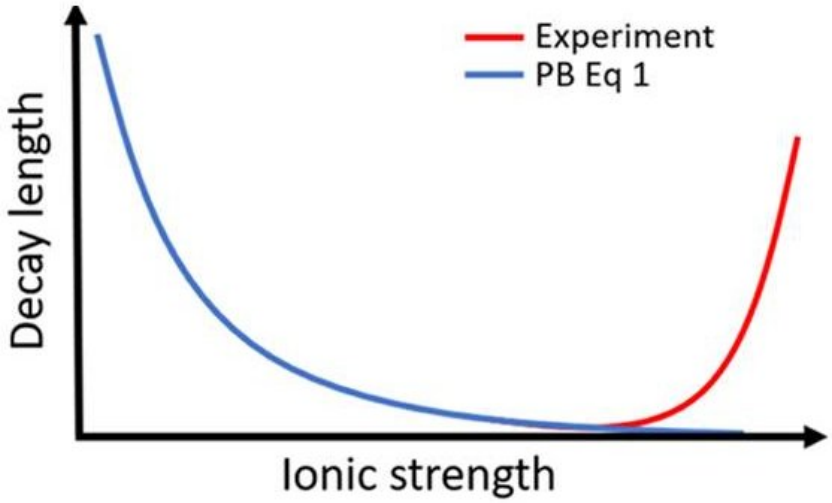


FIGURE 5.3: Decay length vs concentration plot. figure was taken from [6]

number was measured as a function of film thickness. If the decay length of the surface potential is much less than the separation between the plates, then the number of dye molecules near the mid plane will be the same as that near the surface, otherwise there will be a difference, which is called the surface excess. The main result of article[6] is presented in fig. 5.4. It is seen that the decay length of surface excess fluorescein in the case of NaCl and LiCl is of the order of 10 nm, suggesting the presence of a long range field. If classical Debye-Huckel theory was valid, at that concentrations, the decay length should be of the order of 0.1 nm (eq. 1). The occurrence of positive surface excess of fluroscein is attributed to the charge reversal of the silica surfaces, since both silica and fluroscein acquire negative charge in water. In the case of CsCl no surface excess fluroscein was observed. The authors did not provide any explanation for that. Change in decay length with the salt concentration is shown in fig. 5.5.

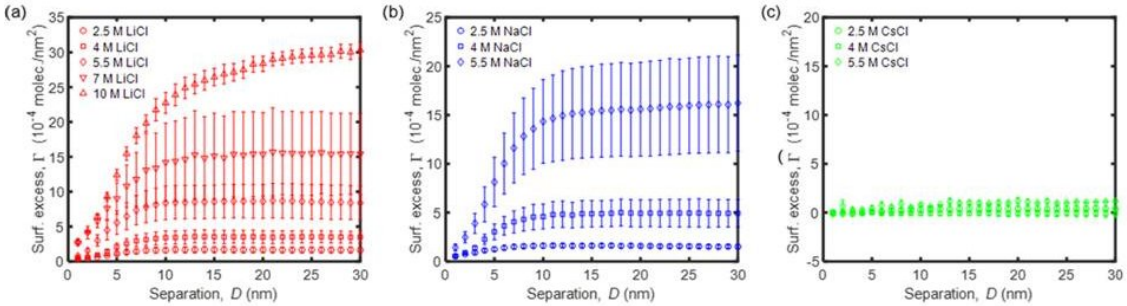


FIGURE 5.4: Surface excess of fluorescein as a function of separation (aqueous film thickness) for various salt concentrations and salt cations. Figure taken from [6]

In the above mentioned experiments the effect of high salt concentration was studied on two rigid flat surfaces made of either mica or silica surfaces. Both of the surfaces acquires negative charge in an aqueous solution. In this chapter we discuss the effect of alkali metal chlorides (LiCl, NaCl, KCl and CsCl) on the lamellar phase formed by didodecyldimethylammonium chloride (DDAC) and 1,2-dimyristoyl-3-trimethylammonium-propane (chloride salt) (DMTAP) bilayers

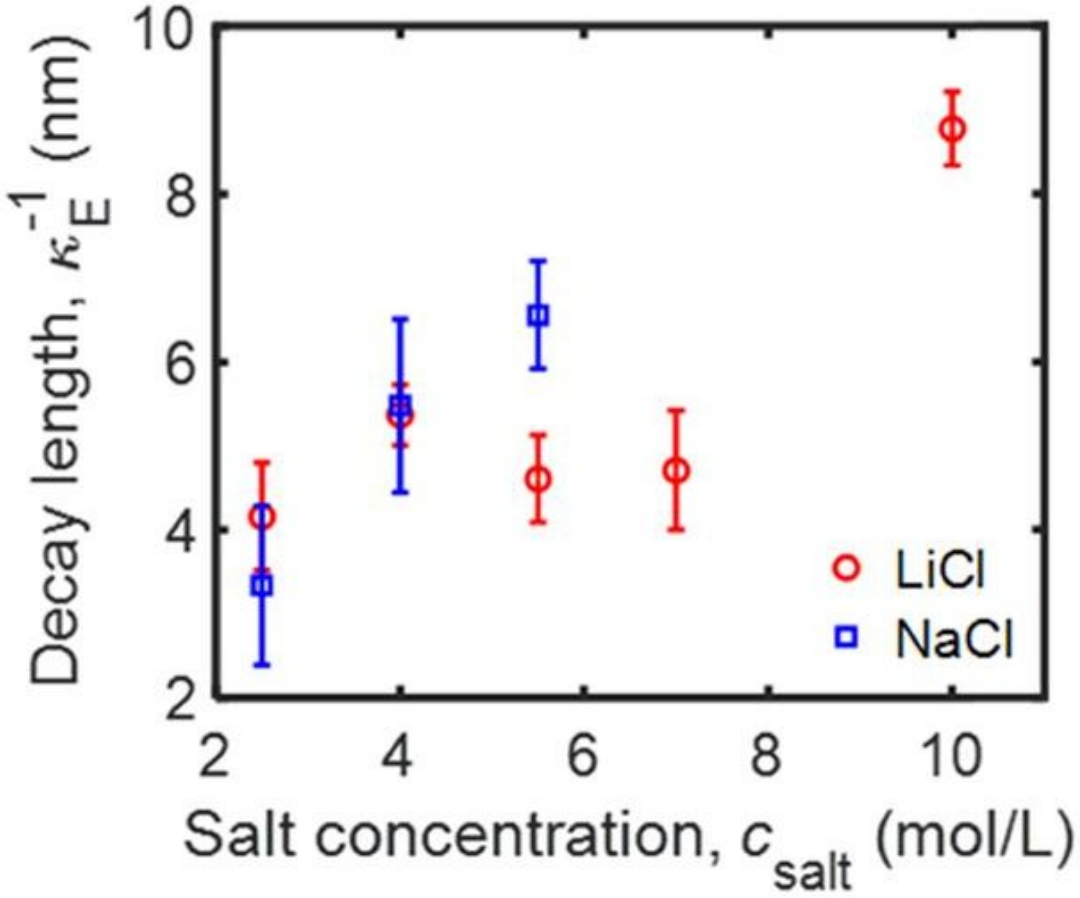


FIGURE 5.5: Decay length vs salt concentration. figure taken from [6]

and that of alkali metal bromides (LiBr, NaBr, KBr and CsBr) on the lamellar phase of didodecyldimethylammonium bromide (DDAB) bilayers using SAXS, POM and cryo-SEM techniques. DDAC, DDAB and DMTAP form lamellar phase in water over a wide range of concentration [7,8]. These amphiphilies acquire a positive charge in the aqueous solution and the surfaces are much more flexible compare to the ones used in the experiments described above. In our study the effect of different alkali metal chlorides (LiCl, NaCl, KCl and CsCl) is found to be different on the lamellar phase ($L_\alpha$) formed by DDAC and DMTAP bilayers. In the case of DMTAP, on increasing the salt concentration of KCl and CsCl, the lamellar periodicity (d) decreases till it reaches minimum. On increasing the salt concentration further the d-spacing does not increase further. In the case of NaCl and LiCl, the d-spacing first reaches a minimum. After a threshold value of salt concentration the d-spacing starts to increase again. The value of the threshold salt concentration is found to be lower in the case of LiCl. The effect of alkali metal chlorides on the $L_\alpha$ phase of DDAC bilayers is found to be qualitatively similar to that of DMTAP. In the case of KCl and CSCl, the d-spacing reaches a minimum and does not change further on increasing the salt concentration. But for NaCl and LiCl, the d-spacing increases after a threshold salt concentration. The threshold is found to be lower for LiCl. At high value of salt concentration ($[C_s]$), the d-spacing for DDAC-LiCl system is found to be lower than that of DDAC-NaCl system. The effect of different alkali metal bromides (CsBr, KBr, NaBr and LiBr) on the $L_\alpha$ phase of DDAB is also found to be ion dependent. In the cases of CsBr and KBr the d-spacing reaches a minimum, on increasing the

salt concentration further the d-spacing does not change significantly. In the case of NaBr after a threshold the d-spacing increases and an optically isotropic phase is found at high NaBr concentration. In the case of LiBr after a threshold a co-existence between of two lamellar phases with different periodicities is observed.

## 5.2 Materials and methods

Same as prvious chapter.

## 5.3 Results

### 5.3.1 Effect of salt on DDAC bilayers

#### DSC studies

DSC thermograms of DDAC samples in water and at different salt concentrations ($C_s$) of different alkali metal salts are presented in fig. 5.6. In the absence of any salt the transition temperature is observed to be around 10°C. The transition temperature is found to increase slightly with increasing salt concentration. At [$C_s$]= 1 M and 4 M, the transition temperature observed is $\sim$ 15°C and $\sim$ 18°C, respectively. The typical transition enthalpy is found to be close to 6 kJ/mol. The peak position corresponds to the Krafft temperature, above which the bilayers are formed.

#### SAXS studies

20 wt% DDAC samples in water forms a lmellar phase ($L_\alpha$) with periodicity (d) $\sim$ 11 nm. SAXS patterns shows 4 peaks, which can be indexed as the 1st, 2nd, 3rd and 4th order peaks of a lamellar structure. SAXS profiles of DDAC-LiCl samples are shown in fig. 5.7. At [$C_s$]= 0.5 M, a lamellar phase is found with periodicity (d) 3.5 nm. The d-spacing remain similar up to [$C_s$] $\sim$ 2 M. At [$C_s$]= 2 M, the lamellar periodicity (d) is 3.87 nm. On increasing the salt concentration to 4 M, the peak becomes broad and the d-spacing increases to 6.4 nm.

SAXS profiles of DDAC- NaCl samples are shown in fig. 5.8. At [$C_s$]= 0.5 M, the lamellar periodicity (d) is 3.41 nm. The dspacing remains same up to [$C_s$] $\sim$ 2.2 M. At [$C_s$]= 2.5 M, a co-existence between two lamellar phases with slightly different periodicity is observed (d= 3.3 nm and 4.95 nm). At [$C_s$]= 3 M, the peak becomes broad, corresponds to a single lamellar phase with periodicity $\sim$ 11 nm . The d-spacing increases to $\sim$ 12 nm at [$C_s$]= 4 M. One noticeable difference between DDAC- NaCL and DDAC-LiCl samples is that their d-spacings at high salt concentrations ([C$s$= 3 M or 4 M] are different. The DDAC- NaCl samples at $\phi$= 20, at [$C_s$]= 3M and 4 M swells to the full extent limited by the water content, whereas for similar salt concentrations of LiCl the d-spacing found is $\sim$ 6.4 nm. To examine that whether this difference is independent of wt% of the samples or not, we have done similar experiment on 10 wt% DDAC samples, at LiCl solution of 4M concentration. The SAXS profile is presented in fig. 5.9. The d-spacing is found be similar for both, $\phi$= 10 and for $\phi$= 20. POM and Cryo-SEM images of DDAC-NaCl samples are shown in fig. 5.10 and fig. 5.11. cryo-SEM image shows layered morphology, POM image shows Maltese cross texture, which are typical of a lamellar phase.

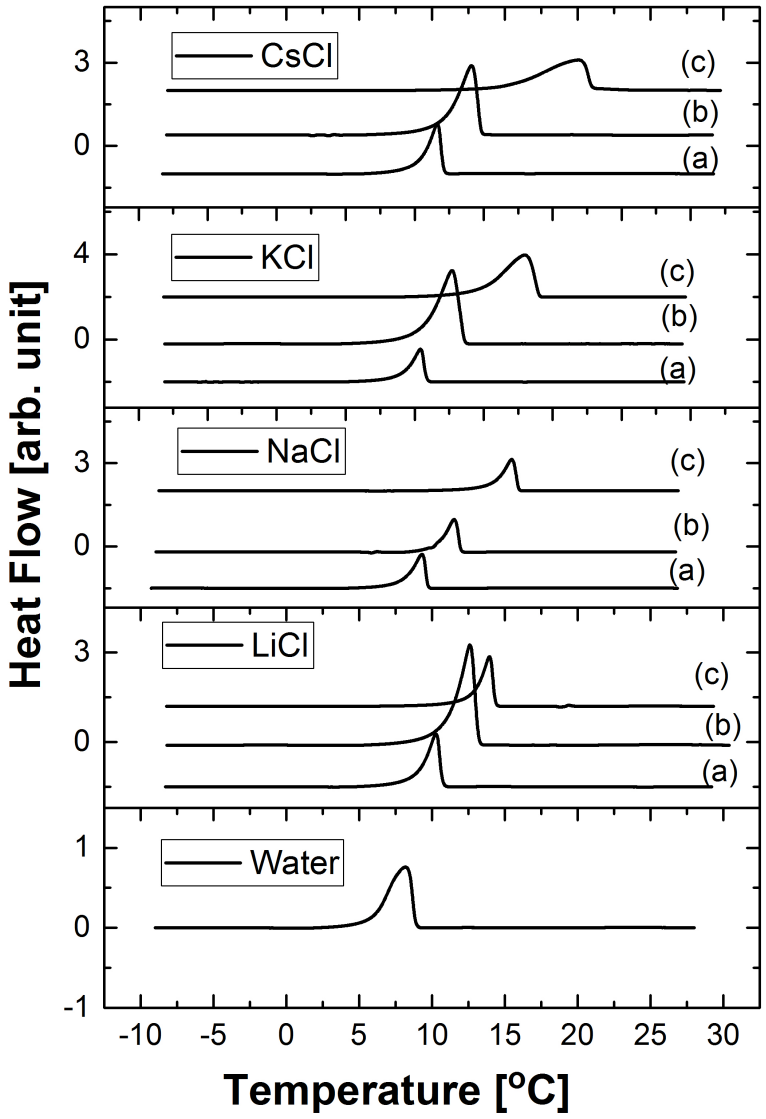


FIGURE 5.6: DSC thermograms of DDAC dispersions in water and in solutions of different alkali metal chlorides at $\phi$ = 20. (a), (b) and (c) represents [$C_s$] = 200mM, 1M and 4M, respectively. The transition was not observed in the cooling cycle due to the super-cooling of the fluid phase.

SAXS profiles of DDAC- KCl and DDAC- CsCl samples are qualitatively similar and they are shown in fig. 5.12 and fig. 5.13. Two sharp peaks are seen in the SAXS profiles, corresponding to a lamellar phase of periodicity $\sim$ 3.5 nm, at [$C_s$]= 0.5 M. On incresing the salt concentration the d-spacing does not change significantly. At [$C_s$]= 4M, the observed d is $\sim$ 3.1 nm. The variation of d-spacing with increasing salt concentration is shown in fig. 5.14 and table. 5.1.

Effect of temperature is also studied for DDAC- salt samples at 4 M, in the temperature range of 30°C - 70°C. SAXS profiles are shown in fig. 5.15, fig. 5.16, fig. 5.17, and fig. 5.18. In the case of LiCl, the peak becomes broad on increasing the temperature, the d-spacing does not change significantly. In the case of NaCl, the peak becomes sharp at 70°C, with a slight increase of d-spacing. For DDAC-KCl and DDAC-CsCl samples the SAXS profile is found to be independent of

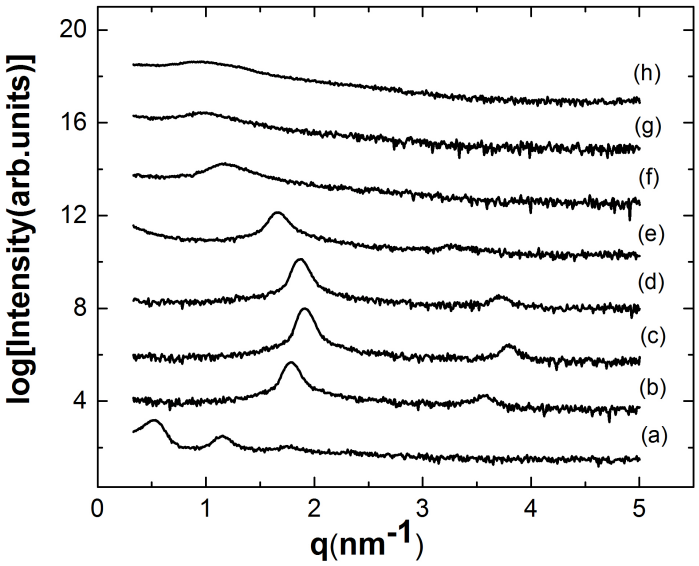


FIGURE 5.7: SAXS profiles of DDAC dispersions in (a) water, and in LiCl solutions of (b) 0.5 M, (c) 1 M, (d) 1.5 M, (e) 2 M, (f) 2.5 M, (g) 3 M, and (h) 4M concentration at $\phi$= 20.

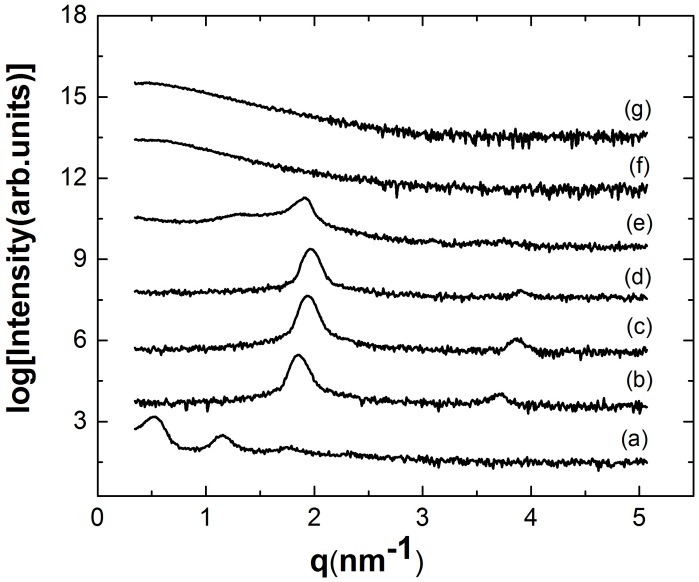


FIGURE 5.8: SAXS profiles of DDAC dispersions in (a) water, and in NaCl solutions of (b) 0.5 M, (c) 1 M, (d) 2 M, (e) 2.5 M, (f) 3 M, and (g) 4M concentration at $\phi$= 20.

temperature. The change of dspacing with temperature is given in table 5.2.

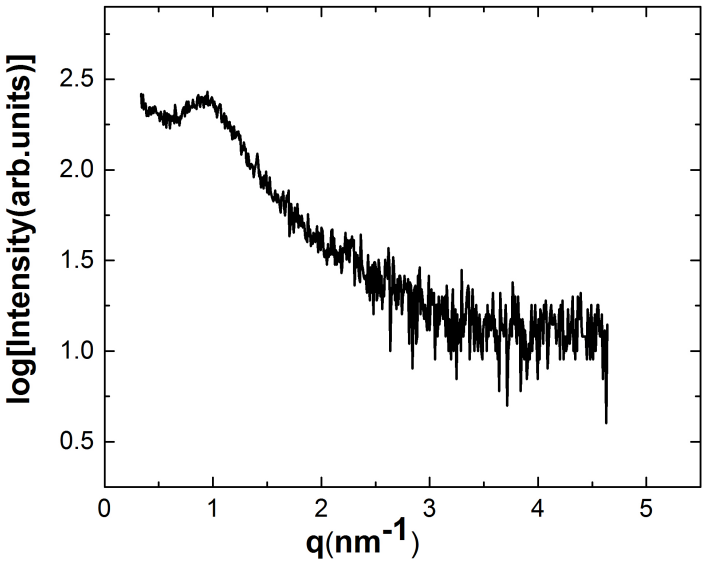


FIGURE 5.9: SAXS profiles of DDAC dispersions in LiCl solution of 4M concentration at $\phi$= 10.

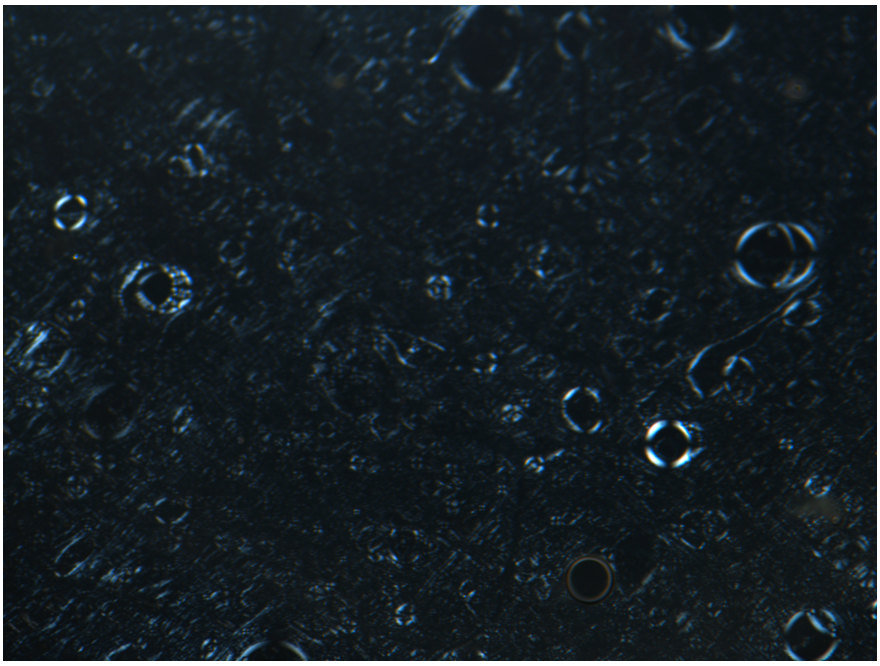

FIGURE 5.10: POM image of DDAC dispersions in NaCl solution of 3.5M concentration at $\phi$= 20.

### 5.3.2 Effect of salt on DMTAP bilayers

#### DSC studies

DSC thermograms of DMTAP samples are shown in fig. 5.19. A large hysteresis is found in heating and cooling cycles ($\sim$ 10°C). Multiple peaks are found in the cooling cycle in some cases. An increase in the transition temperature is observed in the presence of salt. The SAXS data are taken at 50°C, to make sure that the system is in the fluid phase. The typical transition enthalpy

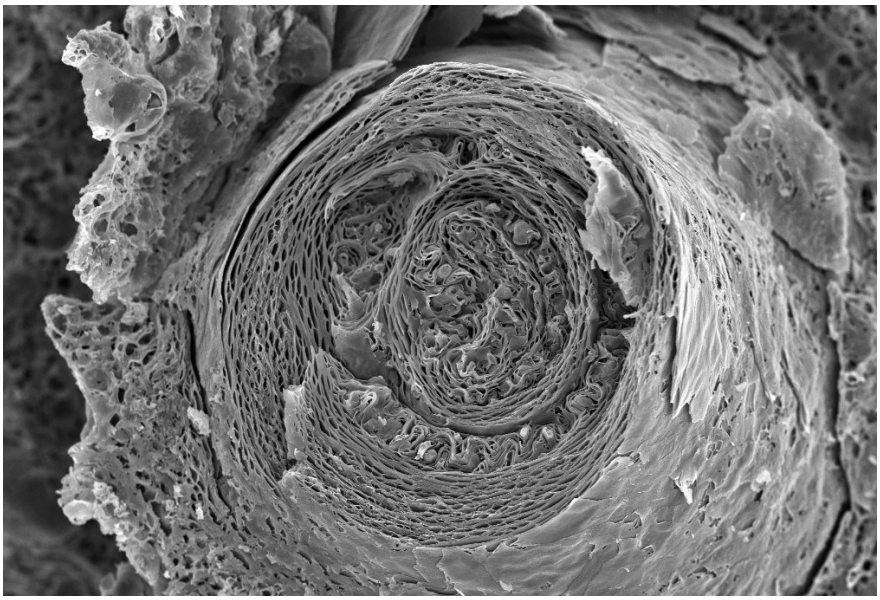

FIGURE 5.11: Cryo-SEM image of DDAC dispersions in NaCl solution of 3.5M concentration at $\phi$= 20.

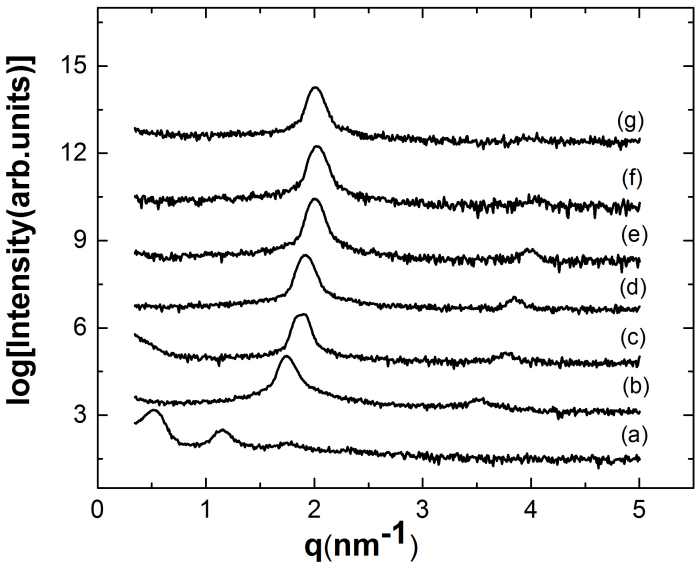


FIGURE 5.12: SAXS profiles of DDAC dispersions in (a) water, and in KCl solutions of (b) 0.5 M, (c) 0.7 M, (d) 1 M, (e) 2 M, (f) 3 M, and (g) 4M concentration at $\phi$= 20.

found is 12 kJ/mol, corresponds to chain melting transition of the lipid.

### SAXS studies

SAXS profiles of DMTAP-LiCl samples are shown in fig. 5.20. Multiple peaks are seen inthe SAXS profile in the absence of salt corresponding to a $L_\alpha$ phase with d= 15.64 nm. In the presence of salt two or three sharp peaks are seen in the SAXS profiles, which can be indexed to h=1, 2 and 3 rd order reflections of a $L_\alpha$ phase,with relatively smaller d-spacing. The variation of d-spacing with salt concentration is shown in fig. 5.21 and table. 5.3. The d- spacing reduces with increasing salt

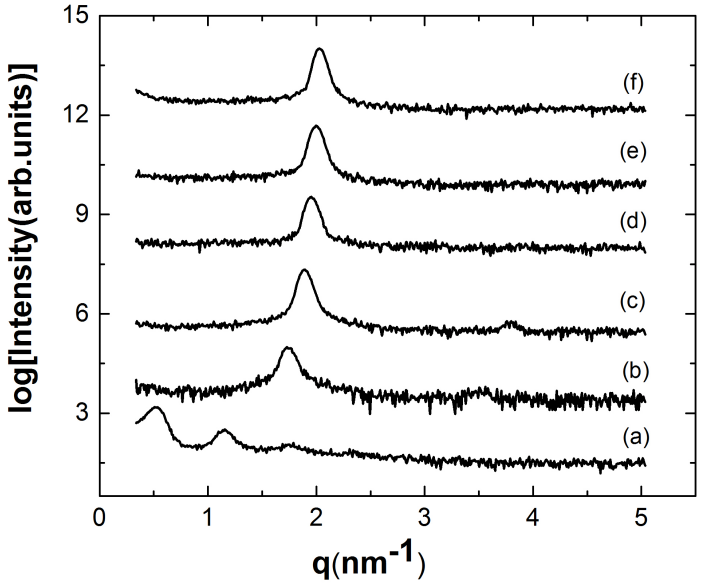


FIGURE 5.13: SAXS profiles of DDAC dispersions in (a) water, and in CsCl solutions of (b) 0.5 M, (c) 1 M, (d) 2 M, (e) 3 M, and (f) 4 M concentration at $\phi$= 20.

| $[C_s]$ (M) | $d_{CsCl}$ (nm) | $d_{KCl}$ (nm) | $d_{NaCl}$ (nm) | $d_{LiCl}$ (nm) |
|---|---|---|---|---|
| 0 | 10.72 | 10.72 | 10.72 | 10.72 |
| 0.5 | 3.52 | 3.41 | 3.54 | 3.52 |
| 1 | 3.33 | 3.35 | 3.28 | 3.31 |
| 1.5 | - | 3.24 | - | 3.35 |
| 1.75 | - | - | - | 3.51 |
| 2 | 3.21 | 3.17 | 3.26 | 3.87 |
| 2.2 | - | - | 3.31 | - |
| 2.5 | - | - | 3.33, 4.95 | 5.36 |
| 3 | 3.13 | 3.13 | 10.45 | 6.20 |
| 3.5 | - | - | 10.59 | - |
| 4 | 3.10 | 3.14 | 12.1 | 6.41 |

TABLE 5.1: Dependence of d on salt concentration for different salts for DDAC system at $\phi$= 20. '-' denotes that data was not taken at that point.

concentration till $[C_s] \sim 1$ M. At $[C_s]$=2 M, the observed d-spacing is higher than that of 1 M salt concentration. d-spacing remains same in the range $[C_s]$= 2 M - 4 M. SAXS profiles of DMTAP-NaCl samples are shown in fig. 5.22. The variation of d-spacing with increasing salt concentration is shown in fig. 5.21 and table. 5.3. The way the d-spacing changes for DMTAP-NACl system, is qualitatively similar to that of DMTAP- LiCl system, with a few differences. In the case of DMTAP-LiCl system the increased spacing is observed at $[C_s]$= 2M, whereas for DMTAP- NaCl system the

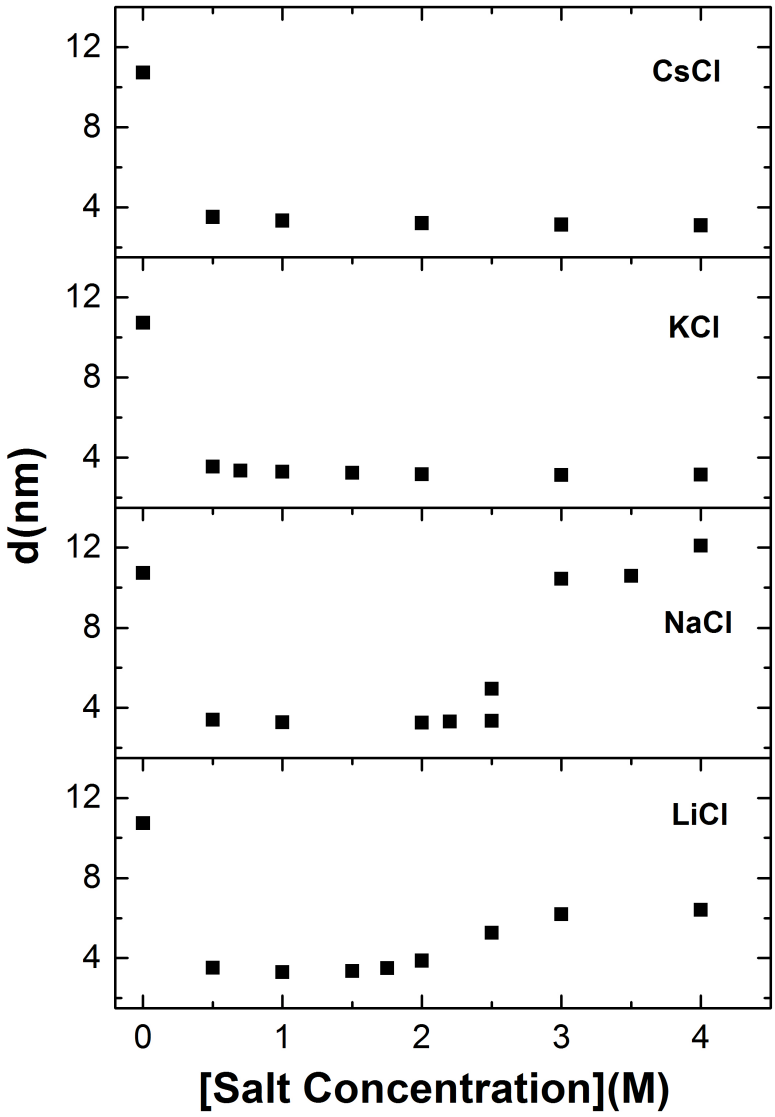


FIGURE 5.14: Variation of d of the $L_\alpha$ phase of 20 wt% DDAC dispersions with salt concentration for different salts.

swelling is observed at [$C_s$]= 3 M. The other difference is the value of the lamellar periodicity (d) is slightly lower at [$C_s$]= 3 M and 4 M, for DMTAP- LiCl system, compared to the DMTAP- NaCl system.

SAXS profiles of DMTAP- KCl and DMTAP- CsCl systems are shown in fig. 5.23 and fig. 5.24. The variation of d-spacing with salt concentration is shown in fig. 5.21 and table 5.3. In both the cases the d-spacing changes in a qualitatively similar way with salt concentration. The spacing reduces to a minimum at [$C_s$]$\sim$ 1 M and does not change much up to [$C_s$]= 4 M.

### 5.3.3 Effect of salt on DDAB bilayers

SAXS profiles of DDAB-LiBr samples are shown in fig. 5.25. In water 20 wt% DDAB samples form a lamellar phase ($L_\alpha$) with d-spacing $\sim$ 11.5 nm, multiple peaks are found in the SAXS pattern.

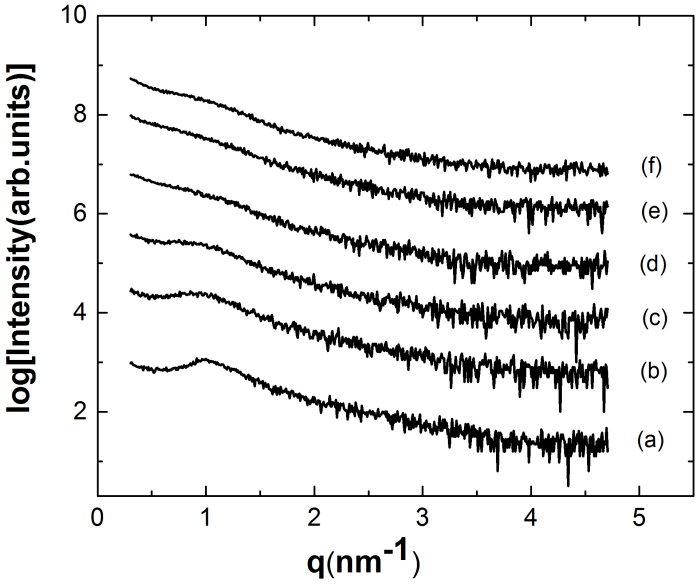


FIGURE 5.15: SAXS profiles of 20 wt% DDAC dispersions in LiCl solution of 4 M concentration at (a) 30°C, (b) 40°C, (c) 50°C, (d) 60°C, (e) 65°C and (f) 70°C.

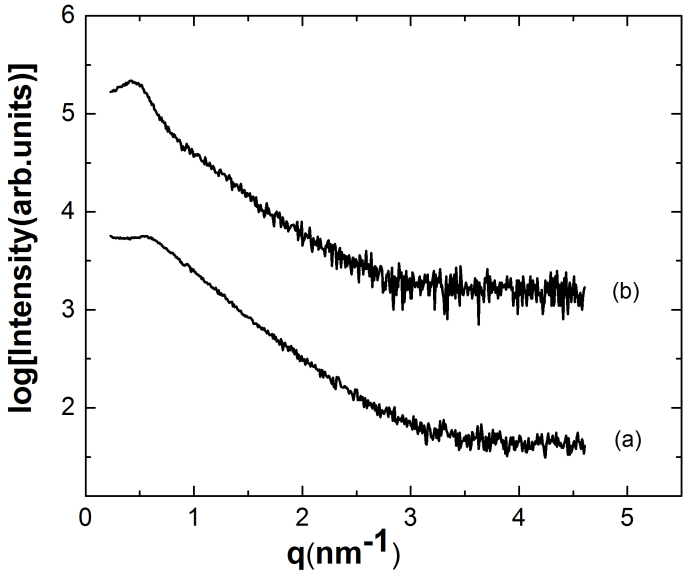


FIGURE 5.16: SAXS profiles of 20 wt% DDAC dispersions in NaCl solution of 4 M concentration at (a) 30°C and (b) 70°C.

At $[C_s] \sim 500$ mM, two sharp peaks are found in the SAXS pattern and the lamellar periodicity (d) reduces to $\sim 3.1$ nm. The lamellar peroidicity remains similar up to $[C_s] \sim 2$ M. At $[C_s]= 2.75$ M, two peaks are found in the SAXS pattern. One sharp peak corresponding to a d-spacing of $\sim 4.1$ nm and one broad peak corresponding to a periodicity of $\sim 9$ nm. The patterns remain similar up to $[C_s]= 4$ M. The variation of d-spacing with salt concentration is represented in fig. 5.28 and table. 5.4. SAXS profiles DDAB- NaBr samples are shown in fig. 5.26. At [NaBr]= 0.5 M, a lamellar phase is found whose periodicity is $\sim 3$ nm. The d-spacing remains same up to [NaBr]=

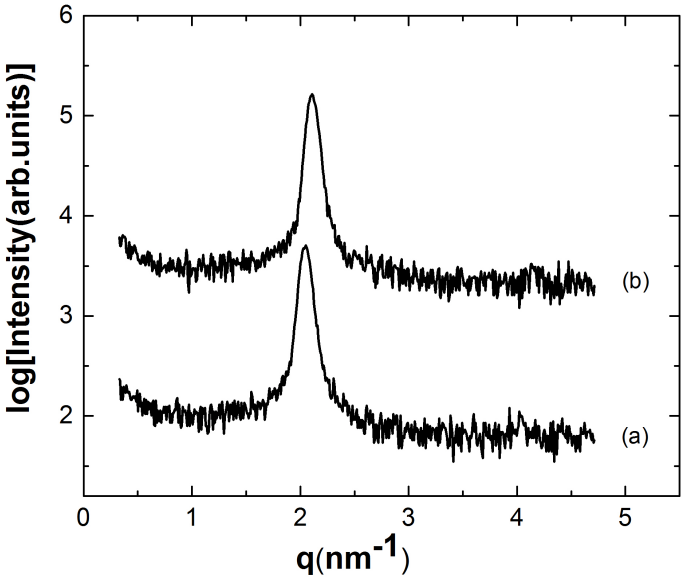


FIGURE 5.17: SAXS profiles of 20 wt% DDAC dispersions in KCl solution of 4 M concentration at (a) 30°C and (b) 70°C.

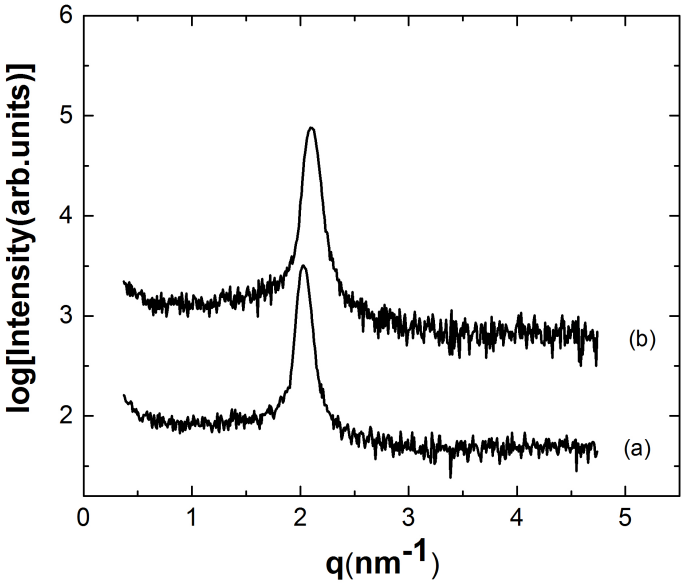


FIGURE 5.18: SAXS profiles of 20 wt% DDAC dispersions in CsCl solution of 4 M concentration at (a) 30°C and (b) 70°C.

2.5 M. At [NaBr]= 3 M, a change in SAXS pattern is observed. unlike the previous cases, where two peaks where found, which can be indexed to first and second order reflections of a $L_\alpha$ phase, a broad peak is found in the SAXS profile corresponding to a spacing of $\sim$ 8.5 nm. The spacing does not change significantly till [NaBr]= 4 M. This new phase is found to be optically isotropic, when viewed under a polarizing optical microscope 5.27.

The SAXS profiles of DDAB- KBr and DDAB- CsBr smaples are shown in fig. 5.29 and fig. 5.30, respectively. The SAXS profiles look similar. The variation of d-spacing with KBr and CsBr

| T (°C) | $d_{CsCl}$ (nm) | $d_{KCl}$ (nm) | $d_{NaCl}$ (nm) | $d_{LiCl}$ (nm) |
|---|---|---|---|---|
| 30 | 3.05 | 3.05 | 10.74 | 6.36 |
| 40 | - | - | - | 6.81 |
| 50 | - | - | - | 6.99 |
| 60 | - | - | - | * |
| 65 | - | - | - | * |
| 70 | 2.98 | 2.97 | 13.14 | 6.93 |

TABLE 5.2: Temperature dependence of d-spacing for 20 wt% DDAC dispersions at 4 M salt concentration of different alkali metal chlorides. '-' denotes that data was not taken at that temperature and '*' denotes no peak in the SAXS was observed at that temperature.

| $[C_s]$ (M) | $d_{CsCl}$ (nm) | $d_{KCl}$ (nm) | $d_{NaCl}$ (nm) | $d_{LiCl}$ (nm) |
|---|---|---|---|---|
| 0 | 15.64 | 15.64 | 15.64 | 15.64 |
| 0.5 | 8.21 | 6.01 | 5.04 | 5.43 |
| 0.7 | 4.89 | 4.74 | 4.73 | 4.75 |
| 1 | 4.67 | 4.59 | 4.62 | 4.79 |
| 2 | 4.51 | 4.51 | 4.54 | 5.56 |
| 3 | 4.48 | 4.48 | 6.01 | 5.58 |
| 4 | 4.48 | 4.48 | 5.96 | 5.58 |

TABLE 5.3: Salt concentration vs d for different salts for DMTAP system at $\phi$= 20.

concentrations are shown in fig. 5.28 and table 5.4. The spacing reduces to $\sim$ 3 nm at $[C_s] \sim 0.5$ M and does not change significantly till $[C_s]$= 4 M.

### 5.3.4 Effect of salt on unmixed samples

The SAXS profiles of DDAC-XCl (X= Cs, K, Na, Li) samples, which were not mixed during the time of preparation is shown in fig. 5.31 , fig. 5.32, fig.5.33 and fig. 5.34. With increasing LiCl concentration the d-spacing reduces till [LiCl] $\sim$ 1 M. At [LiCl]= 2 M, the spacing is more compared to that at [LiCl]= 1 M. The spacing increases further at [LiCl]= 3 M and does not change much at [LiCl]= 4 M. The effect of NaCl is qulatitavely same as compared to LiCl. A two lamellar phase co-existence is observed at [NaCl]= 2.5 M. From [NaCl]= 3 M, only one broad peak is observed corresponds to a spacing of $\sim$ 5.3 nm. In the case of mixed samples at [NaCl]= 3M (or 4 M) a fully swollen phase is observed, with a d-spacing of $\sim$ 11 nm. The variation of d-spacing with salt concentration is shown in fig. 5.35 and table. 5.5. The effect of KCl and CsCl is found to be similar. The d-spacing decreases with salt concentration till it reaches a minimum and does not increase on increasing the salt concentration further.

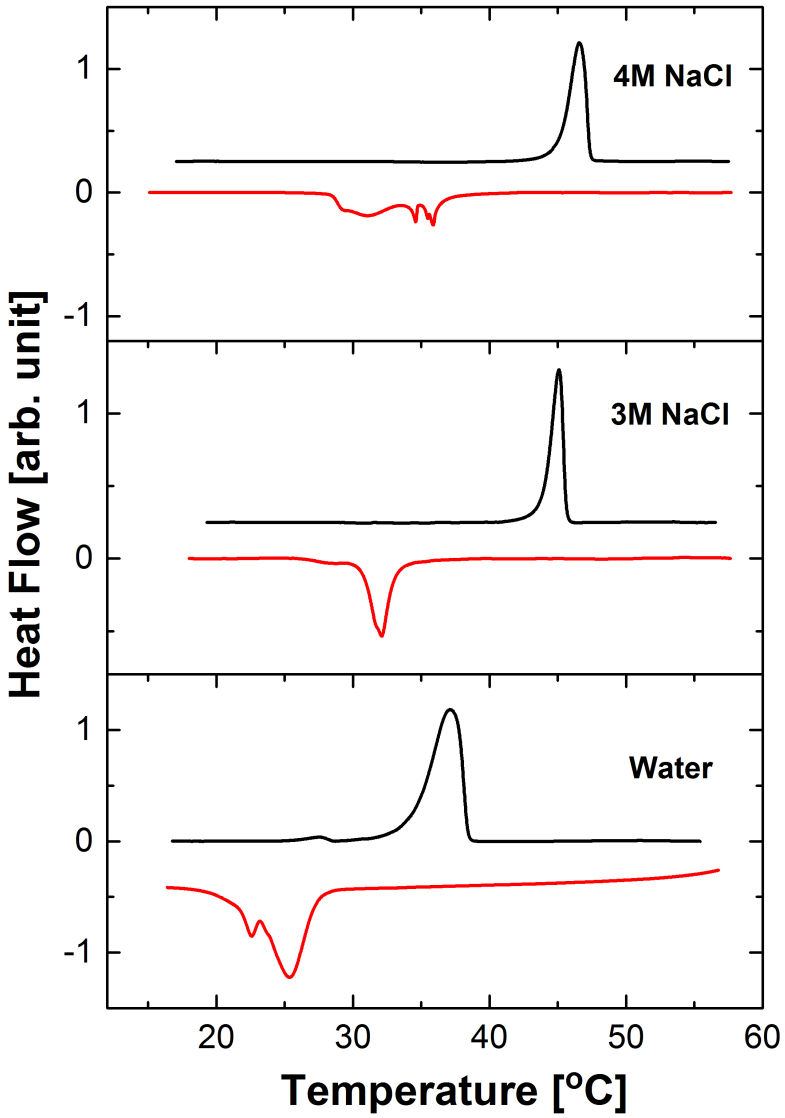


FIGURE 5.19: DSC thermograms of 20 wt% DMTAP dispersions in water and in NaCl solutions of 3 M and 4 M concentrations. The black and red traces correspond to the heating and cooling cycles, respectively.

## 5.4 Discussions

The d-spacing of lamellar phase made of ionic amphiphiles in water or at low salt concentration is determined by inter bilayer electrostatic repulsion[9]. With increasing salt concentration the surface charges of the bilayers get screened. At moderate value of $C_s$, the periodicity of the lamellar phase becomes close to the bilayer thickness ($L_\alpha^c$ phase). The interactions in the lamellar phase and the formation of $L_\alpha^c$ phase can be described in terms of DLVO theory. A detailed discussion of the variation of d up to 1 M salt concentration is given in the previous chapter.

The effect of different alkali metal chlorides on the variation of d-spacing for DMTAP-system at $\phi$= 20, is given in table 5.3. At [$C_s$]= 1 M, the d-spacing is $\sim$ 4.7 nm, which is about 1 nm higher than the thickness of bilayers in the fluid $L_\alpha$ phase[10]. There is a thin layer of water separating

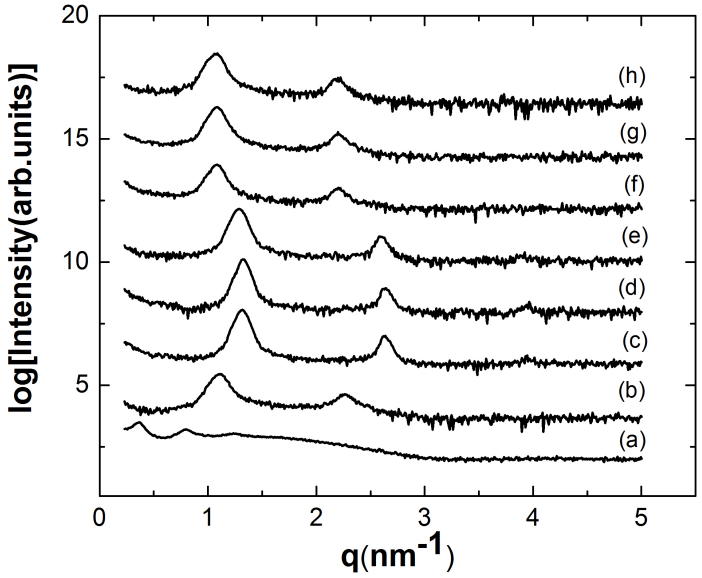


FIGURE 5.20: SAXS profiles of DMTAP dispersions in (a) water, and in LiCl solutions of (b) 0.5 M, (c) 0.7 M, (d) 0.8 M, (e) 1 M, (f) 2 M, (g) 3 M, and (h) 4 M concentration at $\phi$= 20.

| $[C_s]$ (M) | $d_{CsBr}$ (nm) | $d_{KBr}$ (nm) | $d_{NaBr}$ (nm) | $d_{LiBr}$ (nm) |
|---|---|---|---|---|
| 0 | 11.9 | 11.9 | 11.9 | 11.9 |
| 0.5 | 3.06 | - | 3.1 | 3.07 |
| 1 | 3.05 | 3.0 | 3.01 | 3.07 |
| 1.5 | - | - | - | 3.13 |
| 1.8 | - | - | - | 3.2 |
| 2 | 2.99 | 2.98 | 2.99 | 3.29 |
| 2.5 | - | - | 3.07 | - |
| 2.75 | - | - | - | 4.12,8.97 |
| 3 | 2.94 | 3.01 | 8.76 | 4.19,8.96 |
| 3.5 | - | - | 8.38 | 4.23,9.23 |
| 4 | 2.92 | 2.95 | 8.11 | 4.54,9.19 |

TABLE 5.4: Salt concentration vs d for different salts for DDAB system at $\phi$= 20. '-' denotes that data was not taken at that point.

two bilayers, due to the presence of the short-range hydration repulsion[11]. In the case of CsCl and KCl, the d-spacing does not change up to$[C_s]$= 4 M, but of NaCl and LiCl it shows a non monotonic behaviour. In the case of LiCl, the d-spacing shows an increase at $[C_s]$= 2 M, and does not change further up to $[C_s]$= 4 M. For NaCl, the increase in spacing is observed at $[C_s]$= 3 M and does not change much up to 4 M concentration. The value at d-spacing at high salt

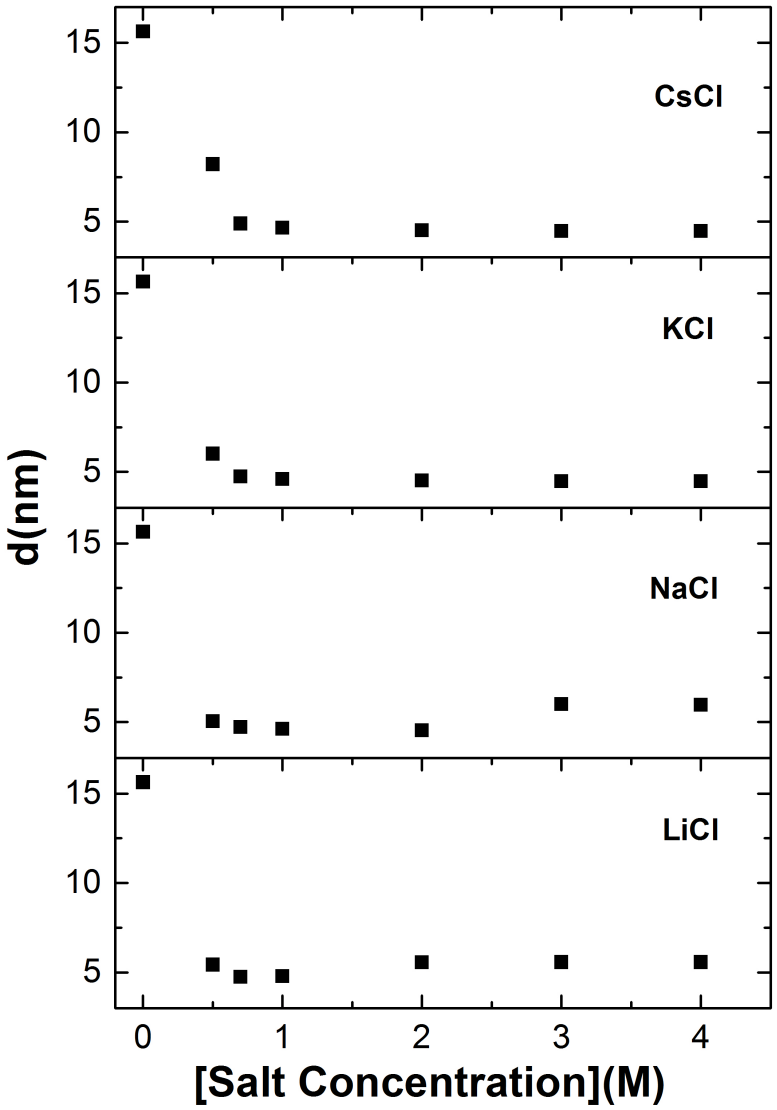


FIGURE 5.21: Variation of d of the $L_\alpha$ phase of 20 wt% DMTAP dispersions with salt concentration for different salts.

concentration( 3 M or 4 M), is found to be slightly higher in the case of NaCl compared to LiCl. The effect of different alkali metal chlorides on the variation of d-spacing for DDDAC-system at $\phi$= 20, is given in table 5.1. Like in the case of DMTAP, for DDAC the d-spacing does not increase on increasing the salt concentration for KCl and CsCl. But it increases in the case of LiCl and NaCl, after a threshold salt concentration. The threshold is lower for LiCl. A graphical representation of electrostatic decay length with salt concentration is presented in fig. 5.3[(6)]. One possible reason for observing the increase in d-spacing after a threshold of salt concentration in the case of DDAC and DMTAP system may be the increase in the electrostatic screening length at high salt concentration as reported in refs. 6 and 11. The salt concentration at which the increase in Debye length is reported in refs 6 and 11, is comparable to that at which we observe the increase in the lamellar periodicity. But their are a few important differences. In the above mentioned

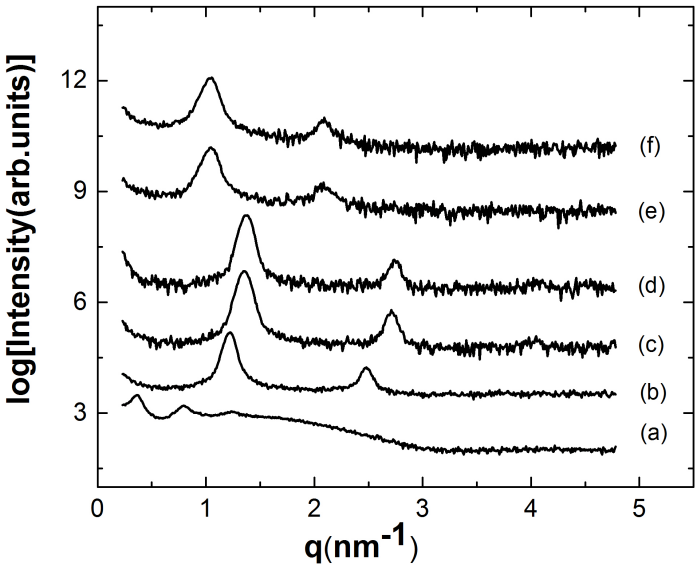


FIGURE 5.22: SAXS profiles of DMTAP dispersions in (a) water, and in NaCl solutions of (b) 0.5 M, (c) 1 M, (d) 2 M, (e) 3 M, and (f) 4 M concentration at $\phi$= 20.

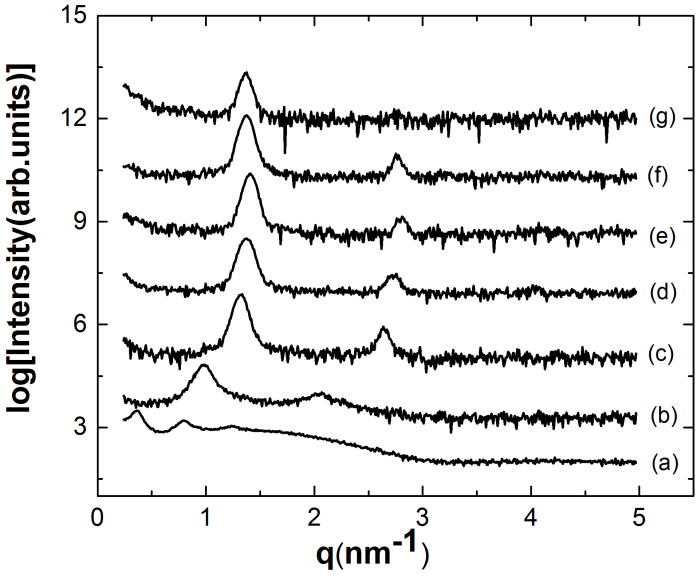


FIGURE 5.23: SAXS profiles of DMTAP dispersions in (a) water, and in KCl solutions of (b) 0.5 M, (c) 0.7 M, (d) 1 M, (e) 2 M, (f) 3 M, and (g) 4 M concentration at $\phi$= 20.

experiments two rigid flat surfaces were used. In our case flexible bilayers are used. The other important difference is that, both mica and silica get negatively charged in aqueous solution, so the cations of different alkali metal chlorides work as counter-ions. But in our case, we have used cat-ionic lipids and surfactants, so the cations from the of different alkali metal chlorides work as a co-ions. Another striking difference is in both studies described in[1,6], they have noticed an increase in Debye length, after a threshold salt concentration. If that was a general phenomenon,

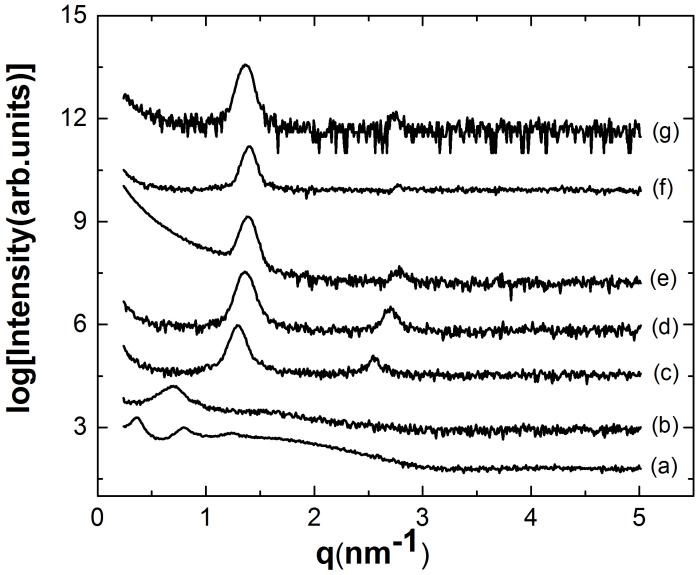


FIGURE 5.24: SAXS profiles of DMTAP dispersions in (a) water, and in CsCl solutions of (b) 0.5 M, (c) 0.7 M, (d) 1 M, (e) 2 M, (f) 3 M, and (g) 4 M concentration at $\phi$= 20.

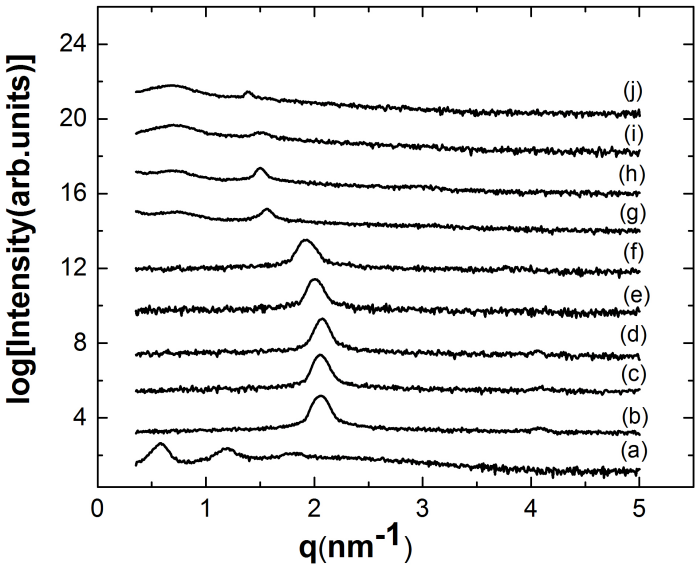


FIGURE 5.25: SAXS profiles of DDAB dispersions in (a) water, and in LiBr solutions of (b) 0.5 M, (c) 1 M, (d) 1.5 M, (e) 1.8 M, (f) 2 M, (g) 2.75 M, (h) 3 M, (i) 3.5 M, and (i) 4 M concentration at $\phi$= 20.

the same should have been observed for all the salts. But we do not observe any increase in d-spacing in the case of KCl and CsCl. Lee et al. suggest a scaling relation between Debye length and radius of ion[12],

$$\lambda \sim l_B c_b a^3 \tag{5.2}$$

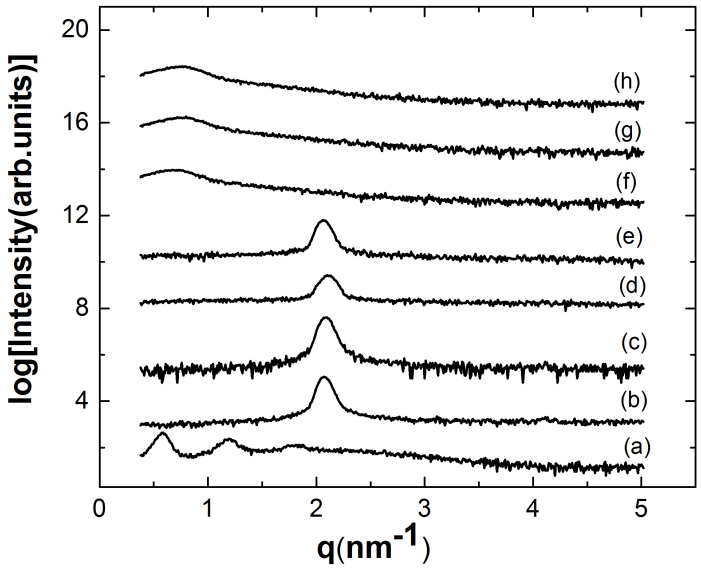


FIGURE 5.26: SAXS profiles of DDAB dispersions in (a) water, and in NaBr solutions of (b) 0.5 M, (c) 1 M, (d) 2 M, (e) 2.5 M, (f) 3 M, (g) 3.5 M, and (h) 4 M concentration at $\phi$= 20.

FIGURE 5.27: POM image of DDAB dispersions in NaBr solution of 3.5M concentration at $\phi$= 20.

where, $l_B$ is the Bjerrum length of the solution, a is the ion diameter, $c_b$ is the salt concentration. But this argument can not explain the fact that we do not observe an increase in d at high concentrations KCl and CsCl.

The activity of species i, is related to the concentration (mol/liter) with the following equation,

$$[i] = \gamma_i m_i \tag{5.3}$$

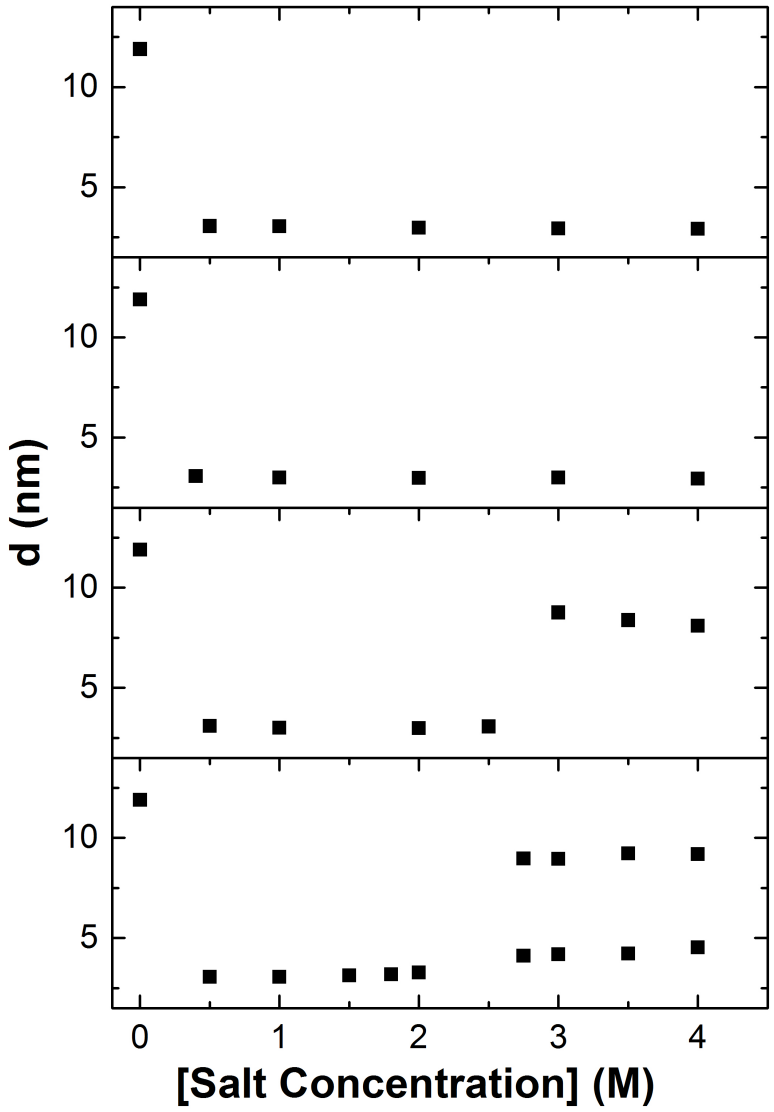


FIGURE 5.28: Variation of d-spacing with salt concentration for different salts for DDAB samples at $\phi$= 20.

$\gamma_i$ is called activity coefficient, which is a measure of deviation from the ideal behaviour. If $\gamma_+$ is activity coefficient of a cation and $\gamma_-$ is activity coefficient of an anion, then in 1:1 electrolytes (e.g. NaCl), the activity coefficient is given by[13],

$$\gamma_\pm = \sqrt{\gamma_+\gamma_-} \tag{5.4}$$

variation of activity coefficient with salt concentration for different alkali metal chlorides are given in[14–17]. There is a non-monotonic behaviour of activity coefficients in the case of NaCl and LiCl, but for KCl and CsCl it decreases monotonically with concentration. Fig. 5.36 shows the change in the activity coefficient with concentration for NaCl and KCl. But if we replace the concentration of the salt solution with the activity, i.e., concentration $\times$ activity coefficient, we were not able to reproduce the non monotonic behaviour of Debye length as described in[1,6]. The

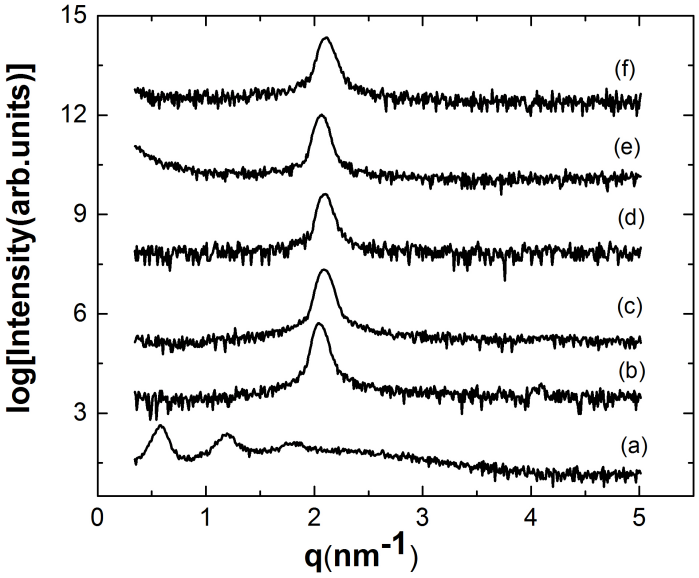


FIGURE 5.29: SAXS profiles of DDAB dispersions in (a) water, and in KBr solutions of (b) 0.4 M, (c) 1 M, (d) 2 M, (e) 3 M, (f) 4 M concentration at $\phi$= 20.

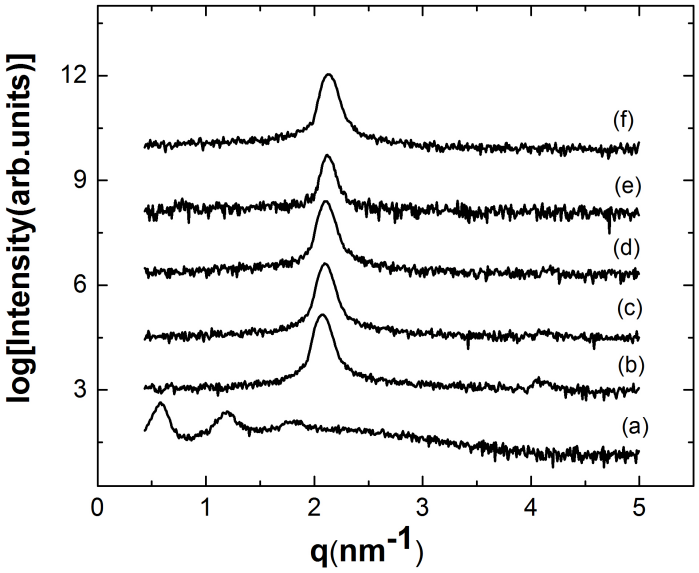


FIGURE 5.30: SAXS profiles of DDAB dispersions in (a) water, and in CsBr solutions of (b) 0.5 M, (c) 1 M, (d) 2 M, (e) 3 M, (f) 4 M concentration at $\phi$= 20.

variation of Debye length with and without activity coefficient in presented in figure 5.37. In both the cases a decrease in Debye length is observed with increasing NaCl concentration. The ion-specificity of the non monotonic behaviour of d-spacing, for the $L_\alpha$ phase of DDAC and DMTAP bilayers we are no able to explain. Further work need to be done to understand this.

At [NaCl] $\sim$ 2.5 M, a coexistence between a the collapsed lamellar phase ($L_\alpha^c$) and a swollen phase (d$\sim$ 5 nm) is observed. Such phase was not seen for DDAC-LiCl system. The spacing after the thresold salt concentration ($\sim$ 2 M) is found to be different for DDAC-LiCl and DDAC- NaCl

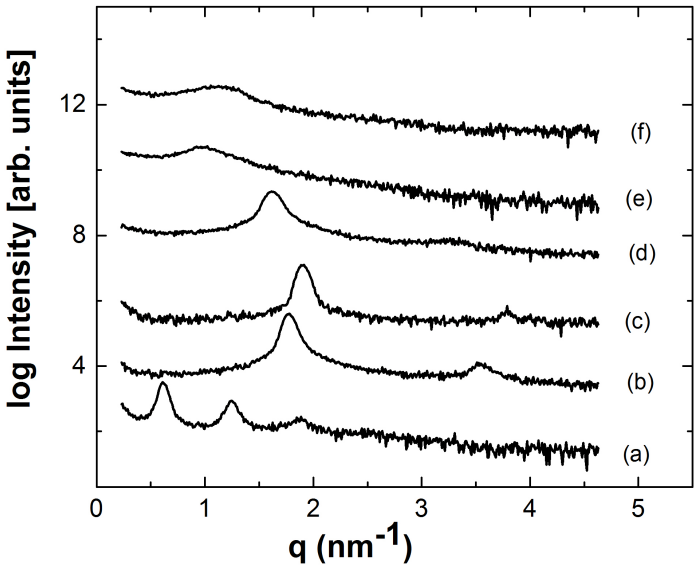


FIGURE 5.31: SAXS profiles of DDAC dispersions in (a) water, and in LiCl solutions of (b) 0.5 M, (c) 1 M, (d) 2 M, (e) 3 M, and (f) 4 M concentration at $\phi$= 20. These samples were not mixed during preparation.

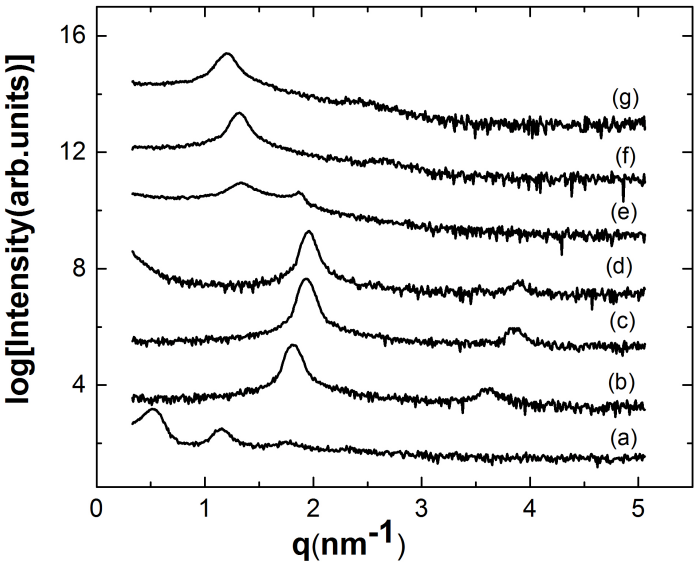


FIGURE 5.32: SAXS profiles of DDAC dispersions in (a) water, and in NaCl solutions of (b) 0.5 M, (c) 1 M, (d) 2 M, (e) 2.5 M, (f) 3 M and (f) 4 M concentration at $\phi$= 20. These samples were not mixed during preparation.

system. The spacing is found to be much higher in the case of DDAC-NaCl, which is close to the fully swollen $L_\alpha$ phase. But in the case of LiCl, it is around 6.5 nm. At present we don't know the origin of this difference. The spacing after threshold salt concentration (after $\sim$ 2 M LiCl and NaCl) is found be different for DMTAP and DDAC systems. In the case of DMTAP the spacing is lower. This is most probably due to the higher bare bending rigidity of the lipid bilayers (of the

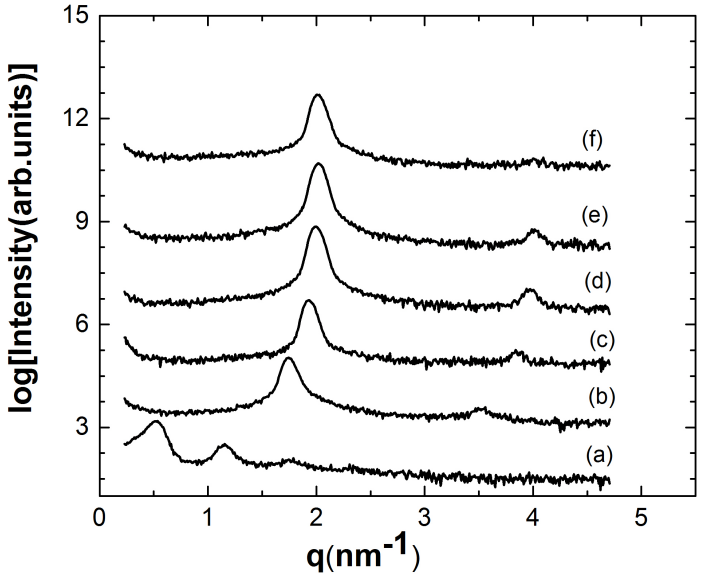


FIGURE 5.33: SAXS profiles of DDAC dispersions in (a) water, and in KCl solutions of (b) 0.5 M, (c) 1 M, (d) 2 M, (e) 3 M, and (f) 4 M concentration at $\phi$= 20. These samples were not mixed during preparation.

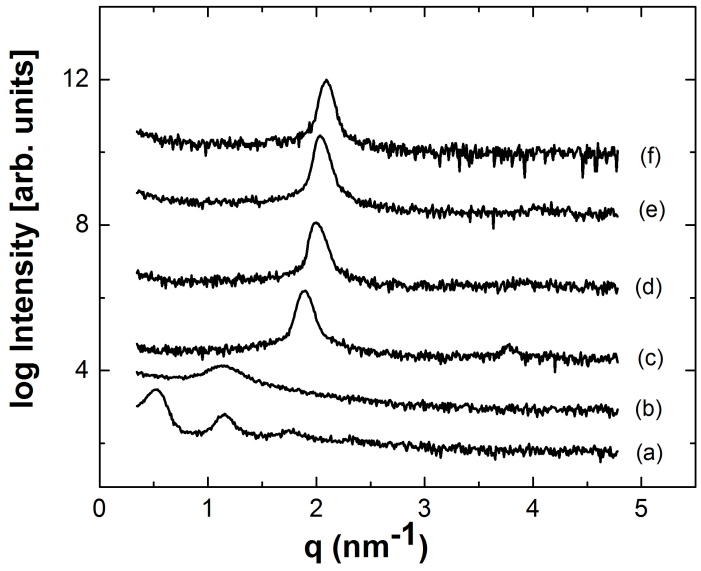


FIGURE 5.34: SAXS profiles of DDAC dispersions in (a) water, and in CsCl solutions of (b) 0.5 M, (c) 1 M, (d) 2 M, (e) 3 M, and (f) 4 M concentration at $\phi$= 20. These samples were not mixed during preparation.

order of 10 $K_BT$)[18,19] compared to that of surfactant bilayers (of the order of $K_BT$)[20,21].

Effect of temperature has been studied in the case DDAC -salt samples. In the case of DDAC-KCl and DDAC-CsCl no significant change is observed on increasing the temperature (table. 5.2). In the case of NaCl an increase in spacing is observed, which can be attributed to increase in the undulation repulsion on increasing the temperature[22]. For DDAC-LiCl samples a broadening

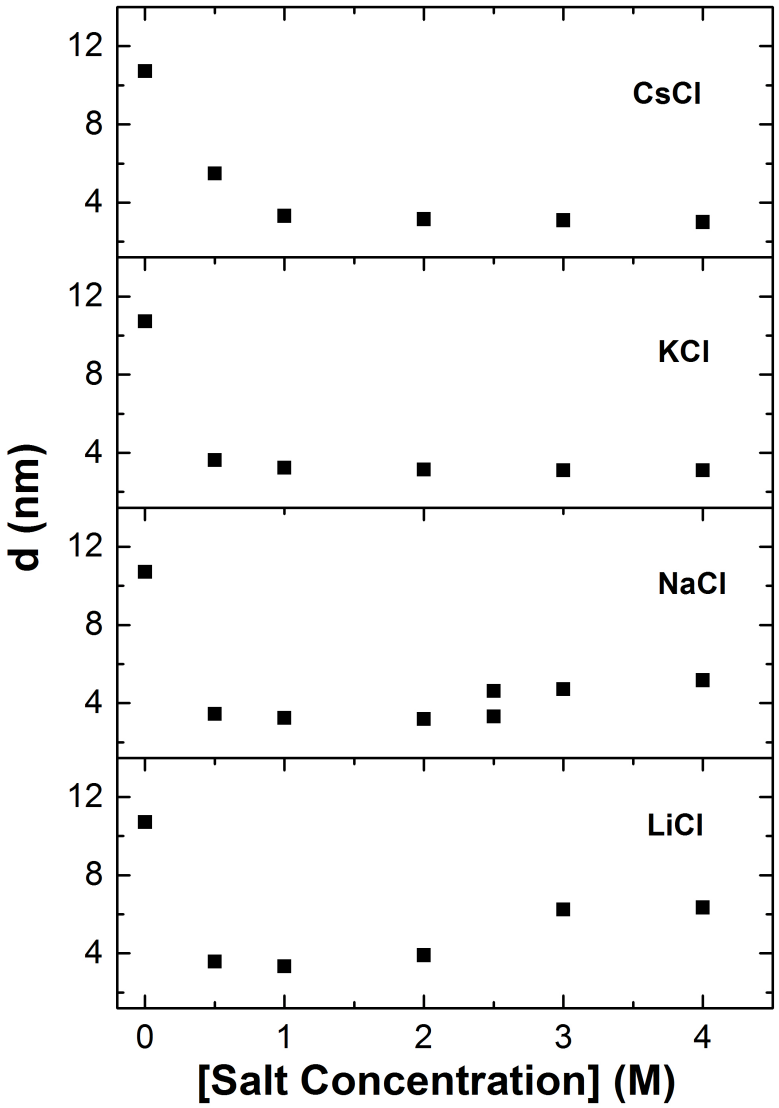


FIGURE 5.35: Variation of d-spacing with salt concentration for different salts for DDAC samples at $\phi$= 20. These samples were not mixed during preparation.

of the peak is observed on increasing the temperature. Which maybe similar to the unbinding transition of lipid membranes[23], discussed in the previous chapter.

Effect of different metal alkali bromides ( CsBr, KBr, NaBr and LiBr) is studied on the $L_\alpha$ phase made by DDAB bilayers. No significant change of d-spacing was observed in the case CsBr and KBr (table5.4). In the case of NaBr after a threshold a broad peak is observed with a much higher periodicity. The phase was found to be optically isotropic. Previous study have shown the formation of an optically isotropic phase ($L_3$) in the case of DDAB-water system, which gives a very broad peak in the SAXS pattern[20]. Another study have shown formation of sponge phase upon adsorption of polyelectrolytes on DDAB bilayers[24]. We were not able to get a good-fit of the scattering data of DDAB-NaBr system at high salt concentration ( e.g. [NaBr]= 4 M) to that expected from a sponge phase, following the procedure described in ref.[25]. A much better fit is obtained

| $[C_s]$ (M) | $d_{CsCl}$ (nm) | $d_{KCl}$ (nm) | $d_{NaCl}$ (nm) | $d_{LiCl}$ (nm) |
|---|---|---|---|---|
| 0 | 10.72 | 10.72 | 10.72 | 10.72 |
| 0.5 | 5.5 | 3.63 | 3.45 | 3.58 |
| 1 | 3.32 | 3.25 | 3.24 | 3.35 |
| 2 | 3.15 | 3.15 | 3.19 | 3.91 |
| 2.5 | - | 3.31,4.62 | - | - |
| 3 | 3.10 | 3.12 | 4.71 | 6.25 |
| 4 | 3.0 | 3.12 | 5.17 | 6.35 |

TABLE 5.5: Salt concentration vs d for different salts for DDAC system at $\phi$= 20. These samples were not mixed during preparation. '-' denotes that data was not taken at that point.

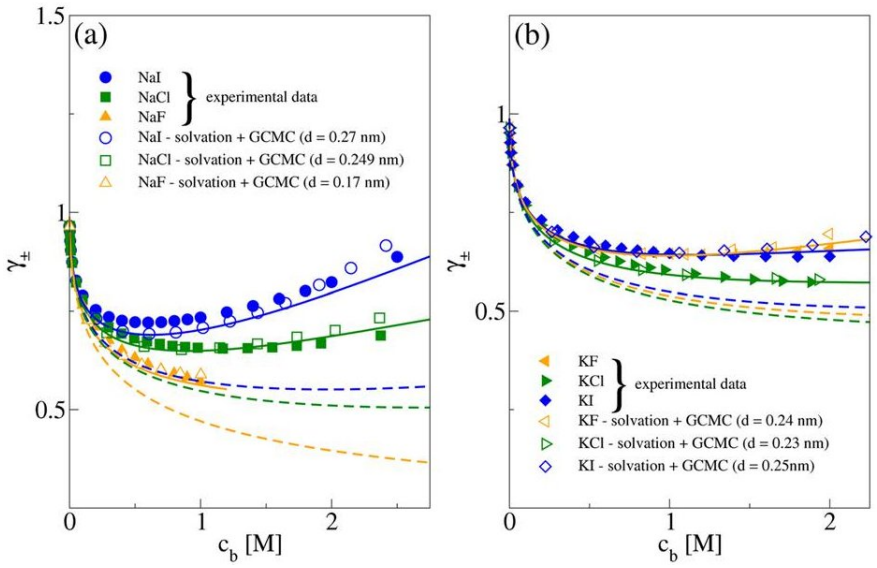


FIGURE 5.36: Variation of activity coefficient with salt concentration for NaCl and KCl. Figure was taken from [15]

when the data was fitted to a scattering from a lamellar phase (fig. 5.38), following the method described in [26]. The fitting parameters obtained from the best fit are given in table 5.6. So this phase can be recognized as an isotropic phase made of bilayers ($L_x$ phase). Formation of the $L_x$ phase is reported in the surfactant system previously [27]. In the case of LiBr after a threshold one sharp peak and one broad peak is observed in the SAXS pattern, which indicates a two phase coexistence. At present we are not able to figure out, what is responsible for this behaviour. Variation of the activity coefficient with salt concentration for different alkali metal brides is given in [28]. In the case of KBr and CsBr the activity coefficient decreases monotonically with salt concentration. For NaBr and LiBr a non monotonic behaviour is observed. The activity coefficient increases after a threshold. In our case also the d-spacing does not change significantly for DDAB-CsBr and DDAB-KBr system on increasing the salt concentration (0.5 M - 4 M). But in the case LiBr and NaBr the d-spacing increases after a threshold. Further work needs to be done to establish the

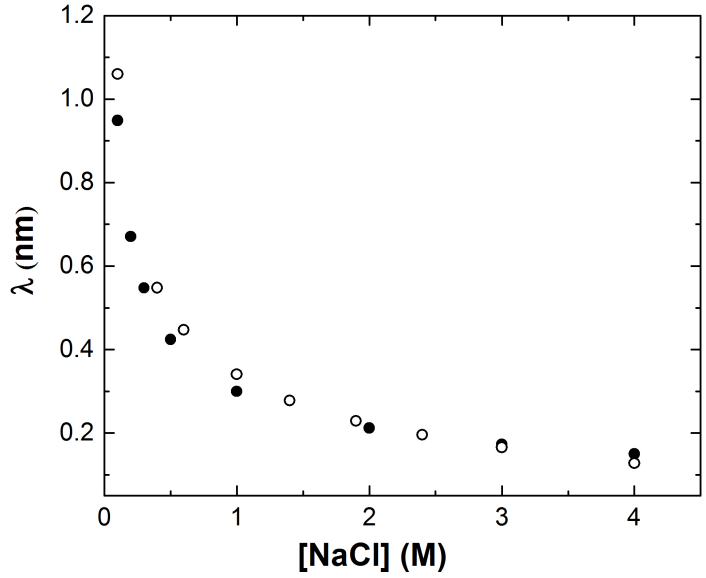


FIGURE 5.37: Variation of Debye length with NaCl concentration. The closed circles represent values without including the activity co-efficient, the open circles are including activity coefficient.

correlation between the trend of the activity coefficient changes with the trend of d-spacing.

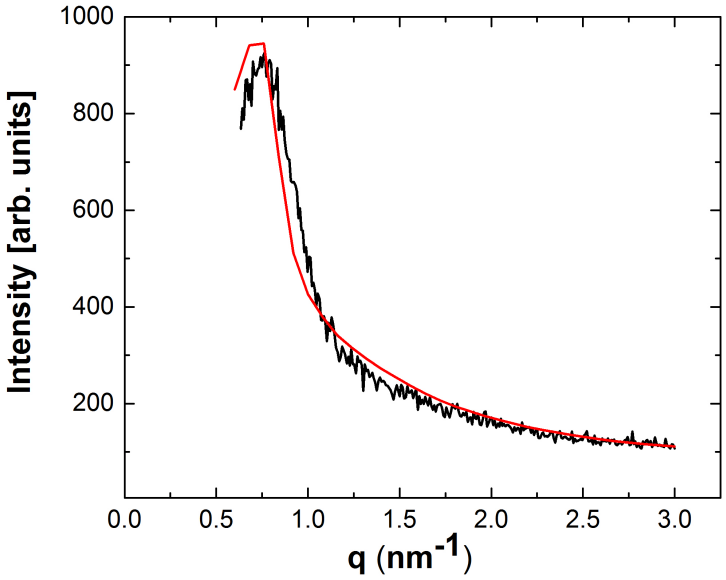


FIGURE 5.38: Fitted data for 20wt% DDAB samples in NaBr solution of 4 M concentration. The black line represents the experimental result and the red line represents the best fit profile obtained from the model.

Variation of d-spacing of DDAC samples which were not mixed during preparation is shown in fig. 5.35 and table.5.5. Like in the case of mixed samples, here also an increase in d-spacing is observed after a threshold for NaCl and LiCl. But it was not observed for CsCl and KCl. The spacing is found to be less for unmixed DDAC-NaCl samples, compared to the mixed one. Earlier

| $[C_s]$ (M) | $z_h$ (nm) | $\sigma_H$ (nm) | $\sigma_C$ (nm) | $\bar{\rho_H}$ / $\bar{\rho_C}$ | $\eta$ |
|---|---|---|---|---|---|
| 4 | 1.31 | 0.13 | 0.49 | -0.32 | 0.64 |

TABLE 5.6: Values of the model parameters obtained from the best fit.

study on DDAB bilayers has shown the formation of a very dilute meta stable sponge phase ($L_3$), which disappears after long incubation time (∼90 days)[20]. The presence of such a dilute phase in the present samples can apply an osmotic pressure on the lamellar phase, leading to the observed behaviour.

## 5.5 Conclusions

In this chapter we have studied the effect of salt on the phase behaviour of fluid lamellar phase formed by ionic surfactants and lipids at high salt regime. For LiCl and NaCl, on increasing the salt concentration after a threshold (∼ 2 M), an increase in d-spacing is observed. But for KCl and CsCl such significant change in spacing is seen. The trend of the d-spacing changes follows the trend of activity coefficient of alkali metal chlorides with concentration. The spacing of DDAC-NaCl (or DDAC-LiCl) samples at high salt concentration (∼ 3 M) is found to be higher than the DMTAP- NaCl (or DMTAP-LiCl) samples. This maybe due to the higher bare bending rigidity of lipid bilayers. The effect of different alkali metal bromides on the $L_\alpha$ phase of DDAB is also studied. No change in spacing is observed for DDAB-KBr and DDAB-CsBr samples. For DDAB-NaBr an optically isotropic phase is found at high NaBr concentration ([NaBr] ∼ 3 M). The spacing also increases. A single broad peak is found, that can be fitted to a scattering from a lamellar phase. For LiBr at similar salt concentration (∼ 3 M), a broad peak (corresponding to a higher periodicity) and a sharp peak (corresponding to a lower periodicity) are observed. The pattern in which d-spacing changes with salt concentration follows the similar trend of activity coefficient of alkali metal bromides. At present we are no able to figure out the ion specificity of such behaviour and further work needs to be done to understand the behaviour.

# Bibliography

[1] Smith AM, Lee AA, Perkin S. The electrostatic screening length in concentrated electrolytes increases with concentration. J Phys Chem Lett. 2016;7(12):2157-63.

[2] Gebbie MA, Valtiner M, Banquy X, Fox ET, Henderson WA, Israelachvili JN. Ionic liquids behave as dilute electrolyte solutions. Proceedings of the National Academy of Sciences. 2013;110(24):9674-9.

[3] Kjellander R. Nonlocal electrostatics in ionic liquids: The key to an understanding of the screening decay length and screened interactions. The Journal of Chemical Physics. 2016;145(12):124503.

[4] Kjellander R. Focus article: Oscillatory and long-range monotonic exponential decays of electrostatic interactions in ionic liquids and other electrolytes: The significance of dielectric permittivity and renormalized charges. The Journal of Chemical Physics. 2018;148(19):193701.

[5] Baimpos T, Shrestha BR, Raman S, Valtiner M. Effect of interfacial ion structuring on range and magnitude of electric double layer, hydration, and adhesive interactions between mica surfaces in 0.05–3 M Li+ and Cs+ electrolyte solutions. Langmuir. 2014;30(15):4322-32.

[6] Gaddam P, Ducker W. Electrostatic screening length in concentrated salt solutions. Langmuir. 2019;35(17):5719-27.

[7] Robb ID. Specialist surfactants. Springer Science & Business Media; 1996.

[8] Kang C, Khan A. Self-assembly in systems of didodecyldimethylammonium surfactants: Binary and ternary phase equilibria and phase structures with sulphate, hydroxide, acetate, and chloride counterions. Journal of colloid and interface science. 1993;156(1):218-28.

[9] Israelachvili JN. Intermolecular and surface forces. Academic press; 2011.

[10] Nagle JF, Tristram-Nagle S. Structure of lipid bilayers. Biochimica et Biophysica Acta (BBA)-Reviews on Biomembranes. 2000;1469(3):159-95.

[11] Parsegian VA, Fuller N, Rand RP. Measured work of deformation and repulsion of lecithin bilayers. Proceedings of the National Academy of Sciences. 1979;76(6):2750-4.

[12] Perez-Martinez CS, Smith AM, Perkin S, et al. Scaling analysis of the screening length in concentrated electrolytes. Physical review letters. 2017;119(2):026002.

[13] Meyers RA. Encyclopedia of physical science and technology. Academic; 2002.

[14] Hamer WJ, Wu YC. Osmotic coefficients and mean activity coefficients of uni-univalent electrolytes in water at 25° C. Journal of Physical and Chemical Reference Data. 1972;1(4):1047-100.

[15] Dos Santos AP, Uematsu Y, Rathert A, Loche P, Netz RR. Consistent description of ion-specificity in bulk and at interfaces by solvent implicit simulations and mean-field theory. The Journal of Chemical Physics. 2020;153(3):034103.

[16] Partanen JI. Mean activity coefficients and osmotic coefficients in dilute aqueous sodium or potassium chloride solutions at temperatures from (0 to 70) C. Journal of Chemical & Engineering Data. 2016;61(1):286-306.

[17] Lewis GN, Randall M. The activity coefficient of strong electrolytes. Journal of the American Chemical Society. 1921;43(5):1112-54.

[18] Purushothaman S, Cicuta P, Ces O, Brooks NJ. Influence of high pressure on the bending rigidity of model membranes. The Journal of Physical Chemistry B. 2015;119(30):9805-10.

[19] Faizi HA, Frey SL, Steinkühler J, Dimova R, Vlahovska PM. Bending rigidity of charged lipid bilayer membranes. Soft Matter. 2019;15(29):6006-13.

[20] Dubois M, Zemb T. Phase behavior and scattering of double-chain surfactants in diluted aqueous solutions. Langmuir. 1991;7(7):1352-60.

[21] Roux D, Nallet F, Freyssingeas E, Porte G, Bassereau P, Skouri M, et al. Excess area in fluctuating-membrane systems. Europhys Lett. 1992;17(7):575.

[22] Helfrich W. Steric interaction of fluid membranes in multilayer systems. Zeitschrift für Naturforschung A. 1978;33(3):305-15.

[23] Lipowsky R, Leibler S. Unbinding transitions of interacting membranes. Physical Review Letters. 1986;56(23):2541.

[24] Gupta SP, Thomas M, Chowdhury A, Raghunathan V. Effect of adsorbed polyelectrolytes on the interactions and elasticity of charged surfactant bilayers. J Phys: Condens Matter. 2020;32(19):194004.

[25] Porcar L, Hamilton WA, Butler PD, Warr G. Scaling of structural and rheological response of L3 sponge phases in the "sweetened" cetylpyridinium/hexanol/dextrose/brine system. Langmuir. 2003;19(26):10779-94.

[26] Pabst G, Rappolt M, Amenitsch H, Laggner P. Structural information from multilamellar liposomes at full hydration: full q-range fitting with high quality x-ray data. Physical Review E. 2000;62(3):4000.

[27] Gupta SP. Studies on novel phase behavior of ionic amphiphile-water systems. Raman Research Institute, Bangalore.; 2014.

[28] Salis A, Ninham BW. Models and mechanisms of Hofmeister effects in electrolyte solutions, and colloid and protein systems revisited. Chemical Society Reviews. 2014;43(21):7358-77.

# Chapter 6

# Effect of pH on the phase behaviour of PC bilayers

## 6.1 Introduction

Lipids are of fundamental importance as they are the basic building blocks of cell membrane[1]. Due to their amphiphilic nature, they self-assemble in to a variety of structures when hydrated ([2],[3]). The hydrophobic region of many lipids is made up of two hydrocarbon chains and they typically exhibit lamellar phases in water, consisting of bilayers. The fluid $L_\alpha$ phase occurs above the chain melting transition called the main-transition. At lower temperatures the gel phase is formed, where the lipid chains are mainly in the all-trans confirmation and are ordered on a two-dimensional lattice in the plane of the bilayer. The ordered gel phase is denoted as $L_{\beta'}$ phase if the chains are tilted with respect to the bilayer normal; otherwise it is referred to as the $L_\beta$ phase. Lipids that form the $L_{\beta'}$ phase often exhibit an intermediate ripple ($P_{\beta'}$) phase in between the gel and fluid phases, and the $L_{\beta'} \rightarrow P_{\beta'}$ transition is referred to as the pre-transition[2,4–6]. The relative cross-sectional area of the lipid headgroup in comparison to that of the chains determines whether the chains are tilted or not in the gel phase. Lipids having small head group area such as dimyristoylphosphatidylamine (DMPE), exhibit the $L_\beta$ phase, whereas those with larger head groups such as DMPC form $L_{\beta'}$ phase[7]. If the headgroup area is even higher, chains from two opposite leaflets can interdigitate to form the interdigitated gel phase, with a much lower membrane thickness that is comparable to the length of a lipid molecule[8].

Some biological membranes, such as the one lining the stomach of animals, are exposed to highly acidic environments[9]. Intracelluar pH is also known affect the structure, integrity and softness of membranes[10]. Hence determining the behaviour of lipids under such conditions is important in understanding their function. Phosphoatidylcholines (PCs) are major component of many biological membranes and hence by far the best studied class of lipids[1]. The PC headgroup is zwitterionic around neutral pH, due to deprotonation of the phosphate group and protonation of the quaternary nitogen. The positive charge of the quaternary nitrogen is neutralized at extremely high pH, above 12[11]. On the other hand, the intrinsic pK of the phosphate group is around 1[11]. Therefore, the fraction of PC lipids with a net positive charge increases as the pH of the solution is lowered, reaching the value 1/2 when pH $\sim$ 1. Calorimetric and fluorescence studies have shown that the chain melting transition temperature of PC lipids increases considerably as the pH of the solution is lowered below 3[12–14]. Protonation of the phosphate group also affects the polarity of the bilayer interface and leads to increasing hydrogen bonding between adjacent

headgroups in the bilayer[13,14]. In the case of dihexadecylphosphatidylcholine (DHPC) bilayers this drives a transition from interdigitated gel phase to bilayer gel phase, having much higher bilayer thikness, on lowering pH[13]. There are also a few reports of decreasing bending rigidity of PC lipids in the fluid phase at low pH[15,16]. Although the effect of pH on the PC bilayers in the fluid lamellar phase has been the subject of a few studies mentioned above, their phase behaviour under low pH condition has not been probed in much detail.

In this chapter we present experimental studies on the phase behaviour of 1,2-dimyristoyl-sn-glycero-3-phosphocholine (DMPC) and 1,2-dilauroyl-sn-glycero-3-phosphocholine (DLPC) at acidic pH. Using differential scanning calorimetry and x-ray scattering, dispersions of DMPC in HCl solutions of pH=4 and pH=3 are found to exhibit identical behaviour as dispersions in water, with the pre-transition ($T_p$) and main-transition ($T_m$) temperatures remaining at around 14 and 24°C, respectively. At low pH, $T_m$ increases for both the lipids (DMPC and DLPC) and the pre-transition disappears. An untilted gel phase with relatively larger periodicity is observed at pH=2 and pH=1, in contrast to tilted gel phase found in higher pH. The larger periodicity of the gel phase indicates presence of long-range inter-bilayer repulsion due to the charging of the head groups as the pH of the solution approaches the pK of the phosphate group. On the other hand, absence of chain tilt in this phase points to the concomitant dehydration of the head groups, which reduces the cross-sectional area. Incubation of the samples for a few days at pH=2 and pH=1, results in the formation of crystallites at low temperatures and an inverted hexagonal phase at higher temperatures. The occurrence of these phases can be attributed to the dehydration of headgroups at very low value of pH[17].

## 6.2 Materials and methods

DMPC and DLPC were obtained from Avanti Lipids. Samples at different pH were prepared by adding appropriate amounts of stock solutions of HCl in water to the dry lipid. These samples were vortexed and incubated at 60°C for at least one day to ensure homogeneity. Concentration of DMPC and DLPC in these samples was typically 20 wt %. For DSC measurements, 30-40 $\mu$l of these samples were taken in sealed metal cups. A Metler Teledo DSC 3 was used for all the experiments with a scanning rate of 3 °C/min. For small angle x-ray scattering (SAXS) studies, the samples were filled in 1 mm capillaries and flame sealed.

## 6.3 Results

### 6.3.1 Effect of pH on DMPC bilayers

At pH=4 and pH=3, DSC thermograms are very similar to that of the DMPC-water system. $T_p$ and $T_m$ remain at 14°C and 24°C, respectively. The small hysteresis which is found on cooling may be due to rate of the cooling used. The phase behaviour changes at lower pH. A small increase in $T_m$ is observed for pH=2. For pH=1, $T_m$ is found to be around 45°C, which is much higher compared to that of the DMPC-water system. Two distinct peaks are observed on cooling for pH=2 samples at 35°C and 25°C, respectively (fig. 6.1b).

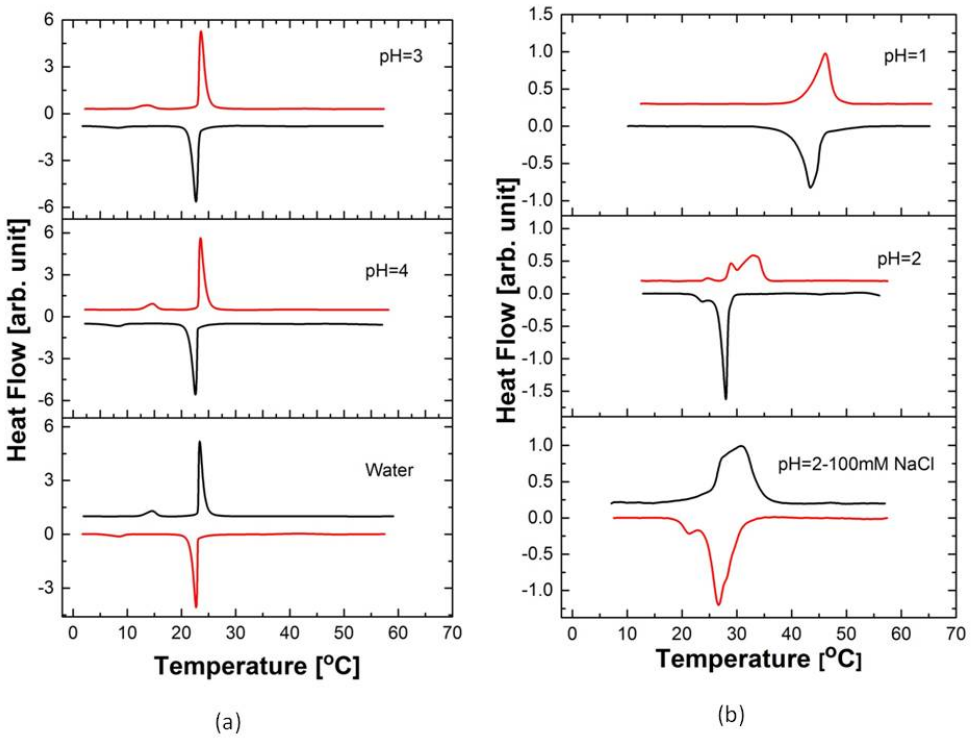


FIGURE 6.1: DSC thermograms DMPC dispersions in water and HCl solutions of different pH. The upper curves correspond to heating cycle and the lower curves correspond to cooling cycle.

SAXS profile of DMPC dispersions at pH=4 and pH=3 are similar to that of the DMPC-water system. The d-spacings found in the fluid phase in all the three cases are similar and is about 6.2 nm (fig.6.2).

SAXS profile of pH=2 samples incubated for one day is shown in (fig.6.3 ). These profiles consist of two or three peaks superposed on a much broader hump. The weak peaks can be indexed to h=2,3 and 4 reflections of a lamellar phase of periodicity about 20 nm. The broad hump arises from uncorrelated bilayers. The pattern doesn't change significantly on cooling except the narrowing of the hump at 20°C. The weak peaks disappears few days after incubation but the broad peak remains (fig.6.4 ). Drastic changes are observed after incubating for many days (fig.6.5). Firstly, a sharp peak appears at 30°C corresponding to a spacing of 3.1nm, which coexists with a broad hump and a correlation peak at 6.5nm, arising from a lamellar phase. The peak from the lamellar phase disappears at 40°C. Scattering from uncorrelated bilayers becomes weaker at 50°C and the SAXS profile is dominated by the sharp peak at 3.1 nm. The pattern changes at 55°C, with the appearance of peaks whose spacings are in a ratio $1:1/\sqrt{3}:1/2$. These can be indexed to a two dimensional hexagonal lattice with a lattice parameter of 6.8 nm. The hexagonal phase remains at 60°C, with the lattice parameter decreasing slightly to 6.3 nm.

WAXS patterns of pH=2 samples are shown in (fig. 6.6 ). Samples incubated for 1 day show a broad peak at around 0.45 nm at 40°C. On cooling to 28°C a sharp peak appears at 0.42 nm. On further cooling the broad peak disappears and the sharp peak becomes more intense. Samples incubated for 15 days show a similar broad peak at higher temperatures, but show multiple sharp peaks at lower temperatures (fig. 6.7 ). The width of these peaks is much lower that that of the single sharp peak seen at lower temperatures in the WAXS profiles of samples incubated for a day.

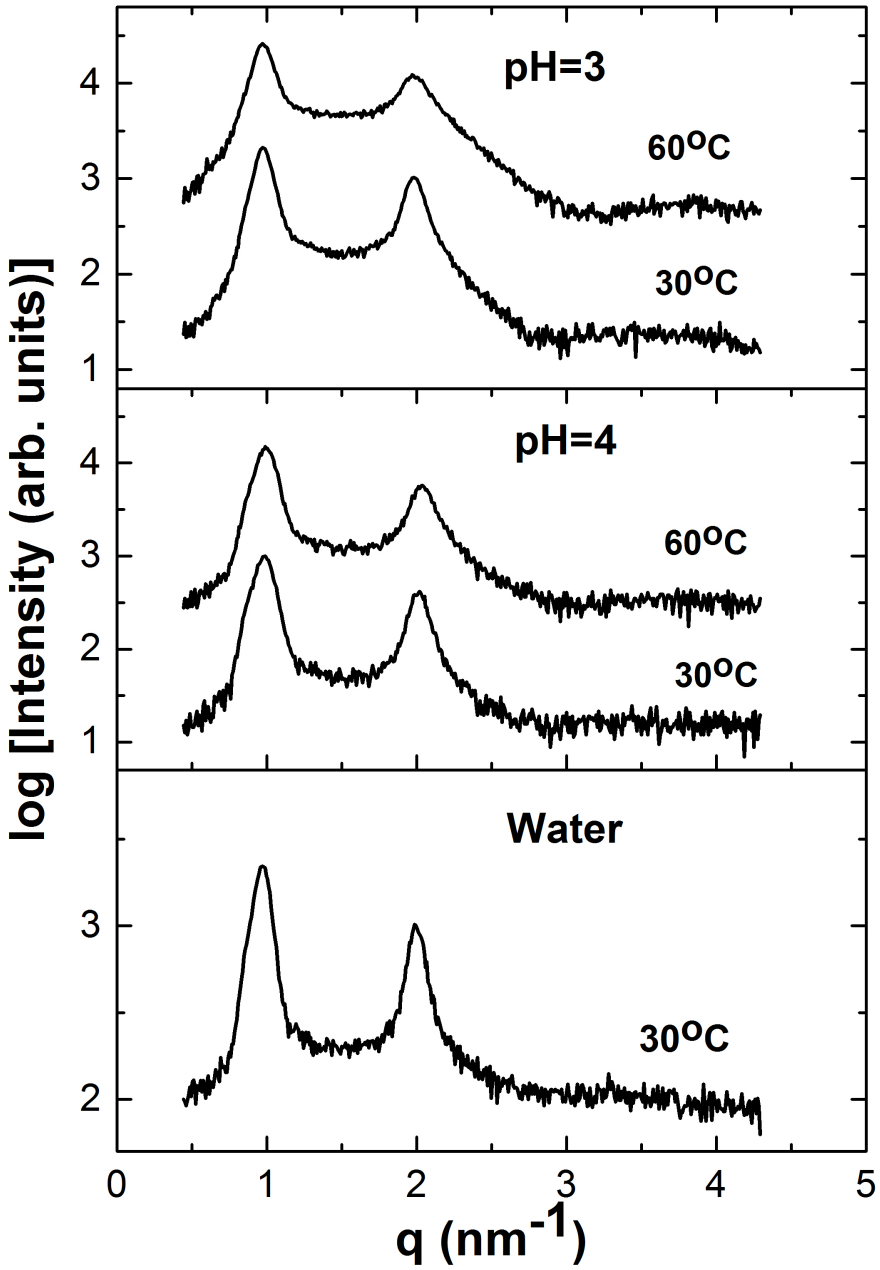


FIGURE 6.2: SAXS patterns of DMPC dispersions in water and in HCl solutions of pH=4 and pH=3.

SAXS profiles of samples at pH=1 are shown in fig 6.8, fig. 6.9 and fig. 6.10. Samples incubated for a day, show two peaks at 60°C arising from a swollen lamellar phase of 14.3 nm periodicity. These peaks are superposed on a broad hump arising from uncorrelated bilayers. The pattern remains unaltered on cooling down to 50°C. Additional lamellar peaks appear at 40°C, but the intensity of the original peak decreases considerably. At this temperature the lamellar periodicity is 13.8 nm. The original peak disappears at 30°C, but the periodicity does not change significantly.

On incubating for three days the periodicity of the swollen lamellar phase decreases to 8.7

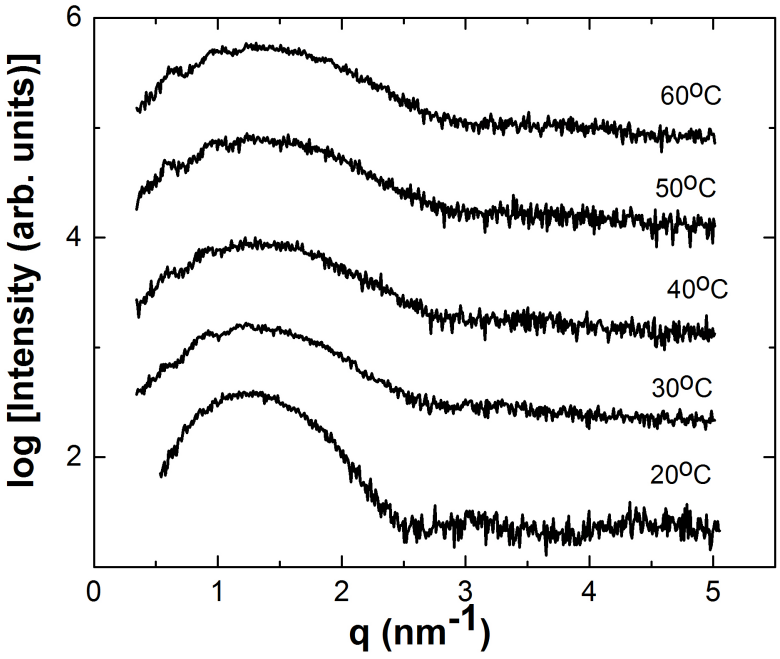


FIGURE 6.3: SAXS profiles of DMPC dispersions in HCl solutions of pH=2 on day 1.

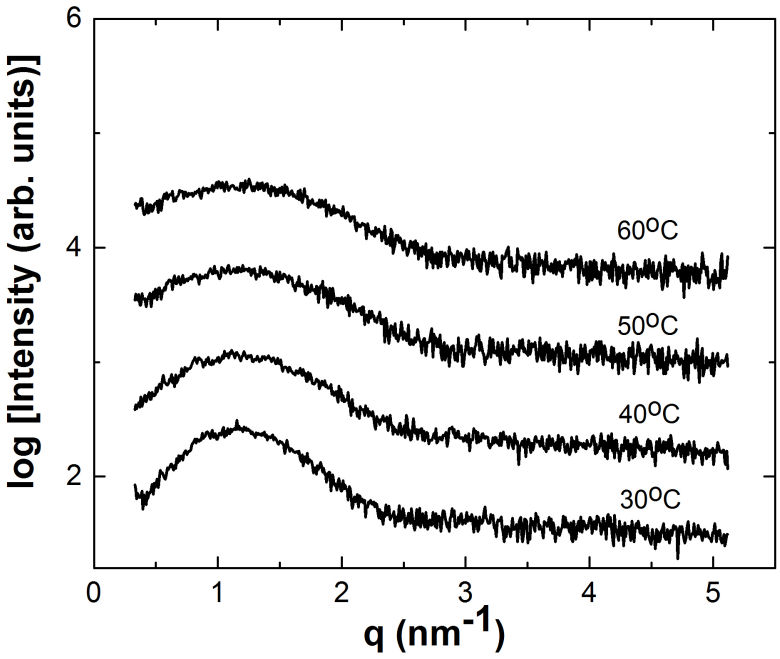


FIGURE 6.4: SAXS profiles of DMPC dispersions in HCl solutions of pH=2 on day 5.

nm at 30°C. In addition, two sharp peaks are observed at this temperature corresponding to a lamellar phase of 3.1 nm periodicity. The pattern remains unaltered at 40°C, but the peaks from the swollen lamellar phase become broader at 50°C, with the periodicity increasing to 9.7 nm. The swollen lamellar phase disapperars at 55°C and three additional peaks appear, two of them falling

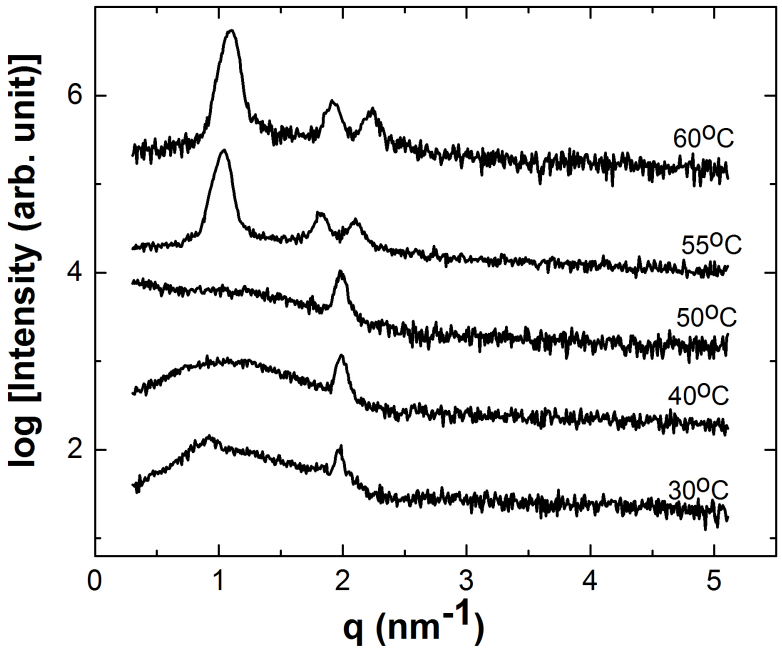


FIGURE 6.5: SAXS profiles of DMPC dispersions in HCl solutions of pH=2 on day 14.

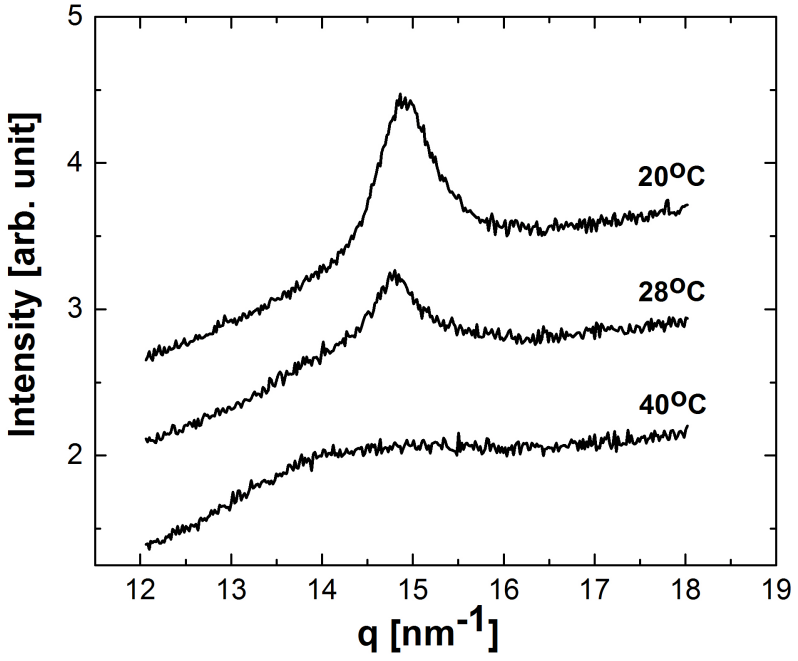


FIGURE 6.6: WAXS profiles of DMPC dispersions in HCl solution of pH=2 on day 1.

very close and on either side of the first peak of the swollen lamellar phase. These peaks can be indexed to a two dimensional hexagonal lattice of lattice parameter 6.8 nm. On heating to 60°C only a broad peak corresponding to a spacing of around 5.5 nm is observed.

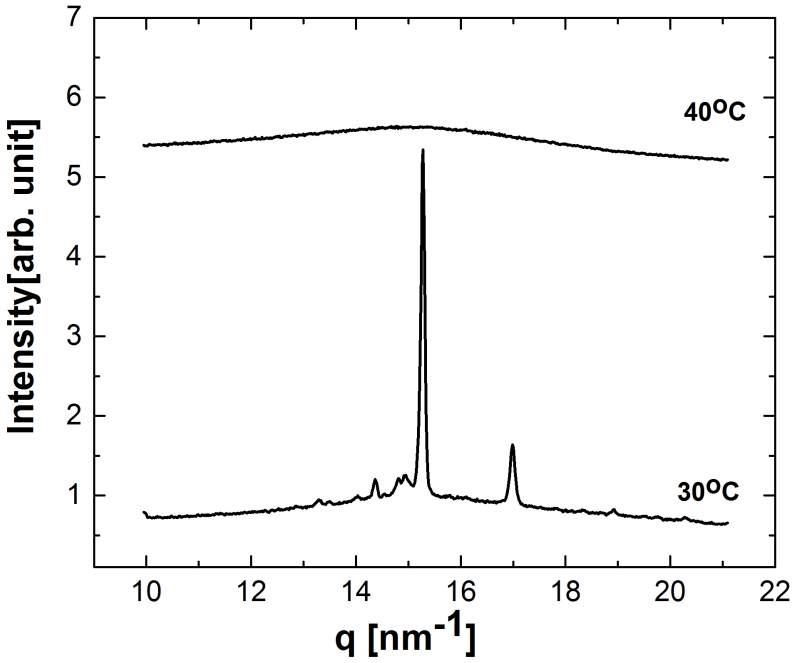


FIGURE 6.7: WAXS profiles of DMPC dispersions in HCl solution of pH=2 on day 15.

Relative intensity of the peaks from the second lamellar phase of periodicity 3.1 nm increases substantially on incubating the samples for 6 days. At 30°C an additional faint peak is observed at a spacing of 6.6 nm, which becomes fainter on heating and disappears above 55°C. No peaks are observed on heating the samples to 60°C.

WAXS patterns of the samples at pH=1 are shown in fig.6.11, fig. 6.12 and fig. 6.13 . A broad peak is observed at 0.45 nm at 45°C, and on cooling below 40°C a sharp peak appears at 0.42 nm. At lower temperatures the broad peak disappears and only the sharp one remains. Width of the peak is considerably less than that of the peak seen at lower temperatures in the WAXS patterns at pH=2 on day 1 (fig. 6.11). After 5 days the patterns seen at lower temperatures changes significantly, with the appearance of multiple sharp peaks. Along with this, the broad peak appearing at high temperatures becomes very faint. On further incubation the number of peaks present in the pattern at lower temperature increases considerably. Polarising optical microscopy of these samples incubated for about a week show plate-like birefringent crystallites dispersed in the aqueous solution, which melt into isotropic droplets at around 60°C (fig. 6.14).

### 6.3.2 Effect of pH on DLPC bilayers

Like DMPC samples a increase of $T_m$ is observed for DLPC dispersions in HCl solutions of lower pH. $T_m$ for DLPC at neutral pH is around -2°C[18]. At pH=2 a peak is seen at around 10°C on heating and cooling. For pH=1 samples the peak is observed at around 15°C (fig. 6.15).

DLPC samples at pH=2, which are incubated for one day, show SAXS profiles given in fig.6.16 . These profiles consist of two peaks which can be indexed as the h=3 and 4 reflections of a lamellar phase with periodicity of about 18 nm. The weak peak disappears after a few days of incubation

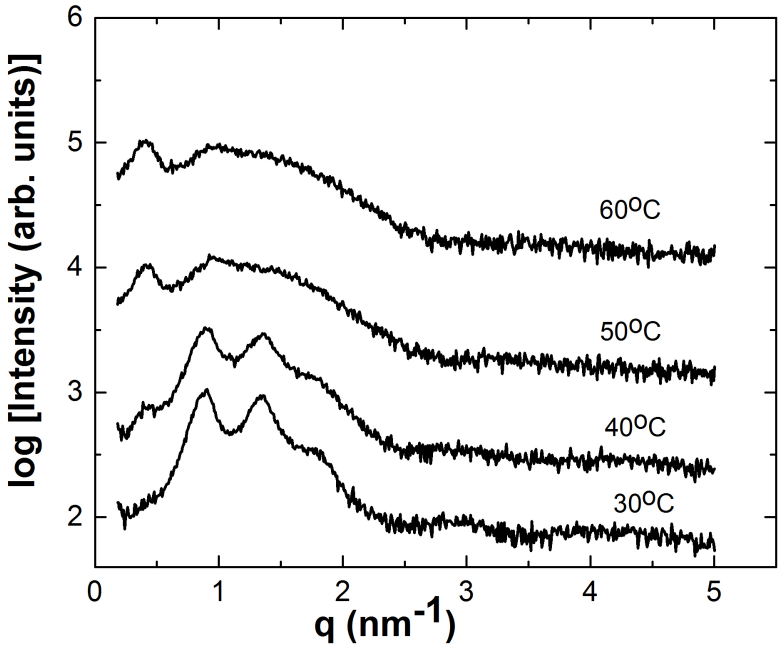


FIGURE 6.8: SAXS profiles of DMPC dispersions in HCl solutions of pH=1 on day 1.

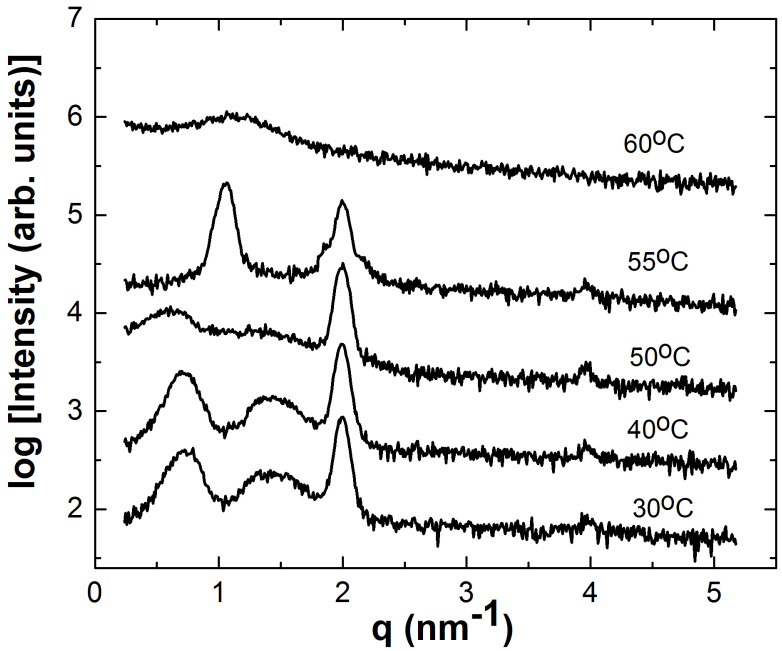


FIGURE 6.9: SAXS profiles of DMPC dispersions in HCl solutions of pH=1 on day 3.

and the broader hump remains (fig.6.17). Drastic changes are observed after incubating for many days (fig.6.18). at -5°C a lamellar phase of periodicity 2.8 nm is found to co-exist with another lamellar phase of 6.4 nm. A change in SAXS pattern is observed on heating to 15°C. The peak correspond to 2.8 nm periodicity remains and h=2,3 and 4 reflections from a lamellar phase of

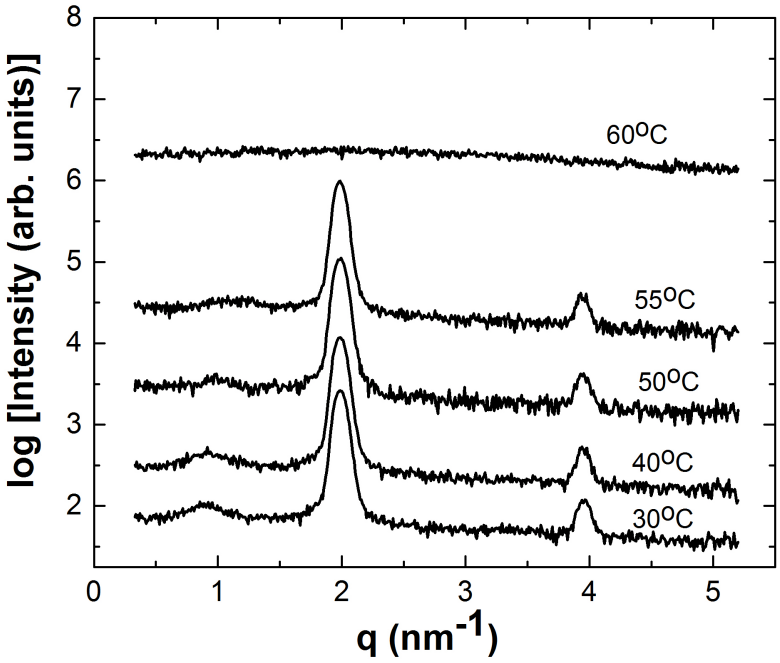


FIGURE 6.10: SAXS profiles of DMPC dispersions in HCl solutions of pH=1 on day 6.

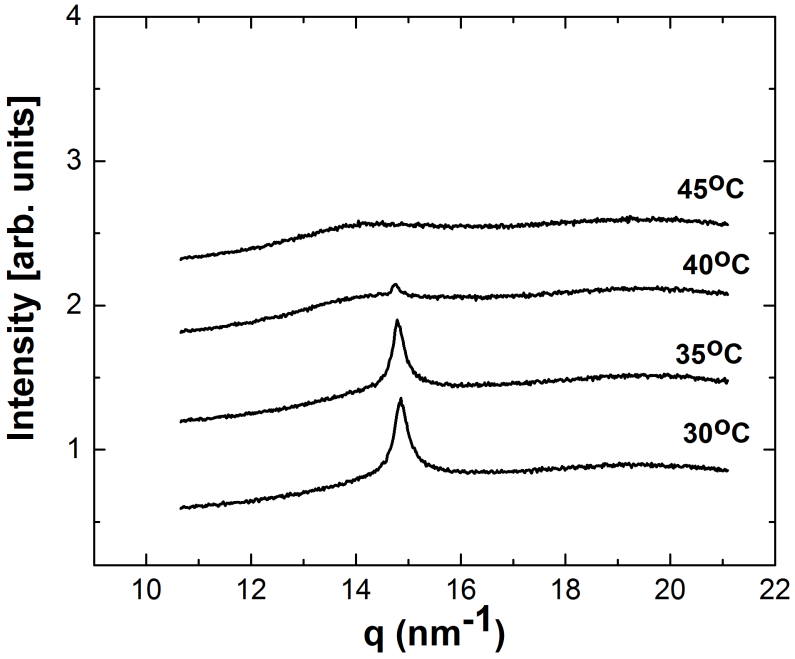


FIGURE 6.11: WAXS profiles of DMPC dispersions in HCl solution of pH=1 on day 1.

periodicity around 18 nm is found. The first peak of the swollen lamellar phase appears on heating to 25°C. Three peaks are found at 45°C, which can be indexed to a two dimensional hexagonal

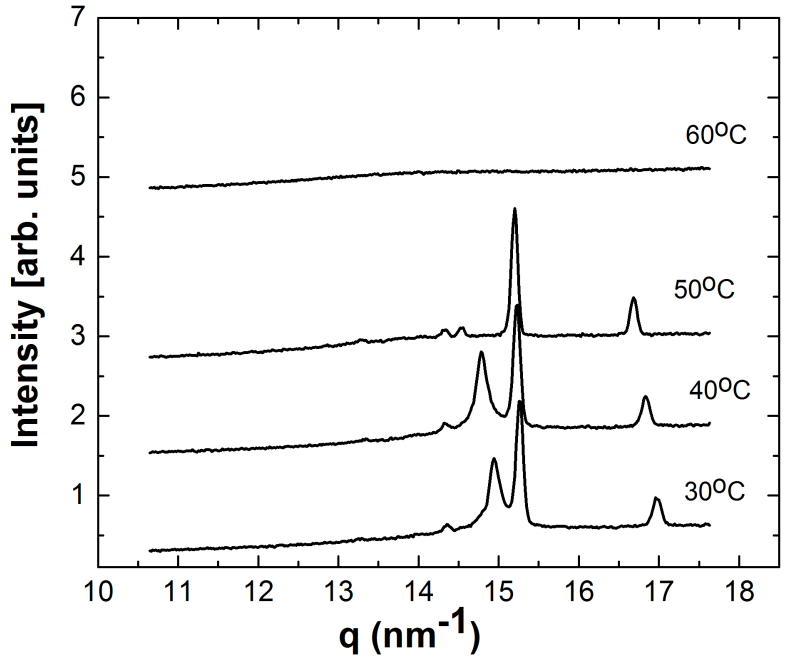


FIGURE 6.12: WAXS profiles of DMPC dispersions in HCl solution of pH=1 on day 5.

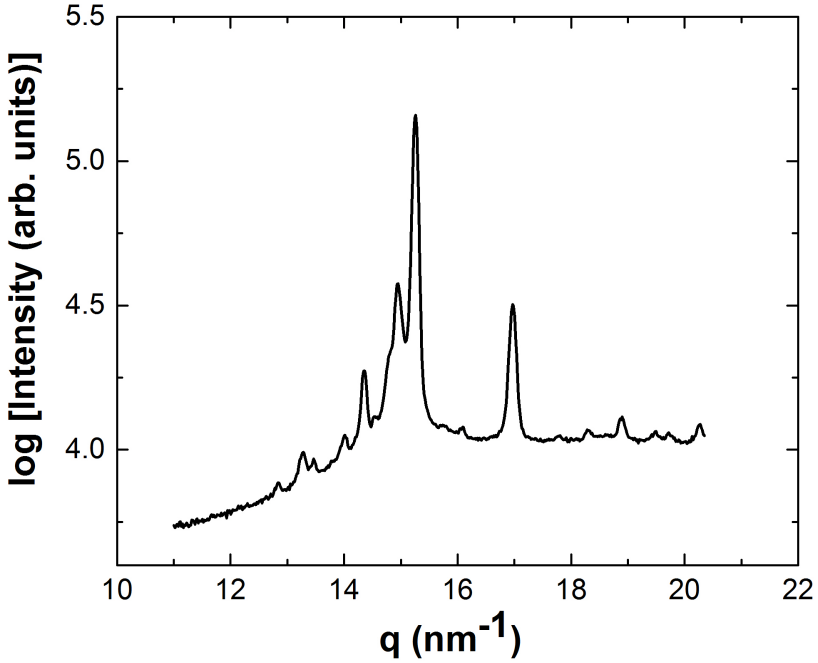


FIGURE 6.13: WAXS profiles of DMPC dispersions in HCl solution of pH=1 on day 8.

phase with a lattice parameter of 6.5 nm.

SAXS patterns of DLPC samples at pH=1 are shown in fig.6.19, fig. 6.20 and fig. 6.21. Samples

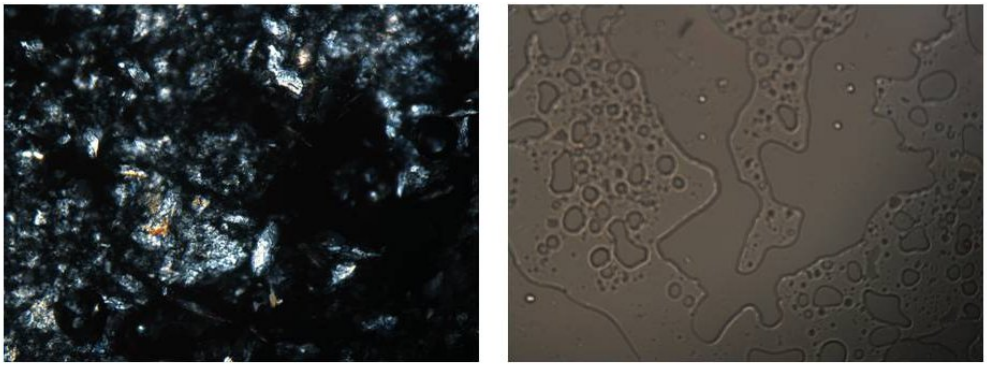

(a) (b)

FIGURE 6.14: POM images of DMPC samples at pH=1, incubated for about a week, showing birefringent crystallites at 30°C (a), and isotropic droplets dispersed in the aqueous medium at 60°C (b).

incubated for a day show 3 peaks below the main transition temperature, arising from a swollen lamellar phase of periodicity around 14 nm. On heating a broad peak is observed, where the SAXS pattern is dominated by scattering from uncorrelated bilayers (fig.6.19). The peaks disappear on day2, and only the broad hump remains (fig.6.20 b). On incubating for 4 days a new lamellar phase appears with a periodicity of 2.7 nm (fig.6.21 c). On heating to 20°C the pattern changes, and at 30°C the first order peak of the swollen lamellar phase appears. At 45°C three peaks are observed which can be indexed on a two dimensional hexagonal lattice with lattice parameter of 6.5 nm.

## 6.4 Discussion

Results of DSC studies clearly show that the phase behaviour of DMPC dispersions at pH=4 and 3 is identical to that of DMPC dispersions in water. $T_m$ and $T_p$ remain unaltered in this pH range. This conclusion is borne out by SAXS experiments, which show a fluid lamellar phase ($L_\alpha$) of comparable periodicity above the main transition over this range of pH. This is expected since over this range of pH the protonation state of the head group is unaltered, the pK of phosphate group being around 1 [11]. We did not probe the phase behaviour of these samples below $T_m$, since these are well documented in the literature [4,5,19].

Both for DMPC and DLPC, $T_m$ increases at pH=2. The DSC thermogram for DMPC at pH=2 shows two closely spaced peaks and relatively large hystersis between the heating and cooling cycles. SAXS profiles do not contain much information about structural changes across this transition since they are dominated from the scattering from uncorrelated bilayers. In order to confirm the origin of this scattering, we have fitted some of these profiles to the form factor of the bilayer derived from the 3 Gaussian model, which is given by [20,21],

$$F(q) = 2\sqrt{2\pi}\bar{\rho_h}\sigma_h exp[-q^2\sigma_h^2/2]\cos(qz_h) + \sqrt{2\pi}\bar{\rho_c}\sigma_c exp[-q^2\sigma_c^2/2] \quad (6.1)$$

Here $\bar{\rho_c}$=$\rho_c$-$\rho_m$ is the relative electron density of the chain region with respect to the methylene group and $\bar{\rho_h}$=$\rho_h$-$\rho_m$ is the relative electron density of the headgroup region. $\sigma_h$ and $\sigma_c$ are the

widths of the Gaussians describing the head group and tail regions, respectively. $z_h$ is the distance between the center of the bilayer and that of the head group region, so that $2z_h$ is a measure of the bilayer thickness.

Data collected from a more dilute DMPC dispersion (5 wt%) at pH=2 were fitted to eq.6.1, in order to minimize correlation effects. These are shown in fig.6.22 and values of the model parameters reported from the fit are presented in table 6.1, which are comparable to the values obtained in the literature for similar lipids[21]. The fit confirms that the scattering is from uncorrelated bilayers. Furthermore, values of the bilayer thickness ($2z_h$) obtained at 10°C and 40°C are found to be comparable to those reported in the gel and fluid phases of DMPC[7,19].

TABLE 6.1: Values of the bilayer electron density model parameters obtained on fitting eqn. 6.1 to SAXS data collected from a 5 wt% DMPC dispersion at pH = 2.

| T°C | $z_h$(nm) | ($\bar{\rho_h}$ / $\bar{\rho_c}$ ) | $\sigma_h$(nm) | $\sigma_c$(nm) |
|---|---|---|---|---|
| 10 | 2.00 | -1.70 | 0.10 | 0.38 |
| 40 | 1.64 | -1.58 | 0.20 | 0.65 |

In both DMPC and DLPC, observation of a highly swollen lamellar phase and spontaneous formation of uncorrelated bilayers point to the existance of long range repulsion between the bilayers, which can arise from charging of the bilayers since the pH is close to the pK of the phosphate group. In order to confirm the origin of this repulsion, we have studied the effect of 100mM NaCl on DMPC dispersions at pH=2. Incorporation of salt is found not to affect the phase behaviour in any way, as can be discerned from DSC thermograms given in fig 6.1b. However SAXS patterns of the $L_\alpha$ phase are altered significantly by the salt (fig.6.24). As described earlier, salt free system gives patterns consisting of a few peaks superposed on a back ground. The multiple peaks correspond to a lamellar periodicity of around 20 nm, whereas the background correspond to the form factor of the bilayer. Hence it can be concluded that DMPC and DLPC form mainly unilamellar vesicles (ULVs) and a few multilamellar vesicles (MLVs) in the dispersion; former giving rise to the broad background and latter giving rise to the peaks (fig.6.25). SAXS patterns obtained in the presence of 100mM NaCl resemble those obtained from DMPC at higher pH, and consist of two peaks corresponds to a lamellar structure, with a periodicity of 7.0 nm, which is close to the value of 6.2 nm reported for DMPC dispersions in water[22]. Hence we can conclude that these samples moslty consist of MLVs. The much lower periodicity of these samples, which leads to the enhanced stability of MLVs, indicates screening of inter bilayer repulsion by salt, thus confirming its elecrostatic origin in the case of PC lipids.

SAXS patterns of samples containing salt change considerably when they are cooled down to gel phase. Peaks corresponding to lamellar periodicity disappear and only a broad peak from the bilayer form factor is observed. This indicates a transformation of the MLVs present at $T>T_m$ into ULVs below $T_m$. On heating back to the fluid phase the SAXS pattern remains almost unaltered , showing that the ULVs do not transform back into MLVs. Narrowing of the profile can be accounted for by the thickening of the bilayers in the gel phase , as found in the salt-frree system (fig.6.22). Presence of ULVs above $T_m$ is most probably due to the very slow kinetics of their conversion into MLVs, and not an indication of their inherent stability in the fluid phase. Transformation of MLVs into ULVs corresponds to the unbinding of the bilayers, and is driven by a relative enhancement of the long range inter bilayer repulsion, which overwhelms the attractive

van der Waals interaction between them[23]. For example, an unbinding transition has been reported on melting from the gel into fluid phase, caused by steric repulsion between the bilayers, which arises from their thermal undulations[24]. Since the bilayer bending modulus in the fluid phase is very much lower than in the gel phase, there is an abrupt increase in the amplitude of thermal undulations of bilayer across the chain melting transition, and hence in the steric repulsion, leading to the unbinding of bilayers[24]. In the present system unbinding occurs on cooling from the fluid to gel phase and hence can not be attributed to steric repulsion. The only other long range inter bilayer repulsion is electrostatic repulsion. But it is difficult to imagine an abrupt increase in electrostatic repulsion on going from the fluid to gel phase. An abrupt decrease in the attractive van der Waals interaction across this transition is also very unlikely. One possibility is that this MLV $\longrightarrow$ ULV transformation is not driven by a relative increase in the inter-bilayer repulsion, but by a relative change in the Gaussian and bending rigidities of the bilayer due to contributions arising from electrostatic interaction, which are known to have opposite signs in the two cases[25]. It has been shown that different bilayer morphologies, such as ULVs and flat bilayers, are stable over different ranges of the ratio of these two elastic moduli[26,27]. Hence it is conceivable that the observed change in the bilayer morphology results from variations in the elastic moduli on approaching the chain melting transition from above. Further work is needed to understand the origin of this unexpected behaviour.

For DMPC, DSC traces of pH=2 samples with and without salt, are ver similar, but for an increase in the width of the peak in the presence of 100 mM NaCl. On cooling they show a large peak followed closely by a smaller one. They are reminiscent of the main and the pre transitions of DMPC at higher value of pH, but with the two transition occurring very close in temperature. Since the salt free samples consists mainly of ULVs, as deduced from the SAXS data, these transitions should correspond to changes in each bilayer. It may be mentioned here that the pretransition is believed to occur in isolated bilayers[28], hence the possibility of the smaller peak corresponding to such a transition can not be ruled out. However, in the absence of a periodic stacking of bilayers, it is no possible to deduce the occurrence of this transition from our SAXS data. We have tried to probe this temperature range in detail in samples with salt, since they form MLVs at high temperatures. However, the formation of ULVs on cooling prevented us from gaining an understanding of the structural changes in the system over this temperature range.

WAXS profiles of DMPC samples at pH=2, collected after 1 day of incubation, which are comparable to the samples used in DSC studies, show a fluid to gel transition at around 30°C. Presence of one sharp peak in the wide angle region shows that the lipid chains are not tilted with the respect to the bilayer normal, and the gel phase can be identified as $L_\beta$. In contrast, two or three peaks are observed in the $L_{\beta'}$ phase, depending on the direction of chain tilt with respect to the chain lattice ([5],[19]). Since DMPC forms the $L_{\beta'}$ phase at higher pH, observation of the $L_\beta$ phase suggests a reduction in the headgroup cross-sectional area at pH=2. As suggested in the literature, the PC headgroups are dehydrated at lower pH[13,16]. Although repulsion between the headgroups also increases due to their charging, the effect of dehydration dominates in determining their cross-sectional area. This leads to the formation of the $L_\beta$ phase at lower temperatures at pH=2. Since the chains are ordered on a two-dimensional hexagonal lattice in the $L_\beta$ phase, the area per lipid can be calculated using the relation, $A = (4/\sqrt{3})d^2$, where d is the spacing of the WAXS peak (0.42 nm). This gives A=0.41 $nm^2$, which is in good agreement with the value

found in the $L_\beta$ phase of 1,2-Dilauroyl-sn-glycero-3-phosphorylethanolamine (DLPE), which has a much smaller head group compared to DMPC[7]. In comparison, A=0.47 $nm^2$ in the $L_{\beta'}$ phase of DMPC[19]. DLPE has shorter chains compared to DMPC, but the area per lipid is not affected by this difference. Thus the reduction in A at low pH is quantitatively borne out by our results. Occurrence of a swollen $L_\beta$ phase clearly demonstrates the two concurrent effects of low pH on the headgroups, namely, charging and dehydration. Similar WAXS studies were not done in the case of DLPC. But the trend in the SAXS profile and DSC thermograms of DLPC are very similar to that found in DMPC. As the effect of dehydration at low pH is independent of chain size, it is expected that the WAXS pattern of DLPC also will be very similar to that of DMPC.

A new phase appears at low temperatures after days of incubation, giving rise to a SAXS pattern similar to that of a lamellar phase of 3.1 nm periodicity in the case of DMPC and of 2.8 nm periodicity for DLPC. From the WAXS profile of DMPC this phase can be identified as a crystal, as it consists of many sharp peaks. Formation of a crystalline phase can be attributed to the drastic reduction in the head group hydration at lower pH. These observations suggest that the reported ability of acetic acid to promote crystallization of lipids results from a lowering of the solution pH caused by dissociation of this weak acid[29]. We have not probed the structure of these crystallites to see if it differs from the reported crystal structure[30]. These crystallites coexist with a gel phase at low temperatures. They both melt on heating leading to the formation of hexagonal phase, which can be identified as an inverted phase as it coexists with an aqueous solution. The appearance of the inverted hexagonal phase ($H_{II}$) at high temperatures again points to the reduction in the head group size due to dehydration, as this phase is exhibited by aqueous dispersions of lipids such as DPPE and DLPE, which have a much smaller phosphatidylethanolamine (PE) headgroup, but saturated hydrocarbon chains similar to those of DMPC[3]. Changes in the SAXS profile suggest that the $H_{II}$ phase melts into a more disordered structure, such as an isotropic phase of inverted micelles, at higher temperatures.

The phase behaviour at pH=1 is very similar to that at pH=2, with a few minor differences. Increase of $T_m$ is more at pH=1, for both DMPC and DLPC, in agreement with earlier report[12–14]. The crystalline and inverted hexagonal phases appear much faster here compared to pH=2 samples, probably due to a higher degree of dehydration. In the case of DMPC, the scattering data show the coexistence of gel and crystalline phase at 30°C and suggests an $L_\beta \longrightarrow L_\alpha$ transition at 50°C. On heating further, the $L_\alpha$ phase gets converted into the $H_{II}$ phase at around 55°C. In the case of DLPC the conversion to $H_{II}$ phase takes place at around 45°C. This sequence of phases is usually exhibited by aqueous dispersions of lipds with smaller headgroups such as DPPE and DLPE[3], illustrating the key role played by the head group size in determining the phase behaviour. A careful observation on DMPC dispersions at pH=1 shows that the swollen gel phase almost disappears after a few days of incubation and only the crystalline phase is observed. These crystallites melt at around 60°C and form a dispersion of isotropic droplets in the aqueous medium (fig.6.14b). The high temperature liquid phase scatters X-rays very weakly and does not give any noticeable SAXS signals. The inability of the crystallites to form any liquid crystalline phases on melting is a clear indication of the extreme dehydration of head groups at pH=1. Observation of lamellar peaks in the pH=1 samples may be due to the reduction of interbilayer repulsion compared to pH=2. This can be attributed to the lower Debye length at pH=1, which is of the order of 1 nm, compared to 3 nm at pH=2. Although the surface charge density is higher at pH=1, the

lower Debye length leads to increased correlation between the bilayers.

Crystallization is a slow process, it is expected that the crystals of PC lipids will form at lower pH only a few days of incubation. The duration of incubation is much shorter at pH=1, as a result of much higher degree of dehydration of the headgroups. On the other hand, the delay in the appearance of the $H_{II}$ phase is rather surprising. This phase can be expected to form only when the headgroup size is reduced sufficiently due to dehydration. Hence the appearance of the $H_{II}$ phase many days after incubation suggests that the kinetics of headgroup dehydration is very slow.

In order to further probe the observed dehydration of the PC headgroups at low pH, we have studied the pressure-area isotherms of DMPC monolayers at air-water interface for three different values of the pH of the subphase at T=25°C. We do not find any significant differences between the isotherms measured at pH=7,3,2 and 1 (fig.6.26)[17]. This suggests that the area per molecule in the monolayer is not affected by the pH of the aqueous solution, in contrast to the case of bilayers. It may be noted here that DMPC monolayers are in the liquid expanded phase at ambient temperature, irrespective of the applied pressure[31]. It would be interesting to see if lipid monolayers exhibiting the liquid condensed phase also exhibit this insensitivity to the pH of the subphase.

It is difficult to correlate the results of the present study on a simple model membrane system to the behaviour of multi-component biological membranes. However, since animal membranes typically contain an appreciable amount of cholesterol[1], which is known to significantly alter the phase behaviour of DMPC[32], a natural extension of the present study will be to probe the influence of low pH on DMPC-cholesterol membranes.

## 6.5 Conclusions

We have studied the effect of acidic pH on the phase behaviour of two zwitterionic lipids, namely DMPC and DLPC. Dispersions of DMPC in HCl solution of pH=4 and pH=3 behave identical to dispersions in water. PC bilayers get charged at lower pH on approaching the pK of the PC headgroup. At the same time head group size is reduced due to dehydration. This results in the formation of the untilted gel phase at low temperatures and the inverted hexagonal phase at higher temperatures. Headgroup dehydration leads to the formation of crystals after a few days of incubation at pH=2 and pH=1.

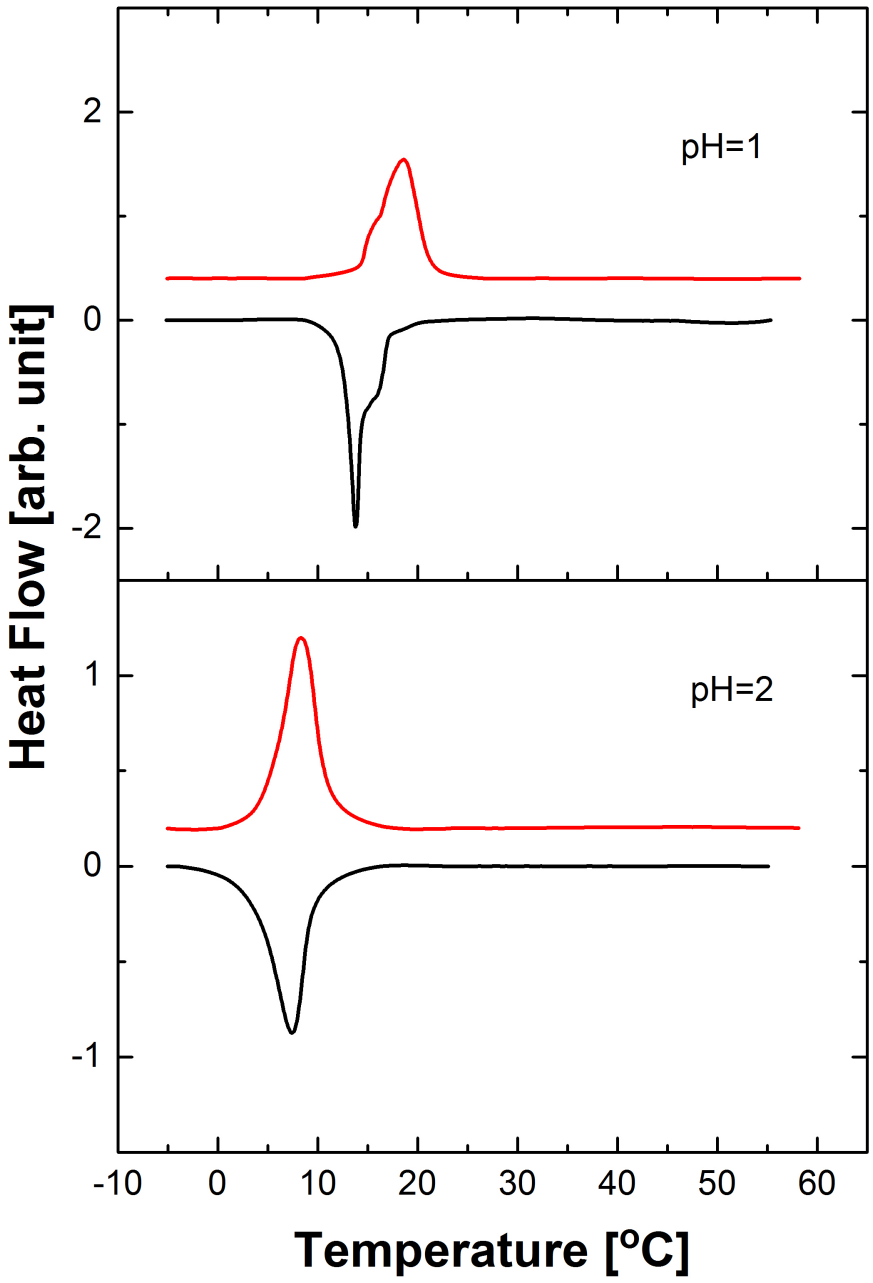


FIGURE 6.15: DSC thermograms of DLPC dispersions in water and HCl solutions of pH=2 and pH=1.

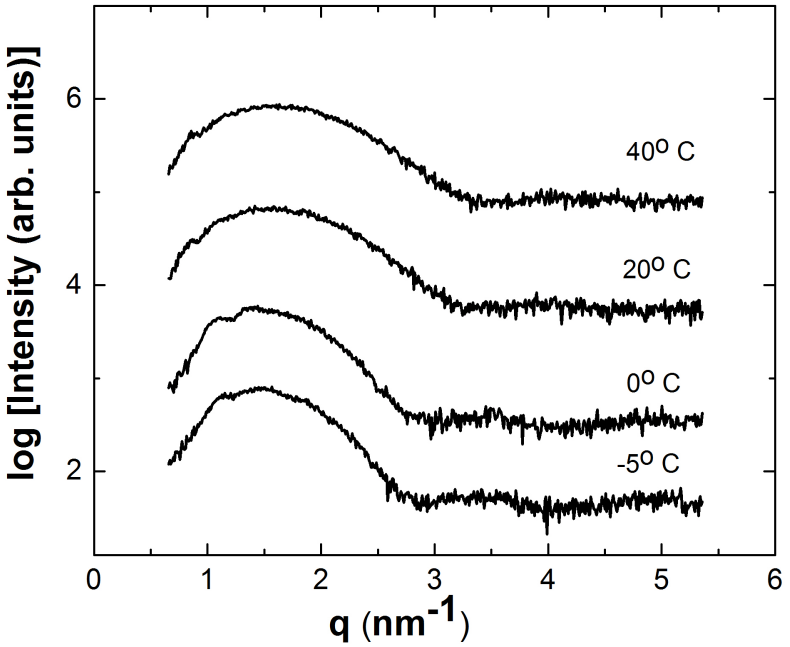


FIGURE 6.16: SAXS profiles of DLPC dispersions in HCl solution of pH=2 on day 1.

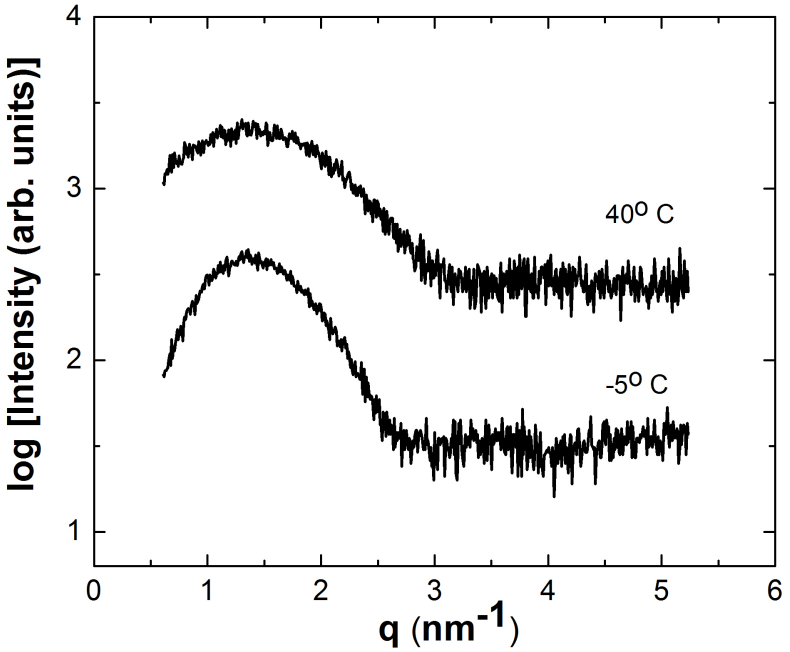


FIGURE 6.17: SAXS profiles of DLPC dispersions in HCl solution of pH=2 on day 4.

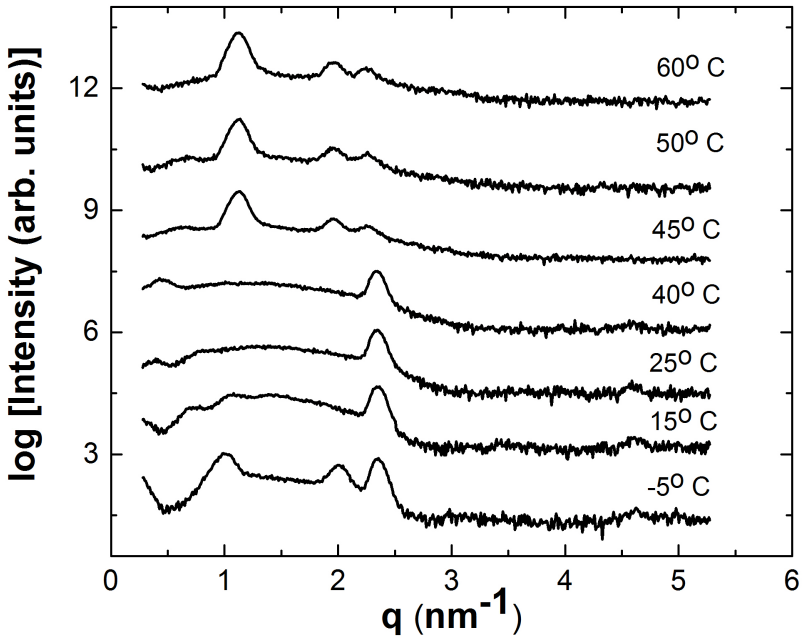


FIGURE 6.18: SAXS profiles of DLPC dispersions in HCl solution of pH=2 on day 10.

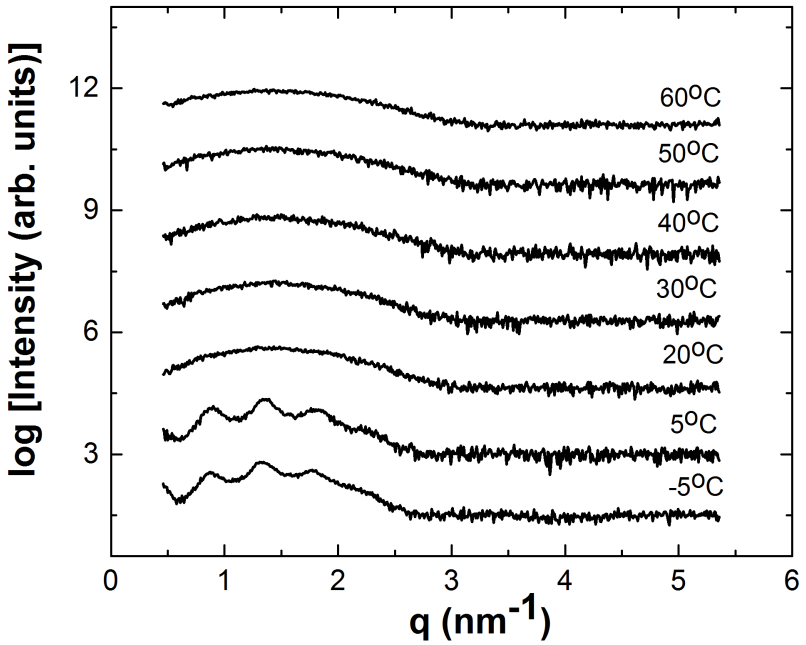


FIGURE 6.19: SAXS profiles of DLPC dispersions in HCl solution of pH=1 on day 1.

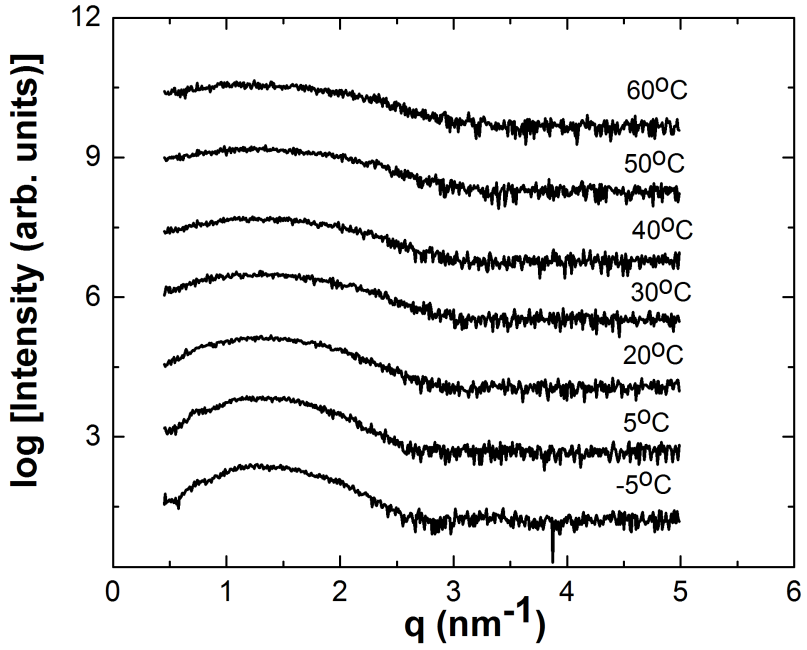


FIGURE 6.20: SAXS profiles of DLPC dispersions in HCl solution of pH=1 on day 2.

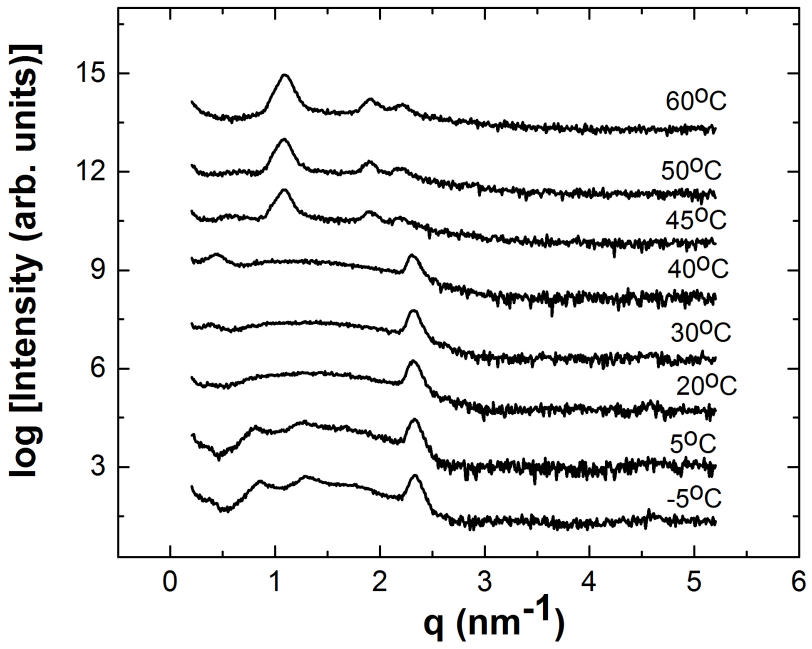


FIGURE 6.21: SAXS profiles of DLPC dispersions in HCl solution of pH=1 on day 4.

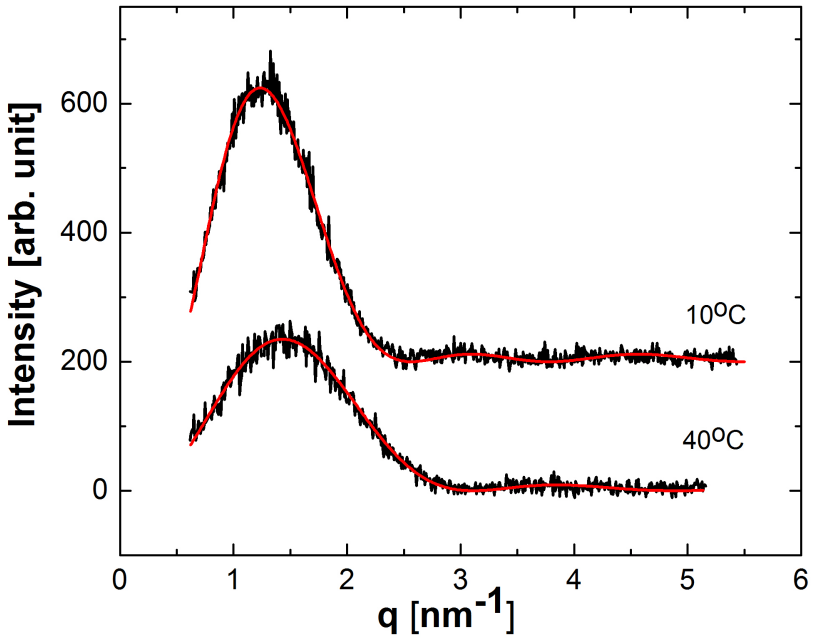


FIGURE 6.22: SAXS pattern of a 5wt% DMPC dispersion at pH=2, in the gel (T=10°C) and fluid (T=40°C) phases. The smooth lines are fits to the bilayer form factor given by eq.6.1.

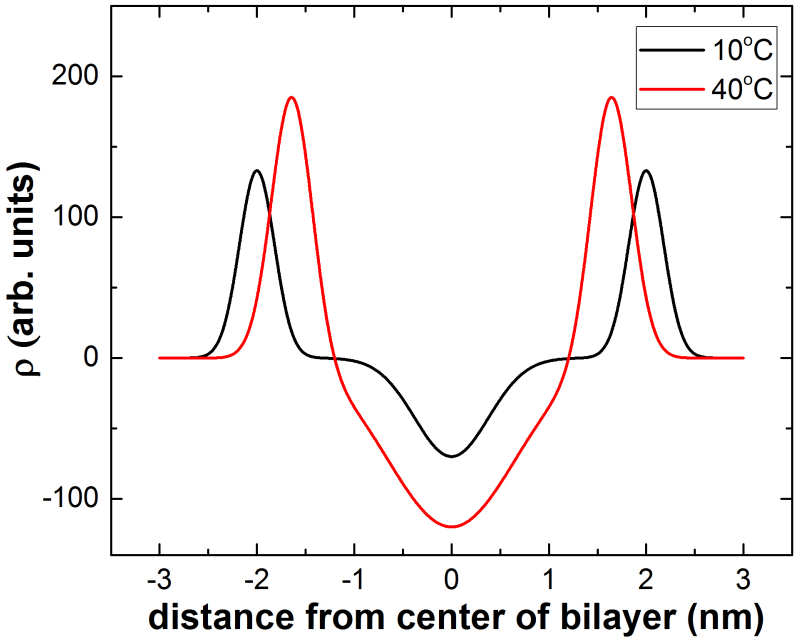


FIGURE 6.23: electron density profiles obtained from the model.

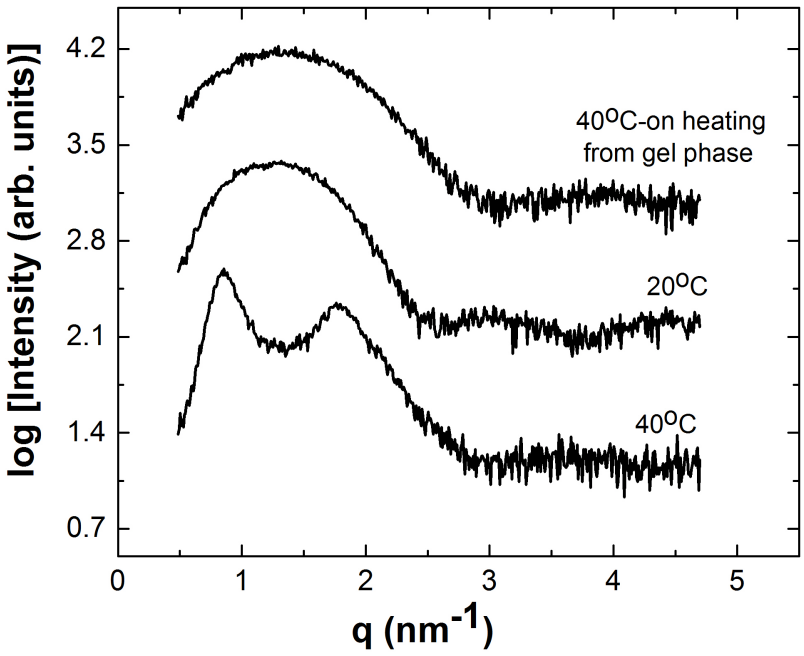


FIGURE 6.24: SAXS patterns of DMPC dispersion at pH=2 in the presence of 100mM NaCl. The sample was prepared at 40°C in the fluid phase and cooled down to 20°C in the gel phase. It was subsequently reheated to the fluid phase.

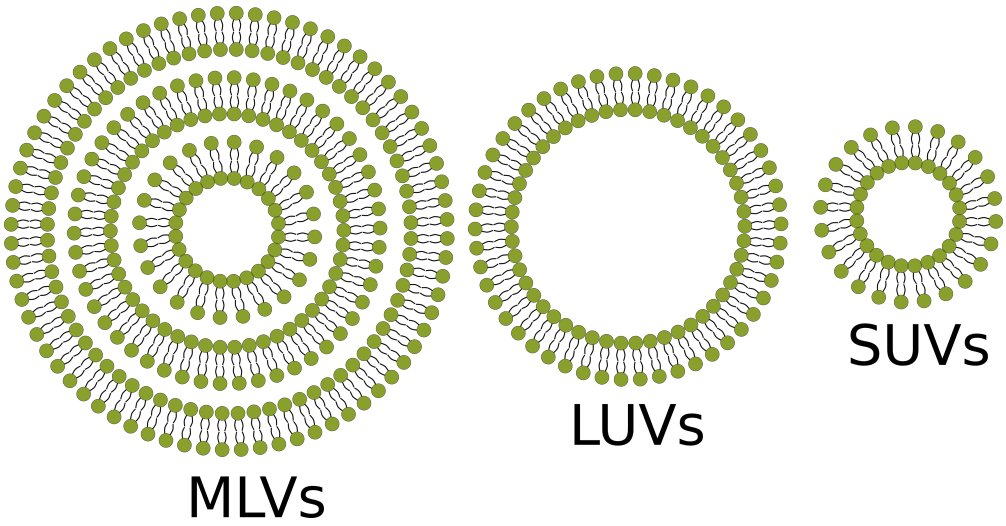


FIGURE 6.25: schematic of two bilayer morphologies, namely, multilamellar vesicles (MLVs) and unilamellar vesicles (ULVs), observed in the present study. ULVs are often referred to as large unilamellar vesicles (LUVs) and small unilamellar vesicles (SUVs), if their diameters are more or less than 100 nm, respectively.

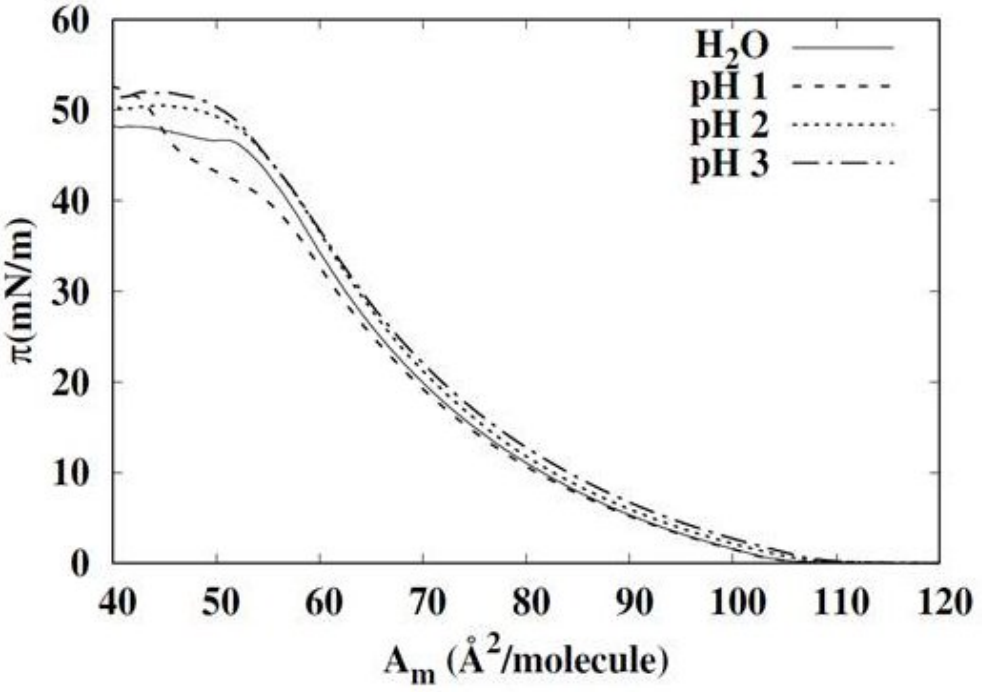


FIGURE 6.26: Surface pressure – Area per molecule ($\pi$–$A_m$) isotherm for DMPC monolayer at different pH.

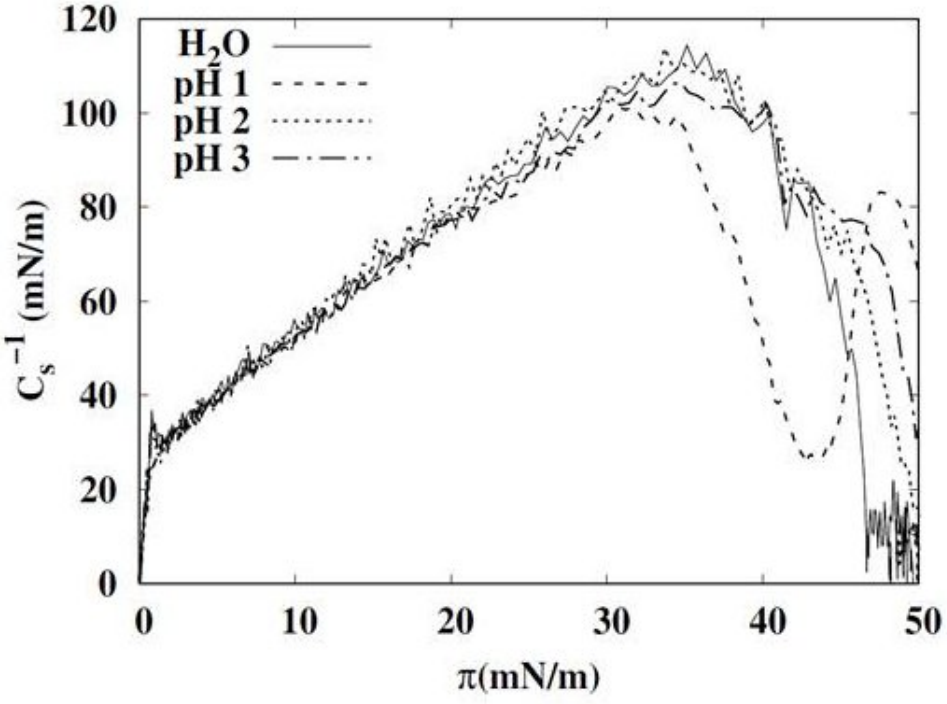


FIGURE 6.27: Variation of the compression modulus ($C_s^1$ with surface pressure ($\pi$) for DMPC monolayer at different pH.

# Bibliography


[1] Small DM. The Physical Chemistry of Lipids. New York: Plenum; 1986.

[2] Tardieu A, Luzzati V, Reman F. Structure and polymorphism of the hydrocarbon chains of lipids: a study of lecithin-water phases. Journal of molecular biology. 1973;75(4):711-33.

[3] Seddon JM, Templer RH. Polymorphism of lipid-water systems. In: Lipowsky R, Sackmann E, editors. Handbook of biological physics. vol. 1. Elsevier science B. V.; 1995. .

[4] Wack DC, Webb WW. Synchrotron x-ray study of the modulated lamellar phase P $\beta$'in the lecithin-water system. Physical Review A. 1989;40(5):2712.

[5] Smith G, Sirota E, Safinya C, Plano R, Clark NA. X-ray structural studies of freely suspended ordered hydrated DMPC multimembrane films. The Journal of chemical physics. 1990;92(7):4519-29.

[6] Akabori K, Nagle JF. Structure of the DMPC lipid bilayer ripple phase. Soft matter. 2015;11(5):918-26.

[7] Nagle JF, Tristram-Nagle S. Structure of lipid bilayers. Biochimica et Biophysica Acta (BBA)-Reviews on Biomembranes. 2000;1469(3):159-95.

[8] Rowe ES, Campion JM. Alcohol induction of interdigitation in distearoylphosphatidylcholine: fluorescence studies of alcohol chain length requirements. Biophysical journal. 1994;67(5):1888-95.

[9] Lichtenberger LM. Membranes and barriers: with a focus on the gastric mucosal barrier. Clin Invest Med. 1987;10:181-8.

[10] Guiral M, Neitzel C, Castell MS, Martinez N, Giudici-Orticoni M, Peters J. The effect of pH on the dynamics of natural membranes. The European Physical Journal E. 2018;41(2):1-8.

[11] Tocanne JF, Teissié J. Ionization of phospholipids and phospholipid-supported interfacial lateral diffusion of protons in membrane model systems. Biochimica et Biophysica Acta (BBA)-Reviews on Biomembranes. 1990;1031(1):111-42.

[12] Träuble H, Eibl H. Electrostatic effects on lipid phase transitions: membrane structure and ionic environment. Proceedings of the National Academy of Sciences. 1974;71(1):214-9.

[13] Furuike S, Levadny VG, Li SJ, Yamazaki M. Low pH induces an interdigitated gel to bilayer gel phase transition in dihexadecylphosphatidylcholine membrane. Biophysical journal. 1999;77(4):2015-23.

[14] Boggara MB, Krishnamoorti R. Small-angle neutron scattering studies of phospholipid-NSAID adducts. Langmuir. 2010;26(8):5734-45.

[15] Zhou Y, Raphael RM. Solution pH alters mechanical and electrical properties of phosphatidylcholine membranes: relation between interfacial electrostatics, intramembrane potential, and bending elasticity. Biophysical journal. 2007;92(7):2451-62.

[16] Boggara MB, Faraone A, Krishnamoorti R. Effect of pH and ibuprofen on the phospholipid bilayer bending modulus. The Journal of Physical Chemistry B. 2010;114(24):8061-6.

[17] Chowdhury A, Sasidharan S, Xavier P, Viswanath P, Raghunathan V. Effect of pH on the phase behavior of DMPC bilayers. Biochim Biophys Acta. 2021;1863(11):183695.

[18] Matsuki H, Miyazaki E, Sakano F, Tamai N, Kaneshina S. Thermotropic and barotropic phase transitions in bilayer membranes of ether-linked phospholipids with varying alkyl chain lengths. Biochimica et Biophysica Acta (BBA)-Biomembranes. 2007;1768(3):479-89.

[19] Tristram-Nagle S, Liu Y, Legleiter J, Nagle JF. Structure of gel phase DMPC determined by X-ray diffraction. Biophysical journal. 2002;83(6):3324-35.

[20] Wiener M, Suter R, Nagle J. Structure of the fully hydrated gel phase of dipalmitoylphosphatidylcholine. Biophysical journal. 1989;55(2):315-25.

[21] Pabst G, Rappolt M, Amenitsch H, Laggner P. Structural information from multilamellar liposomes at full hydration: full q-range fitting with high quality x-ray data. Physical Review E. 2000;62(3):4000.

[22] Kučerka N, Liu Y, Chu N, Petrache HI, Tristram-Nagle S, Nagle JF. Structure of fully hydrated fluid phase DMPC and DLPC lipid bilayers using X-ray scattering from oriented multilamellar arrays and from unilamellar vesicles. Biophysical journal. 2005;88(4):2626-37.

[23] Lipowsky R, Leibler S. Unbinding transitions of interacting membranes. Physical Review Letters. 1986;56(23):2541.

[24] Pozo-Navas B, Raghunathan V, Katsaras J, Rappolt M, Lohner K, Pabst G. Discontinuous unbinding of lipid multibilayers. Physical review letters. 2003;91(2):028101.

[25] Winterhalter M, Helfrich W. Bending elasticity of electrically charged bilayers: coupled monolayers, neutral surfaces, and balancing stresses. The journal of physical chemistry. 1992;96(1):327-30.

[26] Morse DC. Topological instabilities and phase behavior of fluid membranes. Physical Review E. 1994;50(4):R2423.

[27] Golubović L. Passages and droplets in lamellar fluid membrane phases. Physical Review E. 1994;50(4):R2419.

[28] Chen CM, Lubensky T, MacKintosh F. Phase transitions and modulated phases in lipid bilayers. Physical Review E. 1995;51(1):504.

[29] Hitchcock PB, Mason R, Thomas KM, Shipley GG. Structural chemistry of 1, 2 dilauroyl-DL-phosphatidylethanolamine: molecular conformation and intermolecular packing of phospholipids. Proceedings of the National Academy of Sciences. 1974;71(8):3036-40.

[30] Pearson RH, Pascher I. The molecular structure of lecithin dihydrate. Nature. 1979;281(5731):499-501.

[31] Miyoshi T, Kato S. Detailed analysis of the surface area and elasticity in the saturated 1, 2-diacylphosphatidylcholine/cholesterol binary monolayer system. Langmuir. 2015;31(33):9086-96.

[32] Karmakar S, Sarangi B, Raghunathan V. Phase behaviour of lipid–cholesterol membranes. Solid state communications. 2006;139(11-12):630-4.

# Chapter 7

# Conclusions

In this thesis we study the structure, phase behaviour and polymorphism of different selfassembled aggregates of ionic amphiphilic molecules in the presence of polyelectrolytes and salt. In addition, the influence of pH on the phase behaviour of zwitterionic bilayers has also been probed. Various experimental techniques, such as small angle x-ray scattering (SAXS), polarising optical microscopy (POM), cryogenic scanning electron microscopy (cryo-SEM) and differential scanning calorimetry (DSC), are used to probe the structure of different phases and the underlying interactions.

In chapter 1 we give a brief introduction to amphiphilic molecules and principles of their self-assembly. Then we present a short description of the phase behaviour of amphiphilewater systems. We provide an outline of relevant interactions present in systems probed in this study. We also describe the basic principles of experimental techniques, such as xray scattering, polarising optical microscopy and cryo-SEM. SAXS data modelling for the determination of various structures observed in our systems is also discussed.

In chapter 2 we have studied the structure of complexes of DNA with cationic alkyltrimethylammonium bromide ($C_n$TAB) surfactants for n varying between 8 and 18. These complexes are found to have a two-dimensional hexagonal structure for n $\geq$ 14. On the other hand, a two-dimensional square phase is observed for n = 10. In the intermediate case of n = 12, the square phase is observed at relatively higher surfactant concentrations, but a hexagonal phase, distinct from the one exhibited by complexes of longer chain surfactants, is observed at lower surfactant concentrations. Formation of the square phase at lower surfactant-chain length can be attributed to higher DNA–DNA repulsion in the hexagonal phase. At presenet we do not know what is the reason behind formation of $H_s$ phase for $C_{12}$TAB-DNA complexes. Further work is needed to understand this phase behaviour. Structural polymorphism of these complexes demonstrate the delicate interplay between entropy and electrostatic energy in these two-dimensional macroion crystals.

In chapter 3 we have studied the effect of an oppositely charged polyelectrolyte on the interaction between ionic surfactant bilayers, as a function of salt concentration in the solution. At low salt concentrations, polymer bridging between adjacent bilayers creates an effective interbilayer attraction, that results in a condensed lamellar complex. At high salt concentration the polyelectrolyte does not bind to the bilayers and the van der Waals inter-bilayer attraction leads to the formation of a collapsed lamellar phase. A swollen complex occurs over intermediate salt concentrations, which forms a bicontinuous sponge phase in the case of DDAB and a swollen lamellar phase for DDAC and DOAC. A speard in the spacing is observed in the swollen phase. Further

work is needed to understand the reason behind it. Formation of the sponge phase can be attributed to an increase in the Gaussian rigidity of the bilayers due to polymer adsorption, as has been theoretically predicted.

In chapter 4 we have studied the effect of salt on the phase behaviour of fluid lamellar phase formed by ionic surfactants and lipids at low salt regime. In the case of surfactant bilayers (DDAC an DDAB) the system goes from an electrostatically stabilized phase to a undulation stabilized phase on increasing the salt concentration in the solution, before it goes into a collapse lamellar ($L_\alpha^c$) phase. The value of salt concentration at which the collapsed phase appears is different for DDAC and DDAB. This can be attributed to the difference in the counter-ions in the two systems. A specific-ion effect is also observed as the value of $C_s$ at which the $L_\alpha^c$ phase appears in the case of DDAC, is slightly higher for LiCl and CsCl compared to NaCl or KCl. Further work needs to be done to understand such specific ion effect. A temperature driven $L_\alpha^c \rightarrow L_\alpha$ transition is observed in the case of lamellar phase formed by DDAC. The transition temperature depends on the salt concentration. In the case of charged lipid bilayers (DMTAP), whose bare bending rigidity is a order of magnitude higher compared to the surfactant bilayers, a gradual reduction of d-spacing is observed with increasing $C_s$.

In chapter 5 we have studied the effect of salt on the phase behaviour of fluid lamellar phase formed by ionic surfactants and lipids at high salt regime. For LiCl and NaCl, on increasing the salt concentration after a threshold ($\sim$ 2 M), an increase in d-spacing is observed. But for KCl and CsCl such significant change in spacing is seen. The trend of the d-spacing changes follows the trend of activity coefficient of alkali metal chlorides with concentration. The spacing of DDAC-NaCl (or DDAC-LiCl) samples at high salt concentration ($\sim$ 3 M) is found to be higher than the DMTAP- NaCl (or DMTAP-LiCl) samples. This maybe due to the higher bare bending rigidity of lipid bilayers. The effect of different alkali metal bromides on the $L_\alpha$ phase of DDAB is also studied. No change in spacing is observed for DDAB-KBr and DDAB-CsBr samples. For DDAB-NaBr an optically isotropic phase is found at high NaBr concentration ([NaBr] $\sim$ 3 M). The spacing also increases. A single broad peak is found, that can be fitted to a scattering from a lamellar phase. For LiBr at similar salt concentration ($\sim$ 3 M), a broad peak (corresponding to a higher periodicity) and a sharp peak (corresponding to a lower periodicity) are observed. The pattern in which d-spacing changes with salt concentration follows the similar trend of activity coefficient of alkali metal bromides. At present we are no able to figure out the ion specificity of such behaviour and further work needs to be done to understand the behaviour.

In chapter 6 We have studied the effect of acidic pH on the phase behaviour of two zwitterionic lipids, namely DMPC and DLPC. Dispersions of DMPC in HCl solution of pH=4 and pH=3 behave identical to dispersions in water. PC bilayers get charged at lower pH on approaching the pK of the PC headgroup. At the same time head group size is reduced due to dehydration. This results in the formation of the untilted gel phase at low temperatures and the inverted hexagonal phase at higher temperatures. Headgroup dehydration leads to the formation of crystals after a few days of incubation at pH=2 and pH=1. Since animal membranes typically contain an appreciable amount of cholesterol, which is known to significantly alter the phase behavior of PC lipids, a natural extension of the present study will be to probe the influence of low pH on DMPC–cholesterol (or DLPC- cholesterol) membranes.